ABSTRACT

HOSSAIN, MD MILON. Carbon Nanotube E-Textiles for Multifunctional and Wearable Electronic Applications. (Under the direction of Dr. Philip D. Bradford).

Textile-based wearable electronics are seeing a surge in attention due to their many potential applications in sportswear, health care, military, lifestyle and fashion. With these systems, it is essential to integrate electrical functionality while maintaining the comfort and fit of conventional apparel for truly wearable electronics. Conductive yarns are a basic building block of e-textiles that are needed for transferring power and signal. The requirements for the commercial success of e-textiles are strength, elasticity, flexibility and durability. Most commercially available e-textiles are based on metallic or metal-coated yarns which have good conductivity and mechanical strength but have relatively poor comfort, the chance of skin irritation, can corrode and have durability issues, all of which lower their appeal in apparel applications. Among conductive materials, carbon nanomaterials possess the advantages of high flexibility and electrical conductivity, as well as mechanical, thermal and chemical stability. Carbon nanotube (CNT) is a promising material for multifunctional wearable electronic applications due to their excellent electrical conductivity, low density, and superior strength. However, the shorter length of CNTs and nanoscale dimension restricts them for macro assembly and bulk scale processing. Therefore, different synthesis methods emerged for the macro-assembly of the CNTs for wearable electronic applications. Most of these process produces thin diameter yarn unsuitable for textile processing and the coating-based process is susceptible to laundering. It is, therefore, necessary to develop a CNT yarn with a higher diameter and durable to washing for advancing sustainable e-textiles.

Here, a solid-state and straightforward process of producing CNT-wrapped textile yarns was developed for multifunctional wearable electronic applications. Highly aligned and millimeter tall CNTs were synthesized on a quartz substrate by chemical vapor deposition. Two CNTs arrays were placed on a custom-made spinning device, and the textile yarn was inserted as a core. Both the arrays were wrapped over the textile yarns for producing highly conductive and strong yarn. Both the strength and conductivity of the CNT-wrapped yarn can be customized for various applications. Thermoplastic polyurethane dissolved in acetone was applied and the impact on the structure and properties were evaluated. Microcomputed tomography revealed the alignment and packing of the fibers. The thermal stability of the developed yarns was determined.

The textile processability of conductive yarns is critical for wearable electronic applications. The produced yarn has a diameter similar to the conventional textile yarns essential for the bulk production of electrodes. The CNT-wrapped yarns are suitable for textile processing such as weaving and knitting, sewing, and embroidering into apparel. The yarn was used in different multifunctional applications such as motion sensors, powering LEDs and heating garments. Seamless integration into a glove and wristband demonstrated the suitability of the yarn for Textile 4.0.

The versatility of the spinning device allows inserting almost all textile yarns. When the same spinning system was applied to the spandex core, a highly elastic yarn was produced. The yarn was used to produce different braid structures. Woven, knitted and braided structure containing CNTY was visualized by laser profilometer and these CNT textile electrodes demonstrated

excellent performance as electrocardiography (ECG). The remarkable body conformability of the electrodes revealed high stability against motion artifacts. Further investigation on washability demonstrated no significant deterioration in ECG signal. The CNT-wrapped cotton yarn was functionalized using titanium carbide (Ti3C2) for enhanced strain sensing and supercapacitor applications. The elemental composition, surface morphology and microstructure of the modified yarn were analyzed. Evaluation of strain sensing and supercapacitance revealed that their performance increased multifold compared to the unmodified yarns.

Carbon Nanotube E-Textiles for Multifunctional and Wearable Electronic Applications

by
Md Milon Hossain

A dissertation submitted to the Graduate Faculty of
North Carolina State University
in partial fulfillment of the
requirements for the degree of
Doctor of Philosophy

Fiber and Polymer Science

Raleigh, North Carolina
2022

APPROVED BY:

_____	_____
Dr. Philip Bradford Committee Chair	Dr. Jesse Jur
_____	_____
Dr. Xiangwu Zhang	Dr. Jacob Adams

DEDICATION

To my family.

BIOGRAPHY

Md Milon Hossain was born in Magura, Bangladesh on December 31st, 1987. He is the older of two children, having a younger sister, Farzana. After graduating from the high school in Jessore, he went to Mawlana Bhashani Science and Technology University, Tangail. He graduated with Bachelor and Master in Textile Engineering in 2011 and 2014. During his Master's thesis, he worked on carbon-Kevlar/polypropylene composites under Dr. Mobarak Ahmad Khan at the Institute of Radiation and Polymer Technology, Dhaka. After graduation, Milon worked in a textile company and later joined Khulna University of Engineering and Technology as a lecturer. He was promoted to Assistant Professor in 2015 and joined the University of Nebraska-Lincoln for PhD. He worked on soy protein fiber extraction and wet spinning for a year. His research interests transitioned to e-textiles and thus, moved to the Wilson College of Textiles, North Carolina State University in Fall 2017.

He joined Carbon Nanotube Textile Research group as a Research Assistant under the direction of Dr. Philip Bradford in Fall 2017. Here, he assisted in catalytic vapor deposition of highly aligned carbon nanotube and developing a spinning system for carbon nanotube yarn. He optimized and investigated the carbon nanotube wrapping system over different textile yarns. Then he demonstrated the textile manufacturability of the yarns and successfully knit the yarn using the whole garment knitting machine for the first time. The different textile structures produced by the CNT-wrapped textile yarn demonstrated excellent performance in different wearable electronic textile applications. He is a recipient of the German Academic Exchange Service (DAAD) RISE Professional Scholarship and spent three months at the Fraunhofer Research Institution for Casting, Composite and Processing, Augsburg, Germany and assisted in developing tensile test standards for unidirectional thick carbon composites.

ACKNOWLEDGMENTS

I would like to express my sincere appreciation to Dr. Philip Bradford for accepting me into his research group. I am grateful to Dr. Bradford for trusting me in this unique research area and guiding me along the way. You have been an invaluable contributor to my development as a researcher and scientist. At the same time, I learned to enjoy life and develop a positive outlook in any hardship. I would like to thank Dr. Jesse Jur and his NEXT research lab for providing instrumental facilities, advice and enthusiasm. I am also thankful to Dr. Xiangwu Zhang and Dr. Jacob Adams for continual support as committee members.

I am incredibly grateful to Dr. Jon Rust for the opportunity to work in the Knitting Lab, Zeis Textiles Extension. I am indebted to Lab Manager, Brian Davis who trained me with the whole garment knitting machine and without it, this work would have been incomplete. I am fortunate to have Dr. Braden Li for his tremendous support and assistance with the mechanical testing and electrocardiography data analysis. I also want to thank Dr. Nanfei He and Dr. Gao for providing me MXene and helping with voltammetry. Special thanks to Dr. Andre West and Dr. Ericka Ford for their encouragement and guidance. I would like to thank my lab members especially Dr. Ozkan and Dr. Lubna who smoothen my transition to the lab and introduced the chemical vapor deposition system. I also would like to thank Dr. Karim, Sara, Jakub, Pat and Walaa for their encouragement and support.

This work would not have been possible without the support and assistance of so many: Judy Elson, Birgit Anderson, Joyce Cole, Busra Sennik, and the AIF lab managers and research associates especially Chuck, BB, and Phillip Strader who helped me in doing many advanced characterizations and taught me the techniques.

I can’t imagine my development, education, and progress without the tremendous sacrifice of my parents who always trusted me and did everything for my comfort. Finally, I would like to thank my wife Shahida and my lovely daughter Mifrah for their unwavering patience and love which have made the completion of this dissertation possible

TABLE OF CONTENTS

LIST OF TABLES

LIST OF FIGURES

Chapter 2

Chapter 3

Chapter 4

Chapter 5

Chapter 6

Chapter 1: Introduction

Nanomanipulation has revolutionized the future of material science with unprecedented properties. Materials at nanoscale often demonstrate superior electrical, mechanical, thermal and optical properties compared to their bulk counterparts. The molecular composition, dimensions, and structures of nanomaterials can be controlled to tailor their properties for diverse applications. Assembling them into macroscale structures enables the development of materials with multi-functionality. Nanostructured materials have led to breakthroughs in the design of high-performance electrical devices by tremendous miniaturization of circuitry[1]. In addition to the high speed and performance, the next-generation electronics are expected to have high portability and flexibility, easily integrating structure in a single device system[2]. To meet these requirements, fiber-based structures are being explored as a promising platform and substrate for wearable electronics owing to their softness, deformability, and stretchability[3]. Miniaturization of electric components has enabled further advances in wearable electronics by attaching, incorporating, or merging them into fiber-based structures using a variety of techniques and processes[4] and eliminates the process of hiding bulky electronics through clever garment design[5]. These garments enhanced with electrical functionality are termed as electronic textiles (e-textiles) and composed of sensors, actuators, data processors, power supply and a communication interface[4]. Electrically conductive yarns, films and fabrics are the major components of e-textiles and are used to connect different sensors, modules, MCU and power sources to form a wearable body area network[6]. The widely used electroconductive materials for e-textiles are carbon materials[7,8,9,10,11,12] intrinsic conducting polymers (ICPs)[13,14,15] metallic nanowires (NWs)[16,17,18] and metallic nanoparticles (NPs)[19,20,21].

Ideal electrically conductive materials for e-textiles would offer low resistance and electrical performance to the textile structures. The very high aspect ratio, excellent flexibility, high tensile strength, modulus and superior electronic properties of carbon nanotubes (CNTs) make them one of the most promising materials for e-textiles. CNTs can be integrated into e-textiles in three ways- CNT yarns, CNT-polymer composite yarns and CNT-coated yarns/fabrics[22]. CNT-based e-textiles have applications in sensing[23,24] and actuating[25,26], energy storage and conversions[27,28], Joule heating[29], electromagnetic shielding[30,31], field emission[32,33], transistors[34,35], biomedical[36,37] etc. CNT-polymer composites yarns are produced by melt or wet spinning process. The poor processability and agglomeration characteristics of CNTs makes the process complicated. Moreover, the CNT loading is low due to the lower percolation threshold. The hydrophobic nature of CNTs shows poor adhesion to textiles during the coating process. CNT yarns are produced by direct assembly of highly aligned CNTs into macroscale and the yarns possess high mechanical strength and electrical conductivity[22]. This macroscopic CNT yarn can further be textile processed for 2-dimensional fabric production at a large scale. The reduction of outstanding individual CNT properties at nanoscale is the major issue of assembling CNTs in macroscale. The alignment of CNT decreases at bulk scale and defects may induced during assembly resulting in a drop in CNTs performance. This is the major challenge to be solved for e-textile applications.

CNTs can be assembled macroscopically in 1, 2 and 3-dimension architectures. Wet spinning, direct spinning and dry (array) spinning are examples of assembling CNTs in fibers, yarns, films, ribbons, foams etc. Not all CNT arrays are spinnable and it depends on the CNTs morphology, lengths, diameters and density[38]. A large amount of CNTs is required to assemble them into a macroscale yarn to match the diameter of conventional textile yarns for processing by

textile technologies for seamless integration into e-textiles. There is a need for developing techniques to spin CNTs into yarn to produce large diameter CNT yarn by using a small amount of CNTs to make it sustainable for e-textile applications. The CNT array spinning process will be used in this dissertation to assemble CNT e-textiles for multifunctional wearable electronic applications. CNT assemblies produced from vertically aligned CNTs (VACNTs) have been demonstrated in the literature and a good understanding of different spinning parameters for pristine CNTs has been established. However, the different spinning parameters for CNT-wrapped textile yarns are rarely reported. Wrapping CNTs over textile yarns are required to produce yarn with a larger diameter for textile processing. Understanding the structure-property relationship of CNT wrapped sheath-core textile yarn is important for e-textile fabrication and is presently not well understood. The flexibility and strength of the sheath-core yarn determine the textile processability for multifunctional and wearable electronics applications. For certain applications, it is required to improve the functionality of CNT wrapped textile yarns while retaining their processability. Most of the functionalized CNT research focused mainly on increasing active materials loading regardless of their textile processability. In this dissertation, we aim to solve several of these research problems in the wearable e-textile field. The main research objectives of this dissertation are mentioned below:

- Objective 1: Develop a spinning system to wrap CNT over textile yarns while maintaining conductivity and mechanical properties suitable for textile processing
- Objective 2: Understand the structure-property behavior of CNT wrapped textile yarns and their impact on wearable electronic applications
- Objective 3: Design highly wash durable CNT-based textile electrodes for biosensing

Chapter 2: Literature Review

2.1 E-Textile Yarn

Yarn as a smart and conductive material is attractive for various applications and the textile processing of yarn into fabric facilitates the greater control of composition, surface area and porosity. Using the proper fiber geometries and processing techniques, the properties of yarn can be tailored to produce complex architectures. The next-generation wearable technology should be tiny and lightweight and should be enabled by yarns. However, the critical importance of all these applications is the need for yarns with excellent electrical conductivity and mechanical stability. At the same time, the yarns are required to be flexible, stretchable and durable[39]. Electrically conductive textile yarn should be used for connectors, passive components, and in some cases building blocks for active components. Conductive yarns can be produced using different materials and methods and could be intrinsically or extrinsically conductinge[40].

2.1.1 Metallic Yarn

Metallic yarn has been used from ancient times especially for aesthetic purposes. Metallic yarn has a very low electrical resistance which is essential for e-textile applications. Copper, stainless steel, silver, brass nickel and their alloys are commonly used as conductive yarns for producing e-textiles. The metallic yarn could be used in textiles in three different ways such as: metal filament (monofilaments) or multifilament (wires) yarns spun from metal, metal filaments combined with textile yarns (plied yarns) by twisting and core-sheath structures (either metal as core or sheath - both configurations are possible)[41]. Wire drawing, bundle wire drawing, melt spinning and shaving process are used to produce very thin metallic filaments with diameters ranging from 1 – 80 μm to millimeters. Threads produced from stainless steel have an electrical conductivity of 1.3×10^6 S/m. Copper is an excellent conductor (58×10^6 S/m) but suffers from oxide formation in the air. While aluminum shows good conductivity of 37×10^6 S/m, the

formation of the passivation layer (aluminum oxide) limits their usability. Silver and gold also have an excellent electrical conductivity of 62 x 10^6 S/m and 44 x 10^6 S/m respectively but due to their higher cost, they are the least used in practical applications[42]. The tough metallic yarn has very high conductivity but they are heavier and stiffer than conventional textile yarns. This adds weight to the textiles and makes the garments uncomfortable. Additionally, their thin filaments are brittle which makes them susceptible to breaking and they also may corrode over time[43,44]. The high cost and complicated textile processing (weaving/knitting) of the stiff yarns make them less attractive materials for wearable and e-textile applications.

2.1.2 Intrinsically conductive (ICP) polymer-coated yarn

Polymers are commonly considered insulators because of their poor electrical conductivity (10^{-18} S/cm)[42]. However, a new class of polymer known as intrinsically/inherently conductive polymers (ICPs) has been extensively investigated in the past 50 years and fiber/yarn based on ICPs were first reported around 1980[44]. The most used ICPs are poly (3,4-ethylenedioxythiophene) (PEDOT), polypyrrole, polyaniline, polythiophene and derivatives/copolymers thereof[45]. ICPs have the advantages of high conductivity, lightweight, and environmental stability and their conductivity range from 10^{-8} – 10^5 S/cm[42]. ICPs offer a wide range of colors and unlike metal, they do not suffer from skin irritation and long term toxicity under direct contact[46]. However, it is very challenging to produce all-organic fibers from ICPs and the process is expensive. Generally, melt spinning, solution spinning and electrospinning are used to produce ICPs fibers/yarns. Melt spinning is not a suitable technique since ICPs are mostly non-thermoplastic. Poor solubility, rigid backbone structure and low molecular weight are the main issues with the electrospinning of ICPs and make them unfavorable[47,48]. Therefore, wet spinning is the most appropriate method for producing ICPs fibers. Conductive fibers obtained from polyaniline, PEDOT, and PEDOT:PSS (poly (styrene sulfonate)) showed conductivity of 150 – 250 S/cm[42] which is comparatively lower

than metallic yarn. However, secondary doping can significantly improve the electrical conductivity of ICPs. Poor mechanical strength and low strain at break, microscale size, slow production rate, brittleness and difficult processing make their usability very limited for different commercial applications. Therefore, they are often combined with other polymeric materials to enhance their application areas sacrificing their electrical conductivity. This can be done by either mixing ICPs with insulating polymers or coatings on other polymers. Processes like dip coating, vapor phase deposition, electrochemical coating and in-situ polymerization are widely used to coat textiles with ICPs due to their excellent scalability and easy processing.

2.1.3 Nanoparticles (NPs)/nanowires (NWs) coated yarn

Various types of nanostructured materials such as nanorods, nanowires, nanoneedles, nanoflowers, nanobelts, nanoflakes, nanotubes, nanoparticles etc. can be grown or coated on textiles[49]. They are mainly used for surface modification and functionalization of textile materials. Among the various nanostructures, nanoparticles (NPs) and/or nanowires (NWs) are widely used for textile yarn due to their high aspect ratio (NWs) and better dispersibility (NPs). Metallic nanomaterials have high conductivity and their solution-based synthesis process enables them to be applied on textile surfaces easily. NPs/NWs of copper, gold, nickel, silver and aluminum are commonly used to impart electrical conductivity to textile structures. Nanomaterials of silver are extensively used due to their excellent electrical conductivity and solution processability. Copper being the cheaper (1% the cost of silver) and more abundant is also an attractive nanomaterial. In contrast, NWs of copper has a lower aspect ratio, higher oxidation tendency and poor solvent dispersion compared to silver NWs[50]. Though gold nanomaterial has superior resistance to oxidation and biocompatibility, it is the least used material for textiles due to their high cost and complex synthesis process[51]. Vapor phase deposition and electrodeposition are the most favorable for NPs/NWs application in textiles whereas the coating process is suitable for bulk scale

production. However, NPs/NWs greatly affect the inherent characteristics of the textile structure. It is essential to consider the attributes like size, shape, dispersibility and purity of nanomaterials/NWS[52]. Two major problems of nano induced electrical conductivity enhancement of textiles are that i) nanomaterials/NWs tend to aggregate themselves due to electrostatic and van der Waals attractions making it difficult to apply them uniformly onto the surface of textile structures and ii) poor adhesion and durability due to the absence of surface functional groups which makes it hard to bond them with textile fibers. The difference in surface energy between inorganic nanoparticles and polymeric materials is very high resulting in repellency in the interface between them. Moreover, the high surface area of NPs escalates this issue further. This is reflected in the poor wash stability of NPs/NWs coated textiles[53]. Binding agents/cross-linking are commonly used to improve the adhesion of NPs/NWs to textiles[52]. Additionally, the electrical conductivities of NPs/NWs deposited in textile yarns may decrease dramatically under repeated mechanical deformation.

2.1.4 Carbonaceous yarn

Electrical conductivity is an important parameter of the e-textile yarn for various wearable electronics applications and can be tailored as required. However, e-textile yarn is also required to meet some additional criteria such as they must be able to withstand mechanical stress during processing and end-uses. The yarn also needs to maintain the functionality in different environments including ambient atmosphere, which is challenging for volatile dopants used with ICPs, exposure to water (during washing) and sweat (during use) and chemical agents - for example, detergent. These additional requirements are sometimes overlooked but critical for commercial success and applications of e-textile products[54]. Electrical conductivity and Young's modulus of different types of fibers and yarns have been compared as shown in Figure 2.1[54]. The modulus and electrical conductivity vary widely according to different yarn types. It is interesting

to note that, yarns with higher electrical conductivity showed higher modulus because both the electron transport and mechanical load transfer benefit from the alignment of fiber along the yarn axis. Carbon-based yarns showed higher electrical conductivity and modulus than polymer blends, coated fibers and nanocomposites.

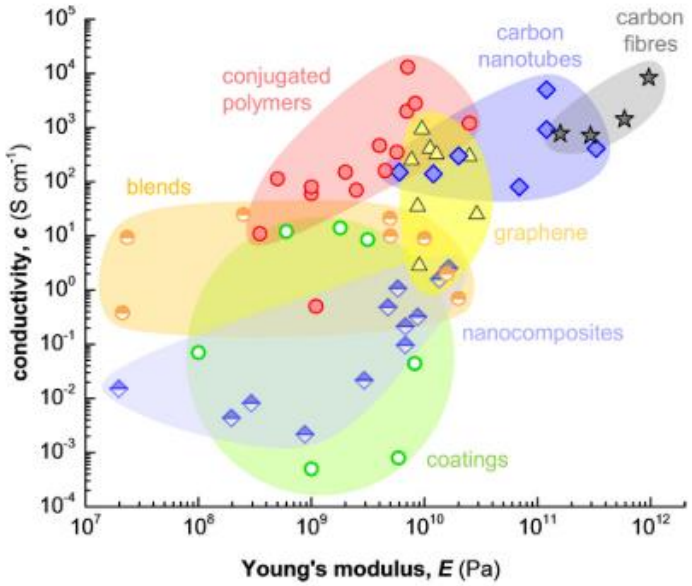

Figure 2. 1 Ashby plot of electrical conductivity vs Young's modulus of fibers/yarns

Description: (grey stars) carbon fibers, (blue diamonds) carbon nanotubes, (yellow triangles) graphene, (red circles) conjugated polymers, (orange/white circles) blends of conjugated and insulating polymers, (blue/white diamonds) nanocomposites of carbon black, carbon nanotubes or graphene embedded in an insulating polymer matrix and (green/white circles) coatings of textile fibers with conjugated polymers, carbon nanotubes or graphene[54]

In the past, metals and ICPs were the most popular electrically conductive materials for e-textiles. Recently, carbon materials are being extensively studied for use in e-textiles due to their excellent electrical conductivity, lightweight, and chemical resistance characteristics. They are cost-effective and abundantly available in different shapes and sizes making them an excellent candidate for e-textile applications. Based on the carbon materials' morphology and synthesis

process, their characteristics also vary widely. Carbon materials can be incorporated into yarn in three different ways[55]- i) Directly spinning carbon-based fibers ii) coating textile yarn with carbon materials and iii) carbonization of textile at high temperature in an inert environment. Different carbon materials such as carbon black (CB), graphene oxide (GO), carbon nanofibers, carbon nanotubes (CNTs) are widely used for producing conductive yarn.

Among these carbon materials, GO and CNTs are the most attractive due to their excellent electrical, thermal, and mechanical characteristics. However, the synthesis process of GO and CNTs affects their processability and performance. Graphene is a two-dimensional monoatomic carbon layer and has excellent electrical and thermal conductivity. In addition to their conductive properties, graphene is also flexible, compressible and transparent[56]. CNTs are a tubular form of graphene sheet mainly available as single-walled (SWCNTs) and multiwalled (MWCNTs) forms and their electrical conductivity is either metallic or semiconductor-based on their chirality[57]. CNT-based conductive yarn can be produced by either spinning CNTs or coating textile yarn with CNTs solution. CNTs yarns are mechanically strong and flexible which makes it the ideal candidate for textile processing. However, for e-textile applications, converting nanoscale CNT fibers/yarns to micro/macroscale is considered the most effective and commercially viable process[58].

2.2 Carbon Nanotube Assemblies

The three methods commonly used in synthesizing CNTs are laser ablation, arc discharge and chemical vapor deposition (CVD)[59,60]. While the first two methods work on the mechanism of evaporating carbon molecules from the solid, the CVD method breaks the hydrocarbon precursors. Then carbon atoms of broken hydrocarbon are rearranged into the desired nanotube structure. Most of the CNTs are obtained by the CVD method because of high CNT yields, high purity, greater control over synthesis and excellent self-assembly[59,61,62]. Though great efforts and significant

achievements have been made on CNT synthesis and their application in different fields, it is still a major challenge to produce CNTs with controlled diameter, conductive properties, chiral selectivity and special structure[63]. Proper control of the morphology of CNTs should improve the electrical conductivity, mechanical and thermal properties. Though some researchers obtained the best mechanical properties but the electrical property is still below aluminum and copper[61]. Geometric differences like defects, chirality, different diameters, and the degree of crystallinity of the tubular structure significantly influence the electronic properties of CNTs. They can be conducting or semi-conducting types based on the type of chirality[64]. It is crucial to realize the selective growth of pure metallic or semiconducting CNTs for effective electronic device applications.

2.2.1 Vertically aligned CNT production by chemical vapor deposition (CVD)

While arc discharge and laser ablation methods can be used to produce CNTs, CVD is the only method to produce spinnable CNTs. Besides, CVD offers the low-temperature operation, low costs and controlled synthesis and it is the most promising method for bulk production[65]. CVD is an efficient method of producing large areas of highly ordered, aligned, and isolated CNTs. Moreover, using CVD, CNTs can be produced on a diverse set of substrates and enable it viable for electronic manufacturing applications. The CVD process used in synthesizing CNTs can be categorized as catalytic chemical vapor deposition (CCVD), plasma-enhanced chemical vapor deposition (PE-CVD), microwave plasma-enhanced chemical vapor deposition (MPECVD) and oxygen-assisted chemical vapor deposition (OCVD). The configuration of the CVD system can be either horizontal or vertical and horizontal furnace configuration is widely used[66]. The floating catalytic synthesis process is popular for producing highly aligned and spinnable CNTs offering different advantages compared to other CVD processes such as continuous process, faster preparation process, and active catalyst[59]. Catalyst plays a crucial role in synthesizing CNTs and

is responsible for breaking bonds and adsorbing carbon at its surface. Then catalyst diffuses carbon through or around an interface to facilitate the reformation of carbon in graphitic planes. The most used catalysts are transition metal iron, nickel and cobalt as well as noncatalytic metals like aluminum, copper is also used[67]. In this CVD synthesis process, the catalyst is heated at a high temperature of 600-1000 °C in a tube furnace where hydrocarbon gas is passed through the tube reactor. The hydrocarbon gas is dissociated and catalyzed. Saturated carbon atoms are precipitated and form tubular carbon in a sp^2 structure[68].

2.2.2 CNT structures

CNTs have a 1D tubular structure with a diameter in nanoscale and length in micrometer and are comprised of sp2-bonded carbon atoms. The structure of CNTs is based on a planar hexagonal lattice of carbon atoms, called graphene, rolled to form seamless tubes and the rolling pattern is known as CNT chirality, as shown in Figure 2.2 (A)[69].

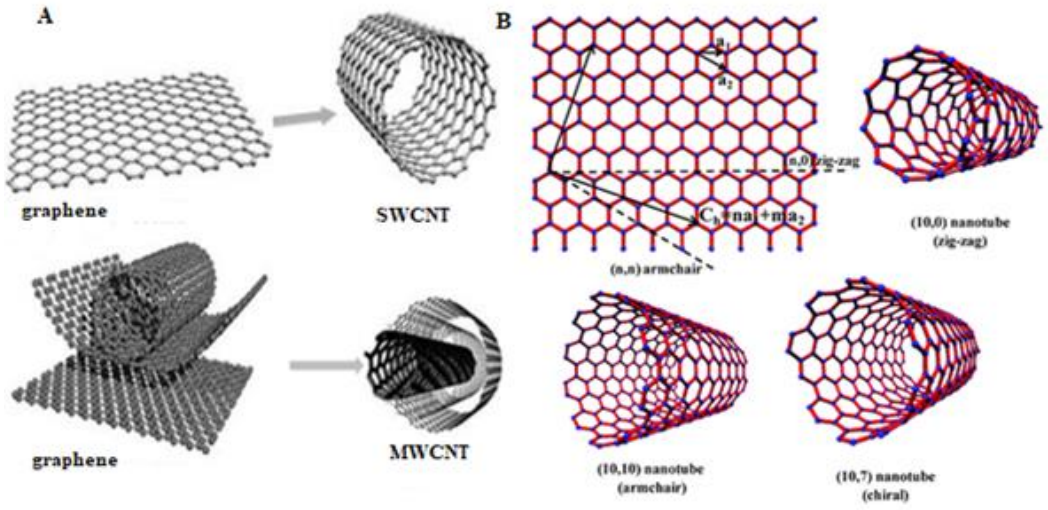

Figure 2. 2 Schematic of CNT formation and different structure

Description: A) CNTs from graphene[69] B) Typical vector representation of the different structures of CNTs[70]

CNTs can be two types, single-wall CNTs (SWCNTs), which consist of a single tube of graphene, and when several numbers of concentric tubes, cylinders insider other cylinders are formed, they are known as multi-wall CNTs (MWCNTs). In MWCNTs, the interlayer spacing of concentric tubes is around 3.4 Angstrom and tube diameter ranges from 0.4 nm to 100 nm from innermost tube to outermost tube. Depending on the orientation of the graphene sheet relative to the tube axis three different structures of SWCNTs are formed[71]. Zig-zag CNT is formed if the hexagonal lattice forms a zig-zag pattern along the circumference of the nanotubes and when the lattice is turned around by 90 degrees about the zig-zag pattern is called armchair CNT and finally any other pattern obtained along the circumference is termed as chiral[61]. These three structures of SWCNTs and the vector representation of planar graphene is illustrated in Figure 2.2 (B)[70].

Chiral vector $\overrightarrow{C_h}$ determines the circumference of SWCNT and is defined by $\overrightarrow{C_h} = m\widehat{a_1} + n\widehat{a_2}$, where m and n are integers and $\widehat{a_1}$ and $\widehat{a_2}$ are unit vectors in the 2D graphene sheet. The values of integers (m, n) and chiral angle θ (angle between the chiral vector and zig-zag direction) determine the structure of SWCNTs. The armchair structure is formed when m = n and θ = 30, zig-zag structure is formed when n or m = 0 and θ = 0. The rest of the structures ($0 < \theta < 30$) are known as chiral or helical nanotubes. Besides, the CNT diameter also depends on the integers (m, n) and is defined by the following equation: $d = \frac{a\sqrt{m^2+mn+n^2}}{\pi}$ where a is the C-C bond length in the graphene sheet and defined by $a = 1.42 \times \sqrt{3} = 0.246$ nm[71]. In metallic conductivity- conduction and valence bands slightly overlap and it is found in armchair CNTs whereas zig-zag and chiral nanotubes may have different widths of bandgaps and show semi-metals to semiconductors properties depending on their diameter and exact chirality[61].

2.2.3 Spinnable CNT arrays

Assembling CNTs in macroscale and realizing the outstanding mechanical properties is very challenging. Buckypaper was the first macroscale CNT structure showing relatively high electrical and thermal conductivity, but the mechanical properties were very poor. Therefore, a lot of effort has been made to assemble CNTs with superior mechanical properties and the most suitable structure is CNT fibers/yarns[72]. The first CNT yarn was spun from vertically aligned CNT arrays/forests by Jiang et al. in 2002[73]. The yarn is like thin ribbons with a diameter of several hundred nanometers and the fibers were arranged parallel to the yarn axis. The process of drawing a thin ribbon out of a vertically aligned CNTs array is shown in Figure 2.3[74]. However, not all CNT arrays are spinnable and the morphology of CNT arrays dictates the spinnability of CNTs[75]. The yarns spun by the Jiang group in 2002 were loosely packed and the load transfer capacity of the yarn was limited. To improve the mechanical performance of the spun CNT yarn, Zhang et al. proposed a modified method of spinning CNTs from the array[76]. They introduced twists during the drawing process of MWCNTs from the array which increased the packing density of the yarn. Twist-spun CNT yarn from long CNT arrays gained tremendous attention to producing continuous CNT yarn. CNT yarn produced from longer CNT arrays has a higher surface area for better load transfer which is essential to fabricate high-strength structural materials[77].

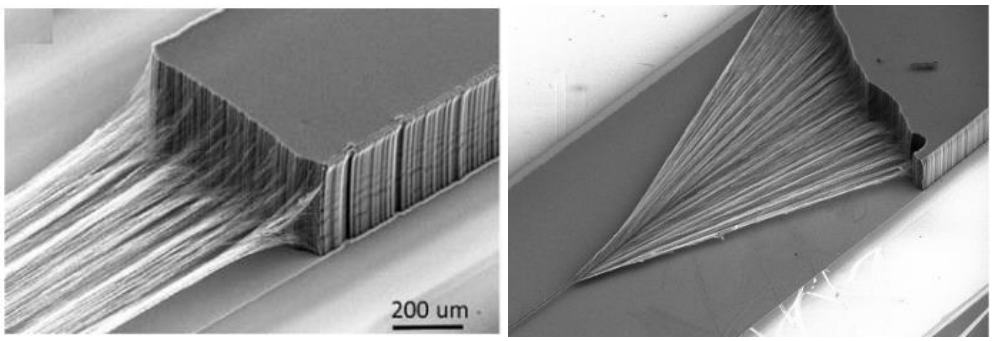

Figure 2. 3 SEM image of Vertically aligned CNT

Description: Ribbon pulled from the array (left)[74] and twist induced CNT yarn formation (right)[76]

2.2.4 Macroscopic CNT assemblies made from spinnable CNT arrays

2.2.4.1 Thin films and ribbons

Thin films and ribbons are the two-dimensional macroscopic assembly of CNT arrays where aligned and CNTs bundle with the neighboring CNTs along their axial direction[78]. The CNT films/ribbons are ultrathin, transparent and highly conductive making them suitable as a substrate for electrical device fabrication[79]. CNT films can be fabricated by different methods such as a dry drawing of vertically aligned CNT arrays, drying dispersion of CNTs, or direct drawing from the CVD reactor. This 2D CNTs structure can be used as catalyst supports, molecular sieves, filter, conductors, capacitors, electromagnetic shields, artificial tissues etc[80].

Fabrication of CNT thin films by drawing is very simple and advantageous for bulk scale production. The thickness and geometry of CNT film can be easily controlled for different application requirements. The as drawn CNT film is extremely light and thickness is tens of nanometers, depending on the height of super aligned CNT arrays it is being drawn. This highly aligned CNT film exhibits a polarization effect in both emitting and absorbing photons which is essential for optical devices[81]. By changing the drawing direction and overlapping of multiple

films, striped CNT films and CNT cross-stack films can be produced. The thin-film of CNT produced from the highly aligned vertical array can be used to produce a stretchable conductor. Due to their alignment in axial direction and capability of sliding against each other, they remain continuous under uniaxial strains. A CNT ribbon is drawn out of aligned CNT arrays and encapsulated in poly(dimethylsiloxane) (PDMS) showed no change in electrical conductivity when strained up to 100%[78].

2.2.4.2 Fibers and yarns

Super aligned CNT sheets can be shrunk into yarn by mechanical and solvent densification. However, a combination of twisting and densification produces yarn with superior mechanical properties[72,82,83]. The first macroscopic CNT yarn was produced by spinning CNT dispersion into a polyvinyl alcohol bath. Inspired by this approach, SWCNTs composite yarn with very high strength was produced by modification of the wet spinning process[72]. The wet spinning process requires low-defect CNTs to form a liquid crystalline phase which is very difficult to obtain by CVD process. In wet spinning, CNTs are dispersed in superacid and highly aligned and dense CNT fiber is produced due to the shear force generated during the spinning process. This process requires time-consuming liquid crystalline phase formation of CNT and purification steps to remove amorphous carbon and residual catalysts[84]. Alternatively, solid-state spinning is a very simple and one-step process, but the produced CNT yarn is highly porous compared to the wet spun CNT yarn.

2.3 Carbon Nanotube Yarn

Recently CNT yarn emerged as the most promising material for yarn-based wearable electronic systems due to their excellent electrical, chemical and mechanical properties. The nanoscale CNT fiber (diameter ~ 10 μm) shows remarkable tensile strength up to 3 GPa, electrical conductivity 4 x 10^4 to 1 x10^5 S/m and thermal conductivity of around 100 W / (mK)[85]. However,

this small diameter CNT yarn is difficult to incorporate in textile processing and it is of the utmost importance to multiply nanoscale CNT fibers into a large diameter CNT yarn (> 100 μm), which is very common in textile processing. Different methods such as i) extrusion from CNT/polymer solution (solution spinning) ii) spinning a yarn directly from an aerogel of CNTs formed in the CVD reactor (direct spinning) and iii) spinning yarn from a vertically aligned MWCNTs array (dry/array spinning) has been developed to assemble the small diameter CNT fiber into a macroscale yarn[65].

2.3.1 Direct spinning of CNT yarns

Direct spinning or solid-state spinning is the predominant method of CNT yarn production, typically accomplished by drawing the CNT either directly from the CVD reactor or vertically aligned arrays. This technique is widely adopted because of the simplicity of the process and direct fabrication method[86]. The first direct spinning of SWCNT yarns from a floating catalyst CVD method was reported by Zhu et al[87] though the product was an isolated strand. The as-spun SWCNT strands were 20 cm long with a diameter of 0.3 mm. SWCNT bundles peeled off from the strands with diameter from 5-20 μm showed strength and stiffness of 1.0 GPA and 100 GPa respectively. However, the pioneering work on continuous CNT yarn spinning from CVD was reported two years later in 2004 by Li et al[88]. Ethanol was used as a carbon source with added ferrocene and thiophene and hydrogen as a carrier gas. The CNT yarn was mechanically drawn directly from the reactor furnace. The direct spinning of CNT yarn is shown in Figure 2.4[89]. CNT yarns spun directly and continuously from the CVD reactor show high strength and stiffness which is comparable to those of commercial high-strength fibers. Different process parameters like carbon source, catalyst concentration, winding rate etc. directly influence the mechanical properties of as-spun CNT yarns. However, iron content has a significant influence on the CNT yarn structure and properties compared to a carbon source. Likewise, the iron content, winding

rate greatly enhance the fiber strength and stiffness by increasing the CNT alignment and density[75]. The yarn-like behavior of CNT was extensively studied by a research group in different conditions such as a knot, cut and bending[90]. The direct spun CNT yarn from aerogel is highly flexible and can be bent to extreme radii without causing any damage to the yarn, unlike conventional carbon fibers. When the CNT yarn is cut using a razor blade, a CNT fiber stretches across the cutting edge of the blade and spreads laterally. Additionally, the yarn was tested for knot formation and it was found that the knot efficiency is as high as 100% and no degradation in strength was found. Continuous multilayered CNT yarns were produced by Zhong et al using acetone and ethanol as the carbon source[80]. The formation of multilayered structure is attributed to the higher concentration of CNTs in the gas flow because of double carbon source gas.

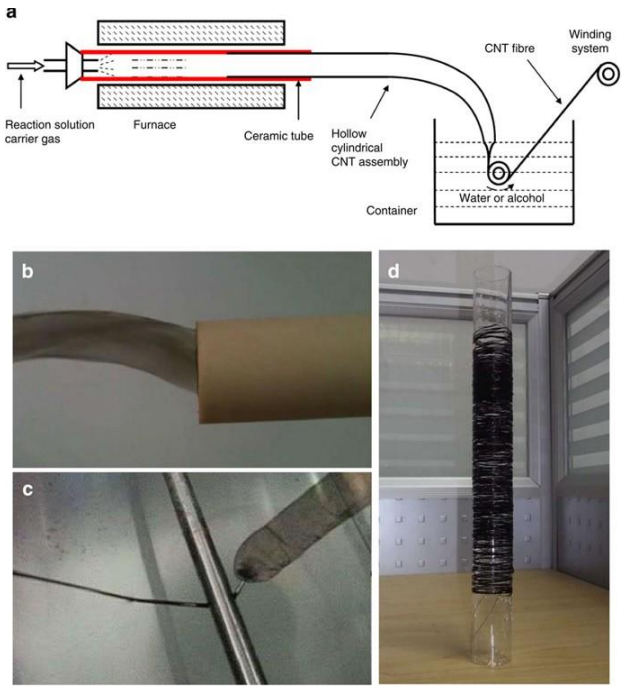

Figure 2. 4 Direct spinning of CNT yarn

Description: a) schematic of direct spinning system b) CNT socks blown out from reactor c) liquid densification of the cylindrical CNT assembly d) spool of CNT yarn wound after densification process[89]

The mechanical performance of CNT yarns greatly depends on the characteristics of individual CNT fibers from which the CNT yarns are produced. Nanotubes with a longer length and a low number of defects can produce high strength yarns. Compared to MWCNTs, SWCNTs or double-walled CNTs have lower defects and tend to align in parallel into bundles. The intertube junction between adjacent nanotubes also contributes to producing high strength CNT yarn. It is easier to maximize the intertube contact area in thin-walled carbon nanotubes than MWCNTs since they tend to flatten[91]. In a recent study, a unique die drawing method along with adhesion agent polyethyleneimine (PEI) was used to produce mechanically robust CNT yarn[85]. The pristine CNT yarn with a diameter of 51 µm showed a tensile strength of 387 MPa and specific strength of 0.50 N/tex. Although the tensile strength of the CNT yarn increased for multiplied yarn, toughness decreases with the higher number of plies. CNT yarn with 6 plies was found to be optimum for higher strength and toughness. CNT yarns multiplied by PEI showed a remarkable improvement of tensile strength. The maximum tensile load for PEI assisted multiplied CNT yarn increased to 5.93 N from 0.79 N for the pristine CNT yarn.

2.3.2 Solution spinning of CNT yarns

Solution spinning/wet spinning is well known for producing industrial fibers. In the solution spinning process, the polymer solution is extruded through a spinneret into a second solution called coagulation bath where the solvent is removed by dissolution from the polymer. This wet spinning process was first adopted by Vigolo et al. in 2000 to produce SWCNT yarns and the process is shown in Figure 2.5[75,92]. The diameter of CNT yarns could be up to 100 micrometers depending on the various processing conditions. This wet spun CNT yarn is very flexible unlike carbon fiber and the tensile strength and modulus were found to be 300 MPa and 40 GPa, respectively. However, this wet spinning method is very slow, and the produced CNT yarn mechanical performance was relatively low. Therefore, Dalton et al. modified and improved

this method to enhance the mechanical performance and produce longer CNT yarn. This method is two steps spinning, unlike Vigolo's method where a reel of nanotube gel fiber was produced and then converted to solid nanotube yarn by a continuous process. The draw rate was 70 times higher than the original method and SWCNT yarn produced by this modified method showed a tensile strength of 1.8 GPa and modulus of 80 GPa[93,94]. However, the residual polymers on the CNT yarn negatively impact the electrical and thermal conductivity. Therefore, a neat CNT yarn was spun using sulfuric acid dispersion of SWCNT[95]. The liquid crystal phase of the solution was spun, and a long pure CNT yarn was obtained. The neat CNT yarn has a lower tensile strength (116 MPa), but higher Young's modulus (120 GPa) compared to the polymer-based spinning of CNT. However, this yarn had higher electrical and thermal conductivity since it does not contain any polymer. Though the modulus and electrical conductivity of acid spun yarn are higher than any other spinning process, the tensile strength is still relatively low[96].

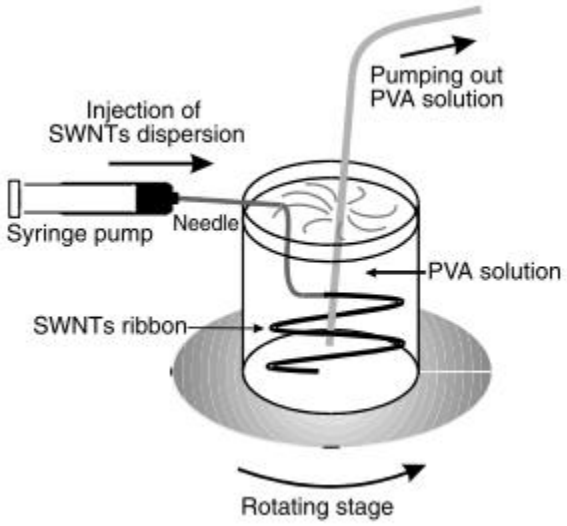

Figure 2. 5 Schematic of wet spinning process of CNT Yarn

Description: SWCNTS are dissolved and extruded into PVA solution to make the yarn[92]

Zhang et al. produced pure MWCNT fibers by dispersing in ethylene glycol unlike superacid and extruded into a diethyl ether bath[97]. After the extrusion, the CNT yarn is heated at 280°C to remove residual ethylene glycol. Though the fiber showed higher electrical conductivity of PVA assisted wet spun CNT, the mechanical properties of this yarn were lower. CNTs length is a major challenge for the successful adoption of the wet spinning process to produce CNT yarn. Behabtu et al. used a longer length of 5 μm CNTs and wet spun them into continuous CNT yarn[98]. This CNT yarn showed an average tensile strength of 1 GPa and modulus of 120 GPa respectively. The wet spun CNT yarn also showed good electrical and thermal conductivity. In a recent study, the CNT length and yarn density dependences of the electrical and mechanical properties of wet spun CNT yarn was reported[99]. The electrical conductivity of the CNT yarn showed a linear correlation with the density. Mechanical properties such as strength, modulus and toughness were also improved with increasing density as well as effective CNTs length. Increasing the effective CNT length improves the CNT junctions per unit fiber length resulting in higher electrical conductivity.

2.3.3 Dry spinning of CNT yarns

Dry/array spinning resembles the characteristics of both traditional staples spun yarn and synthetic filament spinning. The first spinning of CNT yarn was reported by Jiang et al in 2002 and they spun a 30 cm long CNT yarn from a 100 μm tall CNT array[100]. The yarn produced was loosely packed and had poor mechanical properties. Afterward, extensive research has been carried out to produce continuous CNT yarn with superior mechanical properties. Twisting, densification and polymer infiltration are the methods used in improving the mechanical performance of the dry spun CNT yarn.

Zhang et al modified the spinning method and inserted twist during the drawing of the MWCNTs from a nanotube array[76]. The catalytic CVD method was used to produce vertically

aligned MWCNTs with an array height of 300 µm and the CNT yarn drawing process is shown in Figure 2.6. The diameter of the yarn was around 1 – 10 µm and tensile strength range from 150 – 300 MPa. The electrical conductivity was found to be ~ 300 S/cm. However, the yarn diameter depends on the width of the CNT forest sidewall and the forest sidewall was 150 µm to ~3 mm. The drawing process was manual but indicated the possibility of automation. This manual drawing process restricted the yarn length by the arm length of the person drawing the yarn. The produced was single-ply and two-ply yarns were obtained by over twisting a single yarn followed by relaxation.

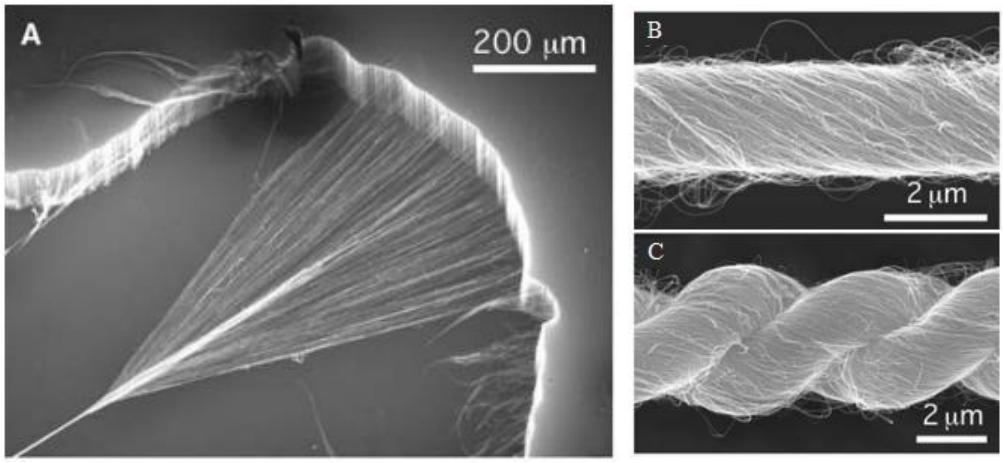

Figure 2. 6 SEM image of the dry spinning process

Description: A) CNT yarn drawing process from VACNT array B) Single yarn C) two-ply yarn[76]

Different modifications have been made to improve the continuous spinning and yarn properties. Simultaneous automatic drawing and twisting systems have been developed to produce continuous CNT yarn[101,102]. However, the spinning rate was very slow and ranges from 0.003 and 0.33 m/s producing a small amount of CNT yarn[103,104]. Alvarez et al. modified the dry spinning process to enhance the draw rate comparable to the natural fiber spinning process by using CNT

array detached from the substrate[105]. This method showed that the CNT yarn can be drawn at ~ 16 m/s rate. In addition to the modification of the spinning system, higher length CNT arrays have been used to produce yarn with superior mechanical properties. In a study, CNT yarn spun from 1 mm high CNT arrays showed a tensile strength of 3.3 GPa[101]. However, the twist might have a negative impact on the strength of CNT yarn as demonstrated by the researcher[74]. This is maybe due to the misalignment of fibers along the yarn axis for over twisting. At a higher twisting angle, the inter-tube spaces reduce and increase the contact junction but lower the fiber strength.

CNT yarn spun from the array has a relatively low density which can be increased by inserting twist. However, the compaction induced by the twist is not uniform from the surface of the yarn to the core. Because the twisting force imparted on the surface transferred to the core making it difficult to obtain a uniform compact across the yarn. Therefore, the liquid shrinking process is used to increase the density of CNT yarn as well as its mechanical properties. Though CNT yarns are hydrophobic they can be wetted by a common organic solvent. The surface tension is considered the prime factor for the shrinking effect of organic solvents for the untwisted yarn. Liu et al. used various solvents such as water, ethanol and acetone to shrink the twisted CNT yarn[102]. Despite high surface tension compared to ethanol and acetone, water does not wet the CNTs and thus, could hardly infiltrate inside the yarn during the short time when the yarn is passed through water. On the other hand, organic solvent wet the CNTs and easily infiltrated into yarn and fill the interspaces of CNT fibers as the CNT yarn passes through them. The shrinking takes place at the interface for the twisted yarn. However, drying the yarn showed a further decrease in yarn diameter suggesting a second shrinkage caused by the evaporation of organic solvents. Therefore, the mechanism of shrinking by water and organic solvent differs. Furthermore, having similar surface tension, acetone diffuses quickly in CNT yarn than ethanol and thus, has a better

wettability with CNTs. Therefore, CNT yarn shrunk by acetone showed higher tensile strength compared to other solvent densification. The twisted yarn showed a tensile strength of 1.10 GPa after shrinking by acetone whereas the tensile strength before shrinking was found to be 0.63 GPa[102].

Polymer infiltration can also enhance the density and mechanical performance of CNT yarn. PVA is a flexible polymer and has very good adhesive characteristics. A simple cost-effective was developed to produce CNT/PVA composite fiber with superior performance[106]. A twisted dry spun MWCNT yarn was passed through PVA/DMSO (dimethyl sulfoxide) solution and the interstice of the fibers in CNT yarn was infiltrated by PVA. The CNT/PVA composite yarn was obtained after vaporizing DMSO upon heating. The composite yarn showed remarkable improvement in the tensile strength of 2.0 GPa while the yarn was flexible. In another study, PEI was used with CNT to enhance the strength of CNT yarn[107]. PEI infiltrated CNT yarn was cured by thermal and metal oxidation and showed tensile strength greater than 2.0 GPa which was 470% higher than pure CNT yarn.

2.3.4 Structure-properties relationships of CNT yarns

Nowadays, the term ‘CNT fiber’ and ‘CNT yarn’ are arbitrarily used. The term ‘CNT yarn’ can be related to its manufacturing from vertically aligned CNT arrays, which is similar to the production method of traditional textile yarn by spinning with twist[74]. To analyze the structure-property relationship of CNT yarns, they are often compared with traditional textile yarns. The number of fibers in the yarn cross-section is the major difference between CNT yarns and textile yarns. The number of CNTs in the yarn cross is in the order of 10^5 -10^6, which is 1000-10000 times higher than the number of fibers in a textile yarn[65]. The interconnection between fibers in conventional textile yarns is due to the fiber-fiber friction which arises from the pressure between fibers. The failure mechanism of textile yarn is dominated by fiber slippage for low twist level and

fiber breakage for high twist level. A similar twist-strength relationship is found in twisted CNT yarn but the interaction between CNT-CNT (fiber-fiber) differs from the conventional textile yarn. CNTs are found as bundles in the yarns due to the van der Waals attraction which is responsible for transferring load between the nanotubes in CNT yarns. However, CNT yarns can also be produced without a twist. In this case, liquid densification and mechanical rubbing are used [74]. The CNT sheet before spinning is aerogel with a porosity of 99.97%. Though the theoretical minimum porosity of CNT yarn is 23.8%, in practice, the porosity of twist densified CNT yarn is as low as 40%. The maximum packing density of a twisted yarn is found in the center compared to the edge of the yarn as shown in Figure 2.7[82]. Initially, the CNT yarn was monolithic in structure, but the researcher modified the spinning method to produce hollow or monolithic CNT yarn with compacted or detached CNT monolayers[80].

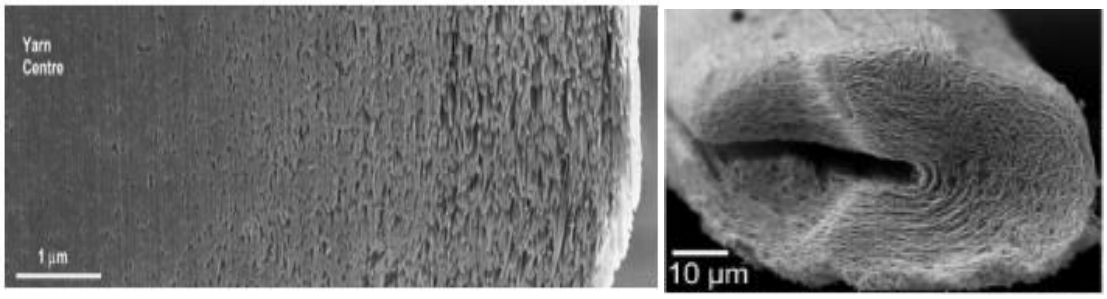

Figure 2. 7 SEM image of different CNT structures

Description: A slice milled through a highly twisted CNT yarn (35,000 turns/m), revealing a densely packed core and a porous sheath (left)[82] and a CNT multilayer yarn (right)[80]

2.3.5 Factors needed for dry spinning CNT yarns

As previously mentioned, not all CNT arrays are spinnable. In the pioneering work, Zhang et al. claimed that CNT yarn can be produced from the CNT array due to the disordered region at the top and bottom of CNT array[108]. Entanglement is the key factor of dry spinning which allows

the arrays of parallel fibers to unfold continuously into a CNTs mat[109]. The entangled network of CNTs is considered as entanglement junctions (Figure 2.8b) and has a significant influence on yarn properties. It was claimed that CNT fibers are moveable provided that the constraint occurred due to the surrounding CNTs changes due to their motion and will disappear upon shifting of CNTs. This phenomenon is modeled as the dual slip-link theory. As seen in Figure 2.8b, the entanglement junction is represented by a slip link through which the CNT fiber chain can move easily and are linked together by slip links.

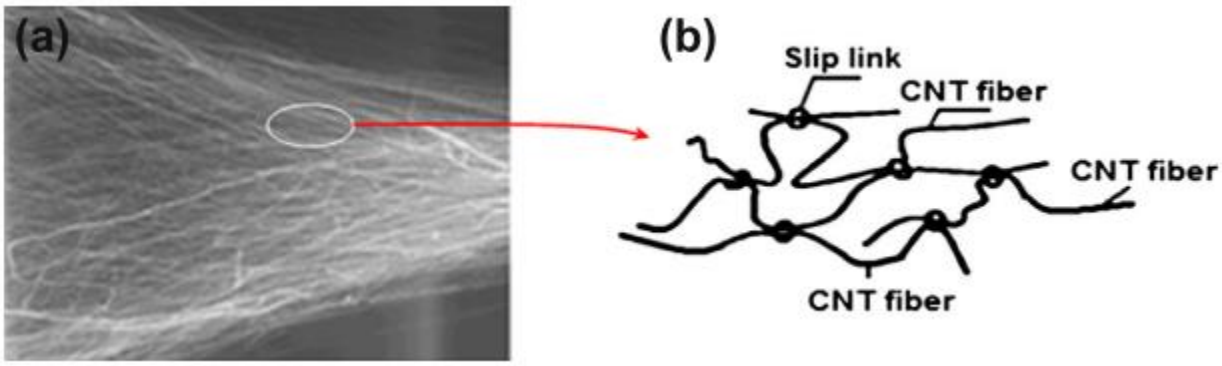

Figure 2. 8 Model of CNT web formation

Description: (a) web formation from a CNT forest and (b) schematic of CNT web using the dual slip-link model[109]

Another group disagreed with this mechanism of CNT yarn formation by comparing the normal array which has more disordered and entanglement than highly aligned arrays[110]. They showed that their super-aligned array has no entanglement and is highly ordered. Therefore, they proposed that van der Waals attraction causes the CNTs to join end to end to form a continuous CNT yarn as presented in Figure 2.9.

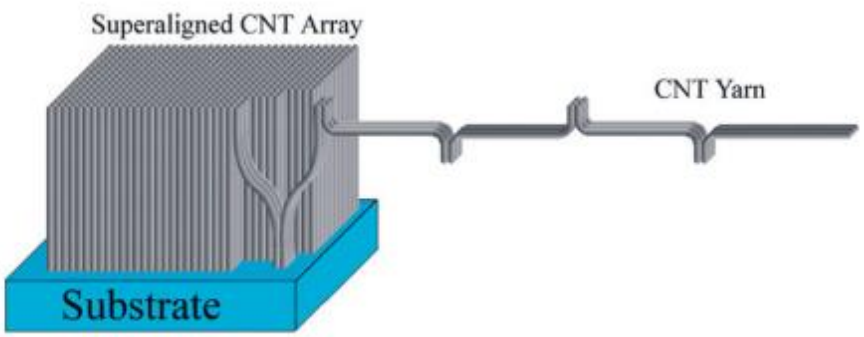

Figure 2. 9 Mechanism of continuous CNT yarn from super-aligned CNTs array

Description: CNTs are attached to each other as a hook when pulling from the array[110]

Twist: The drawn web of CNT from the array is extremely porous and has a low mechanical strength due to the weak inter-tube connection. Researchers found that inserting twist can densify the web increasing the strong connection between CNT junctions. Therefore, twists played a critical role in the early stage of dry spinning CNT yarn and have been extensively studied by researcher[111,112]. Twist can also introduce new properties such as torsional and tensile actuation in addition to improving the strength of the CNT yarn[113]. These twist-induced properties were used to harvest energy by electrochemically converting tensile or torsional mechanical energy into electrical energy from CNT yarn[114]. However, twisted single ply yarn might untwist and snarl if not torsionally tethered and may be a major problem during textile processing. Twist affects the porosity which in turn affects the packing density. Miao demonstrated that with the increase of twist, the electrical conductivity of CNT yarn increases[111]. In addition to increasing strength and electrical conductivity, twist also provides aesthetic values, especially for textile use. The highly twisted yarn has good abrasion resistance and prevents fabric pilling[115].

Alignment: Highly aligned CNT yarns are the prerequisite to maximizing the potential of macro-assembled CNT. Figure 2.10 shows the wavy configuration, misalignment and bundling of

CNTs in the forest and the drawn web[109]. Crimp is present in the original CNTs forest (Figure 2.10A) but most of them are not entangled. When the forest is drawn, they turned 90 degrees from the vertical direction in the forest to the horizontal direction on the web (Figure 2.10B). The web formation by the drawing of vertically aligned array causes entanglement by the formation of loops, hooks, reversal and crossing each other. However, the drawing process removes some crimp from the CNTs present in the original forests. The CNT web is not stretchable like conventional textile web due to the strong van der Waals attraction among CNTs and breaks sharply under tensile load. Thus, the waviness present in the CNT yarn and the straight yarn take up the applied load. Therefore, CNT yarn shows void and porosity due to the presence of waviness and entanglement.

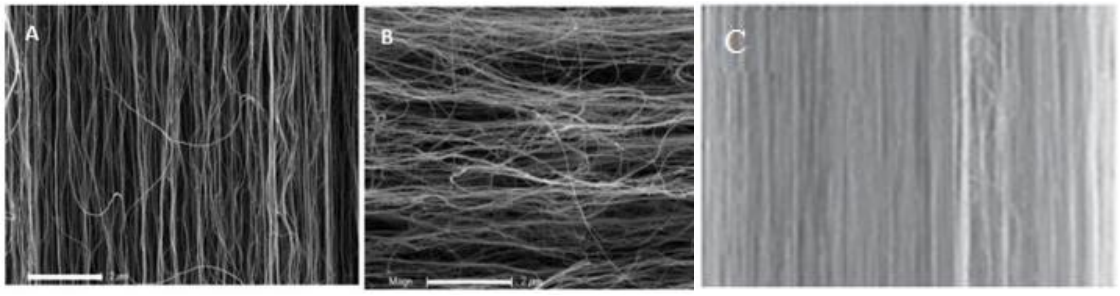

Figure 2. 10 Tortuosity and misalignment of CNTs in the forest and drawn web.

Description: (A) SEM image of CNTs in a vertically aligned CNT array (forest) and (B) SEM image of CNTs in a drawn web[74] (C) SEM image of tensioned induced aligned CNT[109]

Misaligned CNT fibers (web) produce CNT yarn with low packing density. The mechanical tensioning system was developed by Tran[109] to align the CNT fibers along the yarn axis. When the yarn passes through the tensioning system, the CNT fibers align along the yarn axis and can be further enhanced by the capstan rod system (Figure 2.10C). The increased tension

extends and aligns the fibers due to the slip links present in the CNTs. The tensioning system also condenses the fibers which also contributes to the improvement of yarn properties.

Packing density: The packing of CNT yarns is directly related to the van der Waals micro-interaction in CNT-CNT fiber and macro-friction between CNT fibers and provide the required inter-bundle lateral cohesion of the yarn. In CNT yarn, stress transfer in shear modes under tensile loading and better packing results in excellent stress transfer between neighboring CNT fibers[109]. Higher packing ensures maximum contact area which is crucial for higher tensile strength. A maximum packing density can be obtained when all nanotubes are perfectly straight and aligned in a direction. The packing density of the twisted yarn and CNT bundles is demonstrated in Figure 2.11[74]. CNT web drawn from CNT array have a very high porosity of 99.97%. However, the packing density increases with any of the three densification methods discussed earlier. The packing fraction of a highly twisted yarn can be as high as 0.6 which is similar to the fiber packing fraction of a highly densified textile yarn.

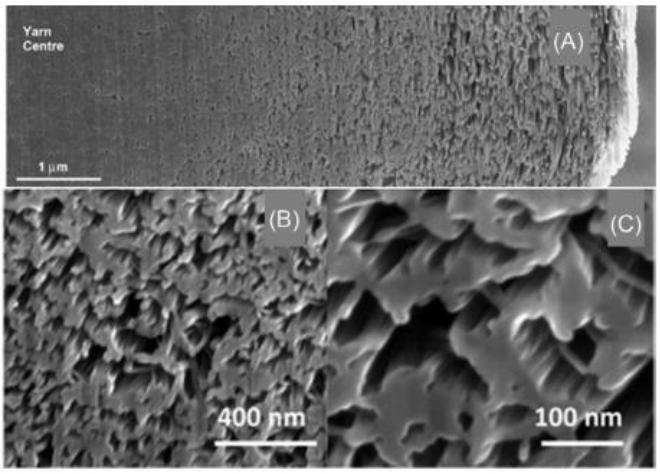

Figure 2. 11 Packing density and pore distribution in twisted CNT yarns and bundles

Description: (A) SEM image of CNT yarn cross-section, showing radial density distribution. (B, C) SEM images showing CNT bundles and pores between CNT bundles[74]

2.3.6 Modifications of CNTs yarns

CNT yarn can be modified by introducing different guest materials for various applications. Additives introduced in the CNT yarn can enhance the performance and multifunctionality of the produced composite yarn. Additionally, new properties can be developed due to the synergistic effect of the CNT and guest materials which is otherwise not available in the individual materials[116]. However, using nanoparticle additives imposes other challenges such as low loading of particles, poor adhesion and durability, decrease in accessible surface area due to processing etc. The spinning of pure nanoparticles is very difficult and most of the time spun together with other polymers. Strong and multifunctional yarn spun from composite yarns could be seamlessly integrated into electronic textiles and electrodes produced from these yarns are flexible and durable. The opportunities of hierarchically engineering the porosity by textile technologies are advantageous over multifunctional films and bulk composites[117]. Different methods like solution mixing, melt mixing, in-situ polymerization, coating, deposition techniques and printing can be used to modify the CNT yarn. Highly conductive metal nanoparticles are used to improve the electrical and mechanical properties of CNT based electrode materials. As already discussed, macroscopically assembled CNT yarns show relatively low conductivity than individual CNTs. The conductivity of CNT yarn could be enhanced by doping, acid treatment and high temperature annealing[118]. Different catalytic nanoparticles like Pt, Pd and Ru are deposited on CNTs for applications in fuel cell electrodes, Li-ion batteries and supercapacitors. CNT decorated by silver nanoparticles can improve the antibacterial activity of textiles fibers[119]. Yarn produced from CNTs has very good cyclic stability, but their low capacitance and energy density restrict them to be used in energy storage applications[120]. Therefore, pseudocapacitance materials such as metal oxide and carbide, conducting materials etc. are used to modify the CNT yarns[121]. Elastomeric polymers are used with CNTs to produce highly efficient and stretchable heaters due to their lightweight, low-

temperature processability, chemical durability and excellent stretchability compared to the metal-based heater. Sun et al. fabricated a stretchable, low voltage drive and thermally stable heater by integrating thermoplastic polyurethane with segregated carbon nanotube networks[122]. The heater showed a high electrical conductivity of 142.6 S/m and could produce a steady-state maximum temperature of 65°C at 6V.

2.4 Textile processing and application of CNT yarns

2.4.1 Processing of CNT yarn by textile technologies

Textile technologies are an outstanding method of producing 2D structures and centuries of industrial development has perfected the process. High-quality and extremely cost-effective products can be produced with great repeatability. The spinning process can assemble short fibers into continuous yarns with a high degree of flexibility and stretchability. Subsequently, this yarn is processed by two prominent methods - knitting and weaving to produce a two-dimensional planar fabric. While the weaving process requires two different yarns interlaced at 90 degrees, knitting can be performed using a single yarn by creating an interloop. The techniques are highly advantageous because of scalable production, wearability, pliability, high surface area which are also essential requirements for wearable electronics applications[123,124,125]. Initially, wearable electronics included miniaturized components and integrated the components by sewing or adhesive onto the textile. This process is aesthetically undesirable and uncomfortable to wear. The development of conductive polymers as well as yarns saw a huge leap in the design of textile-based wearable electronics[5,126]. Different textile technologies and the related supply chains are illustrated in Figure 2.12[4].

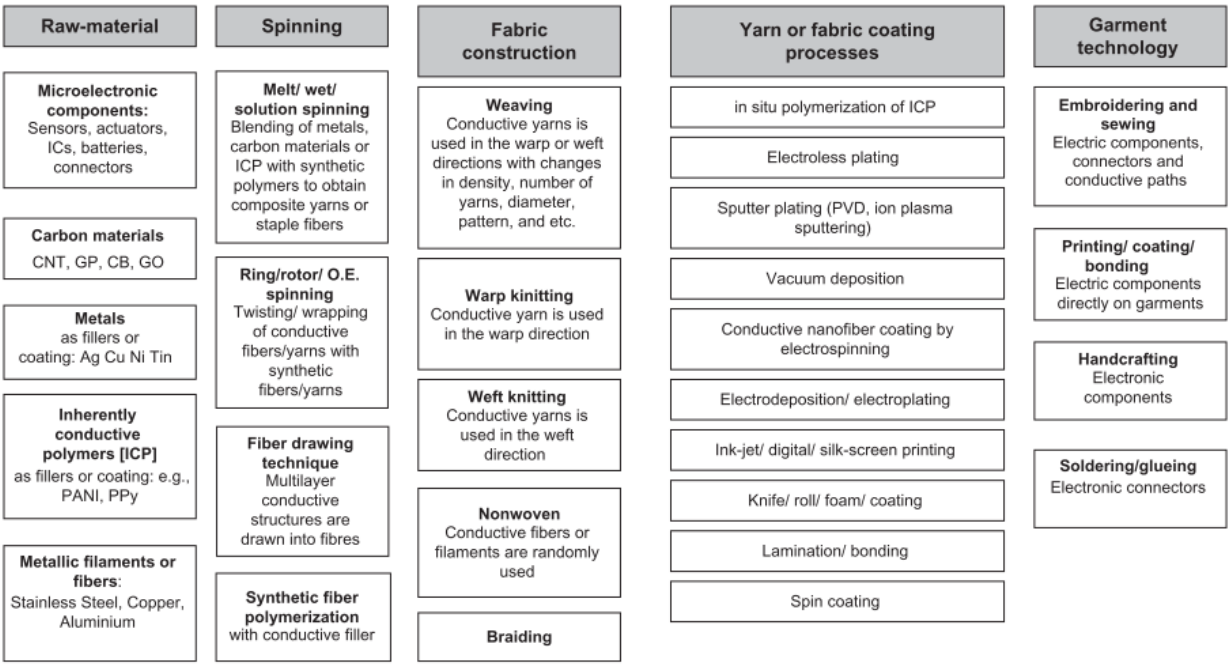

Figure 2. 12 Textile techniques used in producing E-textiles

Description: The process start with raw materials and after processing in different stage final garment is produced[4]

CNT yarn can be processed directly or in combination with other yarn by different textile technologies. A unique method of knitting CNT yarn was reported by Foroughi et al. using spandex as a core yarn[127]. In this process, CNT aerogel was drawn from a spinnable CNT array and wrapped around a spandex yarn and simultaneously feed into a small knitting machine. The CNT loading was adjusted by controlling the CNT to the spandex feed ratio. The knitted fabric showed a very high stretchability and the breaking strain ranges from 600 – 900%. The fabric was electrically conductive and showed a resistance of 3.0 kΩ/m (neglecting contact resistance)[127]. However, the textile processing of pure CNT yarn is challenging due to insufficient mechanical strength and poor abrasion resistance. Luo et al. fabricated a knitted fabric (Figure 2.13) using pure CNT yarn produced by the direct spinning process in lab-scale knitting machine[128]. Multiplied CNT yarn was used for the knitting process from 5 – 10 plies and the diameter of the yarn ranged from 65 μm to

140 µm. The fabric showed electrical conductivity of 110 S/m and thermal conductivity of 0.13 W m^{-1} K^{-1}.

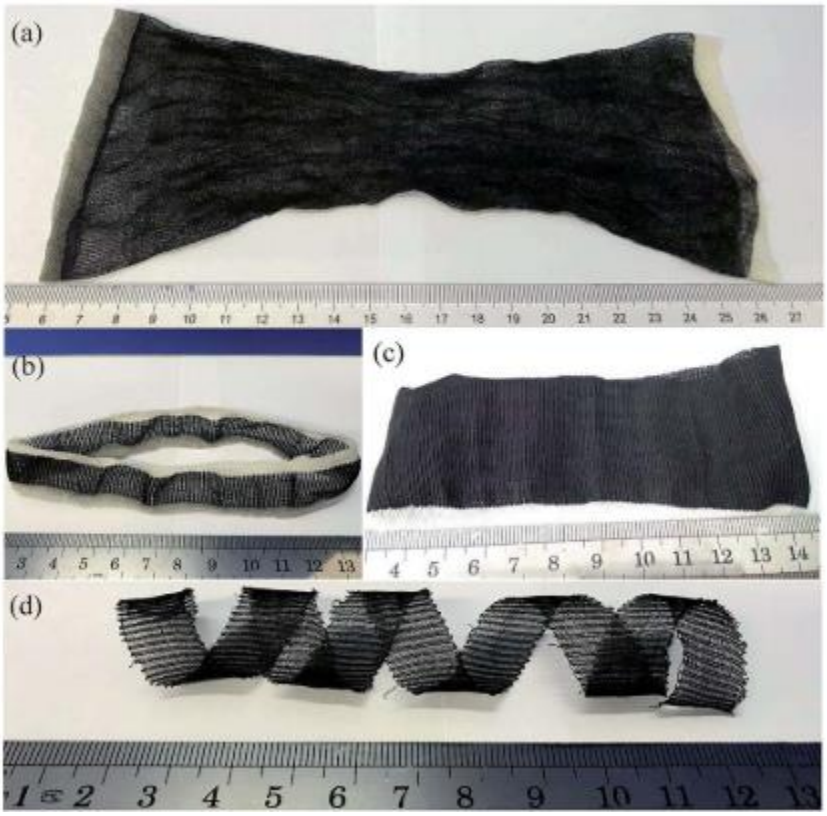

Figure 2. 13 CNT fabric produced by the weft knitting process

Description: a) Fabric produced from 10 ply yarns at 2000 twist level b-c) fabric produced from 5 ply yarns at 2000 twist level d) fabric produced from 5 ply yarns at twist level 2500[128]

A heat-generating textile was developed by weaving CNT yarn with cotton yarn (ratio of 1/2) as weft and copper wire with cotton as warp yarn[129]. Cotton yarn was used as a substrate material for weaving. The fabric showed a rapid response in producing heat when a voltage was applied.

2.4.2 Applications of CNT yarn and their assemblies

2.4.2.1 Strain sensor for wearable body motion monitoring

Wearable devices can be integrated into textiles or directly worn on the human skin for monitoring biophysical signals and motions. Mechanical flexibility is very important to reduce discomfort. Both the structure and materials for wearable electronic devices should be soft and mechanically robust enough to bend, stretch, press and twist in response to motions of the wearer to comply with the curvature, bending and rotational motions of human body[130]. Strain sensing is one of the major applications of wearable sensing devices that measure strain by converting physical deformation into electrical signals. Different type of flexible strain sensors has been reported such as fiber Bragg grating, Raman shift, liquid metal, triboelectricity and piezoelectricity using various materials. Considering the complexity of fabrication, performance and ease of applications, capacitive and resistive type strain sensors are more practical and widely used[130,131]. The conventional metal and semiconductor-based strain sensors cannot meet the requirements of stretchability due to their rigidity and poor stretchability. In contrast, textile-based strain sensors have exceptional wearability, conformability, comfort and washability making them the most promising structures for wearable monitoring purposes[132]. Strain sensors are used in body movement measurement, medical monitoring, sports rehabilitation, human-machine interface, injury prevention, and personal entertainment[133,134]. Textile strain sensors are produced in fiber, yarns and fabric levels using different materials such as conductive polymers, carbon materials, metal nanoparticles/nanowires etc[132]. The coating of textiles by conductive materials is a popular method due to their simple and scalable fabrication process. The coated materials mostly reside on the surface of the textile materials and easily fall off after long-term usage due to the frequent stretching-releasing, bending and twisting, washing etc. This type of strain sensor performs poorly under large mechanical deformations[135]. On the other hand, yarn-based strain sensors have

different advantages such as i) easy to integrate or convert into a textile structure by weaving, knitting, or braiding to provide a variety of sensing performance ii) straight forward readout of strain sensor iii) a high degree of design freedom[131]. However, recently carbon materials, especially CNTs are widely used for flexible strain sensors due to their excellent electrical and mechanical properties. CNTs have a high aspect ratio that enables them to entangle to form a conductive network and the network deforms under stretching and reconstructs when stretch is released showing a measurable electrical resistance change[136]. CNTs exhibit a strong dependence of electrical resistance on the mechanical strain known as piezoresistivity due to the changes in bandgap energy under tensile strain[137]. He et al. fabricated a highly sensitive wearable strain sensor using MWCNT/TPU by wet spinning process[138]. The MWCNT/TPU fiber showed very high sensitivity with a gauge factor of ~2800 in the strain range of 5 – 100%. The yarn was further integrated into a textile fabric by sewing to monitor different human motions. In another study SWCNT thin film was utilized to produce a highly durable and stretchable strain sensor with a fast response rate as shown in Figure 2.14[139]. The sensor could withstand 280% strain and was stable for 1000 cycles at 150% strain. The strain sensor was further assembled into stockings, bandages and gloves to detect different types of human movement including movement, typing, breathing and speech.

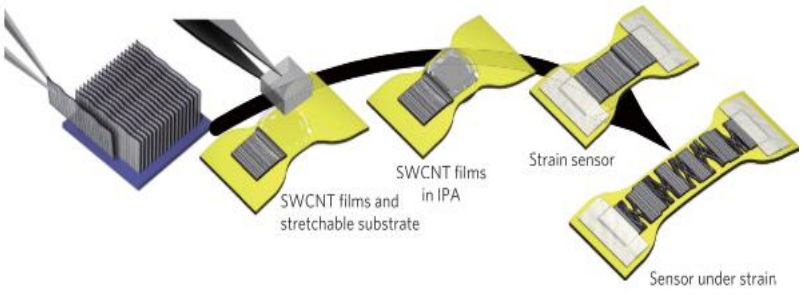

Figure 2. 14 Fabrication of highly durable and stretchable SWCNT strain sensor

Description: CNT were placed on a stretchable substrate[139]

2.4.2.2 Heat generating garments

Heat generation by electrically conductive textiles also known as Ohmic heating/Joule heating/resistive heating is based on the conversion of electrical current into heat. Due to its straight-forward process of producing heat using only electrical power, an electrical heater is used in different applications like de-icing systems, vehicle window defrosters, thermotherapy, joint pain relief, athletic rehabilitation etc[140,141]. Under the applied voltage, inelastic collisions between accelerated electrons and phonons occur and heat is generated. Copper wires are exclusively used for heating applications due to their low cost and abundance. However, copper wires are heavy, inflexible and difficult to cut, sew and textile processes to produce fashionable heated garments[141,142]. A lot of heaters have been developed, but the demand for wearable and skin-mountable heaters are increasing for personal heating systems and healthcare management applications. Furthermore, to broadly adopt wearable devices, it is essential to address different issues such as comfort, aesthetic, haptic perception and weight[141,143]. Therefore, different materials have been explored to replace copper wires to produce heaters for wearable applications. Nanocarbon materials, conductive nanowires/meshes, nanoparticles and conductive polymers have been extensively used as active materials for flexible and skin-mountable heaters. Flexible heaters produced using these materials can generate high temperatures, fast thermal response and uniform heating distribution. However, a high driving voltage to produce targeted temperature, low thermal stability and durability restricts their wearable applications[144,145]. CNTs emerged as promising material over other carbon materials due to their excellent electrical and thermal behavior. Moreover, heating for wearable electronic applications requires flexibility and robustness and stable performance during repeated bending and twisting[140]. Excellent mechanical characteristics, pliability, and flexibility of CNT yarns make them an ideal candidate for wearable electronic heating applications. Liu et al. designed a hierarchically helical structure of aligned CNT

yarn with high mechanical and thermal properties[146]. The hierarchical design provides the CNT yarn with high stretchability and good thermal insulation properties. When the CNT yarn was woven into a textile, it produced a soft and tough fabric with an ultrafast thermal response at low operation voltage. In another study, an aligned CNTs sheet was embedded in a prestrained elastomeric substrate to produce a highly flexible and stretchable heating device[143]. The device was found to be damage tolerant and functional at 400% strain showing excellent thermal stability. The heating device produced 268°C under an applied voltage of 50V at zero strain.

Most of the wearable heaters are used in a non-ionizable ambient atmosphere, whereas, Dudchenko et al. developed a thin, porous CNT film-based Joule heater for a highly corrosive and ionizable environment[147]. Layer-by-layer spray coating of carboxylated CNTs and PVA was used to produce hydrophilic and porous thin film deposited on a hydrophobic porous membrane support. It was found that using alternating currents, the CNT Joule heaters can operate for a long period without degradation in brine water. In another study, a super aligned CNT/polyimide (PI) film heater was developed with high mechanical strength and thermal stability[148]. The tensile test showed that composite film containing 10 layers of CNT has a strength of ~86 MPa whereas, 20 layers sample have a tensile strength of 117 MPa. The thermal heating test depicted a fast response to reach a steady temperature within 5 seconds from room temperature. and stable heating behavior for a longer time at a constant voltage. Jung et al. also used aligned CNT sheets from MWCNTs to produce highly flexible, transparent and conducting heaters and analyzed the impact of different parameters on heating behavior[149]. They showed that mechanical deformation does not affect the heating stability and the addition of metal nanoparticles enhances the heat-generating capacity.

2.4.2.3 Electrodes for energy storage applications

Technologies are continuously being miniaturized and life companions and the next generation electronic devices are expected to be seamlessly integrated into textiles for different

functionalities and applications. However, many of these devices are power-driven and necessitate the development of wearable energy storage devices that also to be integrated into textiles. Flexibility, stretchability and breathability are the major requirements for wearable textile electronics and their power components should also meet these requirements. Therefore, textile-based supercapacitor research is surging to develop a textile-based electrode with higher power and energy density[150,151,152]. In conventional supercapacitor (coin cells), the electrode uses metal current collectors and conductive binders. Some early-stage supercapacitor uses metal or metal-coated wires as current collectors and coating, or hydrothermal methods are used to apply active materials. This results in low specific capacitance due to the weight and volume of metal wire and low mass loading of active material, which has motivated the development of fibers/yarns-based supercapacitors. Yarn-type supercapacitors are lightweight, flexible and stretchable. Conductive polymers, carbon fibers, nanocarbon (CNTs and graphene) and hybrid of these materials are extensively used for yarn type supercapacitors[151,153]. Carbon-based materials have a high surface area, thermal and chemical stability. The major challenge of carbon materials is their limited energy density and capacitance. Therefore, transition metal oxides are often used with carbon materials to enhance their specific capacitance. Transition metal oxide has pseudocapacitive characteristics which are achieved by the redox reactions of transition metal oxides or intercalation of ions. These materials suffer from poor mechanical properties and low electrical conductivity and limit their practical applications. While conductive polymers have very good pseudocapacitive properties and electrical conductivity, but they degraded over time providing a shorter life cycle. An ideal electrode material requires higher electrical conductivity, capacitance and good cyclic stability[154]. Recently, transitional metal carbide also known as MXene showed promising characteristics to be used for energy storage applications owing to their excellent electrical,

electrochemical and mechanical properties[155,156]. Among different materials for potential yarn type supercapacitors, CNTs are promising due to its excellent tensile strength which can be utilized to produce electrodes for structural energy storage. Additionally, CNT based structural electrode exhibit stability in diverse environmental conductions and performs well under mechanical stresses without packaging. Muralidharan et al. fabricated composite electrodes by growing CNTs on stainless steel mesh and layered in an ion-conducting epoxy electrolyte matrix with Kevlar/fiberglass mats[157]. The composite energy storage device showed a modulus of 5 GPa, tensile strength over 85 MPa and energy density up to 3 mWh/kg. Different guest materials are introduced into CNT to improve the capacitance and energy density of the supercapacitor. High capacitive active materials can be loaded into CNT and 90 wt% of active materials can be realized by controlling the yarn diameter and porosity. Different guest materials have been added into CNT yarn-based supercapacitor in the forms of sheath-core, twisted and coiled configurations which effectively utilize the capacitive or pseudocapacitive properties of active materials[151]. MXene/CNT yarn asymmetric supercapacitor was reported by loading 93 wt% of MXene. The co-twisting of MXene particles with CNT sheets by the liquid state biscrolling method was used to produce a negative electrode whereas MnO_2/CNT used as cathode[153]. The yarn supercapacitor showed areal capacitance of 1.56 F/cm^2 and an energy density of 100 μWh/cm^2.

2.5 Wash durability of CNT-based e-textiles

Traditionally, textile durability refers to the ability of fabrics and garments to retain their mechanical and physical performance such as resistance to abrasion, pilling, comfort, and appearance throughout the lifespan of the garment[158]. Garments are expected to be used multiple times and typically undergo some kind of washing/cleaning[159]. However, the washability of e-textiles is very complicated and case dependent. E-textile devices are generally composed of rigid and hard electrical components and flexible areas containing conductive interconnects[160]. It might

not be required to wash the complete e-textiles circuitry because many of the rigid components are detachable or can be encased in waterproofed coatings to make them wash durable[161]. The big challenge is to wash the embedded conductive materials in the garments and have them retain their electrical performance. There are a substantial amount of prototypes/proof of concept prototypes reported in research papers but they are often not commercialized due to reliability issues[162]. Washability of e-textiles is important because the products are expected to go through regular maintenance cycles including washing and cleaning. The mechanical and chemical interaction between garments and washer environment can cause damage to the conductive elements during the washing process and threaten the longevity of the product. Even hydrophobic textiles may absorb water due to the capillary effect and may cause the device to fail[163]. Two major issues need to be solved to make the e-textiles commercially viable- i) the conductive materials on the yarns and fabrics need to be protected during the washing process and ii) the connecting points between rigid electrical components and conductive traces need to be strong enough to sustain the washing cycle. Generally, the interaction during washing can be categorized as mechanical (friction, bending, torsion, twisting etc), thermal (temperature), water stress and influence of detergents[164]. Conductive yarns and fabrics might be more susceptible to mechanical interaction and can damage the connection between soft and rigid components as well as abrade the conductive surfaces[163]. In laboratory-based accelerated washing, the steel balls used can severely damage the conductive traces in the fabric. However, in traditional laundering machines, mechanical stresses may be induced due to the high loading of clothes and interaction with the machine parts. The types and levels of stress produced during the washing process are presented in Table 1[165]. Water also plays a crucial role in wash durability of e-textiles and is considered the second most influential factor.

The soaking, washing and rinsing processes all involve water and the water-induced forces affect the durability of the e-textiles.

Table 2. 1 Different washing stress

Stresses	**Actions**			
	Soaking	Washing	Rinsing	Tumbling
Mechanical	No	High	High	Moderate
Chemical	Moderate	Moderate	No	No
Temperature	Moderate	Moderate	No	No
Water	Moderate	Moderate	Moderate	No

A different researcher reported wash durability of CNT assemblies. SWCNT and PU have been coated on Kevlar fibers by layer-by-layer spray coating[10]. The coated fiber was washed by simply dipping in water and dried by blowing air (no other parameters on the wash conditions were given). After 50 dip water wash cycles, no significant change in electrical conductivity was observed. CNTs have been introduced in nonwoven fabrics using ultrasonication[166]. The conductive nonwoven fabric was washed for 40 hours in water at 700 rpm stirring rate (no other wash durability test parameters were given). After washing for 8 hours, a lot of protruding fibers on the fabric surface was evident due to the strong shear forces exerted by the water, and the electrical conductance was reduced by 10%. However, the inner fibers were not affected and after washing for 40 hours, the conductivity of CNT coated nonwoven fabric only decreased by around 14%. The CNTs were found to be highly attached to the nonwoven fabric making it washable in water. In another study, CNTs were introduced on cotton fabrics by the exhaustion method and stabilized using crosslinking agents[167]. The coated fabric was accelerated machine washed using a

non-ionic detergent at 40°C. The wash durability of the CNT coated fabrics was measured in terms of hue changes of the fabric using greyscale and the degree of staining on the adjacent fabrics after drying. All the samples treated with crosslinking agent demonstrated excellent wash fastness. The authors did not report the electrical conductivity of the coated fabric before and after washing. Cui and Zhou used a dip-coating method to produce conductive cotton fabric using a GO and an MWCNT dispersion[55]. The coated cotton fabric was immersed in an SDS aqueous solution for wash durability testing and stirred at 300 rpm (no textile wash standard was followed). The first four cycles of washing lasted 2 hours each and 12 hours for the fifth cycle and finally bath sonicated for an hour as the sixth wash cycle. Cotton coated with GO six times showed a 47% increase (Figure 2.15a)[55] in resistance after 6 wash cycles whereas the rest of the samples had less than a 10% increase in resistance (Figure 2.15b)[55].

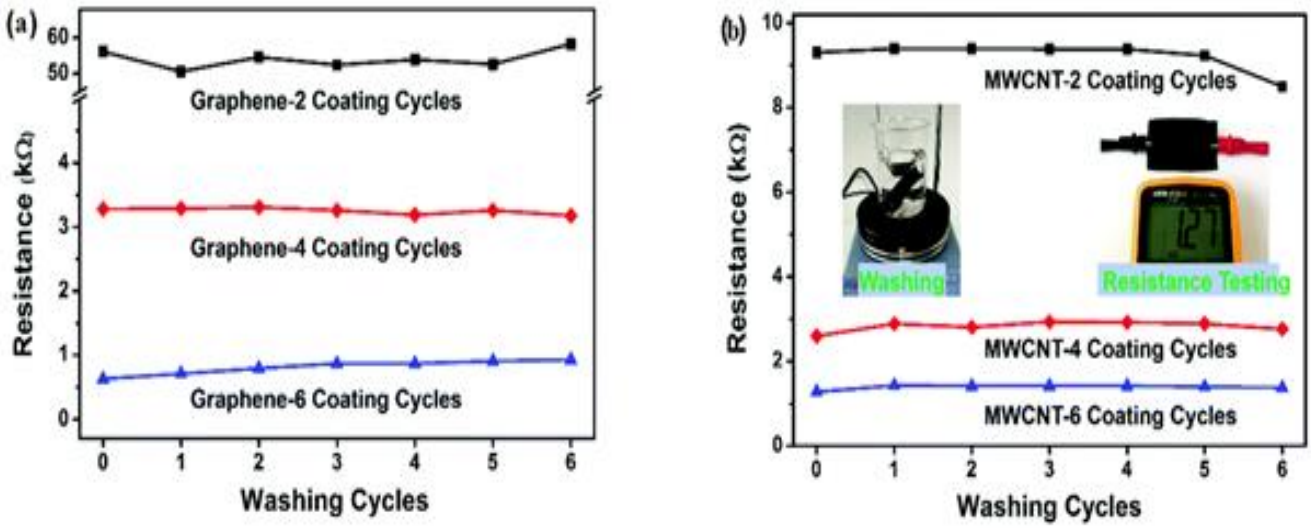

Figure 2. 15 Wash durability test of e-textiles

Description: a) GO coated cotton b) MWCNTs coated cotton[55]

2.6 Critical summary

CNTs show excellent properties in nanoscale which was reported by the voluminous amount of literature that has been published since their discovery by Ijima in 1991[168]. It remains a major challenge to utilize the remarkable properties of CNTs in the micro-macro scale due to the changes in their microstructures and orientation. Large scale continuous production of CNTs was pioneered after more than a decade of its first report. This is because the powdered form of CNTs that had a length in micron-scale was assembled into the solution phase. Increasing the length of CNTs in the millimeter scale enabled the researcher to have better control over the alignment and orientation of CNTs in bulk structure. The breakthrough in spinning CNTs into yarn offers enormous opportunities in producing flexible and multifunctional e-textiles for different wearable applications. The properties of CNTs can be tailored during the spinning process by varying different parameters. For example, the diameter of the CNT yarn is tuned by using multiple CNTs arrays to be used with traditional textile yarns for textile processing. Additionally, CNTs could be wrapped over a textile yarn to obtain larger diameter yarn suitable for seamlessly integrating into textile structures. This process gives wider flexibility of using various textile yarn to customize the properties of CNT-wrapped yarn for desired applications. Wrapping CNT over an elastomeric yarn imparts high flexibility in the assembled structure, as well as high strength core yarn, which can drastically enhance the mechanical properties of the CNT yarn.

On the other hand, guest materials can be introduced into the CNT yarn during the continuous spinning process to enhance the performance of the CNT yarn. When nano CNTs are assembled into micro-CNT yarn, the surface area and electrical conductivity of the CNT yarn decrease resulting in lower capacitance behavior. Guest materials with high capacitance like graphene, MXene can increase the capacitance of CNT yarn due to the better charge transfer.

Furthermore, high flexibility and strength are crucial to producing 2D structures by weaving or knitting for various wearable applications. A 3D whole garment knitting for producing strain sensing gloves for wearable body motion tracking requires yarns to endure high knitting needle friction and superior flexibility to produce knit loop and mechanical intermeshing to produce a fabric. Likewise, for wearable heating applications, the fabric needs to have a high drape ability to adapt the body conformability. A proper intermeshing of CNT yarn is essential for uniform distribution of the heat by providing better contact between loops.

Controlling the alignment of CNTs during the spinning process has a direct impact on CNT yarn properties which greatly affects the mechanical and electrical properties. The researcher demonstrated different methods of improving the properties of CNT yarn by post-processing such as mechanical and solid densification, acid treatment, doping, annealing etc. However, most of the CNT yarn produced by the direct and wet spinning process has a very small diameter which is incompatible for textile processing due to lower strength and abrasion resistance. Multiplying CNT yarns could produce large diameter CNT yarn but require additional equipment and the process is time-consuming. While a few researchers demonstrated the knittability of the fine diameter CNT yarn, but they were produced in either hand or lab scale knitting machines. Hand driven or traditional knitting is very labor-intensive and unsuitable for the seamless fabrication of e-textiles. Furthermore, the knitted fabric produced by thin diameter CNT yarn is an open net structure with poor aesthetics and functionality. Therefore, it is of paramount importance to understand the structure-processing properties of large diameter CNT yarn to realize their potential for fabric-based multifunctional wearable electronic devices. Washing is the critical requirement of wearable textiles which has never been addressed for spun CNT yarn. Though dip-coating based

CNT/Cotton yarn was developed, their washability was extremely poor and unable to meet the laundering requirements[169,170,171.]

This research aims to develop a single step spinning method to assemble CNT in a large diameter yarn similar to traditional textile yarns and incorporate a combined twisting and liquid densification process. This will eliminate the additional densification step making the process faster, continuous and produce CNT yarn with better packing density. The opportunity of inserting any textile yarn as a core and wrapping CNT over the core yarn will provide greater control over CNT yarn geometries, functionalities and improved mechanical properties. Furthermore, this is extremely advantageous of producing very large diameter yarn without increasing the amount of CNT or multiplication of CNT yarns. CNT yarn produced by the spinning system developed in this research will be extensively studied for producing different knit structures using the high speed and automatic industrial knitting machine. The three-dimensional knitted structure will also be fabricated using a seamless whole garment knitting machine to produce next-generation e-textiles and advance manufacturing for Textile 4.0 (4^{th} textile revolution). The unique millimeter long CNT grown in the lab will render the assembled CNT yarn better stability and increase inter-tube junctions. Therefore, the yarn is expected to exhibit excellent durability to washing and meet the existing washing requirement for the commercial viability of e-textiles. Additionally, the unique assembly of CNT yarn is expected to retain their functionality after multiple industrial washing cycles with and without TPU coating.

The morphology of the yarn will be analyzed and compared with mostly used cotton and polyester yarn. The strength requirement and flexibility of the yarn for high-speed industrial knitting will be evaluated by mechanical characterization. The produced yarn will be seamlessly integrated into a 3D hand glove by whole garment knitting and the functionality of the produced

knitted fabric will be exhibited as a strain sensor. Accelerated washing of the yarn will be performed using existing textile washing standards and the durability of the yarn after washing will be evaluated by measuring electrical conductivity and Joule heating application. As mentioned above, the developed spinning method provides greater processing flexibility and therefore, the CNT yarn will be functionalized *in-situ* by transition metal carbide to enhance the capacitance of CNT yarn. Finally, an elastomeric yarn will be used as a core and wrapped by CNT to produce a highly stretchable electrode for multifunctional wearable applications.

Chapter 3: Structure-property relationship of macrostructure carbon nanotube yarn

3.1 Introduction

The impetus for developing carbon nanotube (CNTs) macrostructures such as fibers/yarns, films, aerogels was due to ultrahigh strength and toughness, good chemical stability, high thermal and electrical conductivities, and low density. These molecular level outstanding properties make them ideal multifunctional materials because CNT demonstrates the best-combined properties of carbon fibers, polymers, and metals. However, it remains a major challenge to translate these properties in macroscale [172,75,173,92]. Therefore, different research effort has been made to create CNT macrostructures, especially CNT fibers[174,73,95,96,105,90]. CNT fibers are highly aligned and easy to handle. Besides they could be used for different devices such as sensors, actuators, electrodes, power cables, composites[175,100,176,177]. Neat CNT yarns could be produced by solid-state spinning process or solution extrusion. In solid state spinning process, CNTs are spun either directly from the reaction furnace or from CNT forest grown on a substrate[173]. However, most of these neat CNT yarns have a diameter in 10-100 micron range[77,173,178,179]. Larger diameter CNTs are essential for further processing into different device structures. There are different parameters such as porosity, twist that affects the electrical and mechanical properties of assembled CNT yarns[180]. As spun CNT fibers have weak CNTs-CNTs interaction and limit their load transfer efficiency. A strong CNTs yarn was developed by pi bridging the adjacent CNTs and 2-4 times improvement in tensile strength, toughness and electrical conductivity was observed[181]. The researcher reported that twisting and densification significantly improve the electrical and mechanical properties of CNT yarns[182,183,184]. Anike et al. evaluated the impact of a twist on the tensile strength, elastic modulus, strain-to-failure and toughness[185]. At an optimum twist angle of 30-degree, the maximum tensile strength of CNT yarn was observed due to the enhanced CNT alignment. Besides, affected the elongation at break, packing density and porosity of the CNT yarn. Mechanical and electrical

properties of CNT yarns fabricated from different diameters of multiwalled CNT (MWCNTs) were analyzed[186]. MWCNTs with a diameter ranging from 15 to 41 nm were synthesized by changing the growth recipe of the chloride-mediated chemical vapor deposition system. A significant change in the tensile behavior from nonlinear deformation to elastic was reported. Modification in the spinning system affects the properties of CNT yarn and improvement in tensile strength was reported[187,188]

Different chemical treatment also affects the mechanical properties of the CNT yarn. Liquid infiltration is commonly used to modify the mechanical behavior of CNT yarns[189]. Jia et al. studied the mechanical properties of yarns spun from different CNTs and showed that the strength of the yarn can be improved by 25% by polyvinyl alcohol infiltration[190]. Covalent linkage by polymer binder showed 300% increase in their elastic modulus[191]. Though a good number of reports on different structure-properties relationship of CNT yarns are available, understanding the structure-dependent properties of CNT composites yarns are limited. Besides, diverse applications of CNT are often hindered by the lack of high-rate assembly of CNTs into processable yarns that retain sufficient mechanical properties [192,193.]

Here, we report a modified spinning system for continuous assembly of CNT yarns from dry spun CNT forest. This modified spinning device can simultaneously spin and densify the CNT yarn by both physical and chemical methods. A large diameter yarn was produced by wrapping CNTs over cotton yarn and their structural properties were evaluated and compared with the neat CNT yarns. The impact of wrapping distance and different percentages of thermoplastic polyurethane (TPU) binder is also presented.

3.2 Experimental

3.2.1 Synthesis of vertically aligned CNTs

Vertically aligned CNTs (VACNTs) were synthesized using the modified catalytic chemical vapor deposition (CVD) method. The deposited VACNTs array has an approximate height of ~1mm with an average diameter of 25±10 nm. In short, the process starts with placing iron chloride ($FeCl_2$) catalyst underneath the quartz substrate and both of them are transferred to the CVD furnace in a cylindrical quartz tube. The precursor gas acetylene was used at the flow rate of 600 sccm with argon (398 sccm) and chlorine (2 sccm). The growth was continued for 20 mins at 860 °C and 5 Torr. Argon was purged after the growth process. The quartz tube was removed from the furnace and the quartz substrate containing VACNTs were used for spinning process.

3.2.2 Spinning of CNT and CNT wrapped cotton yarn

Two VACNTs were used for the spinning of CNT yarn (CNTY) and CNT wrapped cotton yarn. The spinning process is initiated by dragging the edge of VACNTs using a tweezer and then they are placed on the spinning device opposite to each other. A core cotton yarn with a linear density of 20 Tex was inserted through a tube inside the spinning mandrel. Then all three yarns are twisted together and passed through a guide. The twisting zone wraps the CNTs over core cotton yarn making an assembled yarn with core-shell structure. Thermoplastic polyurethane (TPU) binder was applied using a syringe pump at different percentages ranging from 0.5 to 5%. Neat CNTY was produced by a similar process without using cotton core. Different yarns were produced and the percentage of TPU used with CNT yarns are denoted as CNTY-0.5 for 0.5% TPU and similarly CNTY-1, CNTY-1.5, CNTY-2, CNTY-2.5, CNTY-3, CNTY-5 variations were produced. CNT-Cotton containing different TPU percentage are designated as CCT-0.5 for 0.5% TPU and CCT-1, CCT-1.5, CCT-2, CCT-2.5, CCT-3, CCT-5 yarns were produced. To evaluate

the impact of wrapping distance, four different wrapping distances were chosen. However, no TPU was applied for the yarn spun at a different distance because the TPU binder may affect the alignment and wrapping angle. CNTY is produced by wrapping at the distance 5 cm from the let-off section is denoted by CNTY-WD5, and similarly, CNTY-WD12, CNTY-WD16 and CNTY-WD20 for the yarn spun at 12, 16 and 20 cm from the let-off zone.

3.2.3 Characterizations of the yarn

The surface morphology of the yarn was characterized using field emission scanning electron microscope (SEM) Verios 460L with a beam voltage of 2 kV and beam current 13 pA. The diameter of the yarns was calculated using the ImageJ, NIH software. Thermogravimetric analysis (TGA) of the yarn was carried out from ambient to 800 °C using Parkin Elmer Pyris 1 instrument with a heating rate of 10 °C/sec. The sample weight for TGA was approximately 5-6 mg for each. The yarn linear density of the yarn was calculated by weighting 20 cm yarn in a microbalance (Anton Per) and multiplying their weight by the unit length of 1000 meters (Tex) which was then divided by the measured length. Xray microcomputed tomography of the yarn was performed on ZEISS Xradia 510 Versa.

3.2.4 Mechanical characterizations of the yarn

The mechanical properties of the yarn were evaluated using MTS Criterion Model 43 instrument. Average results of five test specimens were reported. The tenacity of the yarn was calculated by dividing the tensile load by yarn linear density. The electrical resistance of the yarn was measured using a four-probe method by connecting a Keysight 6 ½ multimeter.

3.3 Results and Discussion

3.3.1 Spinning of the yarn

A one-step spinning and physical and chemical densification process of the yarn is shown in Figure 3.1. The spinning device has three major sections. Section-1 termed as let-off zone

consists of a motor-powered rectangular mandrel where the VACNT arrays are placed. The core yarn is placed in this zone and passed through the mandrel. The tension of the core yarn is adjusted by the spring tensioning system. The core yarn is delivered to the twisting zone and further collected to the powered winding roller. The CNT arrays are securely placed on the mandrel using double-sided tape and a maximum of four arrays can be placed on the mandrel. The tube for the core yarn insertion has a diameter of half millimeters providing the opportunity of using all kinds of regular textile yarns. The spun-initiated array is then pulled through the guiding hole of the mandrel to the second section called the wrapping/twisting zone. Initially, all the yarns are manually twisted here and then released for wrapping by the device. The simultaneous wrapping and twisting densify the CNTY and produce a cylindrical yarn from the CNT ribbon coming from the VACNT arrays. Afterward, the wrapped yarn is passed through a guide and a syringe pump is attached to drop cast TPU. The dropping rate for all TPU concentrations was kept constant and applied on the surface of the twisted yarn. Applying TPU binder further densifies the yarn and removes the protruding fiber from the yarn surface. The last section is the winding zone which is connected to a motor. The spun, wrapped, twisted and densified yarn is collected on a roller. The wrapping angle is controlled by varying the wrapping and winding speed. Important to note that, all the processes are performed simultaneously which saves time and cost.

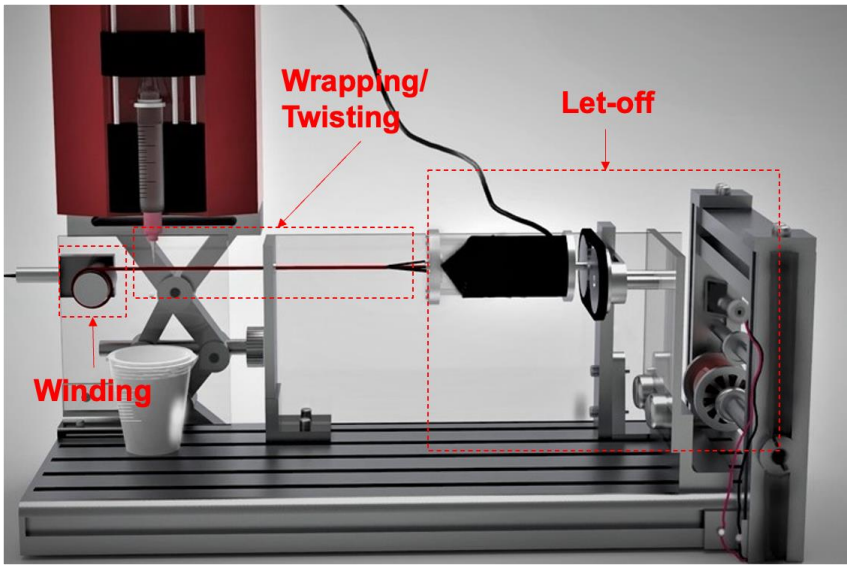

Figure 3. 1 Schematic of the spinning system

Description: Doted box in the right indicates let-off zone, middle is the wrapping/twisting section and the winding section is in the left. The syringe pump is attached at the end of wrapping/twisting section.

3.3.2 Characterization of the yarns

The surface morphology of the yarn spun at different wrapping distances is presented in Figure 3.2a. The diameter and alignment of the yarn did not change significantly against different wrapping distances (Figure 3.2b). Though the wrapping angle slightly increased from 16 degrees (WD5) to 21 (WD20), the standard deviation was very high, and this change is not statistically significant. This can be explained by the wrapping speed which was constant and since there were no additional twisting involved, all the yarn had an almost similar wrap. The magnified morphology of the yarns showed a similar alignment of the yarns (Fig S1). Therefore, changing the wrapping distance did not provide additional densification as reflected in the yarn diameter. In contrast, yarn produced with different TPU percentages, demonstrated significant changes in their linear density (Figure 3.2c). Both the CNTY and CCT yarn revealed similar changes in linear

density after TPU addition and increasing the TPU, the linear density decreases except for 2.5% TPU which was unexpected. This might be due to the changes in TPU concentration. However, all the yarns were densified by TPU addition due to the TPU assisted volume shrinkage of CNTs. Notably, the alignment change on the yarn was mainly on the surface of the yarn rather than across the yarn diameter as demonstrated revealed by the computed tomography (Fig S2). CNTY shows that the fibers are wrapped over the core and a small amount of twist is inserted to the yarn. The wrapping process introduces some level of twist, unlike the regular twisting process. The resistance changes of the yarn after TPU addition showed (Figure 3.2d) an increasing trend for both CNTY and CNTs wrapped cotton yarn. Compared to the CNTY containing TPU, resistance change was higher for CCT yarns and maximum resistance was observed for 5% TPU.

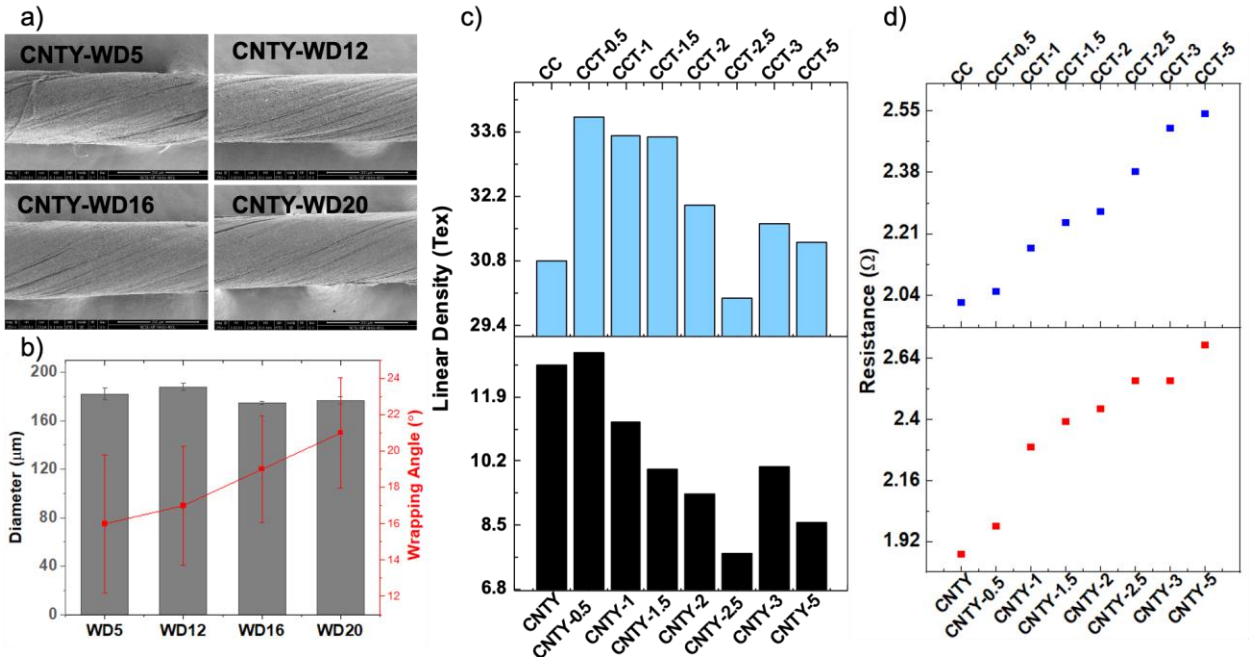

Figure 3. 2 Characteristics of yarns

Description: a) SEM images of CNTY spun at different wrapping distance b) changes in diameter and wrapping angle against wrapping distance (WD). Changes in c) linear density and d) resistance for different TPU percentage

TGA analysis of the yarns are presented in Figure 3.3. CNTY and CCT yarn demonstrated two different thermal transitions. Overall, CCT yarns showed sharp onset in their thermal transition around 230 – 270 degrees Celsius compared to the CNTY with TPU. The first onset for CNTY was above 300 °C higher than CCT yarns. This is due to the lower melting point of core cotton yarns. The absence of cotton in CNTY revealed high thermal stability and the first onset for CNTY was due to the TPU. However, for both cases, TPU degraded far earlier than other yarns and yarns with CNTs have higher thermal stability than TPU as expected.

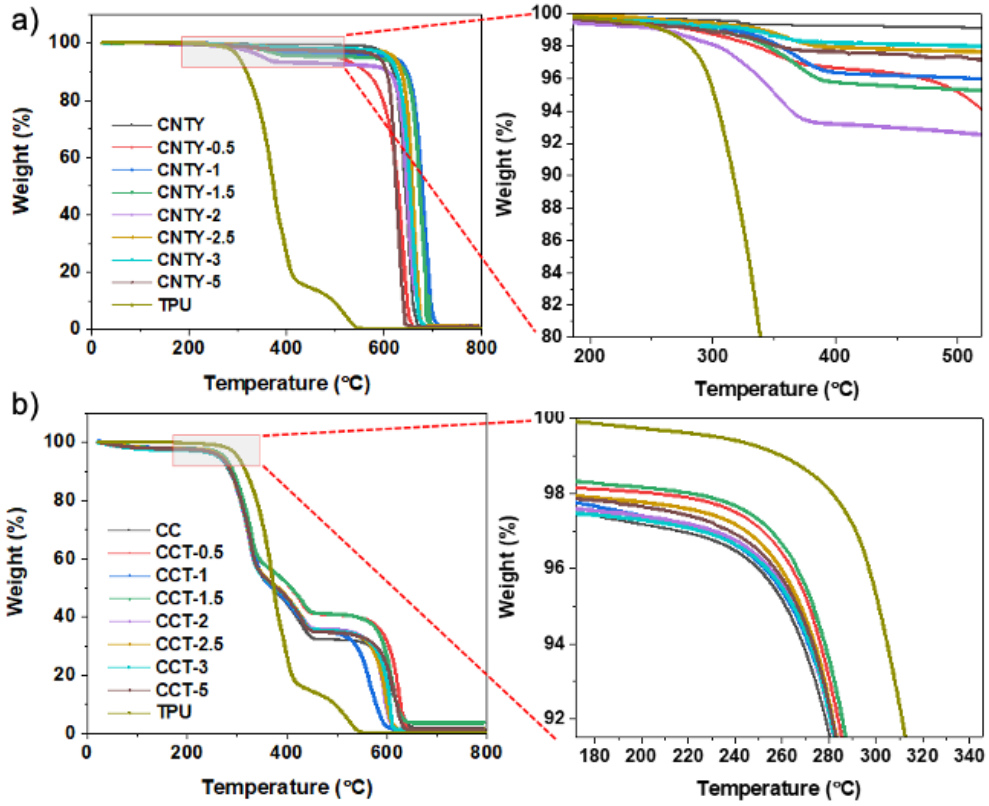

Figure 3. 3 TGA analysis of the yarn

Description: a) TGA of CNTY yarns with TPU b) TGA of CCT yarns

3.3.3 Tensile testing of the yarns

The Tenacity-strain curve of the CNTY and CCT yarns is presented in Figure 3.4 and Fig S3. All the yarns demonstrated improved tenacity after TPU addition compared to the yarn without

TPU. A maximum tenacity was observed for the CNTY-5% due to the increased TPU content on the yarn. TPU acts as a matrix for the yarn and transfers the applied load. Yarns with higher TPU can transfer load better than the yarn with lower TPU. Compared to the CNTY, CNT with cotton core demonstrated higher tensile strain at 5% TPU because core yarn provides more space for aligning the fibers during loading. However, the tenacity of the yarns did not improve linearly with TPU. This can be ascribed to the amount of TPU absorption by the yarns. Though the TPU dropping rate was kept constant, it was uncertain whether all the yarns absorbed all the applied TPU. The Tenacity-strain curve of the yarns spun at different wrapping distances (Fig S4) showed no significant changes except for the yarn spun at 16 cm wrapping distance. Compared to other yarns, CNTY-WD16 yarn exhibited lower tenacity. However, the strain% of CNTY-WD16 was almost twice than that of other yarns.

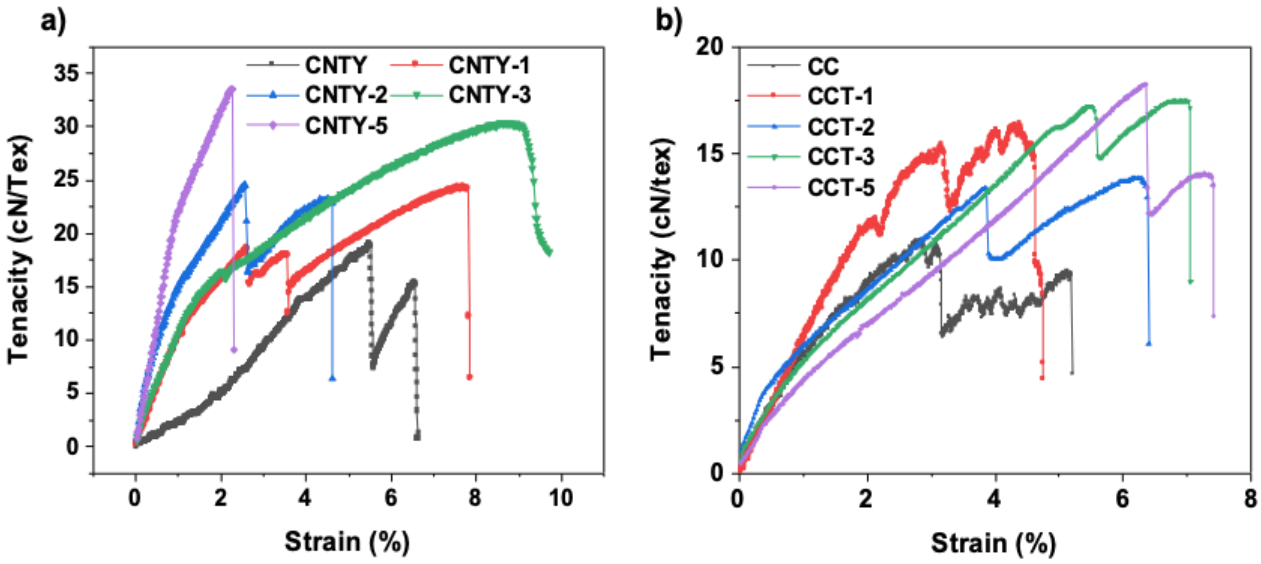

Figure 3. 4 Tenacity-strain curve of the yarns

Description: a) CNTY with different TPU b) CCT yarns

3.4 Conclusion

Different CNTY and CCT yarns by varying TPU loading % and wrapping distance were produced. The wrapping distance does not affect the alignment and densification of the yarn. Compared to other yarns, CNTY-WD16 yarn showed a slight reduction in tenacity but had a higher strain%. On the other hand, different TPU% significantly affects the electrical resistance and linear density of the yarns. In comparison to the CNTY, yarns containing cotton core demonstrated higher weight loss at the first onset of 230 – 270 °C. The tenacity of the yarns was also impacted by the addition of TPU. Maximum tenacity was observed for both types of yarns at 5% TPU addition. Overall, all the yarns with TPU exhibited higher tenacity.

3.5 Supporting Information

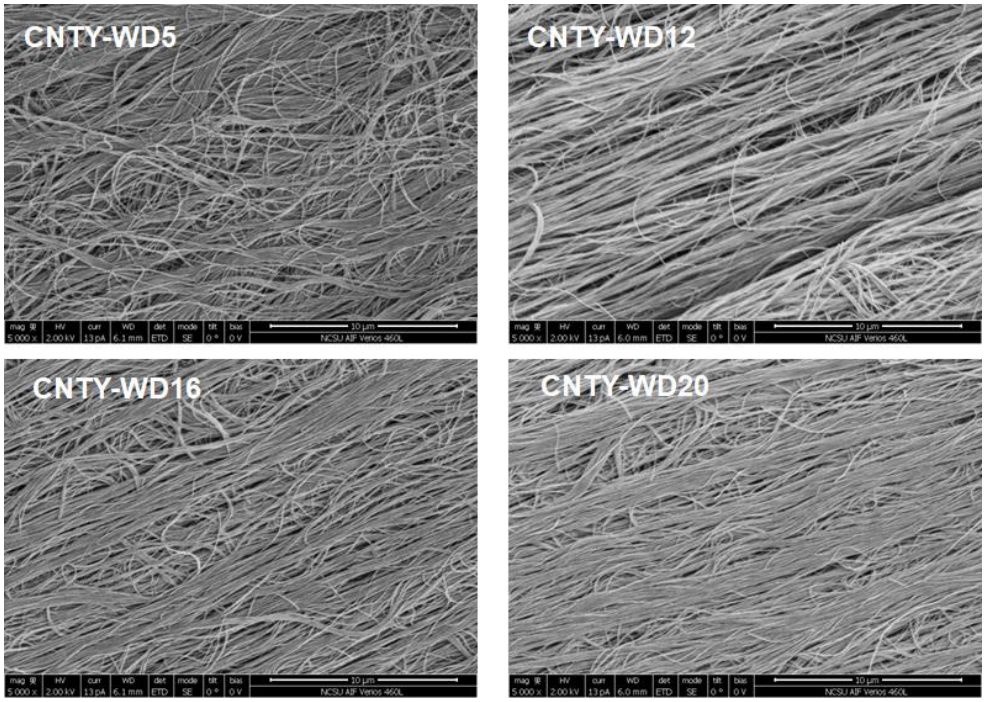

Fig S1: Morphology of the yarns spun at different wrapping distance (5kX)

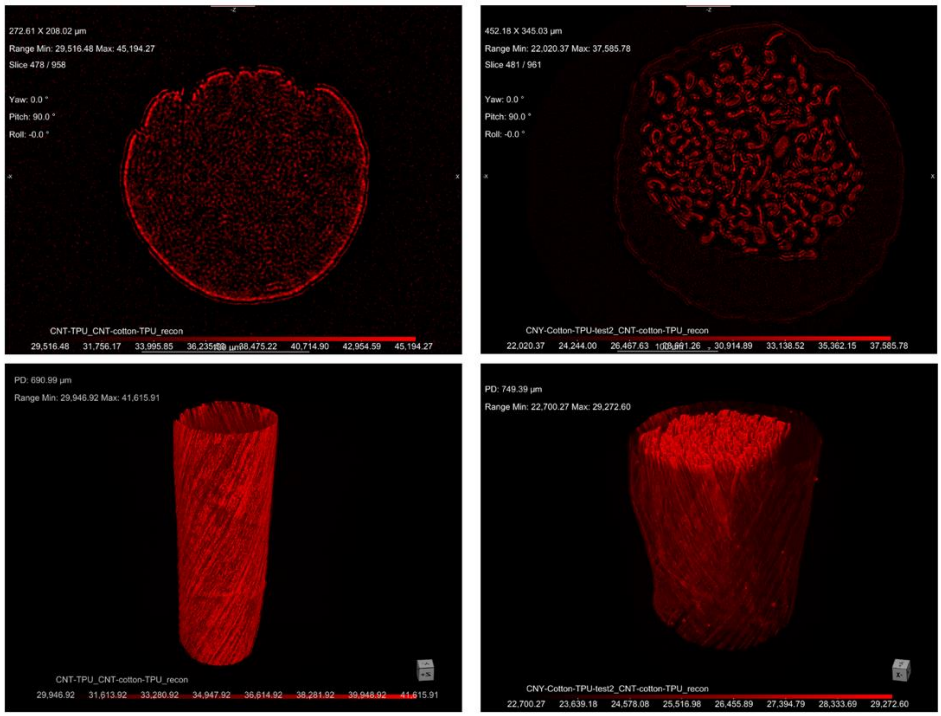

Fig S2: X-ray computed tomography of the CNTY and CNT wrapped cotton yarn after 1% TPU addition

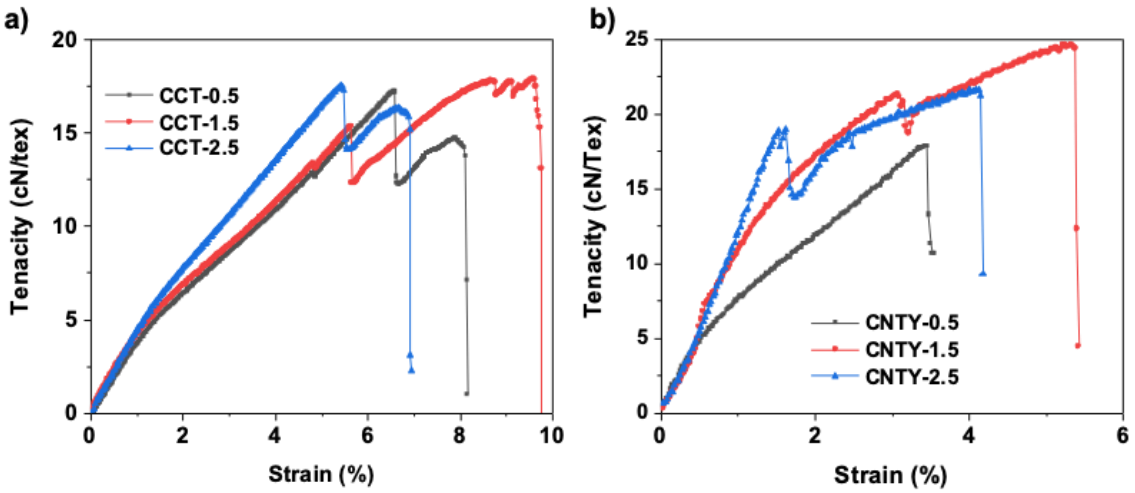

Fig S3: Tenacity-strain curve of yarns with different TPU loading

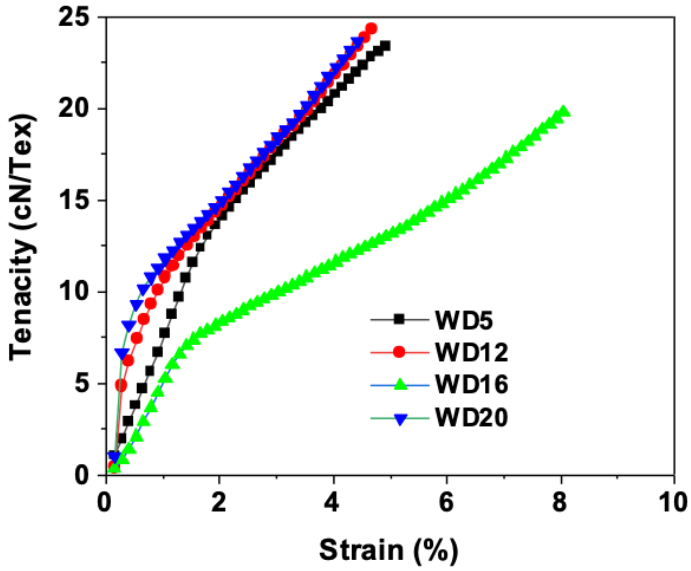

Fig S4: Tenacity-strain curve for different yarns spun at various wrapping distance

Chapter 4: Multifunctional, Highly Flexible, and Washable Carbon Nanotube Wrapped Textile Yarns for Wearable Electronic Fabrics

4.1 Introduction

Wearable electronic textiles (e-textiles) are highly desirable as next-generation smart devices, which combine device functionality with human body compatibility. A variety of approaches are being pursued with the common desirable characteristics of flexibility, wearability, breathability comfort, and wireless operation [194],[195]. With the soaring growth of the 'Internet of Things (IoT), wearable electronics are required to be compact, lightweight, inexpensive, low power consuming, and durable in a range of environments for daily use[196],[197]. To fulfill these combined property demands, researchers focus on developing multifunctional material systems. Significant advances have been made to develop multifunctional wearable electronics for sensing[198,199], energy storage devices[200,201], wearable heaters[202,203], electronic skin[204], artificial muscles[205] and soft robotics[206]. The performance of these reported devices have significantly improved in the past decade, but comfort and washability still require further improvement for seamless integration of next-generation textile based devices. Most of these wearable devices are planar thin-film structures produced by stacking multiple material layers. Thin-film-based devices are not breathable, and their inherent rigidity limits their application in devices conforming to the body [207],[208]. Therefore, flexible, stretchable, and textile-based wearable electronic devices in the forms of fibers/yarns received more attention in the last decade[209],[40]. One approach to fabricating wearable e-textiles is to prepare the device with electronic components (sensors, circuits, etc) in a 2D sheet or film nanocomposite system after integrating it onto the traditional textile by hot-pressing or adhesive binding method. This approach has major challenges regarding stretchability, cyclic durability, and comfort due to the structural incompatibility with textiles (yarn, fabric). To overcome these limitations, many researchers are now focusing on developing electrically

conductive flexible yarn and conductive line pattern printing on fabrics, etc. (1D structure), allowing more comfortable skin contact. Compared to integrating 2D devices on textiles, 1D conductive fiber/yarns are more compatible and provide a better path to producing complex and area-scalable e-textiles in high volume manufacturing processes (weaving, knitting)[210].

To this end, various research approaches have been made to develop conductive fiber/yarn-based wearable electronics using a variety of conductive nanomaterials such as metal nanoparticles and nanowires, graphene, carbon nanotubes (CNTs), conductive polymers, etc. [211],[212]. CNTs are widely used in fabricating wearable devices due to their high aspect ratio, extremely low density, excellent flexibility, mechanical properties, electrical properties, and chemical stability[55]. To incorporate CNTs into wearable e-textiles, fabricating flexible CNT yarns is the most effective design approach. The direct spinning of CNTs grown by chemical vapor deposition (CVD) process, the dry spinning of vertically aligned CNT array (VACNT), and wet/solution spinning of dispersed CNTs are the most common methods of transforming CNTs into flexible yarns[213]. Compared to the solution spinning process of dispersed CNTs, solid-state spinning processes (direct and dry) have several advantages like better nanotube alignment and fewer impurities. They also eliminate the requirement of the complex nanotube dispersion and purification steps.

Additionally, the solid-state spinning of CNT provides greater control over yarn microstructures and surface morphologies for desired applications. CNT yarn produced by the dry spinning of vertically aligned CNT arrays has better nanotube alignment and fewer impurities than the direct spinning process from CVD[214]. However, the web produced by the solid-state spinning process is weak due to the poor inter-tube connections and web bonding. Therefore, CNT webs are densified by solvent and/or mechanical force to produce CNT yarn. Different researchers reported that the performance of CNT yarn could be improved by solvent densification [102] and

mechanical twisting[115] due to the improvement in packing density. In addition, the longer and aligned CNTs ensure close contact with the adjacent CNTs along their aligned direction, enabling efficient load and electron transfer[215]. The dry spinning process facilitates tailoring CNT yarn properties by varying different spinning parameters such as diameter, density, twists and directly impacting CNT yarn properties[216].

The performance of the e-textiles depends on the functionality of the conductive CNT yarns. Though individual CNT possesses extraordinary electrical and mechanical properties, the collective properties of macroassembled CNTs are highly determined by the CNT-CNT junctions and bundling, orientation, and packing density of the structure. The breakthrough in spinning CNTs into macroscopic yarn is a significant step and offers enormous opportunities in producing flexible and multifunctional e-textiles for different wearable applications. In dry spinning, the nanoscale CNTs are assembled into a micro yarn by taking advantage of the inherent property of the π-π stacking tendency of CNTs. Controlled mechanical pulling of vertically aligned CNTs from the as-grown CNT array allows establishing CNT-CNT junctions to make long CNT fibers. It provides scope for twisting and compacting into an industrial-grade yarn required by bulk textile processing. It is important to note that fabricating pristine industrial-grade macroscopic CNT yarn requires many CNTs and slows down the fabrication process with a higher cost [22]. Besides, yarns produced from pure CNTs have a lower linear density; unsuitable for further processing into the 2D fabric using automatic and high-speed textile technologies like weaving and knitting [128].

Unlike weaving, knitting of CNT yarn could produce a fabric with higher flexibility, comfort, and better skin contact, which is an indispensable requirement for wearable sensing applications. Most of the reported CNT fabric was knitted in hand knitting or lab scale knitting machines[217,218,219]. Luo et al. knitted pure CNT yarn using an industrial weft knitting machine for

the first time using multi-plied CNT yarn and the maximum diameter of the yarn was 140 micrometer for 10 plies of CNT yarn[128]. However, plying requires additional processing equipment and the process is time-consuming and incompatible with high-speed textile processing. Unlike the traditional weft knitting process, 3D whole garment weft knitting is a highly advanced state-of-the-art knitting process that seamlessly integrates CNT yarns. In the 3D whole garment knitting, the structure of the fabrics is programmed in computer-aided design using a visual coding language, and each knitting needle and yarn can be controlled. Different textile structures can be produced continuously without human assistance using 3D whole garment knitting[150]. However, the fabrication of seamless 3D fabric using CNTs has not yet been achieved, and no previous reports are available to our knowledge.

3D knitting of CNT yarns requires overcoming the following challenges- i) the yarn diameter should be higher than 150 micrometers and ii) the yarn should have good mechanical properties and flexibility. During textile manufacturing processes, yarns encounter different forces and friction and are subjected to extreme bending and twisting, and this may cause damage or breakage of yarn. In addition to the manufacturability of CNT yarn, truly wearable applications require the fabricated devices to be durable for washing. A few researchers demonstrated the washability of CNT-coated cotton yarn. However, the wash durability of the coated yarn was inferior and unable to meet the laundering requirements [169,170].

Here, we report a single-step spinning and wrapping method to assemble CNT in a large diameter yarn similar to traditional textile yarns and incorporate a combined twisting and liquid densification process. This method eliminated the additional densification step making the process faster, continuous and produce CNT yarn with better packing density. In addition, the unique millimeter-long VACNT grown by catalytic CVD renders CNT with high structural stability by

increasing inter-tube junctions. The developed spinning method also includes a core insertion mechanism and wrapping CNT over the core textile yarns provides greater control over CNT yarn geometries, functionalities, and improved mechanical properties. The core insertion technique can be applied to almost any kind of textile and high-performance yarns. Furthermore, wrapping CNT over core yarns can produce large diameter yarn without increasing the amount of CNT or multi-plying CNT yarns. The morphology of the spun pure CNT yarn and CNT wrapped textile yarn was characterized and compared. A binder of thermoplastic polyurethane (TPU) densified the CNT yarn and increased the alignment of CNTs. The yarns were used in producing seamless 3D knitted structures using an industrial whole garment knitting machine for the first time as a next-generation wearable e-textile. The multifunctionality of the yarn and the knitted fabric was demonstrated by transferring power, strain sensing, and resistive Joule heating applications. Furthermore, for long-term and sustainable applications, the wash durability of the spun yarn was studied intensively, and it was found that the yarn is highly resistant to washing and the conductivity of the yarns remained almost constant after 30 washing cycles. This work exhibited a unique and versatile CNT yarn spinning system to produce CNT-based multifunctional wearable electronics.

4.2 Experimental

4.2.1 Vertically Aligned and Spinnable MWCNTs Synthesis

Vertically aligned MWCNTs CNT (VACNT) arrays were grown in a tube furnace via a modified version of the chlorine mediated chemical vapor deposition (CVD) route [220]. VACNT arrays with an average CNT diameter of ~ 27 ± 8 nm and an average length of ~1 mm, were grown on quartz substrates using iron II chloride ($FeCl_2$) as the catalyst. Iron chloride and the substrate were placed inside a quartz tube, which was loaded into the furnace. The growth gasses, acetylene (600 sccm), argon (400 sccm), and chlorine (2 sccm), were allowed to flow into the chamber after it was sealed and pumped to as low as 6 mTorr. The CNT growth process was carried

out for 20 min at growth temperature and pressure of 760 °C and 5 Torr. Afterward, the system was purged via argon during cool down. Aligned CNT sheets were formed with the aid of sufficient van der Waals interactions between the tubes and the CNT clean surfaces. That allowed the CNTs to align horizontally from the aligned vertical orientation on top of the quartz substrate in CNT sheets. The single sheet had a thickness of approximately 20 μm with a very low density (0.002 g/cm^3) [221]. Then the CNT array was drawn initially using a razor blade and tweezer. After initiating the drawn CNT sheet, it was easily secured to the spinning device.

4.2.2 Fabrication of CNT wrapped textile yarns

Two vertically aligned CNT arrays sized 11.5 x 6 cm were securely placed opposite each other on a rectangular spinning platform developed in the lab. Next, the core textile yarn was inserted through the center of the spinning cylinder. Then, two CNT sheets from the arrays were passed through the guide and wrapped over the core textile yarn to create a single hybrid yarn. Next, a thermoplastic polyurethane (TPU, Desmocoll® 530, Bayer Material Science) solution (1%) containing acetone was deposited on the yarn surface by a syringe pump. The deposition rate was 0.2 μL per minute and the yarn take-up was maintained at ~3.5 rpm. After applying TPU binder, the yarn was collected on a rotating cylinder or spool. The core cotton and polyester yarn has a linear density of 21 Tex and 36 Tex.

4.2.3 Characterization of yarn morphology

Surface morphology and cross-section of CNT and CNT wrapped textile yarn with and without TPU were investigated by field emission scanning electron microscope (SEM) FEI Verios 460L. A 2 kV beam voltage and 13 pA beam current were used during SEM imaging. The as-prepared yarn sample was analyzed in SEM imaging without sputter coating. The Raman spectra of the yarn samples were recorded at room temperature using a WITec confocal Raman microscope system (Alpha 300M). A crystalline Si sample with a characteristic Raman peak at 520.6 cm^{-1} was

used for calibration and the maximum sensitivity excitation wavelength of Raman was 532 nm. The diameter of the yarn was measured using SEM images of the yarn using NIH Image J software. The composition of the yarns were determined by thermogravimetric analysis (TGA) on a Perkin Elmer Pyris 1 TGA at a heating rate of 10°C/min in the air from room temperature to 800°C using 5 – 8 mg of each sample.

4.2.4 Electromechanical characterization of the yarns

The electrical conductivity of the yarn was determined by the four-probe method. Five measurements were taken along the length of the yarns, and the average was reported. Electromechanical characterization was performed using MTS Criterion Model 43 tensile tester. A data acquisition device (NI, USB-6001) was used to record the electrical resistance change in real-time. The yarn was fixed in the grips using a paper frame to ensure no slippage of the yarns. The gauge length of all yarns was 40 mm, and the strain rate was 0.01 mm/s. The dynamic cyclic performance of the yarn was carried out at 5% strain with a strain rate of 0.05 mm/s over 1000 repetitive cycles. Five samples of each yarn were used for electromechanical characterization.

4.2.5 3D knitting of the yarn

The CNT-TPU yarn was knitted on a Shima Seiki SWG061N2 (15 gauge) Whole Garment flat knitting machine. A seamless 3D hand glove design was programmed and simulated in Shima Seiki's SDS-ONE Apex3 design system. The knitting parameters were adjusted based on the design of the knit structure and the knitting speed was 0.7 m/s. The CNT-TPU yarn was integrated continuously using an intarsia pattern, whereas the base yarn of the 3D hand gloves was polyester containing spandex. Using the program a CNT-TPU yarn was seamlessly integrated into the index finger of the glove and used for body motion monitoring demonstration. In addition, a wrist band was also knitted using the CNT-Cotton-TPU yarn using the same knitting parameters. The supporting yarn used for knitting the wrist band was a blend of spandex and polyester fibers.

4.2.6 Piezoresistive Joule heating behavior analysis

The piezoresistive Joule heating behavior of the knitted fabric was studied by connecting it to a DC power supply with alligator clips. CNT-Poly-TPU yarn was used to hand knit a 9 x 0.7 cm swatches of fabric. The alligator clips were attached to the ends of the fabric. The temperature variation and distribution of different fabrics over time were tested by FLIR E4 thermal camera at different applied potentials. CNT-Cotton-TPU yarn was used to produce a knitted wrist band using an industrial-scale 3D whole knitting machine for the wearable Joule heating application. The impact of strain% on the thermal stability of the knitted wrist band was analyzed.

4.2.7 Washability Testing

The developed yarn was sewn onto a cotton fabric for washing according to the AATCC test standard TM 61-1A Test Method for Colorfastness to Laundering: Accelerated. The samples were enclosed in beaker with 200 ml water with 10 steel balls. Then it was washed for 45 min at 40°C without any detergent. After each washing cycle, the fabric containing CNT yarn was dried in the oven at 100ºC for 60 min.

4.3 Results and Discussion

4.3.1 Spinning and Wrapping of CNTs

The single-step dry spinning method used to fabricate the CNT-wrapped textile yarn is presented in **Figure 4.1**. The device has four significant sections: let off, wrapping, coating, and take-up zones. The let-off zone contains the changeable core yarn spool and passes through the spring tensioning device. The core inserting tube has a diameter in the millimeter range, allowing the use of most types of yarns. The tension was optimized, and the tensioning of the core yarn reduces the vibration during the spinning and wrapping process ensuring uniform wrapping of CNTs over the core yarn. The spinnable CNT arrays were securely placed on the sides of the spinning device (wrapping zone). The wrapping zone has a maximum capacity of placing four

CNT arrays, however for this work, two arrays were securely placed opposite each other. A thicker yarn with higher breaking load can be produced by increasing CNT arrays to four and/or using high-performance yarns as the core. Two vertically aligned CNT arrays (Figure S1) were pulled manually through the spinning guide to initiate the spinning process. Then CNT yarns are twisted together with the core yarn approximately 10 cm from the array and pulled to secure on the take-up roller. Later, the let-off and take-up motor was turned on to produce the CNT-wrapped textile yarns continuously. The simultaneous spinning and wrapping process is continuous and can produce around 90 meters of yarn from two CNT arrays.

The third zone of the spinning is the coating and drying zone. The wrapped yarn is passed through a guide for maintaining the tension during the coating process. A TPU solution was deposited on the yarn using a syringe pump. Uses of TPU binder remove any protruding fibers by aligning them to the yarn axis. Unlike the typical cotton yarn, the CNT wrapped yarn containing TPU binder is smoother and uniform in diameter. The drying zone is adjusted so that the ambient temperature can evaporate the acetone before winding on the collecting roller. Unlike the traditional dry spinning of polymeric yarns, the optimized drying distance of CNT spinning eliminates the requirement for heated drying. The take-up zone is where the spun and wrapped yarns are collected. It is very critical to optimize the let-off and take-up speed for uniform wrapping of the CNTs. A yarn spool containing CNT-Cotton-TPU is shown in the left side of Figure 1. Pristine CNT yarn (CNTY) was produced similarly without the core yarn. The two most popular and extensively used textile yarns, cotton and polyester, have both been used as core yarns in our process. CNTY, CNT wrapped cotton (CNT-Cotton) and CNT wrapped polyester (CNT-Poly) yarn were produced without TPU binder. And, TPU binder was applied to all three yarns to produce CNT-TPU, CNT-Cotton-TPU, and CNT-Poly-TPU yarns.

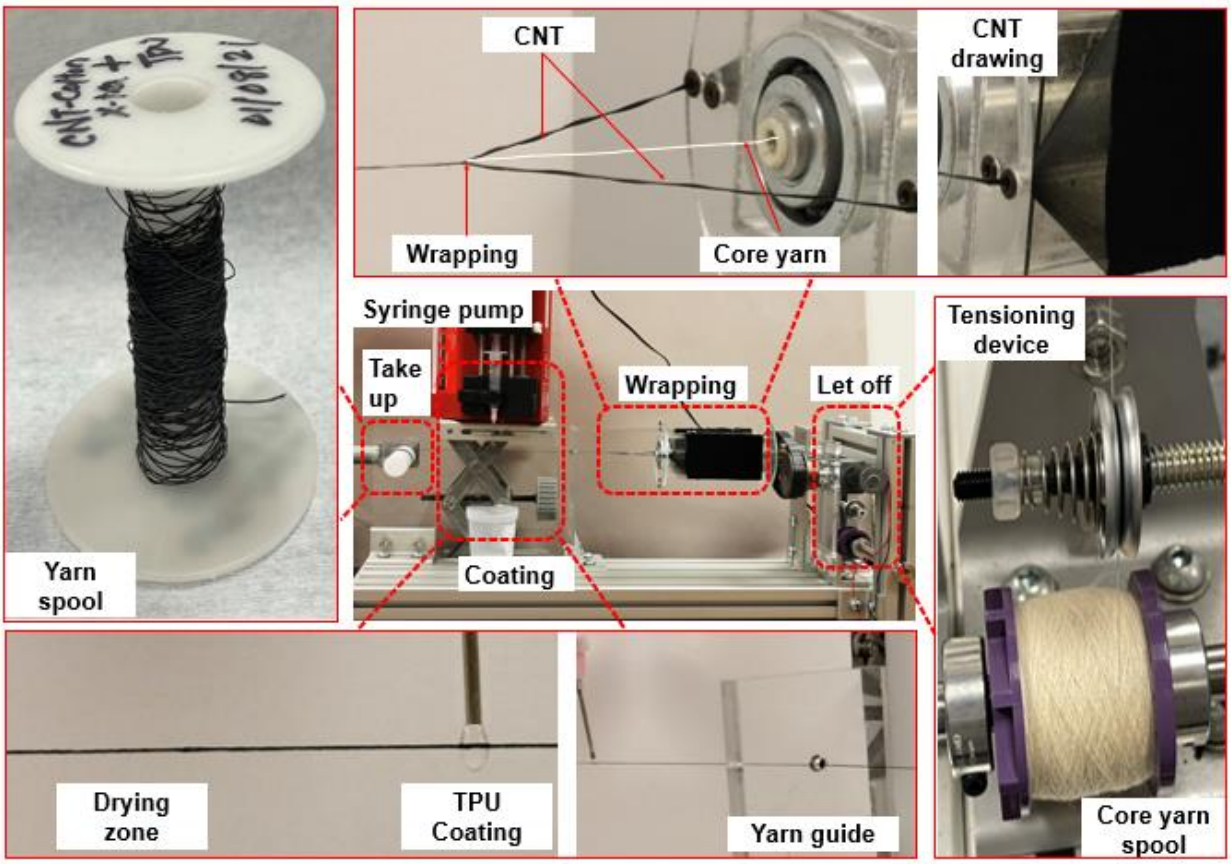

Figure 4. 1 The dry spinning of CNT-wrapped textile yarns.

Description: Two VACNT is secured opposite each other on the rotating cylinder. A core yarn is passed through the inner tube of the cylinder. CNT is wrapped over the core yarn and twisted together. TPU binder is applied using a syringe pump and the yarn is wind up on a roller.

4.3.2 Microstructure of CNTY and CNT wrapped textile yarns

To control the alignment and diameter of the produced yarns, spinning speeds, twisting location, and take-up speeds were kept constant. In other reports of CNT yarn spinning, the diameter of the twisted CNT yarn was 10 – 40 micron [111,222,223,181,102]. In our dry spinning process, the CNT yarn diameter obtained was ~191 microns. The controlled spinning and twisting during the wrapping of CNTs on cotton and polyester yarn allowed to get a uniform CNT wrap on the yarns (confirmed by the SEM images shown in Figure 2), making a CNT nano-fiber shell around

the cotton and polyester yarn. This uniformity in CNT-wrapping helps to achieve a higher cyclic loading performance without compromising the electrical conductivity.

The SEM images of the yarn surface before and after TPU binder application are presented in **Figure 4.2** and the corresponding cross-sections in **Figure S3**. It was found that CNTs were uniformly wrapped over the textile yarns as shown in **Figure S3**. TPU binder smoothed protruding CNT fibers on the yarn surfaces and densified the yarn, as shown in **Figure 4.2 b,d,f**. Yarns without TPU binder have more randomly aligned CNTs on the surface, as demonstrated in **Figure 4.2a** and the yarn microstructure reveals higher porosity than TPU coated yarn (**Figure S2**). However, after applying a small amount of TPU, the diameters and microstructures of CNT changed, as shown in **Figures S2 and 4.3a**. A few CNTs were still aligned in the cross direction (**Figure S2**), bridging the adjacent layers of CNTs and contributing to electron transfer within and between layers [224]. The acetone solvent evaporates quickly after application of the TPU solution and the capillary drying force brings the adjacent CNTs together which results in densified CNT structures. It is important to note that the densification process was uniform throughout the yarn structures and no localized densification was evident. After the densification of the yarns by twist and TPU, the yarns maintained a cylindrical shape which is essential for weaving and knitting. TPU assisted densification also affects the alignment and packing density of the yarns. The high-resolution SEM images (**Figure S2**) showed a reduction in waviness and misalignment of CNTs which also increases density of the CNTs' contact points. The higher packing density and increased contact points are vital for load transfer applications and should also affect mechanical performance, as discussed in the next section.

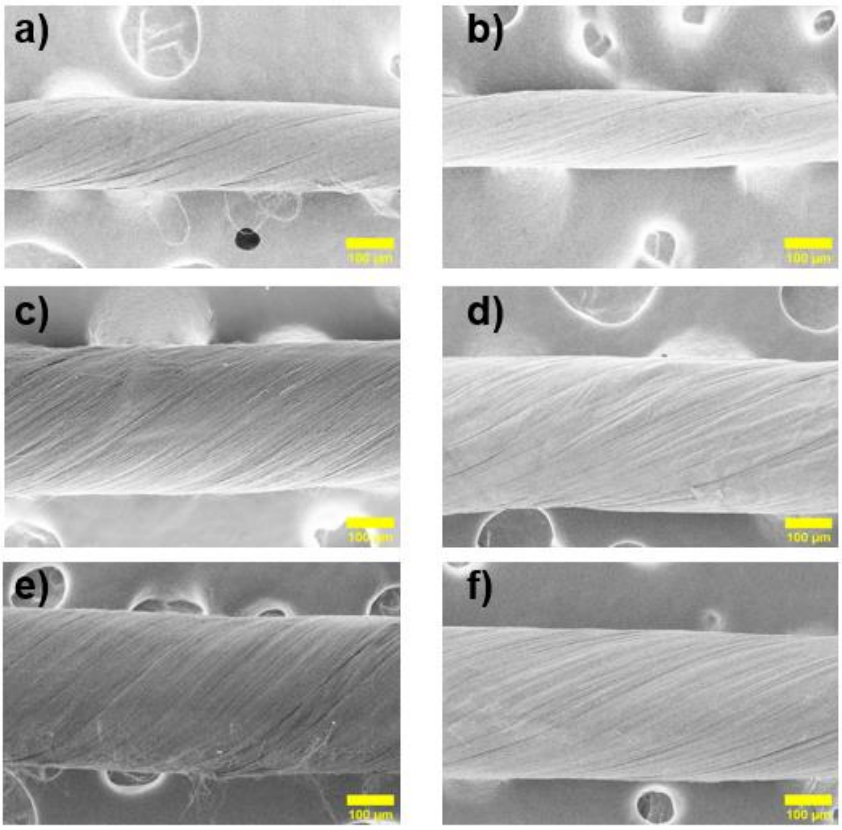

Figure 4. 2 Surface morphology of CNTY and CNT wrapped textile yarns.

Description: a) CNTY b) CNTY-TPU c) CNT-Cotton d) CNT-Cotton-TPU e) CNT-Poly f) CNT-Poly-TPU (scale bar 100 microns)

The TPU binder densifies the CNTY, made the yarn surface smooth, and the yarn diameter shrunk to ~163 microns (**Figure 4.3a**). The SEM images in **Figure 4.2** and **Figure S2** confirmed that TPU smoothed yarn surface with a higher packing density. The diameter and Tex count (gram weight per kilometer of yarn) of the yarns are shown in **Figure 4.3a**. CNT-poly has the maximum diameter due to the high linear density of the polyester yarn. It is important to note that the yarn count Tex increased after 1% TPU coating, whereas the yarn diameter decreased as expected. The diameter change is due to the liquid densification of CNTs which increases the mass per unit length of the yarn. However, the produced CNT-wrapped yarns are highly flexible and can be bent to any

degree essential for textile processing. A knot was inserted in CNT-TPU yarn to evaluate the flexibility and bendability and the SEM image is presented in **Figure 4.3d**.

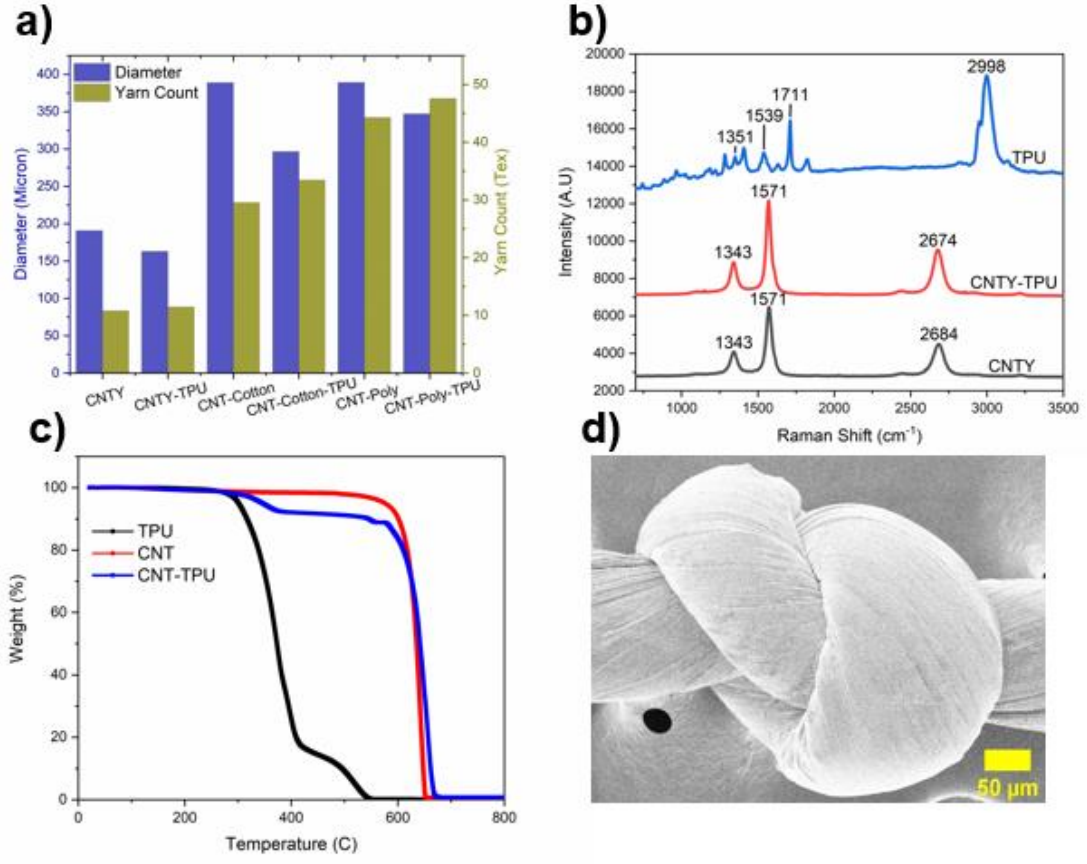

Figure 4. 3 Characterization of CNT yarns

Description: a) yarn diameter and count b) Raman and c) TGA of CNTY, TPU, and CNTY-TPU d) knot in CNT-TPU yarn

The Raman spectra of CNTY, CNTY-TPU, and TPU are illustrated in **Figure 4.3b**. The characteristic peaks of the CNTY were displayed, with a G' band at 2684 cm^{-1}, G band at 1571 cm^{-1}, and D band at 1343 cm^{-1}. These peaks were located on the CNTY-TPU sample at about the same position, suggesting no strong bonding interactions between the CNTY and TPU [225]. The G-band stems from stretching of sp^2 hybridized carbon atom or long chain and D-band is generated by structural defects or disorder (out of plane vibration of carbon atoms). The ratio of

the intensity of D/G peaks indicates the defects and/or geometrical orientation of the CNT structure [226]. A slight increase in ID/IG ratio of CNTY-TPU (0.35) from CNTY (0.34) demonstrates small changes in CNT orientation. The difference in ID/IG ratio might be due to the compaction of the CNTY structure after TPU infiltration as shown by SEM (**Figure S4**). The characteristic peaks of TPU at 1711 cm^{-1} correspond to C = O stretching and amide II and III urethane functional groups results in characteristic peaks at 1539 and 1351 cm^{-1}, respectively [227]. The characteristics Raman peaks of all yarns are presented in **Figure S4**.

The thermal analysis of the yarns tested in the air is shown in **Figure 4.3c**. Pristine CNTY demonstrated a higher onset degradation temperature than TPU and TPU coated CNTY. The first onset for TPU is between 286 and 303 °C due to the cleavage of urethane bonds and losses ~6% weight. Then the soft segment of TPU started to degrade, resulting in sharp weight losses and losses of around 85% weight at 433 °C before slowing down [228]. However, above 600 °C, the char residue of TPU reached below 1%. In contrast, CNTY was very stable up to 600 °C and lost only 10% weight. However, a sharp increase in decomposition was observed in CNTY and char residue was found to be around 5% at 650 °C indicating thermal oxidation of CNTY. The high decomposition temperature of CNTY contributed to the thermal stability of TPU and CNTY-TPU yarn exhibited improved thermal stability compared to pristine TPU and lost 5% weight at 346 °C and 10% at 545 °C. However, the addition of TPU shifted the 2nd onset of CNTY-TPU to 664 °C and retained 5% char residue. This might be due to the more compact structure of CNTY-TPU after the addition of TPU and oxygen takes longer to get into the structure, delaying the onset for a fixed temperature ramp rate. However, no significant impact was observed for the CNT-wrapped textile yarns when TPU was used, as shown in **Figure S5**.

4.3.3 Electromechanical behavior

The electrical behavior of the yarns is presented in **Figure 4.4a**. The electrical conductivity of MWCNT's is dependent on CNT yarn porosity [74]. When twist is applied, the empty spaces between CNTs bundle decreases rather than increasing the intertube connections. Therefore, specific electrical conductivity is more accurate than assuming CNT as a solid cylindrical yarn and the specific electrical conductivity was calculated using $\sigma_{sp} = \frac{l}{RT} \times 10^9$; where l is the length used for measurement of electrical resistance, R and T is the yarn linear density in Tex [74]. As shown in **Figure 4.4a**, CNTY has the maximum specific electrical conductivity of 2.78 x 10^8 S.m/tex. Yarn without TPU have comparatively higher specific electrical conductivity. CNT-Cotton yarn showed a 24% decrease in specific electrical conductivity, whereas a ~22% decrease was found for CNT-Poly yarn after TPU binder. However, the TPU binder did not significantly affect the CNTY, and showed less than 10% decrease in specific electrical conductivity. CNT-wrapped textile yarns have a higher diameter (**Figure 4.2a**) which might affect the alignment of CNTs resulting in lower electrical conductivity. Two CNTY were connected to a 12V LED bulb and power source. The yarn successfully transferred the power for 30 mins without any deterioration in the LED brightness, as illustrated in **Figure 4.4d** (left). The CNT-Cotton-TPU yarn was integrated into a wristband by sewing and connected in series with the LED (**Figure 4.4d, right**). When 3V was applied, a bright LED was observed, demonstrating the flexibility and mechanical robustness of the yarn. The electrical conductivity of the yarns against elastic modulus showed (Figure S7) that our yarn is more flexible than other yarns reported[229] and have better electrical conductivity.

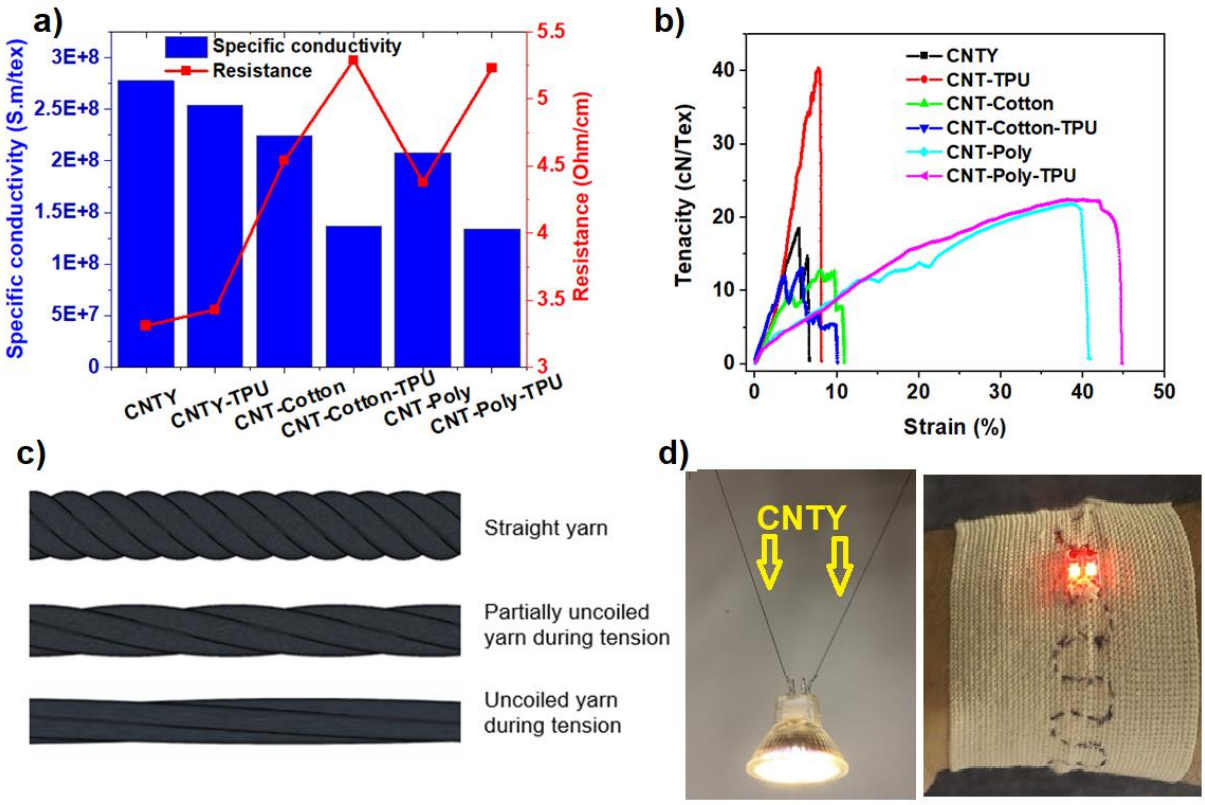

Figure 4. 4 Electromechanical behavior of yarns

Description: a) specific conductivity and resistance of the yarns b) tenacity vs. strain c) deformation of yarn during tension d) CNTY connected to 12V LED bulb e) CNT-Cotton-TPU yarn integrated into a wrist band and connected to LED

Individual CNTs have excellent mechanical properties, but the challenge is to translate the superior mechanical characteristics into macro assembled CNT structures like yarns [230]. Defects induced during the macroscale assembly and porous microstructure of CNTs negatively affect mechanical performance in the bulk. The properties of macroscopic CNTs are determined by the interactions between CNTs, unlike sp^2 C-C bonding within CNTs [231 84]. The typical tenacity-strain curves of different yarns are presented in **Figure 4.4b** and corresponding yarn deformation during tensioning in **Figure 4.4c**. Generally, the TPU coatings improved the tenacity and strain to failure

for all yarns and can be attributed to the reduced CNT waviness, improved directional alignment of CNTs and reduced porosity (**Figure S2**). Besides, TPU assisted in transferring the applied load. A dramatic change in CNTY tenacity was observed, and TPU coating resulted in a maximum 118% increase in CNTY tenacity. In contrast, the rest of the yarns did not exhibit a significant increase in tenacity after TPU coating. This might be due to the maximum densification of CNTY without core yarn making it stronger.

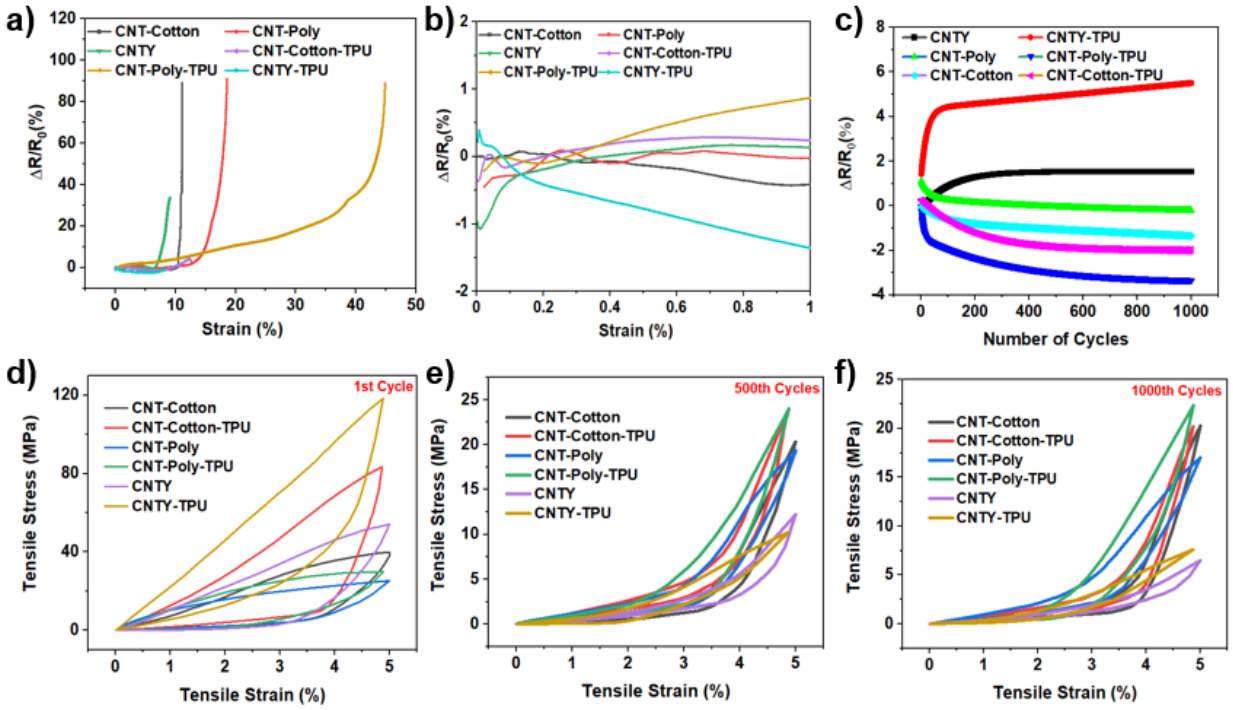

Figure 4. 5 Electromechanical characterizations of the yarns

Description: a) resistance vs strain of different yarns b) changes in resistance under 1% strain, c) changes of resistance vs number of cycles, cyclic stress-strain behavior of different yarns d) 1st cycle e) 500th cycle f) 1000th cycle

Additionally, TPU coating increased the extensibility of all yarns except CNT-Cotton. The maximum 10% increase in extensibility was found for CNT-Poly-TPU. However, CNT wrapped

polyester exhibited above 40% strain due to the inherent plastic behavior of polyester (**Figure S6**). This can be attributed to the wrapping of CNTs over polyester yarn. During the tensioning process, yarn was subjected to stress concentration resulting in necking before breakage. Besides, with the increase of tension, the yarn was uncoiled, and the diameter decreased gradually. The yarn was completely straight and uncoiled (**Figure 4.4c**) and the interconnection points dropped before failure.

CNT structures usually exhibit piezoresistance behavior, which is defined as a change in electrical resistance with applied strain. This behavior is essential to understand to be able to develop wearable body motion sensing garments. **Figure 4.5a** plots the relative changes in resistance against increasing strain, where ΔR is the resistance change and R_0 is the initial resistance. CNT-Poly-TPU showed the maximum extension before losing the electrical conductivity resulting in a sharp increase in resistance. While most of the yarns showed almost negligible changes in resistance until 1% strain (**Figure 4.5b**), CNT-TPU yarn showed a decrease in resistance. This is attributed to the electron hopping mechanism, where the inter-tube conductivity depends on the relative proximity of individual pairs of nanotubes. The TPU coating densified the CNTY and the inter-tube distances decreased with the increased packing density. Moreover, the applied tension might straighten the CNTs along the yarn axis and further increased the contact area between adjacent tubes, resulting in reduced resistance due to higher electron hopping [232]. In contrast, the rest of the yarn maintained stable resistance change under 1% strain. CNT-Poly-TPU yarn showed a maximum of 41% extension before losing the electrical conductivity much higher than the 5% limit of conventional metal strain gauges [139].

Cyclic stability performance was tested to evaluate the mechanical durability of the yarns. The conductive yarns must have excellent mechanical stability to sustain the abrasion, bending,

and twisting during the textile processing. The cyclic resistance change of the yarn for 1000 cycles at 5% strain is presented in **Figure 4.5c**. The results revealed two different resistance change patterns. CNTY without core yarn showed higher resistance change% regardless of TPU coating. This is due to the lower extensibility of the CNTY, as shown in Figure 5b. However, wrapping CNTs over traditional textiles improved the extensibility of the yarns. Therefore, CNTs wrapped yarns demonstrated a rapid decrease in resistance for ~30 cycles and remained stables for the rest of the cycles. The CNTs sheath is greatly affected by the initial tension and subsequently, uncoil and straighten by the tensions. Therefore, the sheath CNTY became parallel to the core yarn axis providing a robust electron conduction pathway. Further increasing the cycles does not influence the alignments of CNTs and exhibited almost constant resistance changes.

The cyclic stress-strain relationship of the yarns is depicted in **Figure 4.5 (d-f)**. All the yarns were subjected to 1000 cycles of tensile loading at 5% strain. The cyclic stress-strain curves demonstrated the anisotropy of CNTs. Likewise, the tenacity CNTY-TPU yarn showed remarkable maximum tensile stress of 118 MPa for the first cyclic loading (**Figure 4.5d**), compared to CNTY (cyclic tensile stress of 54 MPa). CNT yarn spun without core textile yarns are prone to successive cyclic loadings due to the major mechanical deformation caused after the first cycle. However, both yarns demonstrated well recoverable cyclic performance after the first cycle because the reversible fracturing of the CNTY absorbed the successive strain energy. The cyclic tensile stress of CNTY decreased 77% after 500 cycles (**Figure 4.5e**) and increasing to 1000 cycles resulted in a sharp decrease in tensile stress, down to 6 MPa. A similar reduction in tensile stress of CNTY-TPU yarn was also evident after 1000 cyclic loadings (**Figure 4.5f**). This might be due to the lower extensibility of pristine CNTs. Besides, the poor performance of the pristine CNTY was due to the uncoiling of the yarn during tension (**Figure 4.4c**). The application of successive loadings quickly

causes cracks in the uncoiled CNTs resulting in loss of tensile stress. However, the strong van der Waals attraction might facilitate some connection after the failure of CNTs. Therefore, the tensile stress did not go to zero, even breakage after the 1st cycle.

In contrast, CNT-wrapped textile yarns showed significant improvement in the cyclic stress-strain relationship. Unlike CNTY and CNTY-TPU yarns, CNT-Poly and CNT-Poly-TPU yarns exhibited excellent resistance to the cyclic loadings for 1000th cycles. Compared to all yarns, CNT-Poly and CNT-Poly-TPU retained their maximum tensile stress after 500th and 1000th cycles of loading. The tensile stress of CNT-Poly yarn decreased by 33% after 1000th cycles of loading whereas, TPU coating significantly improved the retention of tensile stress. The maximum tensile stress of CNT-Poly after TPU coating decreased only 10% after the 1000th cycle. The outstanding recoverability of the cyclic stress-strain was attributed to the synergistic stretchability of the core polyester yarn and TPU. This enhancement in the cyclic performance of the CNT-wrapped yarn is an excellent way of improving the mechanical performance of the rigid pristine CNTY.

4.3.4 Knitted body motion monitoring garment for wearable applications

Different knitted fabric was produced using seamless whole garment knitting machines to demonstrate a fully automatic next-generation wearable strain sensor. A typical knit structure is present in **Figure 4.6e** where the horizontal row of knit loops is known as ‘course,’ and the vertical column of loops is called ‘wales’. The interloping contacts are critical for the electrical conductivities of the knitted strain sensors and the interloping changes according to the knit architectures. The integration process of the developed yarn was completely automatic, and no cut-sew operation was performed. Unlike flexible polymeric thin film, knitted fabric is comfortable and the highly porous structures endow knitted fabric with excellent breathability suitable for continuous and long-term monitoring. Besides, the loops of knitted fabric undergo extreme deformation under tension and completely recover when relaxed making them highly flexible and

stretchable architectures. Due to these characteristics, knitted structures can conform to the curvilinear body shape and deformation/movement of the skin can be monitored directly and precisely. CNTY-TPU and CNT-Poly-TPU yarn were used to produce different knitted structures and seamlessly integrated without affecting aesthetics. The CNTY-TPU yarn feeding is shown in **Figure S8a,** along with the elastomeric polyester yarn. The different knit construction produced using circular and whole garment weft knitting machine is shown in **Figure S8b-e**. The high flexibility and sufficient stretchability of CNTs allowed excellent knittability of the yarns and no significant surface damage was evident. The knit structures are preferred for wearable applications due to their high structural deformability and breathability. The knit program used for seamless integration of CNT wrapped textile yarns are presented in **Figure S8f** and the movement of the front and back needle is shown in **Figure S8g.**

While jersey knits (**Figure S8b**) are the common knit structure used for regular T-shirt, whole garment knitting are state of the art for producing 3D structures. The seamless manufacturing process of whole garment knitting is the future of textile manufacturing which is the least labor-intensive and automatic. CNTY-TPU yarn was seamlessly integrated into a hand glove produced in the whole garment knitting process (**Figure S9a**) for real-time finger movement tracking. The black region of the hand glove contains the CNTY-TPU yarn, as shown in the inset of **Figure 4.6a-b**. Two ends of the index finger having knitted CNTY-TPU yarn were directly connected to a data acquisition device to record the changes in resistance induced by the deformation of the finger. The resistance changed significantly as the index finger deforms due to the slippage of knitted loops and changes in the contact area, as shown in **Figure 4.6(e-f)**. The intermittent movement of the finger was slow, showing resistance change in the range of 1.7-1.9%. Three repeated bending-releasing cycles were recorded for 200 sec. Alternatively, the continuous

movement was fast, and deformation was higher than the intermittent movement. The continuous movement of the finger exhibited distinctive and higher resistance change % (2.0 – 2.1). Moreover, eleven repeated bending-releasing cycles were recorded for 200 sec. However, a slight variation in resistance change was observed for both intermittent and continuous finger movement. This can be explained by the inconsistent bending-releasing angle of the index finger. The resistance change% for repeated bending-releasing cycles is completely reversible and can be translated to define the state of finger movement.

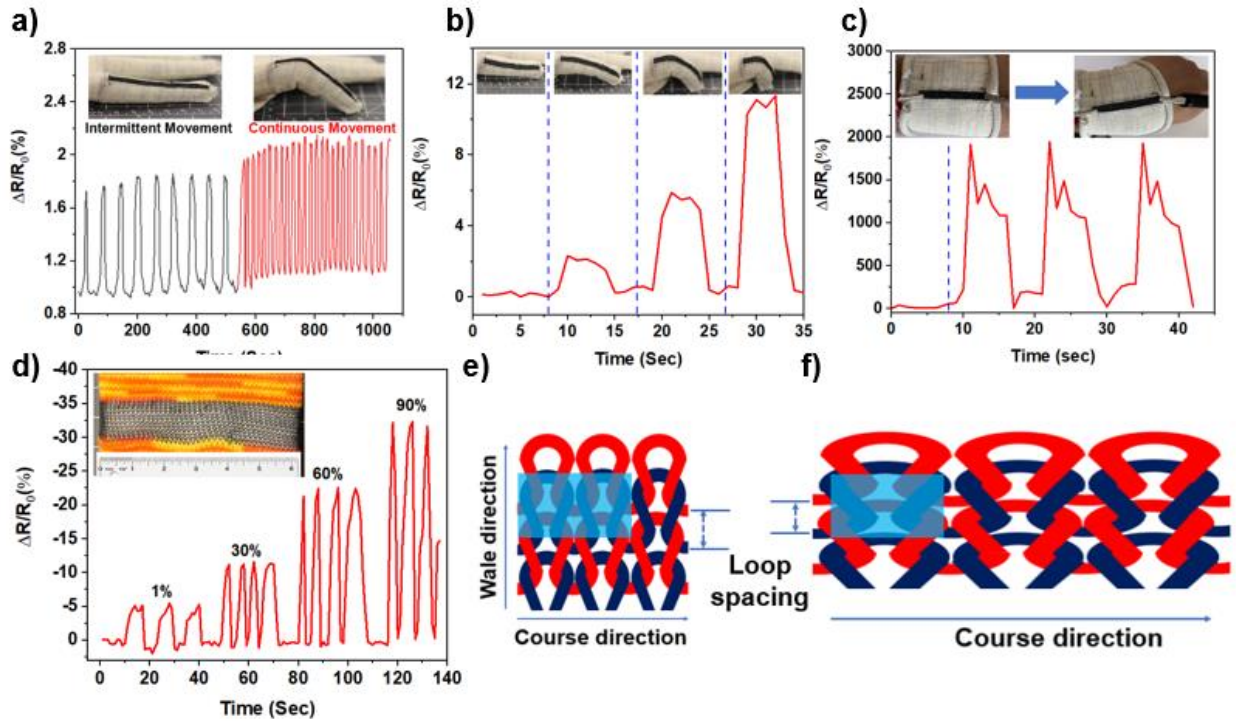

Figure 4. 6 Knitted structures for wearable body motion monitoring.

Description: Finger movement tracking a) continuous and intermittent movement b) finger bending motion at different angles c) wrist bending d) relative resistance change% against different cyclic strain of 1%, 30%, 60%, 90% e) schematic of knitted structure f) deformation of the knitted structure under strain

A wrist band was knitted to detect the wrist movement using CNT-Cotton-TPU yarn, as shown in **Figure S9b**. The directly knitted cylindrical wrist band can be easily fixed on the wrist without additional supports. The knitted band can detect and discriminate the wrist movement by causing a rise to the resistance change%. However, the wrist band was constructed in a rib structure where the face loop is connected alternatively to the back loop, making a stable knit structure. This knit structure is unsuitable for large-scale strain sensing due to the comparatively rigid and compact knit structure [233]. Interestingly, the compact knit structures demonstrate lower resistance and therefore, it is essential to program the required knit pattern for desired applications. **Figure 4.6d** shows the changes in resistance of CNTY-TPU jersey knit under different cyclic strains and the resistance change increased with the strain%. The jersey knit structure (**Figure 4.6e**) makes the fabric highly flexible and stretchable due to the higher loop spacing in course and wales directions. The result revealed that the loop spacing is higher before extending in course direction and the stretching caused a decrease in loop height and flattening of loops throughout the structure. Therefore, the change in the number of loop interconnections resulted in lower contact resistance (**Figure 4.6e,f**). The knitted sensor under different strain% demonstrated a significant relative resistance change and the jersey knitted structure exhibited a maximum of 90% extensibility. This value is much higher than the maximum extensibility range of human skin of 55% [234], which is the key to wearable body motion monitoring applications. With the strain%, the knit loops started to deform in the course direction (**Figure S10**) and decreased contact resistance per unit area (**Figure 4.6e,f**). Besides, the decrease in loop spacing placed the adjacent CNTY-TPU closer facilitating the electron hopping between the adjacent yarns. Therefore, the strain sensing mechanism of the jersey knit structure can be explained in terms of contact resistance and electron hopping. A

synergistic impact of decreased contact resistance and increased electron hopping resulted in a negative resistance change in the strain sensor at the maximum strained conditions.

4.3.5 Knitted garments for wearable Joule heating applications

CNTY and CNT-wrapped textile yarns possess good electrical conductivity and flexibility for wearable Joule heating applications. When voltage is applied to the conductive yarns, a collision occurs between the accelerated electrons and phonons, generating heat. The Joule heating behavior of the CNT-Poly-TPU knitted fabric was studied under the applied voltage ranges from 1 – 5 volts. The surface temperature distribution and the response of the samples were monitored and recorded by a FLIR infrared camera. The time-dependent temperature profile revealed that the knitted fabric instantly generates heat and uniform temperature morphology at the initial low voltage. The rapid heating and cooling profile of the knitted garment is illustrated in **Figure 4.7a**. As observed from the time-dependent temperature profile, the surface temperature of the CNT-Poly-TPU knitted fabric increased from room temperature to 36 °C, at 1 V in less than a minute. In general, the temporal response time of the knitted fabric was 0-80 sec. For example, when 3V was applied to the knitted fabric, the temperature exceeded the skin temperature within 5 seconds (39.8 °C). When the different constant voltages were applied to the knitted sample, the surface temperature immediately increased from ambient temperature to the respective elevated temperature within 20 seconds and gradually reached a steady-state condition. The driving voltage, response time and maximum heat generation of our Joule heater showed better performance compared to other reported Joule heater (Table S1). However, the cooling down of the knitted fabric is rapid initially but significantly influenced by the temperature raised. For better comparison, the power was disconnected at 80 seconds and cooling behavior was recorded until 160 seconds. The cooling behavior showed three distinctive patterns according to the applied voltages. For the voltage range of 1 – 3, the knitted fabric cooled down to the ambient temperature

after 35 seconds. In contrast, increasing voltage to 4 and 5, the fabric produced a very high heat of 111 and 155 °C respectively and cooled down to 37 and 43 °C after 75 seconds. Generally, the fabric showed increased heat-generating capacity with applied voltages, as shown in **Figure 4.7b**. The Joule heating effect resulted in red to yellow conversion depicting the electrochromic transition of knitted fabric under the different applied voltages.

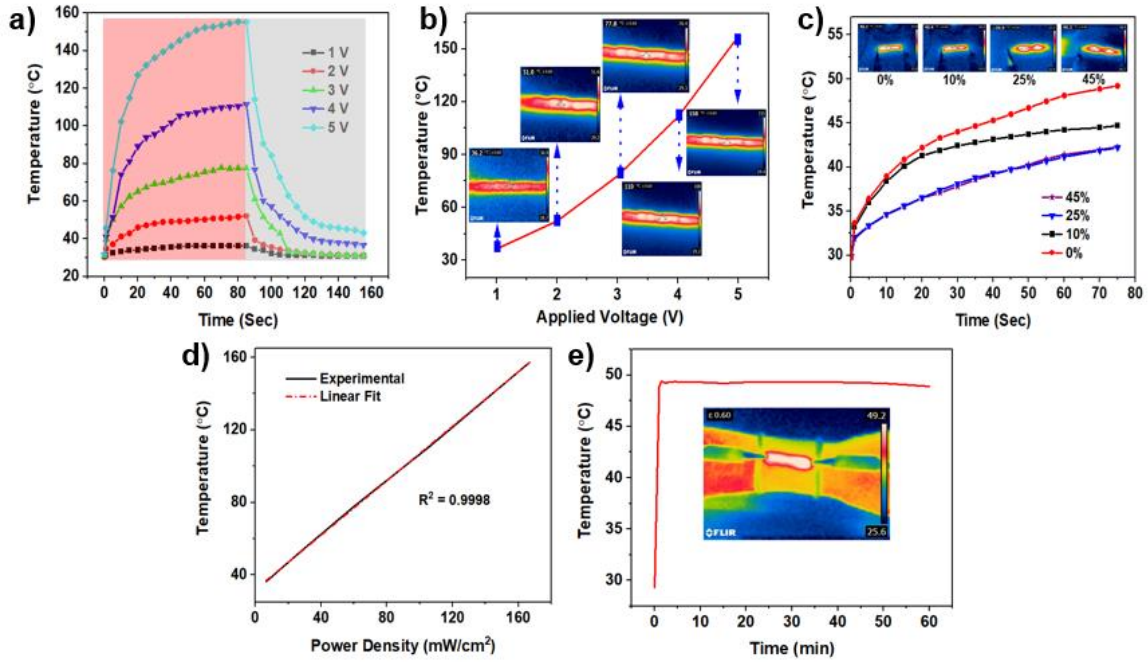

Figure 4. 7 Joule heating applications

Description: a) Time-dependent temperature profile of the knitted garments b) Surface temperature profiles as a function of applied voltages. Inset shows corresponding thermal images at different potentials c) Thermal behavior of knitted garments at different strain% d) power density of the knitted Joule heater e) thermal stability of the knitted Joule heater

A wrist band was knitted in Shima-Seiki 3D Whole garment knitting machine to analyze the wearable thermal stability under different applied strain%. The thermal stability against strain% is crucial for wearable Joule heating applications to meet the extension requirement

generated by the body movement. Generally, the human body undergoes strain% as low as 5% to 50% and the heating garment is expected to maintain stable heat under the strain range of the body parts. The application of different strains from 0 – 45% influenced the thermal stability of the knitted band, as presented in **Figure 4.7c**. The corresponding thermal images under 0 – 45% are shown in the inset taken at 30 seconds (**Figure 4.7c**). The knitted band generated a maximum of 49.2 °C temperature under the unstrained condition at 2V. When the knitted band strained to 10%, the maximum temperature dropped by 9% (44.7 °C). The knitted band demonstrated a lower temperature variation after 15% strain and remained remarkably stable. Straining the knitted band to 25%, the maximum surface temperature decreased by only 5.59% and no change in surface temperature was observed for 45% strain. It is important to note that different strain% affected the heat distribution morphologies (inset figures) and localized hot spot was produced. Heat localization might be due to the distortion of the knitted loop under strain resulting in contact variation of adjacent loops. In knitted fabric, the leg and head of the knitted loops are intermeshed except the side limbs leading to knitted structures highly porous. The porous geometries are greatly affected by straining the knitted structures. Thus, the heat distribution of the knitted band showed localized heat distribution. It can be further proved by the temperature profile of the knitted band under zero strain, as shown in **Figure 4.7e** (inset). The unstrained wearable knitted band showed a uniform temperature profile, and no hot point was observed. This was further validated by the thermal stability of the wrist band for an hour. The knitted wrist band was connected to 2V driving voltage and no temperature variation was observed for 60 minutes, as illustrated in **Figure 4.7e**. However, the thermal profile of the knitted fabric can be optimized by designing a more stable knit structure and preventing the knit loop slippage during the stretching. The temperature of the heater was plotted against power density and a linear relationship was observed (**Figure 4.7d**). The

excellent electrical and thermal conductivity of CNTs enables the knitted heater to convert electrical energy into thermal energy without any significant loss demonstrating the high efficiency of the heater.

4.3.6 Wash Durability

The washability of e-textiles is another crucial requirement for practical applications as wearable devices. The CNTY and CNTs wrapped textiles yarns were sewn into a woven fabric using an industrial sewing machine (**Figure S11**) and were subjected to simulated accelerated washing according to AATCC TM 61D standard without detergent. The surface morphology of the yarn before and after 30 washing cycles are presented in **Figure 4.8 (a-l)**. The application of TPU greatly influenced the wash durability of the yarn. TPU coating protected the yarn from surface damage by the steel ball compared to the yarn without TPU. The resistance change% of the yarn after different washing cycles is presented in **Figure 4.8m** and the resistance of the yarns in **Figure S12**. It was observed that the yarns were able to withstand friction between sewing needle and steel ball during sewing and washing. Though some surface damages were caused by the sharp edge of the sewing needle (**Figure 4.8a-l**), the resistance of the yarn did not change significantly in the successive washing cycles. However, two different patterns in resistance change were observed as presented in **Figure 4.8m**. After the 5 washing cycles, the resistance of the yarns increased except CNTY/TPU and CNT-Cotton-TPU. However, the resistance change% of CNTY decreased negatively after 25 washing cycles.

In contrast, CNT-Poly-TPU demonstrated a maximum increase in resistance % after ten washing cycles and plateaued before slightly dropping at 25 wash cycles. This can be attributed to the partial surface damage to the yarn (**Figure 4.8i-l**) after 10 washing cycles. Among the yarns, CNT-Poly yarn is thicker and might be subjected to more abrasion due to their higher diameter and experience more damage compared to other yarns. However, the wash durability of the yarns

was compared with two commercial silver-coated conductive yarns. While one commercial yarn lost its conductivity completely after five washing cycles (not shown in the figure), the other commercial yarns demonstrated similar resistance change% of CNT-Poly-TPU yarn. The different behavior of the yarns is due to the interaction between yarn and water/steel ball used during washing. Though CNTs are hydrophobic, the water molecules densify their microstructures resulting in changes in alignment and packing of CNTY [102] (**Figure S13**).

The increased packing density of the yarn resulted in an increase in the contact area between adjacent tubes and electron hopping, resulting in better electrical conductivity. The wash durability performance of the yarns was compared to the literature (**Table S2**). Most of the works presented in **Table S2** demonstrated wash stability for a maximum of 10 cycles with very high resistance change%. It is important to note that yarns developed in this study are completely washed durable for 30 washing cycles without significant changes in resistance%. The performance of the CNTY-TPU yarn as a Joule heater before and after washing is presented in **Figure 4.8n**. The yarn was sewn in a cotton fabric and washed following the same standard. There was no change in the heat-generating capacity of the yarn before and after washing was observed and it can readily produce heat when connected to 2V driving voltage. Therefore, this yarn could be used for producing highly wash-durable e-textiles and could be a potential solution to the washability problem of the existing e-textiles.

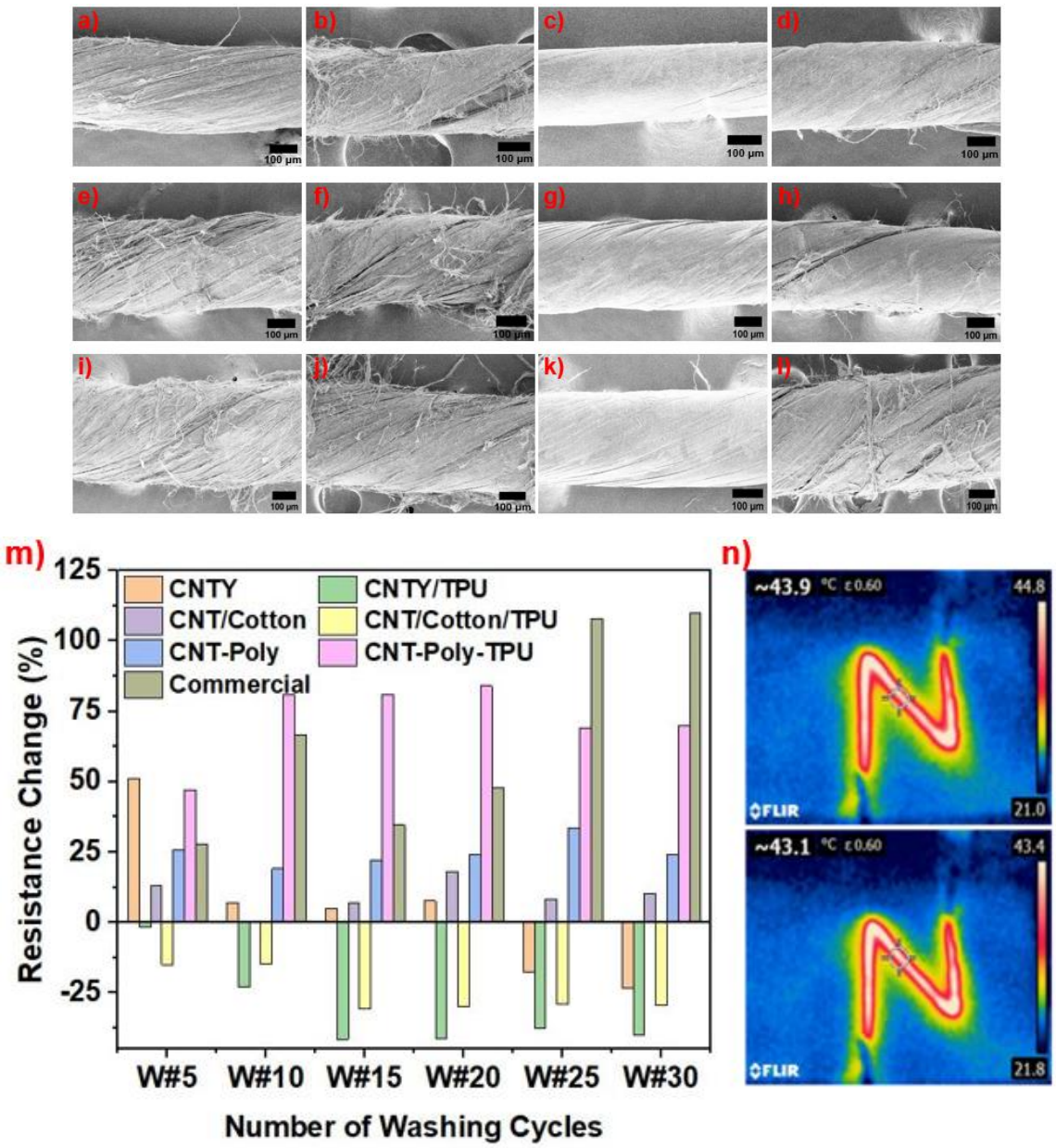

Figure 4. 8 Wash durability of the yarns

Description: CNTY a) before washing b) after washing, CNTY-TPU c) before washing d) after washing, CNT-Cotton e) before washing f) after washing, CNT-Cotton-TPU g) before washing h) after washing, CNT-Poly i) before washing j) after washing, CNT-Poly-TPU k) before washing l) after washing m) resistance change% of different yarns against multiple washing cycles n) Joule heating before and after washing (bottom right)

4.4 Conclusions

CNTs were successfully assembled into microscale yarn and wrapped over traditional textile yarns using a simple, single, and dry spinning method. The diameter of the produced yarn can be tuned by changing the core yarn and the densification process. The microscale CNTY and CNT-wrapped textile yarns have a similar diameter of textile yarn and are successfully knitted into textile structures without affecting aesthetics and breathability. While the small amount of TPU coating did not affect the electrical conductivity of CNTY significantly, the mechanical properties of the yarn increased remarkably. The CNTY and CNT-wrapped yarns showed excellent tenacity and flexibility to knit into different textile fabrics. The seamlessly 3D knitted glove demonstrated excellent piezoresistive response and reversibility under multiple bending-releasing cycles. The jersey knit structure can be extended beyond the maximum extensibility of the human skin. The wearable knitted wrist band exhibited rapid thermal heating behavior under low applied voltages and excellent thermal stability against a wide strain percentage. The yarn demonstrated exceptional wash durability for 30 washing cycles without significant change in resistance. The versatile spinning process developed in this process showed an outstanding possibility of CNTs into multifunctional and wearable electronic applications. Additionally, widen the scope of incorporating functional nanomaterials during the spinning or fabric conversion process for further applications in wearable energy storage, electromagnetic shielding, and soft robotics.

4.5 Supporting Information

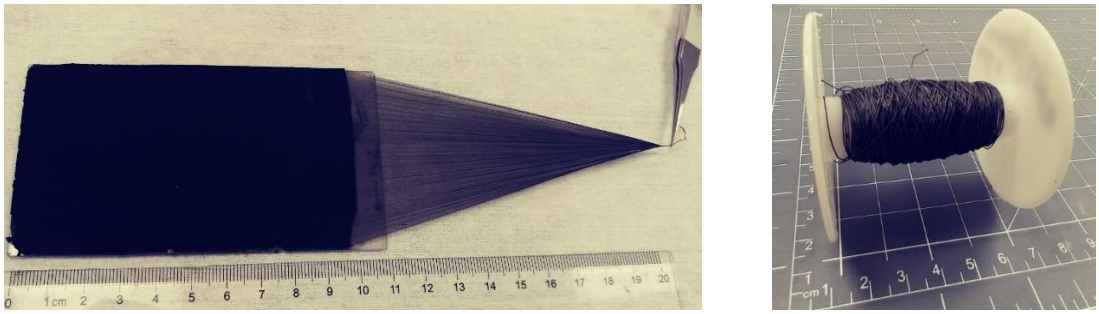

Figure S1: a) Spinnable CNT array b) yarn spool

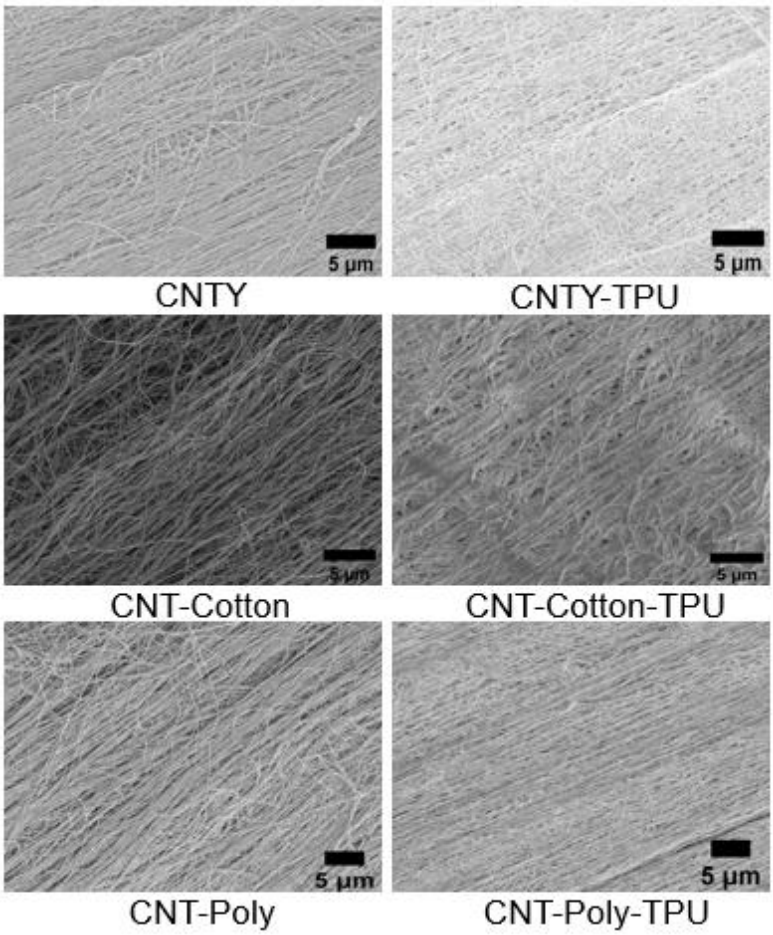

Figure S2: SEM of yarns before and after TPU coating

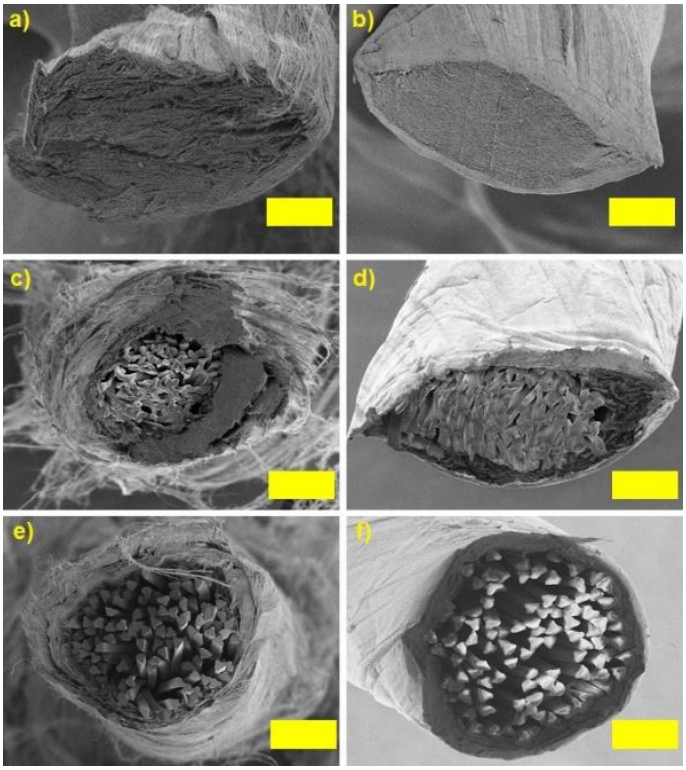

Figure S3: SEM of yarns cross-sections before and after TPU (scale bar 50 micron)

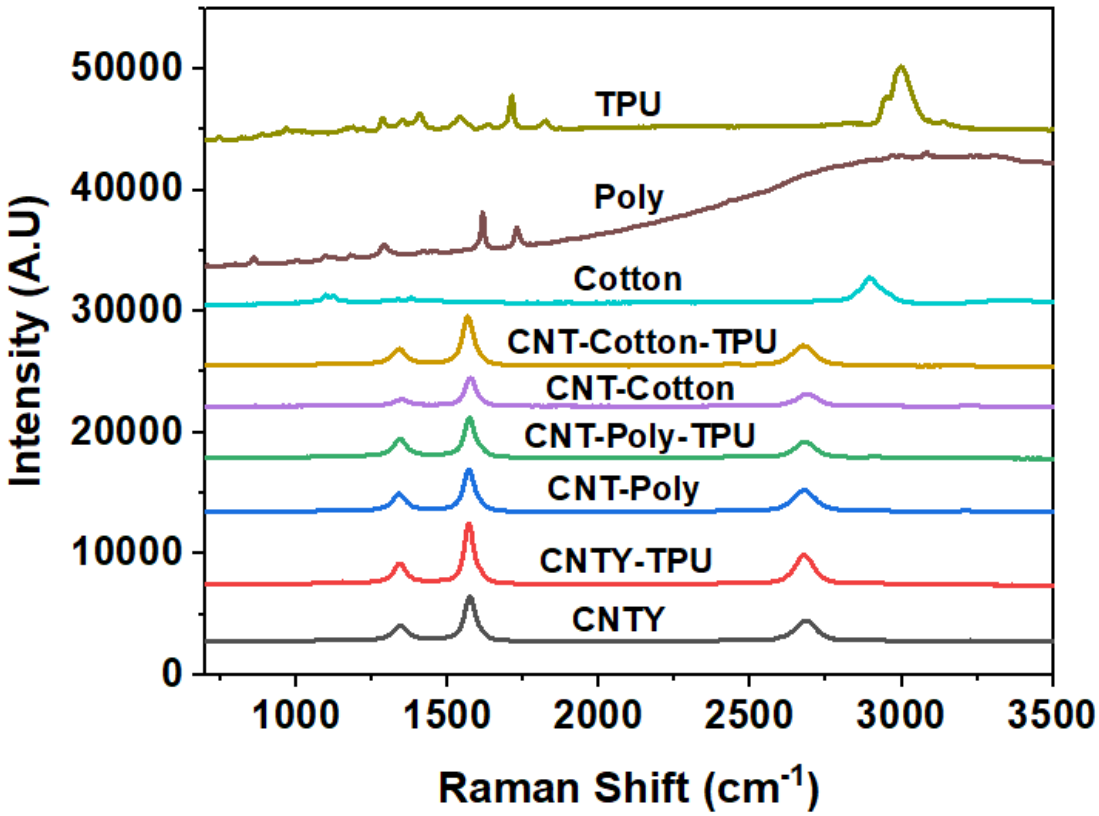

Figure S4: Raman spectra of different yarns

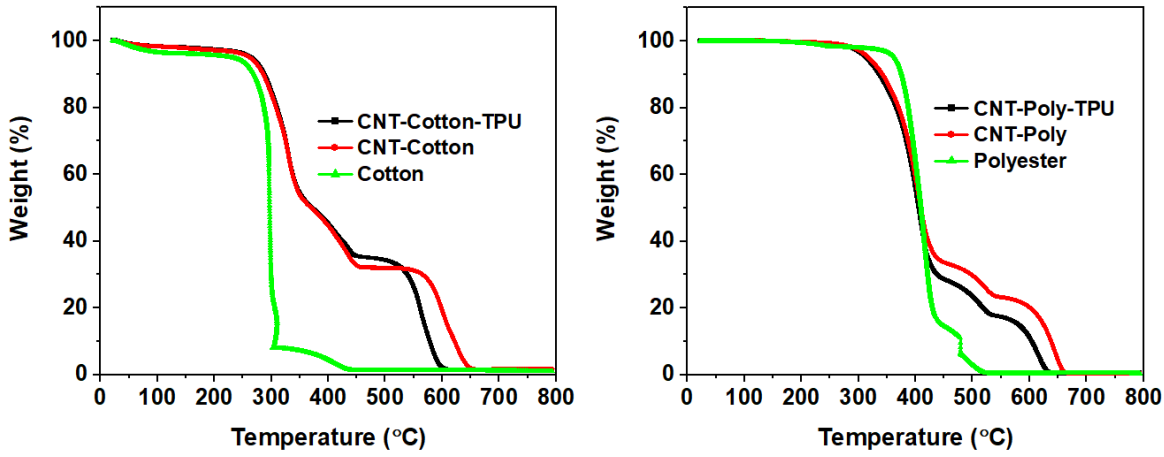

Figure S5: TGA of different yarns

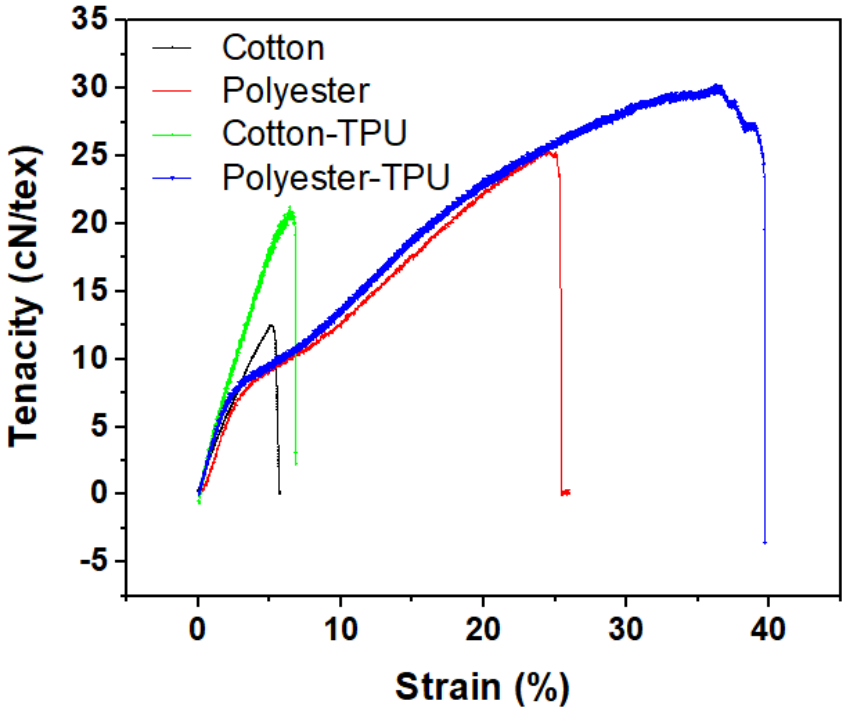

Figure S6: Tensile properties of yarns

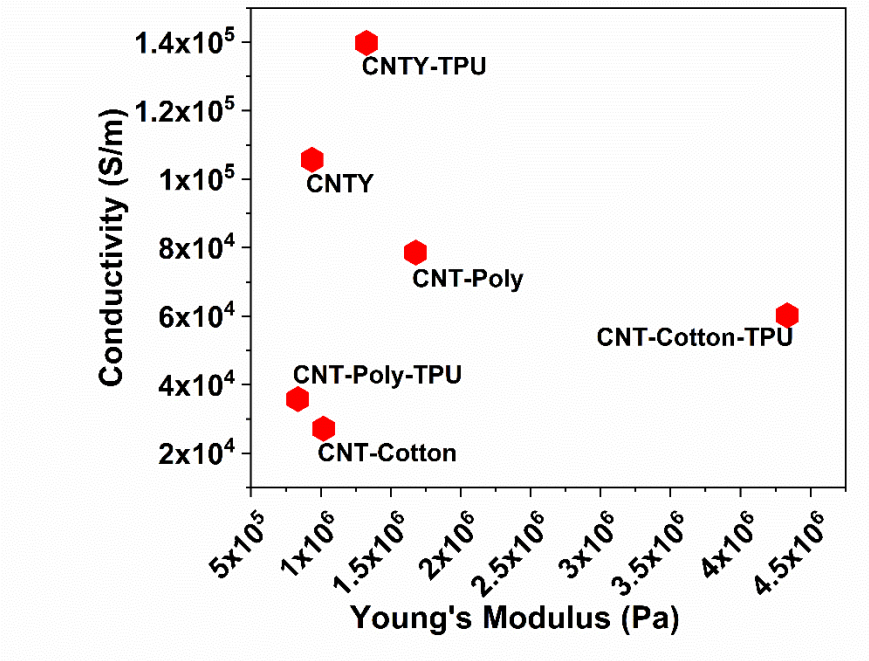

Figure S7: Electrical conductivity Vs modulus of elasticity

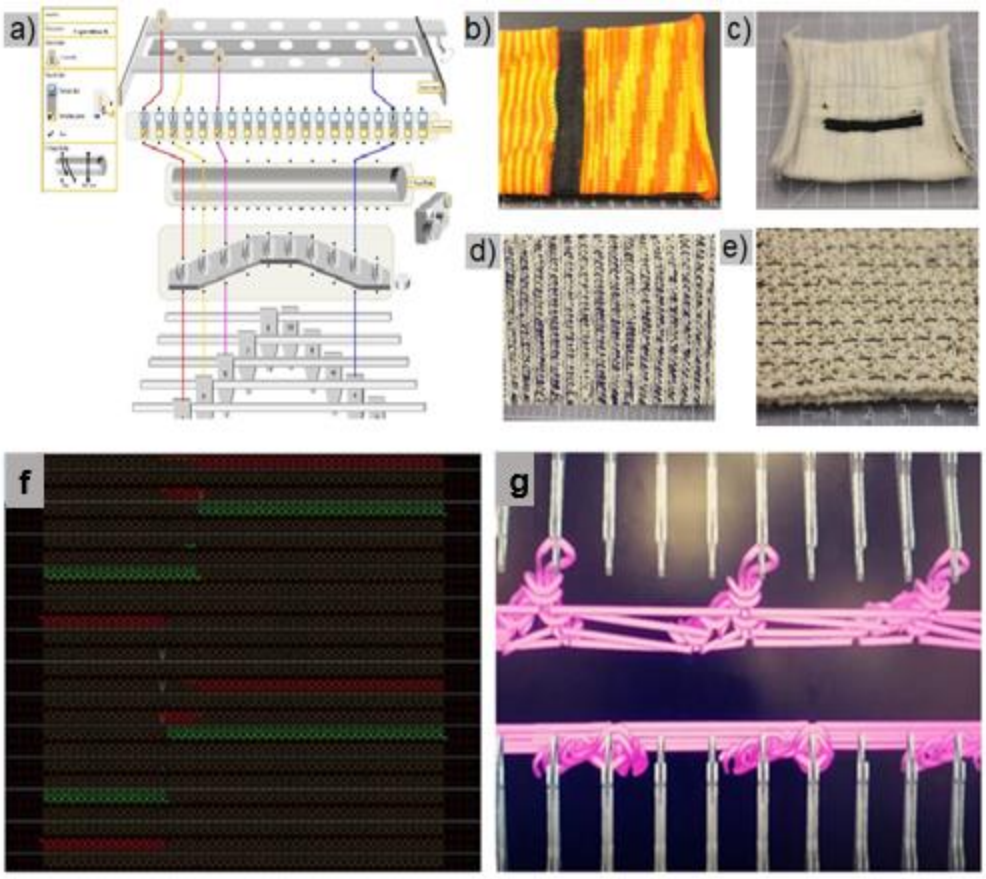

Figure S8: Schematic of CNT yarn feeding and different knit structure a) CNT yarn passing through the guide and a knitting needle (blue color) b) Jersey knit in circular knitting c) Jersey knit in whole garment knitting d) Rib structure with CNT yarn plating e) CNT yarn inlay f) knitting program used for seamless integration of CNT wrapped cotton yarn into hand gloves g) movement of front and back needle bar of the knitting machine

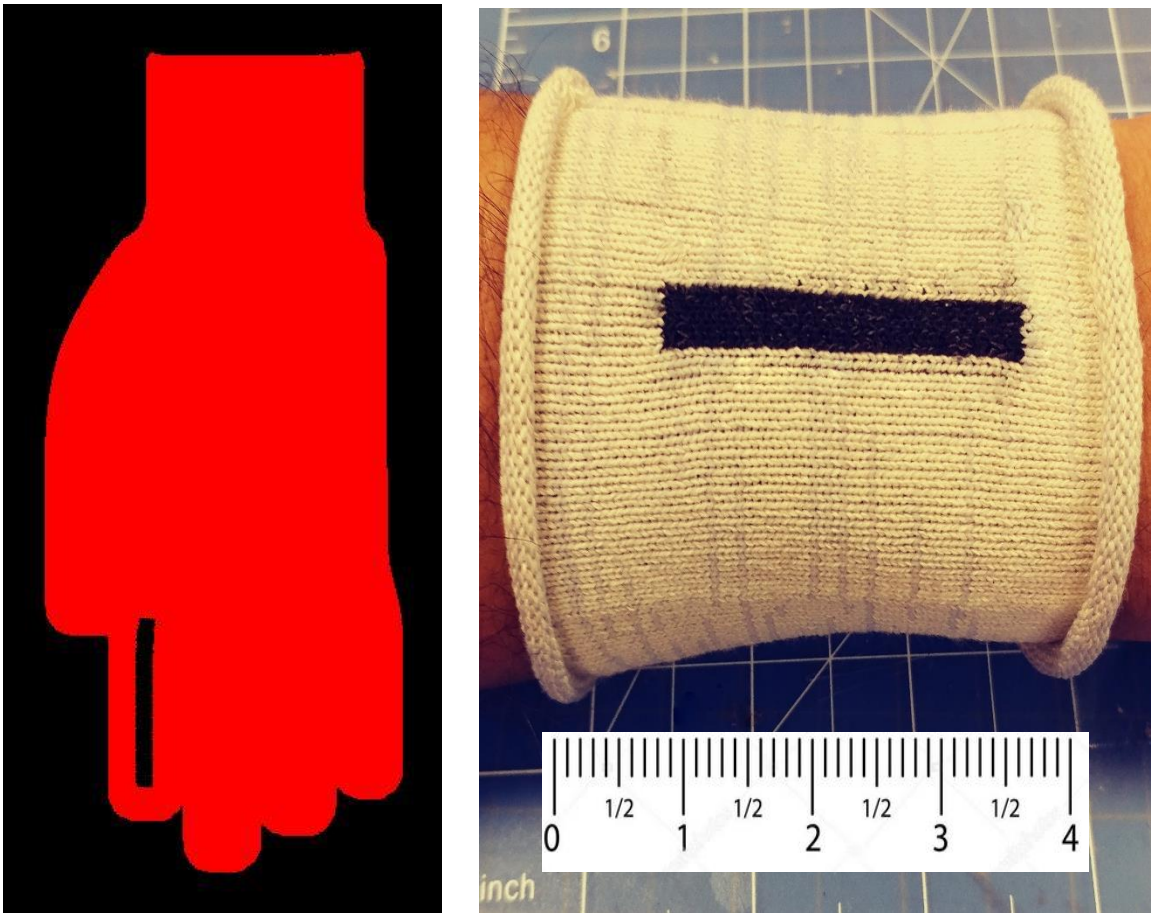

Figure S9: Seamless integration of the yarn using 3D whole garment knitting a) Simulation of the programmed hand gloves containing CNTY-TPU yarn (black region) b) Wrist band knitted on the 3D whole garment knitting machine

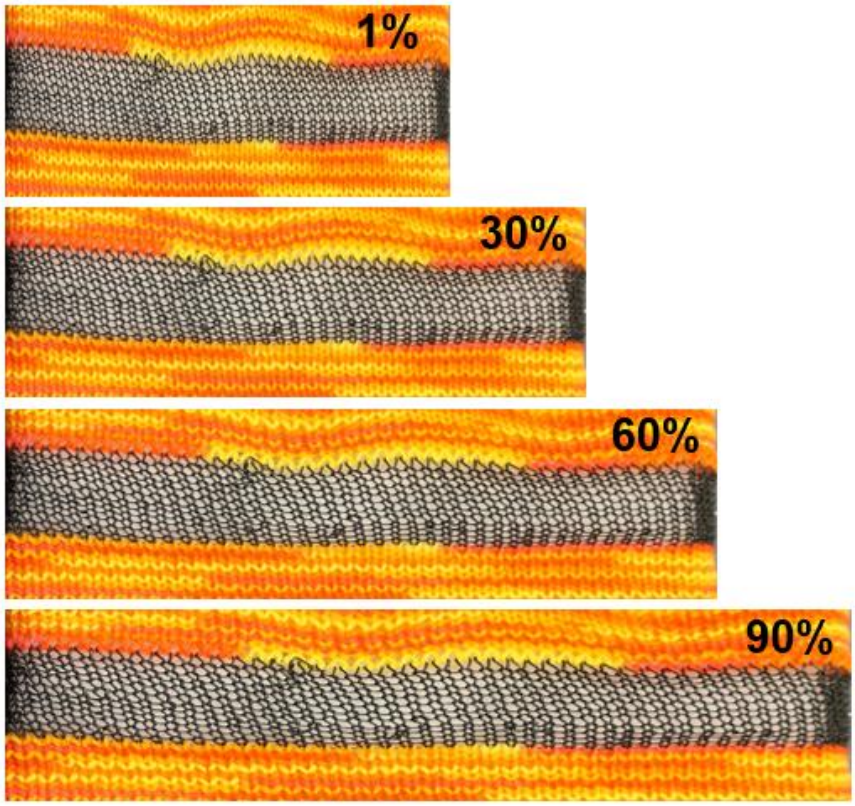

Figure S10: Single jersey knit fabric of CNT-Cotton yarn under various strain%

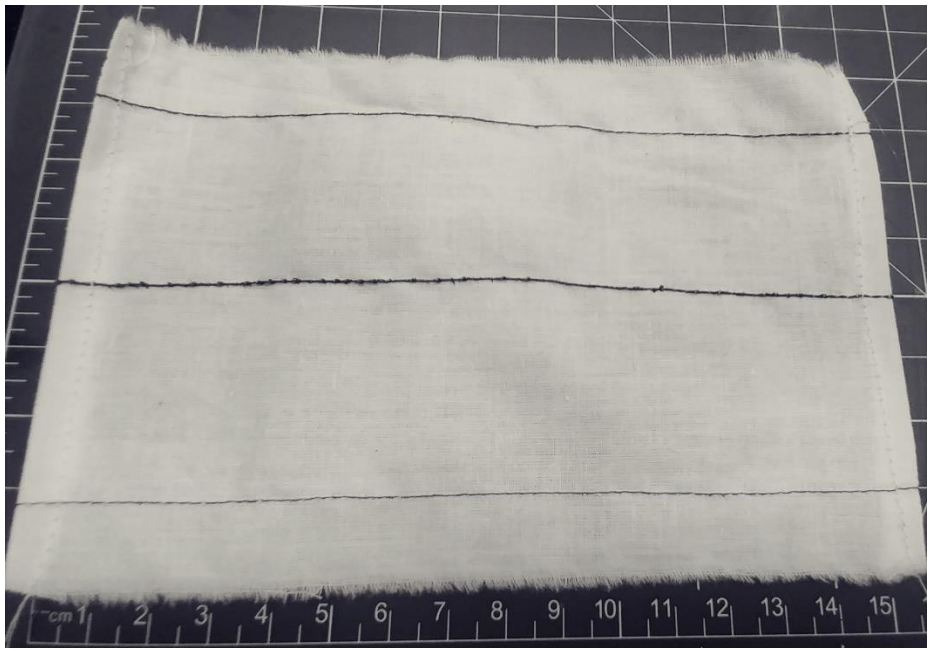

Figure S11: Yarns sewn into a woven fabric for washing

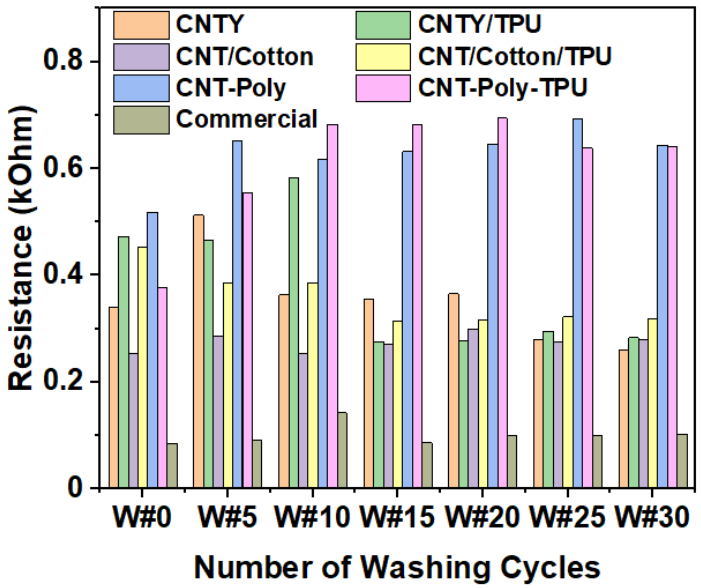

Figure S12: Resistance of yarns before and after different washing cycles

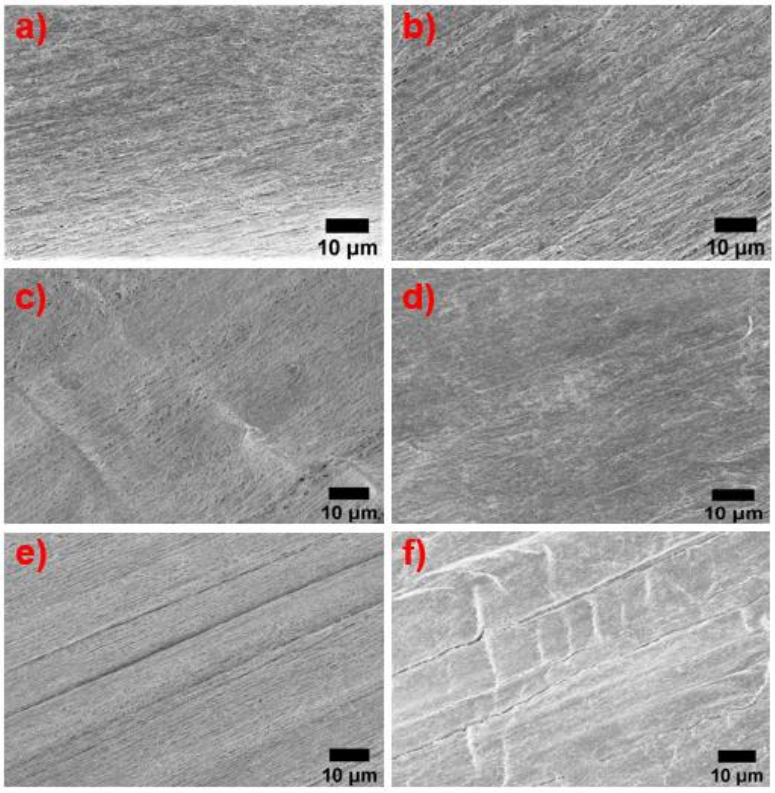

Figure S13: Morphology of the yarns before and after washing. Microstructural changes of CNTY-TPU a) before washing b) after washing, microstructural changes of CNT-Cotton-TPU c) before washing d) after washing, microstructural changes of CNT-Poly-TPU e) before washing f) after washing

Table S1: Comparison of Joule heating performance of different conductive materials

Textile Form Factor	**Electroactive materials**	**Specimen size(cm^2)**	**Driving voltage (V)**	**Response time (sec)**	**Max temperature (℃)**
CNT-Cotton Fabric	MWCNT	9 X 0.7	2 – 5	80	155 **This work**
Cotton fabric[235]	PEDOT:PSS, rGO	3 X 1	5 – 30	15-25	70
Cotton fabric[236]	AgNWs	2 X 2	1.5	20	42
Cotton fabric[237]	PEDOT, MXene	-	12	60	193
Polyamide fabric[238]	SWCNT	2.5 X 9	9	80	149
PET Nonwoven[239]	PPy	15 X 12.5	5 – 30	420	110
Cotton fabric[240]	PPy	-	3–9	60	48
PET fabric[241]	PPy, MXene	4 X 1	1–4	120	79
Cotton fabric[242]	PEDOT	2 X 1	6	20	44
Polyamide fabric[243]	PEDOT:PSS	7 X 6	12	60	64
Cotton fabric[244]	PEDOT:PSS	-	6–12	60	99.6
Cotton fabric[245]	AgNWs	2.54 X 2.54	0.9	300	38
Cotton-nylon-spandex fabric[246]	Ag	-	10	300	119
Aramid fabric (knit)[247]	Graphene	2.54 X 2.54	10–50	250	32
PET fabric (non-woven)[248]	rGO	20 X 20	32.5	600	36
PET/PU Nonwoven[249]	rGO	5 X 5	15–30	400	59

Cotton/elastic rubber[250]	PPy	4 X 2	2–8	120	118
Cotton fiber[251]	CNT, PPy	12	3.5	16	75
Knitted cotton fabric[252]	SWCNT	1 X 3	5–20	120	78
Cotton fabric[253]	SWCNT	1 X 2	10–40	100	96
Airlaid paper[254]	MXene,	2.5 X 2.5	1–4	40	118
PET fabric [255]	MXene	2 X 2	1–3.5	25	100

Table S2: Comparison of wash durability of different conductive materials

Materials	Structure	#wash	ΔR%	Ref
polybutylene terephthalate coated with carbon ink	Coiled helical	3	10	[256]
Cotton Fabric/rGO	2D Fabric	10	277	[257]
GO wrapped Cotton and Polyester yarn by self assembly	core-shell	10	-	[258]
rGO/Nylon/PU	2D Fabric	8	43	[259]
CNT/Cotton/Spandex	yarn	10	40	[260]
CNT printed on fabric	2D Fabric	10	25	[261]
Graphene/CNT/Cotton	2D Fabric	6	6-47%	[262]
CNT ink printed on Nylon/Spandex	2D Fabric	5	1220	[263]
graphene printed on fabric	2D Fabric	10	428	[264]
rGO/Silk Fibroin	electrospun Nonwoven	10	-	[265]
rGO	coated yarn	10	700	[266]
CNT Ink coated on yarn	coated yarn	10	-	[11]
CNT coated cotton	core-shell	8	30-730	[171]
CNT coated cotton	core-shell	10	30	[170]
CNTY and CNT wrapped textile yarns	core-shell	30	-41 -84	**This work**

Chapter 5: Adhesive free, self-tethered and Washable Carbon Nanotube Textile Electrodes for Biosensing

5.1 Introduction

Epidermal electronics have grown exponentially in the past decade with the advancement in miniaturized flexible and wearable bioelectronics. Such skin attachable electronics are widely used in biomedical applications, electrophysiological monitoring (electrocardiogram-ECG, electromyogram-EMG, electroencephalogram-EEG, etc.), human-computer interactions, augmented reality devices[267,268,269,270.] It is critical to record reliable and high-quality electrophysiological data for diagnosing nervous and cardiac systems[271]. Pregelled Ag/AgCl electrodes are the gold standard for clinical ECG recording[272],[273]. Despite their outstanding signal quality, the electrolyte gel dries over time and causes skin irritation restricting long-term application and short-circuit in high-density recording[274,275,276,277,278]. Therefore, soft dry electrodes emerged and exhibited improved wear comfort, reduction of skin irritation and long-term monitoring[279]. High motion artifacts, low signal-to-noise ratio and small area coverage limit the applications of dry electrodes[280], [281]. Besides, adhesive or straps are required for thicker film dry electrodes for reliable mounting on the skin[282]. In contrast, mechanically soft, thin film fabricated by structural engineering of rigid materials are physically attached to the skin by van der Waals interaction or capillary. However, such physical attachments are not robust and debond from dynamic skin over time [283],[284]. Additionally, the rigidity of thin metals results in high noise during body movement[285].

Textiles are ubiquitous in quotidian life and being the closest layer to our body, they provide an ideal platform to develop sensing electrodes[286]. Textile-based electrodes can undergo severe deformations like twisting while providing ultra conformable and comfortable interface with the human skin. Besides, low bending stiffness and stretchability of textile electrodes enable

reliable electrical performances[287],[288]. Textile electrodes are skin-friendly and can be produced in a large scale using a conductive yarn by traditional knitting, weaving, embroidering and braiding process[289], [290]. Additionally, electroactive materials are deposited or electroplated, printed or coated on textiles to fabricate planar electrodes[291]. Advanced carbon materials, metallic nanoparticles and conductive polymers are widely used for fabricating textile electrodes[292],[285],. Among the carbon materials, carbon nanotubes (CNT) demonstrate a high aspect ratio, excellent mechanical properties, ultralight weight, good thermal and electrical properties[293], [294]. However, most of the electrodes fabricated using CNTs are composite film and lack breathability and comfort [295, 296, 297, 298, 299]. Recently, CNT thread electrodes were sewn into garments and exhibited comparable ECG signals to commercial electrodes[300]. However, the sewing process is not suitable for large area and bulk scale manufacturing compared to other textile processing. Therefore, the creation of a large area and seamless textile electrodes demands a new fabrication process.

Here, we offer a comprehensive solution to the large area, seamless, and high-fidelity electrodes by different textile designs and state-of-the-art manufacturing processes. We developed a textile processable yarn by wrapping CNTs over cotton and spandex yarn in a core-shell structure. The spandex core renders the yarn with high stretchability and ultra conformability to the skin providing high reliability against mechanical deformation and motion artifacts. No adhesive and tethering are required for our developed electrode to measure ECG and could be worn and washed like a regular textile. We demonstrated that the systematic design of the electrode will record comparable ECG signals of Ag/AgCl electrode in different body movement conditions.

5.2 Experimental

5.2.1 CNT Synthesis

MWCNTs were vertically grown on a quartz substrate using the catalytic chemical vapor deposition method. An average CNT diameter of ~ 30 ± 8 nm and length of ~1 mm was obtained. Iron II chloride (FeCl2) was used as the catalyst and acetylene as a precursor gas for CNTs. The arrays were grown at 760 °C and 5 Torr under acetylene (600 sccm), argon (400 sccm), and chlorine (2 sccm) flow. The growth process was continued for 20 min and chlorine was purged during the cool down. Detail about the synthesis process was reported in our previous works [301,302,303]. The vertical alignment of the CNTs enables continuous drawing into a yarn.

5.2.2 CNT wrapped textile yarn fabrication

The yarn spinning process was initiated by dragging a razor blade across one edge of the CNT array. Then these two aligned CNTs arrays were placed on a rectangular rotating cylinder opposite to each other. Next, two CNT sheets were pulled through a guide and wrapped together over a core cotton and spandex yarn. The linear density of the cotton and spandex yarn were 20 and 110 Tex (weight in grams per kilometers). The resultant single yarn has a CNT shell and cotton core which was continuously wounded on a cylinder. Next, a thermoplastic polyurethane (TPU, Desmocoll® 530, Bayer Material Science) solution (1%) dissolved in acetone was applied on the yarn surface at a rate of 0.3μL per min by a syringe pump. The yarn was then transferred to a spool for further processing and designing electrodes.

5.2.3 Designing biosensing electrodes

Different textile structures were produced using the CNT wrapped textile yarns. CNTs wrapped spandex yarn was used to produce three knitted braids with dimensions 6 x 0.03 inches denoted as CSP1, 6 x 0.011 inches denoted as CSP2 and 6 x 0.004 inches denoted as CSP3. Woven fabric of CNTs wrapped cotton yarns were used as weft yarn for producing woven fabric. Three

samples with different sizes are 7.1 cm^2 (CF1), 5.8 cm^2 (CF2) and 3.2 cm^2 (CF3) produced using a semi-automatic shuttle weaving machine. A plain woven (1/1) structure was produced with the construction of 80 x 60 warp and weft per inch. A seamless wristband was programmed and simulated in Shima Seiki's SDS-ONE Apex3 design system and knitted on a Shima Seiki SWG061N2 (15 gauge) Whole Garment flat knitting machine using the CNT-Cotton-TPU yarn. The knitting parameters were adjusted based on the design of the knit structure and the knitting speed was 0.8 m/s. The CNT-Cotton-TPU yarn was integrated continuously using an intarsia pattern, whereas the base yarn of the wrist band was cotton yarn.

5.2.4 Morphology of the electrodes

The yarn surface characteristics were measured using field emission scanning electron microscope (SEM) FEI Verios 460L at 2 kV beam voltage and 13 pA beam current. The diameter of the SEM images of the yarn was calculated by NIH Image J software. The surface images and topographic profile of the specimens were visualized through 3D laser scanning confocal microscope (Keyence, model VK-X1000).

5.2.5 Electrical impedance measurements

The electrical impedance of the specimens was determined using a Gamry Instruments Interface 1010 E. Data were obtained at a frequency sweep from 0.1 to 1000 Hz at a voltage of 10 mV. Three electrode configuration was used where 3M wet electrode (3M™ 2560 Red Dot™ ECG Electrodes) as a reference and counter electrode. The working electrodes were different textile structures containing CNTs. All electrodes were placed on the subject arm at 8 cm equilateral distance.

5.2.6 Electrocardiogram measurements

Electrocardiography data was recorded using BIOPAC MP 160 system at a sampling rate of 100 Hz using a 3-lead ECG. 3M™ 2560 Red Dot™ ECG electrode was used as a reference

electrode for the comparison with CNT textile electrodes. However, all three electrodes made from CNT textile were also used to compare with the control 3M™ 2560 Red Dot™ ECG electrode. The electrodes were placed on the lower left arm and upper and lower right arm for the measurement. The measurements of the CNT textile electrodes were taken without skin preparation. The obtained ECG data were analyzed and filtered using MATLAB R2021a software (Mathworks).

5.2.7 Washability testing

The textile electrodes CF1 and CSP 2 was used for washing according to the AATCC test standard TM 61-1A Test Method for Colorfastness to Laundering: Accelerated. The specimens were placed in a beaker with 200 ml water and 10 steel balls were added. The washing cycle was continued for 45 min at 40°C. After each washing cycle, the fabric containing CNT yarn was dried in the oven at 100ºC for 60 min.

5.3 Results and Discussion

5.3.1 Electrode fabrication and characterization

CNT wrapped cotton and spandex yarn was fabricated using the custom-built spinning device Figure 5.1a. First, two CNT arrays were mounted on the let-off zone of the spinning device. Core cotton and spandex yarns were inserted through the inner tube of the let-off cylinder. The core inserting inner tube has a diameter of 0.5 mm to accommodate a wide variety of textile yarns. To ensure smooth feeding of the core yarn, a spring tensioning system was used to control the tension. Besides, the let-off and take-up motor speeds were optimized to reduce the vibration during the spinning. Thus, a smooth wrapping of CNTs over the core yarn was confirmed. Then the vertically aligned CNTs were pulled using a tweezer and aligned horizontally along the yarn axis. The web-like CNTs sheets are then passed through a guide of the cylinder and densified into a ribbon (Figure S1). This ribbon-shaped fiber bundle has lower strength and binding force due to

the less fiber-fiber interaction[304]. The CNT ribbons are then wrapped over the core yarn and a twist is introduced during the wrapping process. The resultant yarn was a cylindrical shape with increased packing density induced by the twist. TPU binder was applied before collecting the yarn on a spool (Figure 5.1c). The CNT yarn produced from two arrays without TPU has a diameter of ~190 microns and the diameter of the CNT-Cotton-TPU and CNT-Spandex-TPU yarn were around 298 and 573 microns. The surface morphology of the yarns is presented in Figure 5.1d. Unlike other yarn fabrication processes, this innovative wrapping process eliminates the separate processing steps such as multiplying CNT yarn, densification etc. for textile processing [300],[305]. The linear density of the yarn increased significantly which is crucial for textile processing[306].

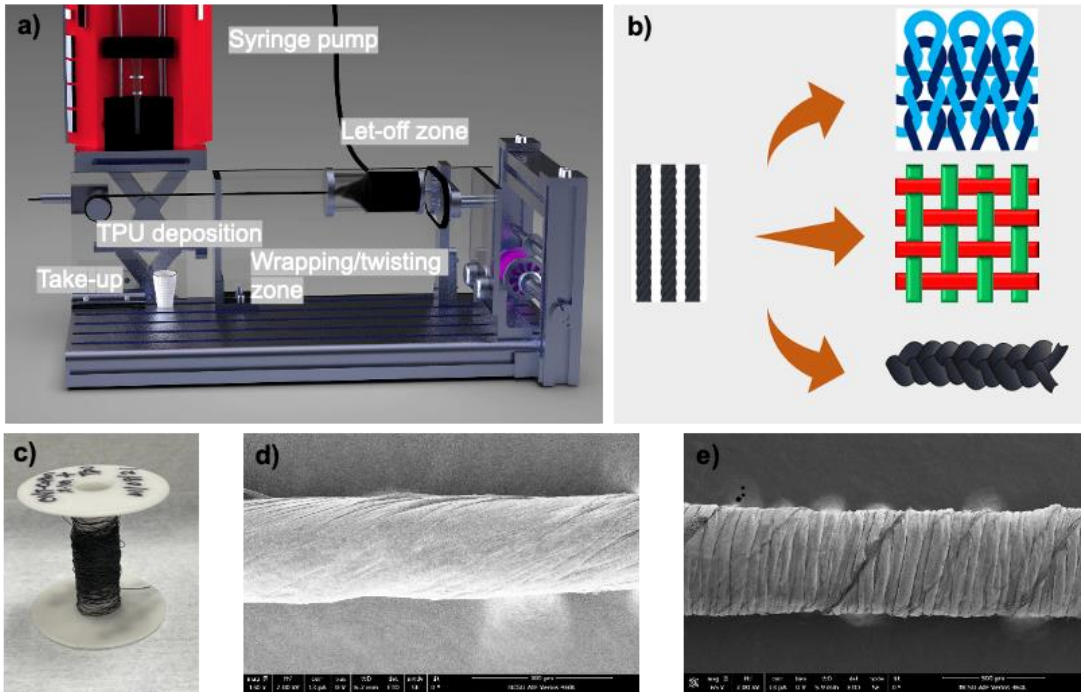

Figure 5. 1 Spinning of CNT yarn and design of ECG electrodes

Description: a) Schematic of the CNT wrapped textile yarn spinning system b) textile process for producing electrodes c) yarn collected on a spool d) SEM image of CNT-Cotton-TPU and e) CNT-Spandex-TPU

The yarn was used for producing different types of electrodes by weaving, knitting and braiding process Figure 5.1b. The geometry and surface characteristics of the different electrodes are presented in Figure 5.2. The woven fabric (Figure 5.2a,b) contains CNT-Cotton-TPU yarn in the horizontal direction known as weft and cotton yarn in warp/vertical direction known as warp. Three CNT-Spandex-TPU yarns were interlaced to produce a braided structure (Figure 5.2c,d). The intermeshing of loop called knitting is known for their superior conformability, comfort, stretchability and rapid prototyping[307], [308]. A rib-knit structure (Figure 5.2e,f) was chosen due to their high structural stability compared to jersey structure. The order of comfortability and wearability are knit>woven>braid structure according to the structural geometry and also affects the skin-electrodes contacts. The braid structures contain a highly stretchable spandex core allowing them to be stretched over 100% which is multiple times higher than the maximum body strain%. On the other hand, knit structures showed a stretchability of 70 % due to their structural geometry without a spandex core (Figure S2).

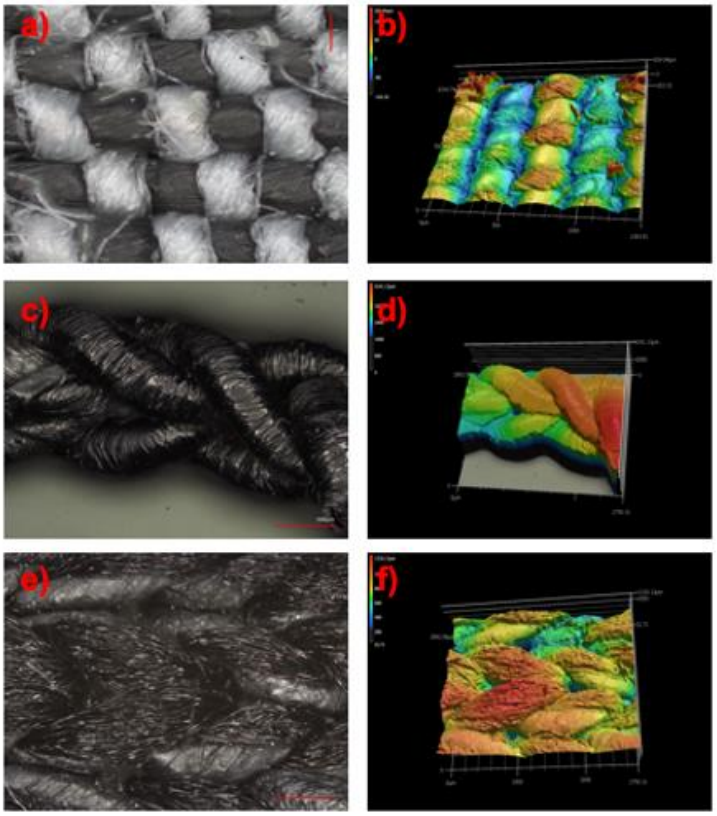

Figure 5. 2 Laser profiling of different electrodes

Description: a) Optical microscopic images (left) and laser profiling images of the electrodes (right) woven, braided and knitted structures b) braid structure and c) knit structure

5.3.2 Impedance behavior

The placement of electrodes for impedance measurement is presented in Figure 5.3a. The interfacial impedance between the skin and electrodes collected from the arm (Figure 5.3b). The impedance of the electrodes varies according to electrode design and sizes. The braided structures have lower skin-electrode impedance compared to woven structures and wrist bands. The knitted electrodes size has a significant impact on the skin-electrode impedance behavior whereas woven electrode sizes do not significantly affect the impedance. In case of woven electrodes, increasing the size does not reduce the impedance because the woven electrode contains insulating cotton yarn. Therefore, increasing electrode size results in more insulating cotton. The woven electrode

was coated with conductive polymer to make the insulating cotton conductive. Unlike woven electrodes, knit electrodes contain all CNT yarn and demonstrate a direct correlation between electrode size and impedance. With the higher electrode size (CSP3), skin-electrode contact impedance decreases as reported in other study[309], 267. However, the biosensing performance of the electrodes was not affected by the lower impedance compared to the 3M wet electrode. All the electrodes exhibited a decreasing trend in impedance with the frequencies. CSP1 electrode has the lowest impedance of 112 kΩ at 100 Hz better than the impedance of CNT yarn electrode[311]. Electrode size does not significantly affect the impedance for woven structure (Figure 5.3c). Changes in braided electrode size affect the impedance and decrease with the size (Figure 5.3d).

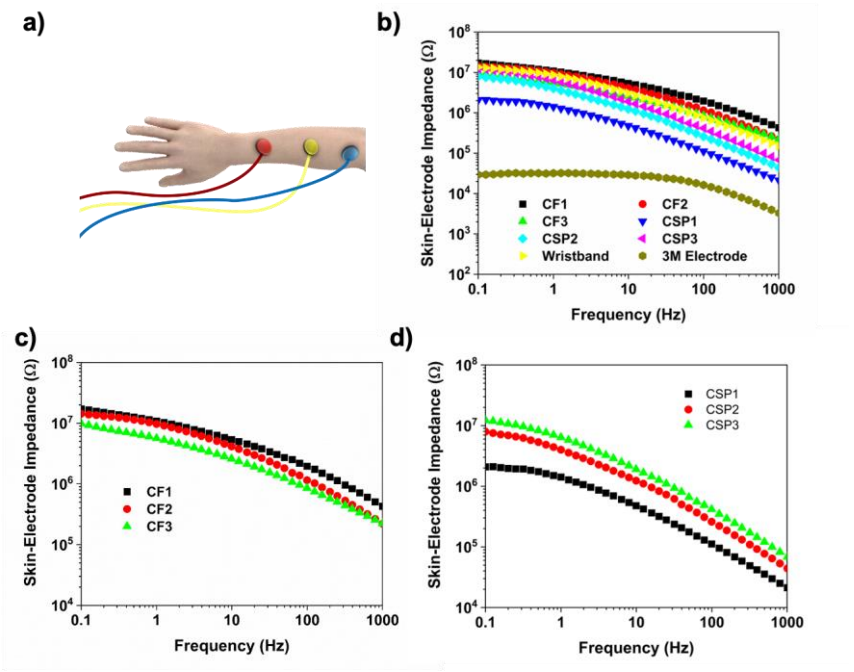

Figure 5. 3 Impedance behavior of the electrodes

Description: a) placement of electrodes for ECG recording b) Impedance of different electrodes impedance variations against different size of c) woven electrodes d) braided electrodes

5.3.3 ECG analysis and monitoring

Electrode design plays an important role in obtaining high-fidelity ECG signals from dry electrodes. Most of the dry electrodes suffer from motion artifacts and are susceptible to environmental conditions such as washing. The setup for ECG data recording is shown in Figure 5.4a where 3M electrode was used as the control sample. An extract of 10s from simultaneous ECG recording of different electrodes exhibited easily distinguishable P-QRS-T complexes (Figure S3). However, the peak amplitude was affected by the active electrode area. A comparison between the 3M electrode and CF3showed a similar ECG signal depicting the high quality of the designed CNT electrode (Figure 5.4b) and a similar result was also found for CSP1 (Figure S4). To further investigate the practical usability of the CNT electrode, the control 3M electrode was replaced with the designed CNT electrode and the recorded ECG signal is presented in Figure 5.4c. All three electrodes used are CSP2 electrode and the ECG signal retain high quality and is comparable to the 3M wet electrode. The comparable performance of CNT textile ECG electrodes is due to the better skin conformability of the electrodes. Skin adhesion force greatly influences the ECG signal quality[312]. Braided CSP electrodes were placed on the wrist as a bracelet, and it was in close contact with the skin enabling the electrode to capture high quality ECG data. Most of the dry electrodes are designed as a square/found flat shape which enables a small surface contact area due to the unevenness of the skin. As a result, the signal transferred from the skin does not completely pass through the electrodes. On the other hand, knitted fabrics are highly conformable to the skin than woven fabric and thus, knitted electrodes are expected to perform better than woven electrodes. While the ECG signal obtained by CNT textile electrodes is comparable to the 3M electrodes, CNT textile electrodes are advantageous because: CNT textile electrodes are reusable, and the signal quality does not degrade over time and has smaller electrochemical noise[313]. Unlike commercial 3M electrode, CNT textile electrodes are washable

and retain their performance after different washing cycles (Figure 5.6). Besides, the 3M electrodes are susceptible to mechanical bending and demonstrate lower performance[314]. It is important to note that, all the ECG data was recorded over 2 months using the CNT textile electrodes and the electrodes were subjected to severe folding and bending. However, all the data were consistent without any changes demonstrating their excellent resistance to regular handling of the CNT textile electrodes.

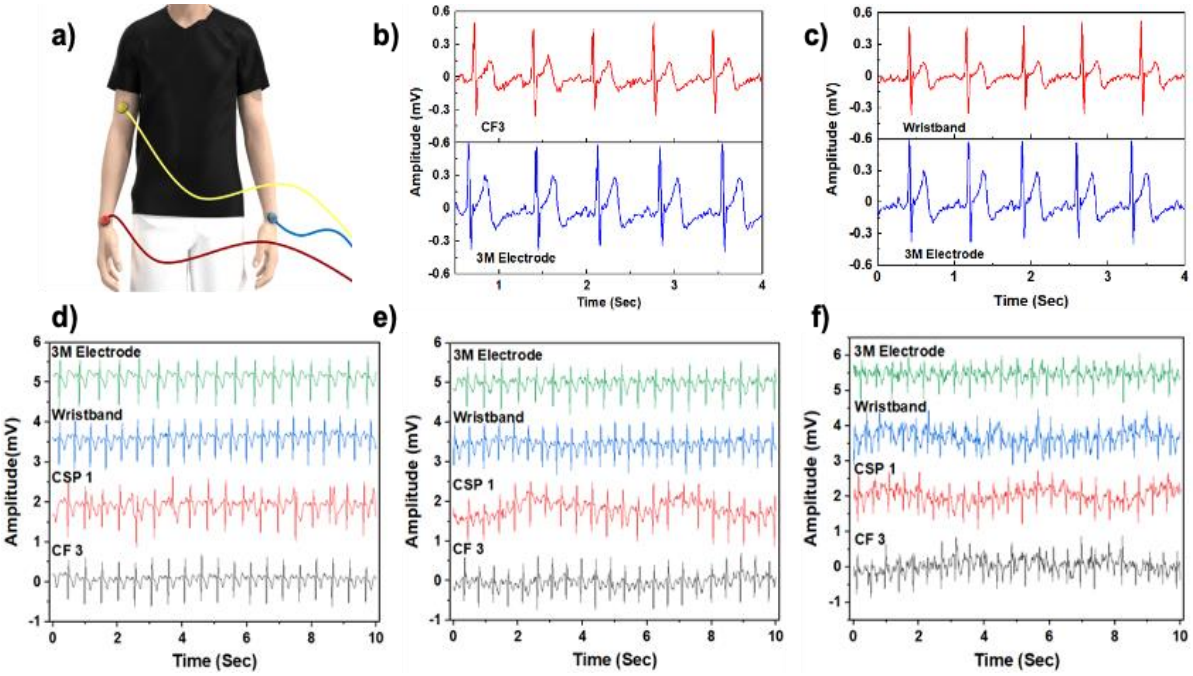

Figure 5. 4 ECG data recording and analysis

Description: a) Placement of electrodes for ECG recording b) comparison of ECG signals between CF3 (top) and commercial 3M electrode (bottom) c) ECG signals of all carbon braided wristband electrode and commercial 3M electrode. ECG signal at different body movement speed d) 2mph e) 4mph and f) 6mph

The signal-to-noise ratio (SNR) of the electrodes are presented in Figure 5.5a,b and compared with the commercial electrode. The SNR of electrodes is greatly affected by the electrode size and design. SNR decreases with the size of the woven electrode while increases for the braided electrode. This is due to the changes in the active electrode area per unit. Braid CSP1 is porous in structure while CSP3 is highly compact resulting in better electrical conductivity. On the other hand, CF3 has a lower active electrode per unit compared to CF1 resulting in a decrease in SNR. Despite their variation in SNR, they are indistinguishable compared to the SNR of 3M electrodes except CF3.

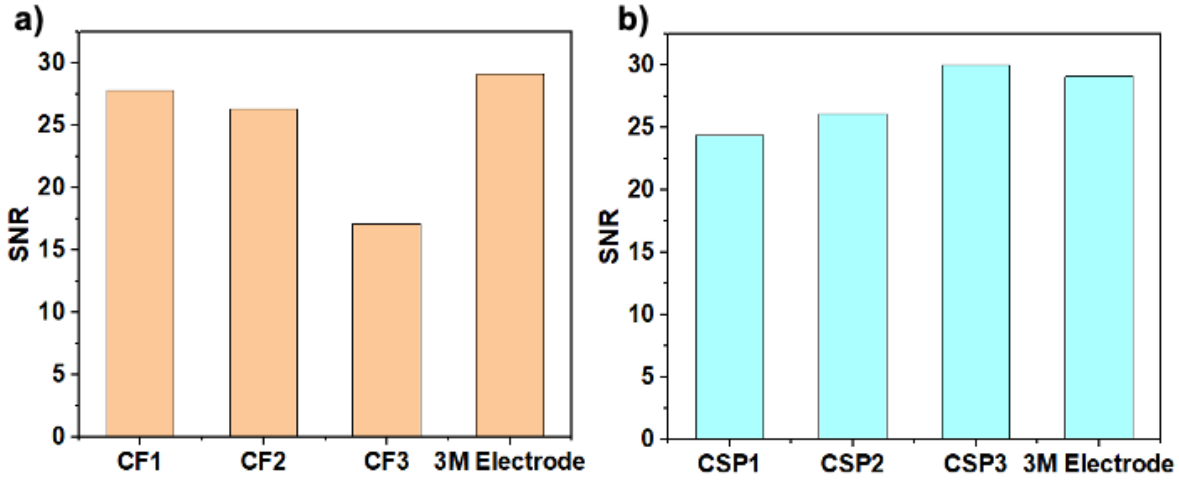

Figure 5. 5 Comparison of SNR of the electrodes

Description: a) SNR of woven electrodes b) SNR of braided electrode

The ECG recording of the electrodes were collected in three different body movement conditions walking at 2 mph, jogging at 4 mph and running at 6 mph (Figure 5.4d-f). The ECG waveforms are distinguishable during walking and jogging conditions. However, noise appears in the ECG signal and with the increase of movement, it becomes more prominent. Comparatively, CF3 and wristband demonstrated high stability against motion artifact than CSP1.

5.3.4 Wash durability of the electrodes

There are a large number of research demonstrated high signal quality using different materials. However, a few of them evaluated their wash durability. Wash durability is critical for long-term and sustainable application of ECG electrodes. The electrode was washed following AATCC TM 61A standard procedure and the comparative ECG signals are shown in Figure 5.6. The ECG signal after 5 washing cycles is very stable and there is no significant degradation was observed. All three electrodes demonstrated comparable ECG signals after washing. Though the signal amplitude after 10 washing decreased slightly, the waveforms are distinguishable. No significant change on the surface of the electrodes before and after washing was observed in the optical microscopic image (Figure S5). The change of electrical resistance after 25 washing cycles (Figure S6) showed no significant changes in resistance and depict the high durability of the electrodes for long term ECG data recording. The performance of different textile electrodes are compared and presented in Table S3.

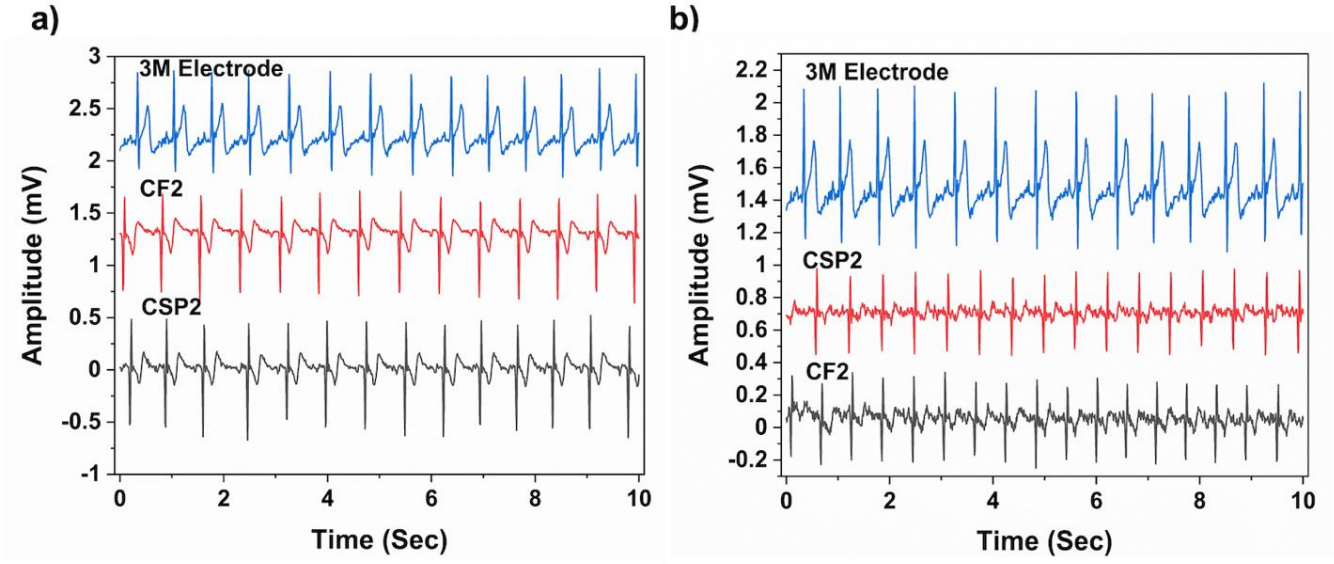

Figure 5. 6 ECG signals after washing a) 5 washing b) 10 washing

5.4 Conclusions

The different electrode has successfully been designed and shown their high-fidelity ECG signals comparable to the conventional wet electrode (3M Red Dot). Besides, SNR of the fabricated electrodes performs like the 3M electrode. The electrodes are highly conformable to the skin and can be produced in bulk using the existing textile processing method. The knitted wristband demonstrated highly advanced seamless fabrication without affecting the comfort and typical characteristics of textiles. This allows the electrode to be mounted on the skin as a regular textile for long-term monitoring. Finally, we showed the wash durability of the electrodes and their robustness to motion artifact.

5.5 Supporting Information

Figure S1: Optical microscopic image of CNT ribbon

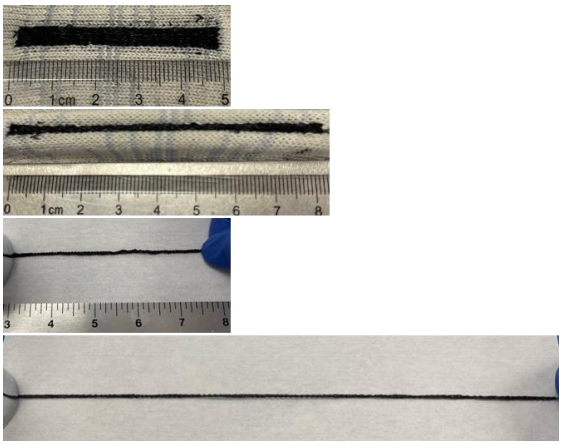

Figure S2: Stretchability of the knitted and braided electrodes

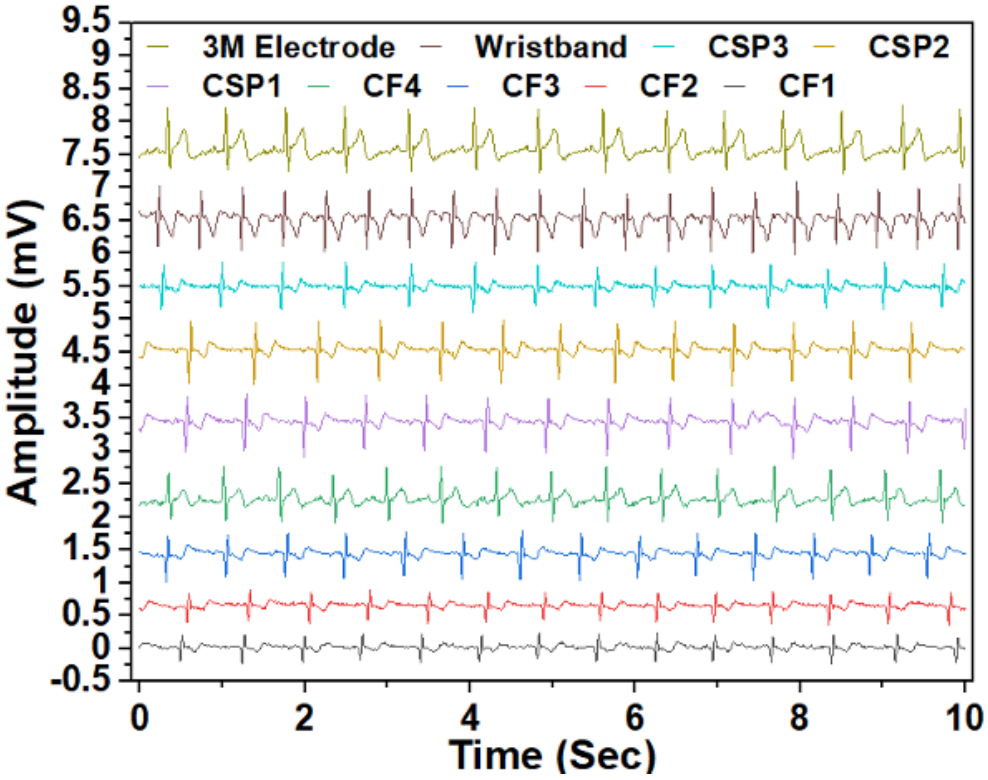

Figure S3: ECG recording of different electrodes

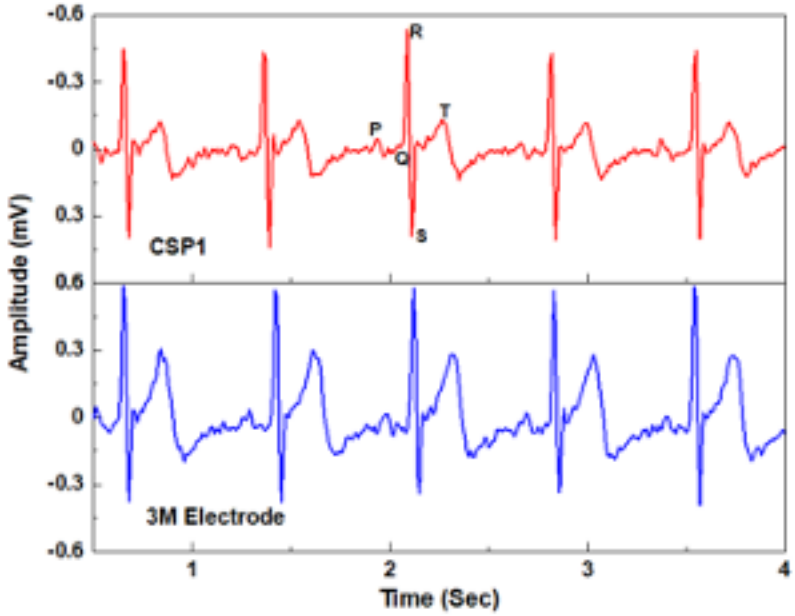

Figure S4: Comparison of ECG signal

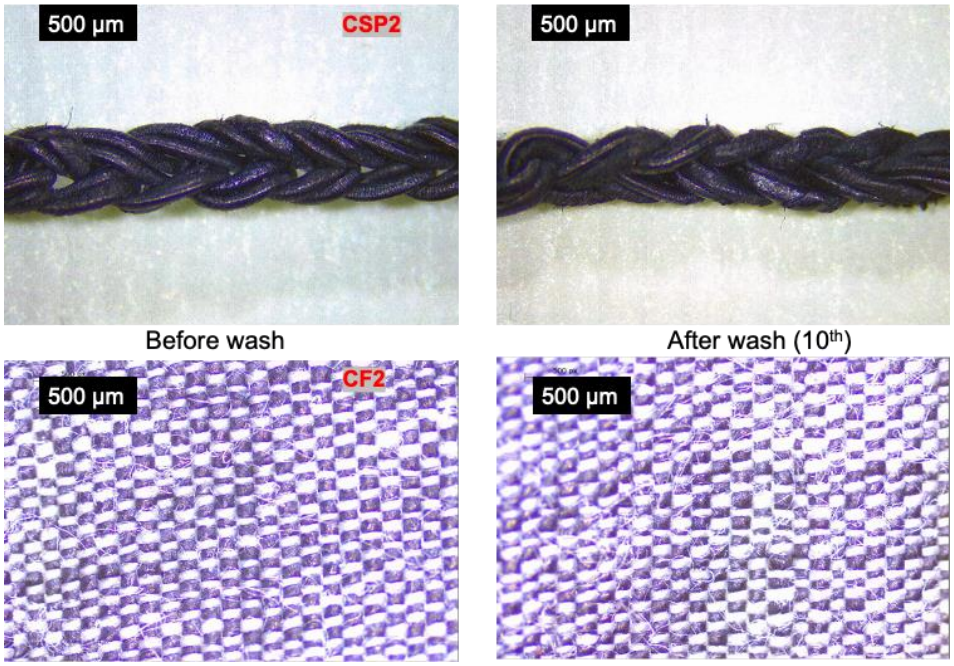

Figure S5: Optical microscope image of the electrodes before and after washing

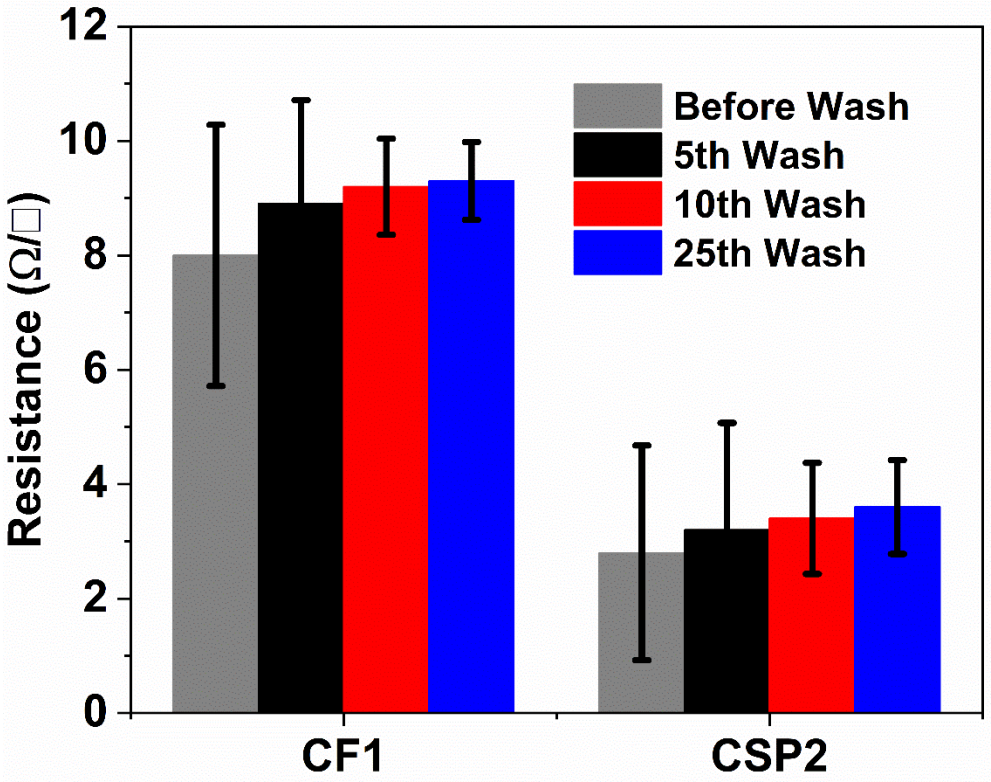

Figure S6: Electrical resistance change after washing (CF1= woven fabric, CSP2= braided fabric)

Table S3: Comparison of dry ECG electrodes and their wash durability

Textile Form Factor	Electrode Materials	Electrical Resistance/Conductivity	Impedance @100 HZ	Signal to noise ratio (dB)	Washability
CNT (woven, knitted, braided)	MWCNTs	1.8-22 Ω/Sq	112 kΩ	16-33	Insignificant change in resistance after 25 washing **This work**
CNT yarn[311]	CNT	6.6 MS/m	>10^6Ω	20-40	Insignificant change in resistance after 10 washing
Cotton fabric[315]	PEDOT:PSS	29 Ω	10^7Ω	-	Impedance increased by two times after 20 washing
PET fabric[316]	PEDOT	~10 Ω/sq	-	32.7	Resistance increased by 58-200% after 1st washing with detergent
Cotton/lycra fabric[317]	PEDOT:PSS	38.3 kΩ	-	27.7	Resistance increased by 3 orders of magnitude after 50 washing
PET fabric[318]	PEDOT:PSS, PDMS	230 Ω/sq	~10^4.5Ω	~16	NA
Cotton fabric[319]	rGO, PEDOT:PSS,	~45 to 190 kΩ	-	21.6	Resistance increased with the 20 washing cycles
Knitted fabric[320]	PEDOT:PSS and rGO	180KΩ to 120Ω	-	21.7	Resistance increased with the 10 washing cycles
Propylene nonwoven fabric[321]	Ag/AgCl ink		300 kΩ	17 – 29	NA
Cotton fabric[322]	Ag yarn	1.5-15 Ω/cm	70 kΩ	21.39	NA
Polypropylene fabric[309]	CNT, PU	380 S/cm	3.4×10^4 – 3.7×10^6 Ω	17.8	Decrease resistance after 20 wash cycles by 6.5%
Fabric (film)[323]	SWCNT/AgNWs/PU	9.4 Ω/cm	370 k Ω	-	NA
Nylon fabric*[324]	rGO		43 k Ω	-	Fairly stable after 5 washing
PET fabric[325]	MWCNT, PDMS	938.8mS/sq	~10^5 Ω	-	NA
Cotton fabric[326]	rGO	~9000 S/m	~10^5 Ω	14-32	NA
PET fabric[327]	Ag	~112Ω	-	~20	NA
Cotton fabric*[328]	Graphene ink	96 Ω/sq	10^5Ω	-	Resistance increases by 35% after 10 wash

*No washing standard was followed

Chapter 6: CNT-Cotton/MXene yarn for multifunctional electronic textiles applications

6.1 Introduction

Thin, lightweight, flexible and wearable electronics are poised to see exponential growth the in next decade. As such, electronic textile (e-textile) emerged and grew rapidly due to the multidisciplinary integration of materials with enhanced functionalities. E-textile with lower dimensions is advantageous because of high flexibility, skin conformability and processability into one-, two- and three-dimensional assemblies [329–332]. Therefore, one-dimensional fiber devices with micron diameter evolving as next-generation and portable electronic device systems. Most of the bulky two/three-dimensional devices are only resistant to unidirectional mechanical deformation for example tension and compression. In contrast, fiber devices are resistant to off-axis mechanical deformations such as bending, torsion, and pressure [333]. Electronic functionality added on or built on the fibers are attractive for various applications such as sensing[334], soft-robotics, electronic skin, and health monitoring[335]. Interestingly, these fiber devices could be self-powered by integrating energy harvesting with energy storage or by integrating energy devices with sensors[336,337]. Utilizing the functionality and ultra conformability of fiber devices, an intelligent system could be developed which can sense, actuate, communicate and harvest/store energy[338]. Generally, electroactive materials are used to impart functionalities to the insulating fibers and/or electroactive materials are directly spun into fibers[339]. Commonly used electroactive materials include conductive polymers, nanocarbon materials, metal nanoparticles/nanowires are integrated into textiles by coating, spraying, and printing[340]. These solution-based techniques have insufficient interfacial adhesion and thus performance degrades over time. On the other hand, fiber spun directly from nanocarbon materials like graphene and carbon nanotube (CNT) are advantageous because they have excellent mechanical, electrical and chemical properties. Besides,

they can be further processed into different fibrous assemblies using the knitting and weaving process.

CNTs demonstrate the best properties stem from strong covalent bonds between the carbon atom and unique atomistic structure. However, CNTs are required to be assembled in a macroscopic scale to utilize the outstanding axial properties[341]. The researcher developed different macrostructures of CNTs like CNT arrays, films and fibers[342]. Spinning strong and conductive fibers by solid-state and solution process from CNT have been reported[343–346] for various applications such as strain sensing[347–349], heating[350], electromagnetic shielding[351], electromechanical[352] and electrochemical[353] energy harvesting. However, this spun CNT fiber are mostly limited to a centimeter length scale and a few micron diameters which restrict their integration into textiles[354]. Besides, upscaling to the macroscopic level, CNT surface area decreases, and pure CNT has lower capacitance and energy density[355].

Different active and pseudo capacitance materials are incorporated into CNTs for improving performance. Transition metal carbide and nitrides, MXenes (e.g $Ti_3C_2T_x$) with high electrical conductivity demonstrated a great promise in different e-textile applications [354,356–359]. Different researchers modified CNT utilizing MXene and demonstrated improvement in performances. A remarkable improvement in capacitance was exhibited by high loading of MXene (up to ~97% wt) by trapping them inside CNT sheets using biscrolling technique[360–362]. Mechanical properties of the functional fiber produced by biscrolling process are often limited for textile processing and difficult to scale up. The high electrical conductivity and electrochemical performance of functional fiber do not necessarily correspond to the versatile manufacturability which is crucial for wearable e-textile applications[363]. Therefore, it is necessary to develop

functional fiber which has intrinsic properties of textiles while offering the required performance for wearable e-textile applications.

Here, we report an MXene modified CNT-Cotton multifunctional fiber for strain sensing and supercapacitor applications. A simultaneous and continuous single-step spinning system was developed to wrap CNT over cotton yarn and deposit MXene during the spinning process. MXene was drop casted in two different zones of the spinning process. First, MXene was deposited on the core cotton yarn and then on the CNT wrapped cotton yarn to increase the MXene loading percentage. The MXene modified yarn demonstrated improvement in electrical conductivity and mechanical properties. The strain sensing and supercapacitance behavior of the yarn was evaluated and significant improvement was observed.

6.2 Experimental

6.2.1 Synthesis of CNT

CNTs with an average CNT diameter of ~ 30 ± 8 nm and an average length of ~1 mm, were grown on quartz substrates via chemical vapor deposition (CVD) process using iron II chloride ($FeCl_2$, anhydrous 99.5% VWR) as the catalyst. Acetylene was used as a precursor gas for CNTs growth with a flow rate of 600 sccm and other gases chlorine and argon was flown at the rate of 2 and 400 sccm. The growth process was carried out for 20 min at 760 °C and 5 torr. CNTs growth on the quartz substrate is vertically aligned (VACNT) known as CNT array/forest. Then the CNT array was drawn initially using a razor blade and tweezer to initiate the spinning process. The thickness of a single CNT sheet is approximately 20 μm and density 0.002 g/cm^3 [364].

6.2.2 Synthesis of MXene

$Ti_3C_2T_x$ MXene were synthesized through etching of Ti_3AlC_2 (MAX phase) powders following MILD method[365]. Specifically, 2.4 g of LiF was dissolved in 30 mL of 9 M HCl. Then 1.5 g of Ti_3AlC_2 powders was added gradually into the above mixture solution and kept at room

temperature (~23°C) for 24 h while stirring. Afterward, the acidic suspension was washed with deionized (DI) water and then centrifuged until pH ≥ 6, followed by vacuum filtration and drying under vacuum to obtain multilayered $Ti_3C_2T_x$.

6.2.3 Spinning of CNT-Cotton-MXene Yarn

CNT-Cotton-MXene yarn was fabricated in a single step and continuously using a custom-built spinning device. Two large CNT array 11.6 x 6.1 cm^2 and a small array 8.08 x 2.54 cm^2 were placed on the spinning device. Then the core cotton yarn was inserted through tube and all of them are twisted together. At the twisting zone, MXene solution was drop casted on the cotton fiber using a syringe pump and another syringe pump was used to deposit MXene on the CNT wrapped cotton yarn. However, MXene was dissolved in acetone solution. The yarn was then collected on a yarn spool for characterization. Different percentage of MXene was loaded on the yarn. CNT-cotton without MXene is denoted as CCO, and CNT-Cotton with 40, 60, 75 and 85% MXene is denoted as CCM1, CCM2, CCM3 and CCM4.

6.2.4 Characterization of CNT-Cotton-MXene yarn

The surface morphology of the yarn was investigated using a field emission scanning electron microscope (SEM) FEI Verios 460L. The beam voltage was 2 kV and beam current 13 pA. No sputtering was done on the samples for SEM image acquisition. Thermogravimetric analysis (TGA) of the yarn was performed using Perkin Elmer Pyris 1 TGA with a heating rate at 10 °C/min in the air. The yarn was heated from ambient to 850 °C using 5-6 gm of each sample.

6.2.5 Electromechanical testing of CNT-Cotton-MXene yarn

A paper coupon was used to evaluate the electromechanical behavior of the yarn. The yarn was sandwiched between the paper coupon and conductive silver epoxy was used to connect a metal wire to connect a multimeter. A five measurements of electromechanical data were taken using MTS Criterion Model 43, and the average was reported. The gauge length was 40 mm and

the strain rate was 0.01 mm/s. The resistance of the yarn was evaluated using a 4 probe station and 1kg weight was applied for a better connection between the yarn and 4 probes lead.

6.2.6 Electrochemical performance characterizations

The electrochemical characterizations of the yarns were performed by an electrochemical workstation (Autolab, Metrohm, USA). Two fibers with a length of 2cm were placed 1 mm apart from each other and soaked with gel electrolyte of H_2SO_4 and dried at room temperature for 3 hours. The fiber supercapacitor was tested at 20 mV/s rate. The ESR is the electrochemical series resistance was calculated using the formula ESR = $U_{drop}/2I$ where, U_{drop} is the voltage drop in the discharge curve and I is the instantaneous current.

6.3 Results and discussion

6.3.1 Synthesis of CNT-Cotton-MXene yarn

The spinning system of producing CNT-Cotton-MXene yarn is presented in Figure 6.1a. The right-side of the spinning device is the let-off zone where the CNT arrays are securely placed. Four CNT arrays (two large and two small) were placed to wrap a cotton core yarn. The yarns are passed over a guide and twisted together 12 cm from the cylinder. The inclined insertion of the yarn creates some open space at the twisting zone and MXene is carefully deposited only on the cotton. This is important to increase the loading of MXene because, unlike planar substrate, fiber has a lower area to accommodate a higher amount of MXene. Besides depositing a very high amount of MXene on the yarn surface may be problematic for further processing. MXene deposition on cotton makes the core conductive and reduces the porosity inside the yarn structures. MXene was then deposited on the surface of the twisted yarn containing MXene deposited cotton core.

6.3.2 Characterization of CNT-Cotton/MXene yarn

The surface morphology and corresponding cross-section of yarns with different MXene loading is presented in Figure 6.1b,d. With the higher MXene loading, the yarn diameter increases. While the MXene was uniformly coated on the CNT-Cotton yarn surface, their cross section shows nonuniform coating thickness around the yarn especially with the increase of MXene loading. However, a small crack was observed for the yarn with higher MXene loading but their continuity was not affected. The layered coating of MXene over cotton and CNT-Cotton is shown in Figure 6.2d. The layers are cotton, MXene, CNT, MXene from inside towards the outer layer and the yarn linear density increases from CCM1 60 Tex (weight in gram per kilometer of yarn) to 275 Tex for CCM4.

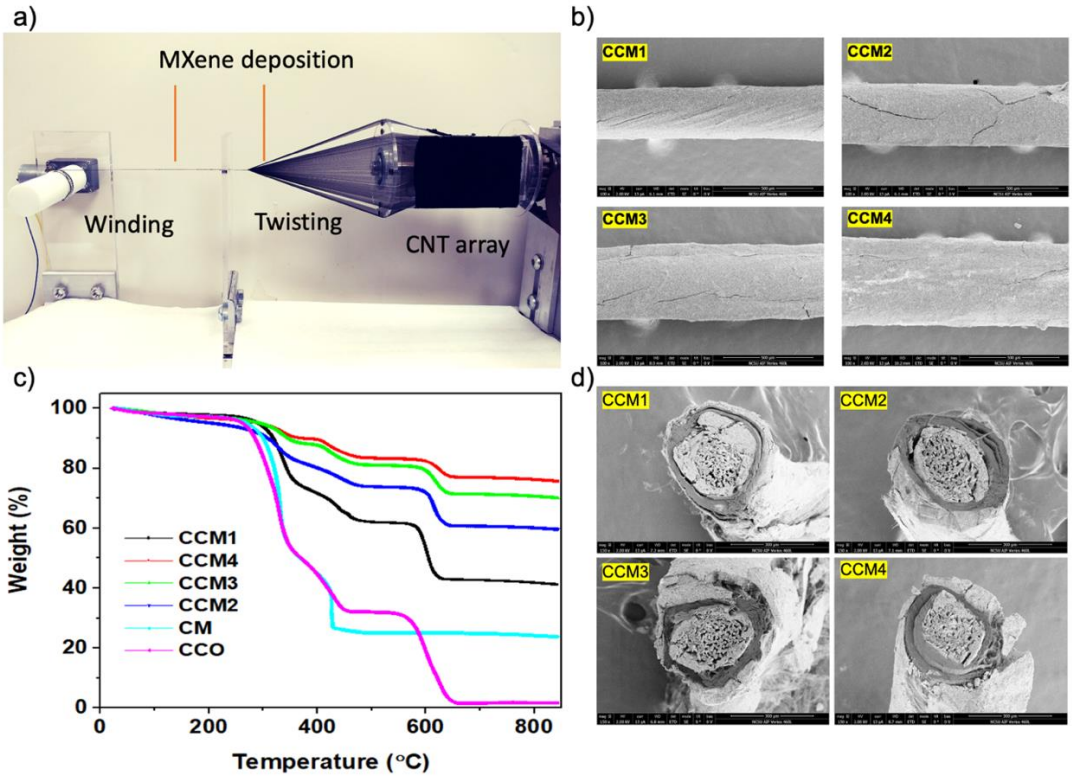

Figure 6. 1 Synthesis and characterizations of the yarn

Description: a) Schematic of CNT-Cotton-MXene yarn spinning device b) SEM images of CNT-Cotton-MXene yarn c) cross-section of the yarns

TGA analysis of the samples is presented in Figure 6.1c. Addition of MXene with the yarns demonstrated significant improvement in the thermal stability. The improvement in thermal stability directly correlates with the MXene loading. Yarn with the highest MXene loading of 85% (CCM4) retained above 70% weight fraction at 850 °C. For all yarns, the first transition of the thermal behavior occurred between 200 - 250 °C temperature and weight loss was around 5%. However, the 2nd onset for CM and CCO yarn at ~430 °C revealed 60 - 70% weight loss depicting decomposition of cotton yarn. However, the char residue for CO yarn was much higher (24%) than CCO because of the MXene.

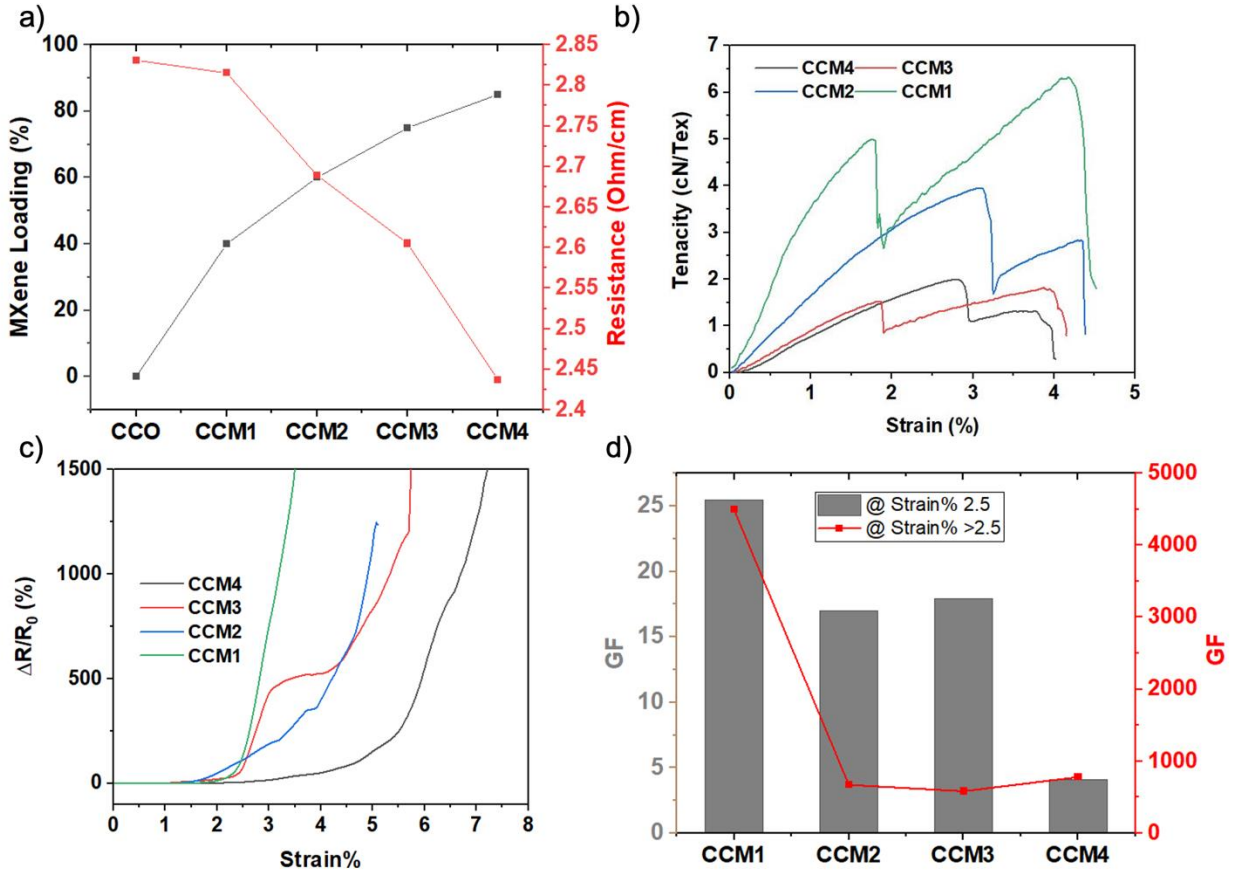

Figure 6. 2 Electromechanical characteristics of different yarns

Description: a) Resistance of yarn against MXene loading b) Tenacity-strain curves c) Relative change% of the yarns at different strain d) Gauge factors of the yarns

6.3.3 Electromechanical evaluation of the yarn

The electrical resistance of the yarns against different MXene loading percentages is presented in Figure 6.2a. With the increase of MXene loading, the electrical resistance decreases and CCM4 demonstrated the lowest resistance of 2.44 ohm/cm. Yarn without MXene, CCO demonstrated electrical resistance of 2.83 ohm/cm. However, similar loading of MXene (40%) had a remarkable difference in electrical resistance for CCM1 and CM yarn (not presented in figure). CM yarn had a maximum resistance of 172 ohm/cm at 40% MXene loading. This demonstrated a synergistic impact of CNT and MXene on electrical resistance.

The tenacity and strain curve of the yarns are shown in Figure 6.2b. Tenacity decreases with the increase of MXene% and the maximum tenacity of 6.32 cN/Tex was found for CCM1 yarn. This might be due to the distribution of MXene nanosheets in the yarn which assists in transferring load[366]. However, increasing the MXene loading also decreased the strain%. This is due to the agglomeration of MXene nanosheets at higher loading resulting in weaker bonding[367].

The relative change in resistance% of the yarns are presented in Figure 6.2c where ΔR is the difference in resistance and R_0 is the initial resistance. All the yarns demonstrated a rapid resistance change after 2% of strain and an overshoot of resistance was observed above 2% strain. However, increasing the MXene loading revealed a small improvement in strain%. Important to note that, lower MXene loading demonstrated sharp change in resistance at 2.4% strain indicating better strain sensing behavior. The calculated gauge factor (GF) of the yarns (Fig 2d) correlates the relative resistance change characteristics of the yarn. At elastic strain 0 – 2.5%, CCM1 had a maximum GF of 25.45 whereas CCM4 showed GF of 4.13. This is due to the flexibility of the yarn which is affected by the MXene loading. CCM3 demonstrated a little higher GF due to the higher relative resistance change but when the GF was calculated in a similar linear region of the curve, the GF was found to be 16.69. In contrast, CCO yarn demonstrated negative GF -0.056 at

0 – 10% strain resulting from the strain-induced increase in electrical conductivity[368]. However, the GF showed exceptional improvement at strain above 2.5%. A maximum GF of ~4492 was observed for CCM4 and the lowest GF was found for CCM3 584. This GF is higher than many other reported strain sensors using MXene[358,369–371].

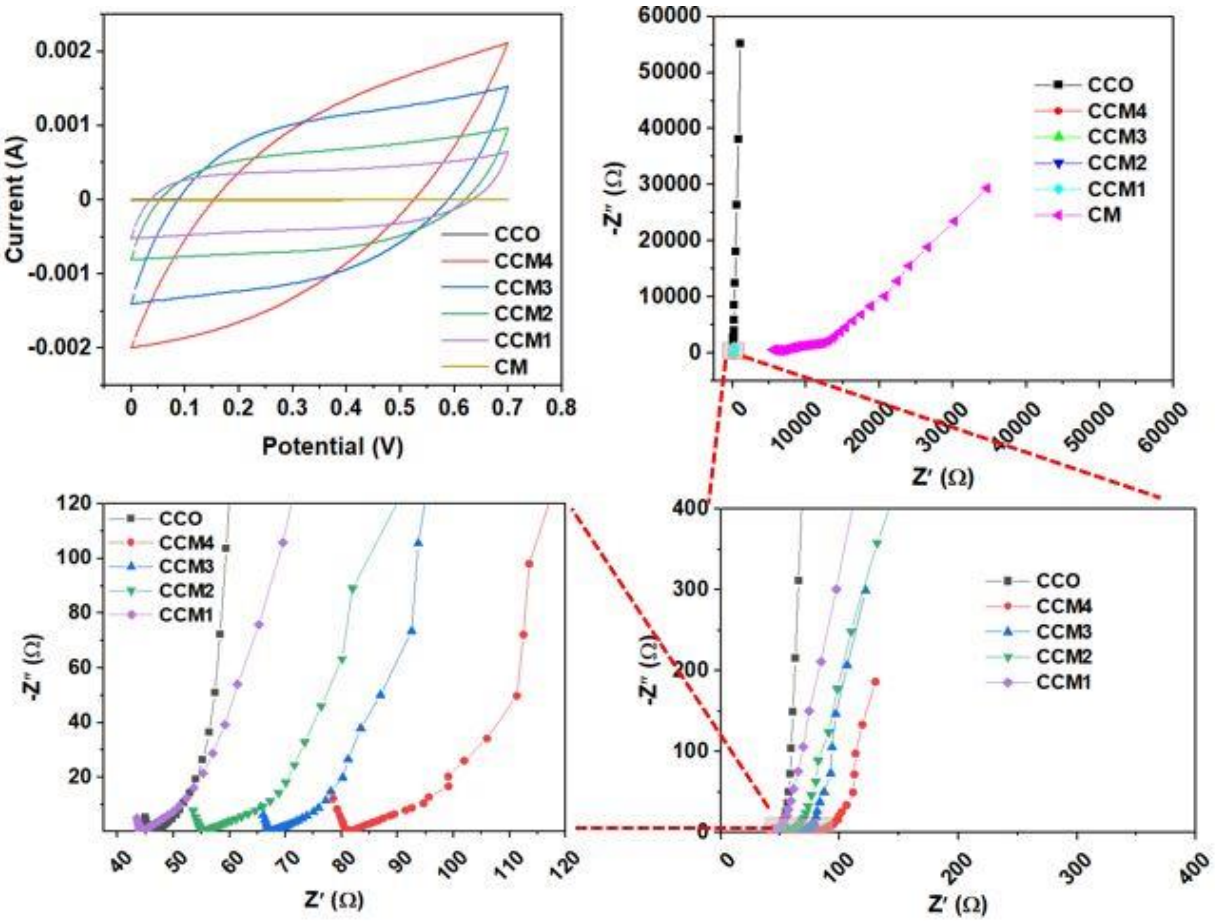

Figure 6. 3 Electrochemical performance of the CNT-Cotton-MXene yarn

Description: a) CV curves at scan rate of 20 mV/s b-d) Nyquist plot (0.01 – 1M Hz)

6.3.4 Electrochemical performance of the yarn

The electrochemical performance of the yarns are presented in Figure 6.3. As shown in the cyclic voltammetry curves (CV) (Figure6.3a), the introduction of MXene into CCO yarns could significantly improve its capacitance. With the increase of MXene loading in the hybrid yarns,

their capacitances increase from 4.43 mF/cm of CCM1 to 14.13 mF/cm of CCM4. Meanwhile, without cotton yarn as core, the MXene loaded pure CM yarn exhibits very low capacitance, indicating the essential role of cotton to facilitate the MXene nanosheets infiltrating CNT layers and thus form reliable interfaces. Electrochemical impedance spectroscopy (EIS) analysis provides information of charge transfer and ion transport (Figure 6.3b-d). As shown in Figure 6.3b-d, the increased MXene loading, however, results in increased equivalent series resistance (ESR) of these hybrid yarns. This is mainly due to the thicker MXene layers out of CNT yarns from high loading lead to larger resistance for the diffusion of gel electrolyte towards inner yarn cores. Meanwhile, a larger amount of MXene brings higher charge transfer resistance.

6.4 Conclusion

CNT-Cotton yarn was modified using MXene and the performance of the modified yarn was evaluated for strain sensing and supercapacitor applications. The sensitivity of the yarn is highly dependent on the MXene loading and optimum MXene loading was 40% for higher sensitivity. The opposite result was observed for supercapacitor applications showing the maximum capacitance at higher MXene loading. MXene loading enhanced the capacitance of CNT-Cotton by five orders of magnitude. The modification process of CNT by MXene provides a promising platform for multifunctional fiber electronics.

Chapter 7: Summary and Future Directions

7.1 Summary

Manipulating nanomaterials in different dimensions provide opportunities for real-world applications. Besides, further processing the nanomaterials and modifications render them with enhanced multifunctionality. This research aimed to design a system for assembling MWCNTs in microscale, evaluate their structure-properties, further process them using textile techniques and modify the assembled MWCNTs by MXene for wearable electronic applications. Based on the literature, the main objectives of this dissertations are following-

- Develop a spinning system to wrap CNT over textile yarns while maintaining conductivity and mechanical properties suitable for textile processing
- Understand the structure-property behavior of CNT wrapped textile yarns and their impact on wearable electronic applications
- Design highly wash durable CNT-based textile electrodes for biosensing

To achieve the above-mentioned objectives, a spinning system were developed accommodating simultaneous wrapping, twisting and liquid densification systems. CNTs were successfully assembled into microscale yarn and wrapped over traditional textile yarns using a simple, single and dry spinning method. The impact of spinning parameters and TPU binder on the yarn properties especially, electrical resistance, linear density, tenacity was evaluated. The diameter of the assembled yarn can be tuned by changing the core yarn and the densification process. After understanding the structure-properties of the yarn, optimized TPU binder and wrapping distance was used to wrap CNT over cotton and polyester yarn for multifunctional e-textiles. Finally, CNT wrapped cotton yarn was modified by MXene to increase the sensitivity and energy storage capacity for wearable applications.

While the structure-property of neat CNT yarn was studied extensively by a different researcher, in this dissertation, we studied the structure-property of large diameter yarn produced by wrapping CNT over cotton yarn. In doing so, we developed an improved dry spinning system to wrap CNT over textile yarn and densify them by twisting and binder. This study revealed that, wrapping distance has no significant impact on the yarn properties. However, a strong correlation between TPU and yarn linear density/resistance was observed, and the detailed analysis is presented in Chapter 3.

The processability of neat CNT yarn is very challenging due to its high rigidity and the thinner diameter of the yarn is not suitable for textile processing. Though multiplication of CNT yarn increases their diameter, low extensibility remained as a major challenge. However, to the best of our knowledge, the knittability of CNT yarn using state-of-the-art whole garment knitting was never studied previously. In this dissertation, we studied the CNT-wrapped textile yarns, characterized them, and demonstrated their textile processability using different instruments for the first time. The detail of this study is presented in Chapter 4. The important research finding of this research is highlighted below:

Inserting core during the spinning system and applying TPU binder provided high flexibility and tenacity to the CNTY and CNT-wrapped yarns. As a result, the yarn exhibited extensibility like the cotton yarn and was further improved by using polyester core.

- The seamlessly 3D knitted glove demonstrated excellent piezoresistive response and reversibility under multiple bending-releasing cycles and the jersey knit structure can be extended beyond the maximum extensibility of the human skin.
- The wearable knitted wrist band exhibited rapid thermal heating behavior under low applied voltages and very good thermal stability against a wide strain percentage.

- The yarn demonstrated excellent wash durability for 30 washing cycles without significant change in resistance.

The versatile spinning process developed in this process showed an outstanding possibility of CNTs into multifunctional and wearable electronic applications.

Most of the reported textile electrodes for biosensing suffer from poor wash durability. On the other hand, CNT thin-film electrodes lack the breathability and comfort required for wearable applications. For the first time, we used the spun CNT yarn to design ECG electrodes by knitting, braiding, and weaving to produce large-area electrodes. Electrodes designed by textile technology ensure excellent breathability and comfort. The freestanding and seamless design allow the electrodes to be mounted on the skin without additional support. We have shown their high-fidelity ECG signals comparable to the conventional wet electrode (3M Red Dot). Besides, SNR of the fabricated electrodes performs like the 3M electrode. Finally, the wash durability of the electrodes and their robustness to motion artifact revealed the suitability of our electrodes for long-term ECG monitoring. The detailed analysis of the CNT textile electrode is documented in Chapter 5.

Different literature studies discussed in Chapter 6, demonstrated strategies for high active materials loading for high performance. However, wearable electronics require the device to be flexible and stretchable along with the performance. Active materials loading into CNT yarn is rarely reported and expected to retain the inherent characteristics of the yarn. Therefore, we modified the wrapping geometry of our spinning system to accommodate MXene as active materials both into the core and surface of the yarn. This strategy allowed higher loading of MXene (~90%) into the CNT yarn. Then the modified CNT-Cotton yarn using MXene was evaluated for strain sensing and supercapacitor applications. It was observed that the higher loading of MXene increased their electrical conductivity. However, the sensitivity of the yarn is highly dependent on

the optimum MXene loading of 40%. The opposite result was observed for supercapacitor applications showing the maximum capacitance at higher MXene loading. MXene loading enhanced the capacitance of CNT-Cotton by five orders of magnitude. The modification process of CNT by MXene provides a promising platform for multifunctional fiber electronics.

7.2 Future directions

7.2.1 Detail study of structure-property relationship

The structure of the developed yarn is critical for different wearable applications. The impact of TPU on tensile properties was evaluated. However, it is essential to investigate the amount of TPU absorbed by the yarn. Besides, how the porosity of the yarns changes with the TPU loading may provide further information about the electromechanical properties of the yarn. During the knitting process, the yarn was caught by the sharp angle of the yarn guide and it might be due to the high coefficient of friction of the yarns. Therefore, evaluating the coefficient of friction and developing a way of reducing the friction could be fascinating for easier processing and fabricating seamless knitted sensors. While the comfort of the textile was assumed to be similar but it would be interesting to determine the comfort of the fabric produced by the developed yarns.

7.2.2 Highly stretchable CNT yarn electrode for sensing

Sensors with high stretchability and sensitivity are desired for different wearable applications. Polyurethane core could be used for stretchability and the sensitivity could be tuned by modifying the yarn surface using conductive polymers. The structure-property of the electrode could be optimized for improved performances. This stretchable electrode could be 3D knitted into a hand glove for human-computer interfacing applications.

7.2.3 Integration of multimodal sensing system and power source

There are demands for wearable health monitoring devices in the form of flexible and stretchable electronics. However, most of the electrodes are limited for single sensing applications. Therefore, incorporating multimodal sensing in the single electrode would be revolutionary for the wearable health industry. CNT modified with different sensing materials could be knitted together enabling them to sense multimodalities.

One of the major challenges for the commercial success of e-textiles is powering the device. The CNT yarn electrode could be converted to a fabric electrode and modified using pseudo capacitance materials or piezoelectric materials for energy harvesting/storage. Developing power sources on e-textile would be remarkable for self-powered e-textiles.

REFERENCES

(1) Li, Z.; Wang, L.; Li, Y.; Feng, Y.; Feng, W. Carbon-Based Functional Nanomaterials: Preparation, Properties and Applications. *Composites Science and Technology* **2019**, *179*, 10–40.

(2) Lah, N. A. C.; Zubir, M. N. M.; Samykano, M. A. Engineered Nanomaterial in Electronics and Electrical Industries. In *Handbook of Nanomaterials for Industrial Applications*; Elsevier Inc., 2018; pp 324–364.

(3) Tao, X.; Koncar, V. Textile Electronic Circuits Based on Organic Fibrous Transistors. In *Smart Textiles and Their Applications*; Elsevier Ltd., 2016; pp 569–598. https://doi.org/10.1016/B978-0-08-100574-3.00025-4.

(4) Bonaldi, R. R. Electronics Used in High-Performance Apparel—Part 1/2. In *High-Performance Apparel*; Elsevier Ltd., 2018; pp 245–284.

(5) Wood, J. Revolutions in Wearable Technology for Apparel. In *High-Performance Apparel*; Elsevier Ltd., 2018; pp 325–339.

(6) Lee, J. C. B.; Liu, W.; Lo, C. H.; Chen, C. C. Laundering Reliability of Electrically Conductive Fabrics for E-Textile Applications. *Proceedings - Electronic Components and Technology Conference* **2019**, *2019-May*, 1826–1832. https://doi.org/10.1109/ECTC.2019.00281.

(7) Sun, G.; Wang, X.; Chen, P. Microfiber Devices Based on Carbon Materials. *Materials Today* **2015**, *18* (4), 215–226. https://doi.org/10.1016/j.mattod.2014.12.001.

(8) Guo, Y.; Dun, C.; Xu, J.; Mu, J.; Li, P.; Gu, L.; Hou, C.; Hewitt, C. A.; Zhang, Q.; Li, Y.; Carroll, D. L.; Wang, H. Ultrathin, Washable, and Large-Area Graphene Papers for Personal Thermal Management. *Small* **2017**, *13* (44), 1–9.

(9) Fugetsu, B.; Sano, E.; Yu, H.; Mori, K.; Tanaka, T. Graphene Oxide as Dyestuffs for the Creation of Electrically Conductive Fabrics. *Carbon* **2010**, *48* (12), 3340–3345.

(10) Xiang, C.; Lu, W.; Zhu, Y.; Sun, Z.; Yan, Z.; Hwang, C. C.; Tour, J. M. Carbon Nanotube and Graphene Nanoribbon-Coated Conductive Kevlar Fibers. *ACS Applied Materials and Interfaces* **2012**, *4* (1), 131–136. https://doi.org/10.1021/am201153b.

(11) Jha, M. K.; Hata, K.; Subramaniam, C. Interwoven Carbon Nanotube Wires for High-Performing, Mechanically Robust, Washable, and Wearable Supercapacitors. *ACS Applied Materials and Interfaces* **2019**, *11*, 18285–18294. https://doi.org/10.1021/acsami.8b22233.

(12) Pahalagedara, L. R.; Siriwardane, I. W.; Tissera, N. D.; Wijesena, R. N.; De Silva, K. M. N. Carbon Black Functionalized Stretchable Conductive Fabrics for Wearable Heating Applications. *RSC Advances* **2017**, *7* (31), 19174–19180. https://doi.org/10.1039/c7ra02184d.

(13) Zhang, L.; Fairbanks, M.; Andrew, T. L. Rugged Textile Electrodes for Wearable Devices Obtained by Vapor Coating Off-the-Shelf, Plain-Woven Fabrics. *Advanced Functional Materials* **2017**, *27* (24), 1–9. https://doi.org/10.1002/adfm.201700415.

(14) Cheng, N.; Zhang, L.; Joon Kim, J.; Andrew, T. L. Vapor Phase Organic Chemistry to Deposit Conjugated Polymer Films on Arbitrary Substrates. *Journal of Materials Chemistry C* **2017**, *5* (23), 5787–5796. https://doi.org/10.1039/c7tc00293a.

(15) Lv, J.; Zhou, P.; Zhang, L.; Zhong, Y.; Sui, X.; Wang, B.; Chen, Z.; Xu, H.; Mao, Z. High-Performance Textile Electrodes for Wearable Electronics Obtained by an Improved in Situ Polymerization Method. *Chemical Engineering Journal* **2019**, *361* (December 2018), 897–907. https://doi.org/10.1016/j.cej.2018.12.083.

(16) Doganay, D.; Coskun, S.; Genlik, S. P.; Unalan, H. E. Silver Nanowire Decorated Heatable Textiles. *Nanotechnology* **2016**, *27* (43), 1–8.

(17) Atwa, Y.; Goldthorpe, I. A. Metal-Nanowire Coated Threads for Conductive Textiles. *Proceedings of the IEEE Conference on Nanotechnology* **2014**, 482–485. https://doi.org/10.1109/NANO.2014.6967994.

(18) Liu, L. X.; Chen, W.; Zhang, H. Bin; Wang, Q. W.; Guan, F.; Yu, Z. Z. Flexible and Multifunctional Silk Textiles with Biomimetic Leaf-Like MXene/Silver Nanowire Nanostructures for Electromagnetic Interference Shielding, Humidity Monitoring, and Self-Derived Hydrophobicity. *Advanced Functional Materials* **2019**, *29* (44), 1–10. https://doi.org/10.1002/adfm.201905197.

(19) Xu, C.; Liu, G.; Chen, H.; Zhou, R.; Liu, Y. Fabrication of Conductive Copper-Coated Glass Fibers through Electroless Plating Process. *Journal of Materials Science: Materials in Electronics* **2014**, *25* (6), 2611–2617.

(20) Guo, R. H.; Jiang, S. X.; Yuen, C. W. M.; Ng, M. C. F.; Lan, J. W. Optimization of Electroless Nickel Plating on Polyester Fabric. *Fibers and Polymers* **2013**, *14* (3), 459–464. https://doi.org/10.1007/s12221-013-0459-y.

(21) Wu, Y.; Yang, Y.; Zhang, Z.; Wang, Z.; Zhao, Y.; Sun, L. Fabrication of Cotton Fabrics with Durable Antibacterial Activities Finishing by Ag Nanoparticles. *Textile Research Journal* **2019**, *89* (5), 867–880. https://doi.org/10.1177/0040517518758002.

(22) Du, D.; Tang, Z.; Ouyang, J. Highly Washable E-Textile Prepared by Ultrasonic Nanosoldering of Carbon Nanotubes onto Polymer Fibers. *Journal of Materials Chemistry C* **2018**, *6* (4), 883–889.

(23) Zhao, H.; Zhang, Y.; Bradford, P. D.; Zhou, Q.; Jia, Q.; Yuan, F. G.; Zhu, Y. Carbon Nanotube Yarn Strain Sensors. *Nanotechnology* **2010**, *21* (30). https://doi.org/10.1088/0957-4484/21/30/305502.

(24) Chen, H.; Su, Z.; Song, Y.; Cheng, X.; Chen, X.; Meng, B.; Song, Z.; Chen, D.; Zhang, H. Omnidirectional Bending and Pressure Sensor Based on Stretchable CNT-PU Sponge. *Advanced Functional Materials* **2017**. https://doi.org/10.1002/adfm.201604434.

(25) Li, Q.; Liu, C.; Lin, Y. H.; Liu, L.; Jiang, K.; Fan, S. Large-Strain, Multiform Movements from Designable Electrothermal Actuators Based on Large Highly Anisotropic Carbon Nanotube Sheets. *ACS Nano* **2015**. https://doi.org/10.1021/nn505535k.

(26) Sachyani, E.; Layani, M.; Tibi, G.; Avidan, T.; Degani, A.; Magdassi, S. Enhanced Movement of CNT-Based Actuators by a Three-Layered Structure with Controlled Resistivity. *Sensors and Actuators, B: Chemical* **2017**. https://doi.org/10.1016/j.snb.2017.06.104.

(27) Choi, C.; Lee, J. A.; Choi, A. Y.; Kim, Y. T.; Leprõ, X.; Lima, M. D.; Baughman, R. H.; Kim, S. J. Flexible Supercapacitor Made of Carbon Nanotube Yarn with Internal Pores. *Advanced Materials* **2014**. https://doi.org/10.1002/adma.201304736.

(28) Sun, J.; Huang, Y.; Fu, C.; Wang, Z.; Huang, Y.; Zhu, M.; Zhi, C.; Hu, H. High-Performance Stretchable Yarn Supercapacitor Based on PPy@CNTs@urethane Elastic Fiber Core Spun Yarn. *Nano Energy* **2016**. https://doi.org/10.1016/j.nanoen.2016.07.008.

(29) Chien, A. T.; Cho, S.; Joshi, Y.; Kumar, S. Electrical Conductivity and Joule Heating of Polyacrylonitrile/Carbon Nanotube Composite Fibers. *Polymer* **2014**. https://doi.org/10.1016/j.polymer.2014.10.064.

(30) Zeng, Z.; Jin, H.; Chen, M.; Li, W.; Zhou, L.; Zhang, Z. Lightweight and Anisotropic Porous MWCNT/WPU Composites for Ultrahigh Performance Electromagnetic Interference Shielding. *Advanced Functional Materials* **2016**. https://doi.org/10.1002/adfm.201503579.

(31) Shajari, S.; Arjmand, M.; Pawar, S. P.; Sundararaj, U.; Sudak, L. J. Synergistic Effect of Hybrid Stainless Steel Fiber and Carbon Nanotube on Mechanical Properties and Electromagnetic Interference Shielding of Polypropylene Nanocomposites. *Composites Part B: Engineering* **2019**. https://doi.org/10.1016/j.compositesb.2019.02.044.

(32) Choi, Y. C.; Kang, J. T.; Park, S.; Go, E.; Jeon, H.; Kim, J. W.; Jeong, J. W.; Park, K. H.; Song, Y. H. High Performance Field Emission and Nottingham Effect Observed from Carbon Nanotube Yarn. *Physica E: Low-Dimensional Systems and Nanostructures* **2017**. https://doi.org/10.1016/j.physe.2016.10.004.

(33) Yang, Y.; Liu, L.; Wei, Y.; Liu, P.; Jiang, K.; Li, Q.; Fan, S. In Situ Fabrication of HfC-Decorated Carbon Nanotube Yarns and Their Field-Emission Properties. *Carbon* **2010**. https://doi.org/10.1016/j.carbon.2009.09.074.

(34) Franklin, A. D.; Farmer, D. B.; Haensch, W. Defining and Overcoming the Contact Resistance Challenge in Scaled Carbon Nanotube Transistors. *ACS Nano* **2014**. https://doi.org/10.1021/nn5024363.

(35) Cao, C.; Andrews, J. B.; Franklin, A. D. Completely Printed, Flexible, Stable, and Hysteresis-Free Carbon Nanotube Thin-Film Transistors via Aerosol Jet Printing. *Advanced Electronic Materials* **2017**. https://doi.org/10.1002/aelm.201700057.

(36) Raphey, V. R.; Henna, T. K.; Nivitha, K. P.; Mufeedha, P.; Sabu, C.; Pramod, K. Advanced Biomedical Applications of Carbon Nanotube. *Materials Science and Engineering C*. 2019. https://doi.org/10.1016/j.msec.2019.03.043.

(37) Khan, A. S.; Hussain, A. N.; Sidra, L.; Sarfraz, Z.; Khalid, H.; Khan, M.; Manzoor, F.; Shahzadi, L.; Yar, M.; Rehman, I. U. Fabrication and in Vivo Evaluation of Hydroxyapatite/Carbon Nanotube Electrospun Fibers for Biomedical/Dental Application. *Materials Science and Engineering C* **2017**. https://doi.org/10.1016/j.msec.2017.05.109.

(38) *Nanotube Superfiber Materials*, 2nd ed.; Schulz, Mark; Shanov, Vesselin; Yin, Zhangzhang; Cahay, M., Ed.; Elsevier Ltd., 2019. https://doi.org/10.1016/c2016-0-03380-6.

(39) Jang, Y.; Kim, S. M.; Spinks, G. M.; Kim, S. J. Carbon Nanotube Yarn for Fiber-Shaped Electrical Sensors, Actuators, and Energy Storage for Smart Systems. *Advanced Materials* **2020**, *32* (5), 1–14.

(40) Lund, A.; Darabi, S.; Hultmark, S.; Ryan, J. D.; Andersson, B.; Ström, A.; Müller, C. Roll-to-Roll Dyed Conducting Silk Yarns: A Versatile Material for E-Textile Devices. *Advanced Materials Technologies* **2018**, *3* (12), 1–6.

(41) Wilson, S.; Laing, R. *Fabrics and Garments as Sensors: A Research Update*; 2019; Vol. 19.

(42) Guo, L.; Bashir, T.; Bresky, E.; Persson, N. K. Electroconductive Textiles and Textile-Based Electromechanical Sensors-Integration in as an Approach for Smart Textiles. In *Smart Textiles and Their Applications*; Elsevier Ltd, 2016; pp 657–693.

(43) Cork, C. R. *Conductive Fibres for Electronic Textiles: An Overview*; Elsevier Ltd., 2015.

(44) Qu, H.; Skorobogatiy, M. Conductive Polymer Yarns for Electronic Textiles. In *Electronic Textiles: Smart Fabrics and Wearable Technology*; 2015; pp 21–53.

(45) Gong, F.; Meng, C.; He, J.; Dong, X. Fabrication of Highly Conductive and Multifunctional Polyester Fabrics by Spray-Coating with PEDOT:PSS Solutions. *Progress in Organic Coatings* **2018**, *121* (November 2017), 89–96. https://doi.org/10.1016/j.porgcoat.2018.04.006.

(46) Guo, Y.; Otley, M. T.; Li, M.; Zhang, X.; Sinha, S. K.; Treich, G. M.; Sotzing, G. A. PEDOT:PSS "Wires" Printed on Textile for Wearable Electronics. *ACS Applied Materials and Interfaces* **2016**, *8* (40), 26998–27005.

(47) Grancarić, A. M.; Jerković, I.; Koncar, V.; Cochrane, C.; Kelly, F. M.; Soulat, D.; Legrand, X. Conductive Polymers for Smart Textile Applications. *Journal of Industrial Textiles* **2018**, *48* (3), 612–642. https://doi.org/10.1177/1528083717699368.

(48) Acar, G.; Ozturk, O.; Golparvar, A. J.; Elboshra, T. A.; Böhringer, K.; Kaya Yapici, M. Wearable and Flexible Textile Electrodes for Biopotential Signal Monitoring: A Review. *Electronics* **2019**, *8* (5), 1–25.

(49) Song, J. Nanowires for Smart Textiles. In *Smart Textiles*; Scrivener Publishing LLC, 2018; pp 127–176. https://doi.org/10.1002/9781119460367.ch5.

(50) Gong, S.; Cheng, W. One-Dimensional Nanomaterials for Soft Electronics. *Advanced Electronic Materials* **2017**, *3* (3).

(51) Yao, S.; Swetha, P.; Zhu, Y. Nanomaterial-Enabled Wearable Sensors for Healthcare. *Advanced Healthcare Materials* **2018**, *7* (1), 1–27.

(52) Parvinzadeh Gashti, M.; Pakdel, E.; Alimohammadi, F. Nanotechnology-Based Coating Techniques for Smart Textiles. In *Active Coatings for Smart Textiles*; Elsevier Ltd, 2016; pp 243–268. https://doi.org/10.1016/B978-0-08-100263-6.00011-3.

(53) Dastjerdi, R.; Montazer, M.; Shahsavan, S. A New Method to Stabilize Nanoparticles on Textile Surfaces. *Colloids and Surfaces A: Physicochemical and Engineering Aspects* **2009**, *345* (1–3), 202–210. https://doi.org/10.1016/j.colsurfa.2009.05.007.

(54) Lund, A.; van der Velden, N. M.; Persson, N. K.; Hamedi, M. M.; Müller, C. Electrically Conducting Fibres for E-Textiles: An Open Playground for Conjugated Polymers and Carbon Nanomaterials. *Materials Science and Engineering R: Reports* **2018**, *126* (January), 1–29. https://doi.org/10.1016/j.mser.2018.03.001.

(55) Cui, J.; Zhou, S. Highly Conductive and Ultra-Durable Electronic Textiles via Covalent Immobilization of Carbon Nanomaterials on Cotton Fabric. *Journal of Materials Chemistry C* **2018**, *6*, 12273–12282.

(56) Neves, A. I. S.; Rodrigues, D. P.; De Sanctis, A.; Alonso, E. T.; Pereira, M. S.; Amaral, V. S.; Melo, L. V.; Russo, S.; De Schrijver, I.; Alves, H.; Craciun, M. F. Towards Conductive Textiles: Coating Polymeric Fibres with Graphene. *Scientific Reports* **2017**, *7* (1), 1–10. https://doi.org/10.1038/s41598-017-04453-7.

(57) Montazer, M.; Asghari, M. S. G.; Pakdel, E. Electrical Conductivity of Single Walled and Multiwalled Carbon Nanotube Containing Wool Fibers. *Journal of Applied Polymer Science* **2011**, *121*, 3353–3358.

(58) Shim, B. S.; Chen, W.; Doty, C.; Xu, C.; Kotov, N. A. Smart Electronic Yarns and Wearable Fabrics for Human Biomonitoring Made by Carbon Nanotube Coating with Polyelectrolytes. *Nano Letters* **2008**, *8* (12), 4151–4157. https://doi.org/10.1021/nl801495p.

(59) Hou, H.; Schaper, A. K.; Jun, Z.; Weller, F.; Greiner, A. Large-Scale Synthesis of Aligned Carbon Nanotubes Using FeCl3 as Floating Catalyst Precursor. *Chemistry of Materials* **2003**, *15* (2), 580–585.

(60) Li, A. W. Z.; Xie, S. S.; Qian, L. X.; Chang, B. H.; Zou, B. S.; Zhou, W. Y.; Zhao, R. A.; Wang, G. Large-Scale Synthesis of Aligned Carbon Nanotubes. *Science* **1996**, *274* (5293), 1701–1703.

(61) Lekawa-Raus, A.; Patmore, J.; Kurzepa, L.; Bulmer, J.; Koziol, K. Electrical Properties of Carbon Nanotube Based Fibers and Their Future Use in Electrical Wiring. *Advanced Functional Materials* **2014**, *24* (24), 3661–3682. https://doi.org/10.1002/adfm.201303716.

(62) Jourdain, V.; Bichara, C. Current Understanding of the Growth of Carbon Nanotubes in Catalytic Chemical Vapour Deposition. *Carbon* **2013**, *58*, 2–39. https://doi.org/10.1016/j.carbon.2013.02.046.

(63) Liu, J.; Lu, J.; Lin, X.; Tang, Y.; Liu, Y.; Wang, T.; Zhu, H. The Electronic Properties of Chiral Carbon Nanotubes. *Computational Materials Science* **2017**, *129*, 290–294. https://doi.org/10.1016/j.commatsci.2016.12.035.

(64) Ibrahim, K. S. Carbon Nanotubes-Properties and Applications: A Review. *Carbon letters* **2013**, *14* (3), 131–144. https://doi.org/10.5714/CL.2013.14.3.131.

(65) Miao, M. Carbon Nanotube Yarns for Electronic Textiles. In *Electronic Textiles: Smart Fabrics and Wearable Technology*; Woodhead Publishing, 2015; pp 55–72.

(66) Rahman, G.; Najaf, Z.; Mehmood, A.; Bilal, S.; Shah, A.; Mian, S.; Ali, G. An Overview of the Recent Progress in the Synthesis and Applications of Carbon Nanotubes. *C* **2019**, *5* (1), 3. https://doi.org/10.3390/c5010003.

(67) Melechko, A. V.; Merkulov, V. I.; McKnight, T. E.; Guillorn, M. A.; Klein, K. L.; Lowndes, D. H.; Simpson, M. L. Vertically Aligned Carbon Nanofibers and Related Structures: Controlled Synthesis and Directed Assembly. *Journal of Applied Physics* **2005**, *97* (4), 1–39. https://doi.org/10.1063/1.1857591.

(68) Brukh, R.; Mitra, S. Mechanism of Carbon Nanotube Growth by CVD. *Chemical Physics Letters* **2006**, *424* (1–3), 126–132. https://doi.org/10.1016/j.cplett.2006.04.028.

(69) Vidu, R.; Rahman, M.; Mahmoudi, M.; Enachescu, M.; Poteca, T. D.; Opris, I. Nanostructures: A Platform for Brain Repair and Augmentation. *Frontiers in Systems Neuroscience* **2014**, *8* (June), 1–24. https://doi.org/10.3389/fnsys.2014.00091.

(70) Rao, C. N. R.; Voggu, R.; Govindaraj, A. Selective Generation of Single-Walled Carbon Nanotubes with Metallic, Semiconducting and Other Unique Electronic Properties. *Nanoscale* **2009**, *1* (1), 96. https://doi.org/10.1039/b9nr00104b.

(71) Dervishi, E.; Li, Z.; Xu, Y.; Saini, V.; Biris, A. R.; Lupu, D.; Biris, A. S. Carbon Nanotubes: Synthesis, Properties, and Applications. *Particulate Science and Technology* **2009**, *27* (2), 107–125. https://doi.org/10.1080/02726350902775962.

(72) Zhang, X.; Li, Q.; Tu, Y.; Li, Y.; Coulter, J. Y.; Zheng, L.; Zhao, Y.; Jia, Q.; Peterson, D. E.; Zhu, Y. Strong Carbon-Nanotube Fibers Spun from Long Carbon-Nanotube Arrays. *Small* **2007**, *3* (2), 244–248.

(73) KAILI JIANG; QUNQING LI; SHOUSHAN FAN. Spinning Continuous Carbon Nanotube Yarns. *Nature* **2002**, *419* (1999), 801.

(74) Menghe, M. *Carbon Nanotube Fibers and Yarns*; Woodhead Publishing, 2020.

(75) Lu, W.; Zu, M.; Byun, J. H.; Kim, B. S.; Chou, T. W. State of the Art of Carbon Nanotube Fibers: Opportunities and Challenges. *Advanced Materials* **2012**, *24* (14), 1805–1833. https://doi.org/10.1002/adma.201104672.

(76) Zhang, M.; Atkinson, K. R.; Baughman, R. H. Multifunctional Carbon Nanotube Yarns by Downsizing an Ancient Technology. *Science* **2004**, *306* (5700), 1358–1361. https://doi.org/10.1126/science.1104276.

(77) Jayasinghe, C.; Chakrabarti, S.; Schulz, M. J.; Shanov, V. Spinning Yarn from Long Carbon Nanotube Arrays. *Journal of Materials Research* **2011**, *26* (5), 645–651. https://doi.org/10.1557/jmr.2010.91.

(78) Zhang, Y.; Sheehan, C. J.; Zhai, J.; Zou, G.; Luo, H.; Xiong, J.; Zhu, Y. T.; Jia, Q. X. Polymer-Embedded Carbon Nanotube Ribbons for Stretchable Conductors. *Advanced Materials* **2010**, *22* (28), 3027–3031.

(79) Zhu, Y.; Xu, F.; Wang, X.; Zhu, Y. Wavy Ribbons of Carbon Nanotubes for Stretchable Conductors. *Advanced Functional Materials* **2012**, *22* (6), 1279–1283. https://doi.org/10.1002/adfm.201102032.

(80) Zhong, X. H.; Li, Y. L.; Liu, Y. K.; Qiao, X. H.; Feng, Y.; Liang, J.; Jin, J.; Zhu, L.; Hou, F.; Li, J. Y. Continuous Multilayered Carbon Nanotube Yarns. *Advanced Materials* **2010**, *22* (6), 692–696. https://doi.org/10.1002/adma.200902943.

(81) Jiang, K.; Wang, J.; Li, Q.; Liu, L.; Liu, C.; Fan, S. Superaligned Carbon Nanotube Arrays, Films, and Yarns: A Road to Applications. *Advanced Materials* **2011**, *23* (9), 1154–1161. https://doi.org/10.1002/adma.201003989.

(82) Miao, M. Yarn Spun from Carbon Nanotube Forests: Production, Structure, Properties and Applications. *Particuology* **2013**, *11* (4), 378–393. https://doi.org/10.1016/j.partic.2012.06.017.

(83) Li, W.; Zhao, J.; Xue, Y.; Ren, X.; Zhang, X.; Li, Q. Merge Multiple Carbon Nanotube Fibers into a Robust Yarn. *Carbon* **2019**, *145*, 266–272. https://doi.org/10.1016/j.carbon.2019.01.054.

(84) Lee, J.; Lee, D. M.; Jung, Y.; Park, J.; Lee, H. S.; Kim, Y. K.; Park, C. R.; Jeong, H. S.; Kim, S. M. Direct Spinning and Densification Method for High-Performance Carbon Nanotube Fibers. *Nature Communications* **2019**, *10* (1), 1–10. https://doi.org/10.1038/s41467-019-10998-0.

(85) Li, W.; Zhao, J.; Xue, Y.; Ren, X.; Zhang, X.; Li, Q. Merge Multiple Carbon Nanotube Fibers into a Robust Yarn. *Carbon* **2019**, *145*, 266–272.

(86) Headrick, R. J.; Tsentalovich, D. E.; Berdegué, J.; Bengio, E. A.; Liberman, L.; Kleinerman, O.; Lucas, M. S.; Talmon, Y.; Pasquali, M. Structure–Property Relations in Carbon Nanotube Fibers by Downscaling Solution Processing. *Advanced Materials* **2018**, *30* (9), 1–8. https://doi.org/10.1002/adma.201704482.

(87) Zhu, H. W.; Xu, C. L.; Wu, D. H.; Wei, B. Q.; Vajtai, R.; Ajayan, P. M. Direct Synthesis of Long Single-Walled Carbon Nanotube Strands. *Science* **2002**, *296* (5569), 884–886. https://doi.org/10.1126/science.1066996.

(88) Li, Y. L.; Kinloch, I. A.; Windle, A. H. Direct Spinning of Carbon Nanotube Fibers from Chemical Vapor Deposition Synthesis. *Science* **2004**, *304* (5668), 276–278. https://doi.org/10.1126/science.1094982.

(89) Wang, J. N.; Luo, X. G.; Wu, T.; Chen, Y. High-Strength Carbon Nanotube Fibre-like Ribbon with High Ductility and High Electrical Conductivity. *Nature Communications* **2014**, *5*, 1–8.

(90) Vilatela, J. J.; Windle, A. H. Yarn-like Carbon Nanotube Fibers. *Advanced Materials* **2010**, *22* (44), 4959–4963. https://doi.org/10.1002/adma.201002131.

(91) Koziol, K.; Vilatela, J.; Moisala, A.; Motta, M.; Cunniff, P.; Sennett, M.; Windle, A. High-Performance Carbon Nanotube Fiber. *Science* **2007**, *318* (5858), 1892–1895. https://doi.org/10.1126/science.1147635.

(92) Vigolo, B.; Penicaud, A.; Coulon, C.; Sauder, C.; Pailler, R.; Journet, C.; Bernier, P.; Poulin, P. Macroscopic Fibers and Ribbons of Oriented Carbon Nanotubes. *Science* **2000**, *290* (5495), 1331–1334.

(93) Dalton, A. B.; Collins, S.; Razal, J. M.; Howard, V. Super-Tough Carbon-Nanotube Fibres. *Nature* **2002**, *886* (423), 703.

(94) Dalton, A. B.; Collins, S.; Razal, J.; Munoz, E.; Ebron, V. H.; Kim, B. G.; Coleman, J. N.; Ferraris, J. P.; Baughman, R. H. Continuous Carbon Nanotube Composite Fibers: Properties, Potential Applications, and Problems. *Journal of Materials Chemistry* **2004**, *14* (1), 1–3.

(95) Ericson, L. M.; Fan, H.; Peng, H.; Davis, V. A.; Zhou, W.; Sulpizio, J.; Wang, Y.; Booker, R.; Vavro, J.; Guthy, C.; Parra-Vasquez, A. N. G.; Kim, M. J.; Ramesh, S.; Saini, R. K.; Kittrell, C.; Lavin, G.; Schmidt, H.; Adams, W. W.; Billups, W. E.; Pasquali, M.; Hwang, W. F.; Hauge, R. H.; Fischer, J. E.; Smalley, R. E. Macroscopic, Neat, Single-Walled Carbon Nanotube Fibers. *Science* **2004**, *305* (5689), 1447–1450. https://doi.org/10.1126/science.1101398.

(96) Behabtu, N.; Green, M. J.; Pasquali, M. Carbon Nanotube-Based Neat Fibers. *Nano Today* **2008**, *3* (5–6), 24–34. https://doi.org/10.1016/S1748-0132(08)70062-8.

(97) Zhang, S.; Koziol, K. K. K.; Kinloch, I. A.; Windle, A. H. Macroscopic Fibers of Well-Aligned Carbon Nanotubes by Wet Spinning. *Small* **2008**, *4* (8), 1217–1222.

(98) Behabtu, N.; Young, C. C.; Tsentalovich, D. E.; Kleinerman, O.; Wang, X.; Ma, A. W. K.; Bengio, E. A.; Ter Waarbeek, R. F.; De Jong, J. J.; Hoogerwerf, R. E.; Fairchild, S. B.; Ferguson, J. B.; Maruyama, B.; Kono, J.; Talmon, Y.; Cohen, Y.; Otto, M. J.; Pasquali, M. Strong, Light, Multifunctional Fibers of Carbon Nanotubes with Ultrahigh Conductivity. *Science* **2013**, *339* (6116), 182–186. https://doi.org/10.1126/science.1228061.

(99) Tajima, N.; Watanabe, T.; Morimoto, T.; Kobashi, K.; Mukai, K.; Asaka, K.; Okazaki, T. Nanotube Length and Density Dependences of Electrical and Mechanical Properties of Carbon Nanotube Fibres Made by Wet Spinning. *Carbon* **2019**, *152*, 1–6.

(100) Jiang, K.; Li, Q.; Fan, S. Spinning Continuous Carbon Nanotube Yarns. *Nature* **2002**, *419* (6909), 801. https://doi.org/10.1038/419801a.

(101) Zhang, X.; Li, Q.; Holesinger, T. G.; Arendt, P. N.; Huang, J.; Kirven, P. D.; Clapp, T. G.; DePaula, R. F.; Liao, X.; Zhao, Y.; Zheng, L.; Peterson, D. E.; Zhu, Y. Ultrastrong, Stiff, and Lightweight Carbon-Nanotube Fibers. *Advanced Materials* **2007**, *19* (23), 4198–4201.

(102) Liu, K.; Sun, Y.; Zhou, R.; Zhu, H.; Wang, J.; Liu, L.; Fan, S.; Jiang, K. Carbon Nanotube Yarns with High Tensile Strength Made by a Twisting and Shrinking Method. *Nanotechnology* **2010**, *21* (4).

(103) Liu, K.; Sun, Y.; Liu, P.; Wang, J.; Li, Q.; Fan, S.; Jiang, K. Periodically Striped Films Produced from Super-Aligned Carbon Nanotube Arrays. *Nanotechnology* **2009**, *20* (33). https://doi.org/10.1088/0957-4484/20/33/335705.

(104) Inoue, Y.; Suzuki, Y.; Minami, Y.; Muramatsu, J.; Shimamura, Y.; Suzuki, K.; Ghemes, A.; Okada, M.; Sakakibara, S.; Mimura, H.; Naito, K. Anisotropic Carbon Nanotube Papers Fabricated from Multiwalled Carbon Nanotube Webs. *Carbon* **2011**, *49* (7), 2437–2443. https://doi.org/10.1016/j.carbon.2011.02.010.

(105) Alvarez, N. T.; Miller, P.; Haase, M.; Kienzle, N.; Zhang, L.; Schulz, M. J.; Shanov, V. Carbon Nanotube Assembly at Near-Industrial Natural-Fiber Spinning Rates. *Carbon* **2015**, *86*, 350–357.

(106) Liu, K.; Sun, Y.; Lin, X.; Zhou, R.; Wang, J.; Fan, S.; Jiang, K. Scratch-Resistant, Highly Conductive, and High-Strength Carbon Nanotube-Based Composite Yarns. *ACS Nano* **2010**, *4* (10), 5827–5834.

(107) Ryu, S.; Lee, Y.; Hwang, J. W.; Hong, S.; Kim, C.; Park, T. G.; Lee, H.; Hong, S. H. High-Strength Carbon Nanotube Fibers Fabricated by Infiltration and Curing of Mussel-Inspired Catecholamine Polymer. *Advanced Materials* **2011**, *23* (17), 1971–1975.

(108) Zhang, M.; Atkinson, K. R.; Baughman, R. H. Multifunctional Carbon Nanotube Yarns by Downsizing an Ancient Technology. *Science* **2004**, *306* (5700), 1358–1361. https://doi.org/10.1126/science.1104276.

(109) Tran, C. D. Dry Spinning Carbon Nanotubes into Continuous Yarn: Progress, Processing and Applications. In *Nanotube Superfiber Materials: Changing Engineering Design*; Elsevier, 2013; pp 211–242.

(110) Zhang, X.; Jiang, K.; Feng, C.; Liu, P.; Zhang, L.; Kong, J.; Zhang, T.; Li, Q.; Fan, S. Spinning and Processing Continuous Yarns from 4-Inch Wafer Scale Super-Aligned Carbon Nanotube Arrays. *Advanced Materials* **2006**, *18* (12), 1505–1510.

(111) Miao, M. The Role of Twist in Dry Spun Carbon Nanotube Yarns. *Carbon* **2016**, *96*, 819–826.

(112) Shang, Y.; Wang, Y.; Li, S.; Hua, C.; Zou, M.; Cao, A. High-Strength Carbon Nanotube Fibers by Twist-Induced Self-Strengthening. *Carbon* **2017**, *119*, 47–55.

(113) Di, J.; Fang, S.; Moura, F. A.; Galvão, D. S.; Bykova, J.; Aliev, A.; de Andrade, M. J.; Lepró, X.; Li, N.; Haines, C.; Ovalle-Robles, R.; Qian, D.; Baughman, R. H. Strong, Twist-Stable Carbon Nanotube Yarns and Muscles by Tension Annealing at Extreme Temperatures. *Advanced Materials* **2016**, *28* (31), 6598–6605.

(114) Kim, S. H.; Haines, C. S.; Li, N.; Kim, K. J.; Mun, T. J.; Choi, C.; Di, J.; Oh, Y. J.; Oviedo, J. P.; Bykova, J.; Fang, S.; Jiang, N.; Liu, Z.; Wang, R.; Kumar, P.; Qiao, R.; Priya, S.; Cho, K.; Kim, M.; Lucas, M. S.; Drummy, L. F.; Maruyama, B.; Lee, D. Y.; Lepró, X.; Gao, E.; Albarq, D.; Ovalle-Robles, R.; Kim, S. J.; Baughman, R. H. Harvesting Electrical Energy from Carbon Nanotube Yarn Twist. *Science* **2017**, *357* (6353), 773–778.

(115) Anike, J. C.; Belay, K.; Abot, J. L. Effect of Twist on the Electromechanical Properties of Carbon Nanotube Yarns. *Carbon* **2019**, *142*, 491–503.

(116) Chen, T.; Cai, Z.; Qiu, L.; Li, H.; Ren, J.; Lin, H.; Yang, Z.; Sun, X.; Peng, H. Synthesis of Aligned Carbon Nanotube Composite Fibers with High Performances by Electrochemical Deposition. *Journal of Materials Chemistry A* **2013**, *1* (6), 2211–2216.

(117) Lima, M. D.; Fang, S.; Lepró, X.; Lewis, C.; Ovalle-Robles, R.; Carretero-González, J.; Castillo-Martínez, E.; Kozlov, M. E.; Oh, J.; Rawat, N.; Haines, C. S.; Haque, M. H.; Aare, V.; Stoughton, S.; Zakhidov, A. A.; Baughman, R. H. Biscrolling Nanotube Sheets and Functional Guests into Yarns. *Science* **2011**, *331* (6013), 51–55.

(118) Dini, Y.; Rouchon, D.; Faure-Vincent, J.; Dijon, J. Large Improvement of CNT Yarn Electrical Conductivity by Varying Chemical Doping and Annealing Treatment. *Carbon* **2020**, *156*, 38–48.

(119) Wang, N.; Pandit, S.; Ye, L.; Edwards, M.; Mokkapati, V. R. S. S.; Murugesan, M.; Kuzmenko, V.; Zhao, C.; Westerlund, F.; Mijakovic, I.; Liu, J. Efficient Surface Modification of Carbon Nanotubes for Fabricating High Performance CNT Based Hybrid Nanostructures. *Carbon* **2017**, *111*, 402–410.

(120) Lin, H.; Weng, W.; Ren, J.; Qiu, L.; Zhang, Z.; Chen, P.; Chen, X.; Deng, J.; Wang, Y.; Peng, H. Twisted Aligned Carbon Nanotube/Silicon Composite Fiber Anode for Flexible Wire-Shaped Lithium-Ion Battery. *Advanced Materials* **2014**, *26* (8), 1217–1222. https://doi.org/10.1002/adma.201304319.

(121) Su, F.; Lv, X.; Miao, M. High-Performance Two-Ply Yarn Supercapacitors Based on Carbon Nanotube Yarns Dotted with Co3O4and NiO Nanoparticles. *Small* **2015**, *11* (7), 854–861.

(122) Sun, W. J.; Xu, L.; Jia, L. C.; Zhou, C. G.; Xiang, Y.; Yin, R. H.; Yan, D. X.; Tang, J. H.; Li, Z. M. Highly Conductive and Stretchable Carbon Nanotube/Thermoplastic Polyurethane Composite for Wearable Heater. *Composites Science and Technology* **2019**, *181* (March), 107695.

(123) Maziz, A.; Concas, A.; Khaldi, A.; Stålhand, J.; Persson, N. K.; Jager, E. W. H. Knitting and Weaving Artificial Muscles. *Science Advances* **2017**, *3* (1), 1–11.

(124) Paradiso, R.; Caldani, L.; Pacelli, M. Knitted Electronic Textiles. In *Wearable Sensors: Fundamentals, Implementation and Applications*; Elsevier Ltd, 2014; Vol. 1, pp 153–174. https://doi.org/10.1016/B978-0-12-418662-0.00003-9.

(125) Kuroda, T.; Takahashi, H.; Masuda, A. Woven Electronic Textiles. In *Wearable Sensors: Fundamentals, Implementation and Applications*; Elsevier Ltd., 2014; pp 175–198. https://doi.org/10.1016/B978-0-12-418662-0.00021-0.

(126) Tao, X.; Koncar, V. Textile Electronic Circuits Based on Organic Fibrous Transistors. In *Smart Textiles and Their Applications*; Elsevier Ltd, 2016; pp 569–598.

(127) Foroughi, J.; Spinks, G. M.; Aziz, S.; Mirabedini, A.; Jeiranikhameneh, A.; Wallace, G. G.; Kozlov, M. E.; Baughman, R. H. Knitted Carbon-Nanotube-Sheath/Spandex-Core Elastomeric Yarns for Artificial Muscles and Strain Sensing. *ACS Nano* **2016**, *10* (10), 9129–9135. https://doi.org/10.1021/acsnano.6b04125.

(128) Luo, X.; Weng, W.; Liang, Y.; Hu, Z.; Zhang, Y.; Yang, J.; Yang, L.; Yang, S.; Zhu, M.; Cheng, H. M. Multifunctional Fabrics of Carbon Nanotube Fibers. *Journal of Materials Chemistry A* **2019**, *7* (15), 8790–8797.

(129) Liu, P.; Li, Y.; Xu, Y.; Bao, L.; Wang, L.; Pan, J.; Zhang, Z.; Sun, X.; Peng, H. Stretchable and Energy-Efficient Heating Carbon Nanotube Fiber by Designing a Hierarchically Helical Structure. *Small* **2018**, *14* (4), 1–6.

(130) Lu, Y.; Biswas, M. C.; Guo, Z.; Jeon, J. W.; Wujcik, E. K. Recent Developments in Bio-Monitoring via Advanced Polymer Nanocomposite-Based Wearable Strain Sensors. *Biosensors and Bioelectronics* **2019**, *123* (August 2018), 167–177.

(131) Li, X.; Hua, T.; Xu, B. Electromechanical Properties of a Yarn Strain Sensor with Graphene-Sheath/Polyurethane-Core. *Carbon* **2017**, *118*, 686–698.

(132) Yu, S.; Wang, X.; Xiang, H.; Zhu, L.; Tebyetekerwa, M.; Zhu, M. Superior Piezoresistive Strain Sensing Behaviors of Carbon Nanotubes in One-Dimensional Polymer Fiber Structure. *Carbon* **2018**, *140*, 1–9.

(133) Wang, Y.; Hao, J.; Huang, Z.; Zheng, G.; Dai, K.; Liu, C.; Shen, C. Flexible Electrically Resistive-Type Strain Sensors Based on Reduced Graphene Oxide-Decorated Electrospun Polymer Fibrous Mats for Human Motion Monitoring. *Carbon* **2018**, *126*, 360–371.

(134) Seyedin, S.; Razal, J. M.; Innis, P. C.; Jeiranikhameneh, A.; Beirne, S.; Wallace, G. G. Knitted Strain Sensor Textiles of Highly Conductive All-Polymeric Fibers. *ACS Applied Materials and Interfaces* **2015**, *7* (38), 21150–21158. https://doi.org/10.1021/acsami.5b04892.

(135) Pan, J.; Hao, B.; Song, W.; Chen, S.; Li, D.; Luo, L.; Xia, Z.; Cheng, D.; Xu, A.; Cai, G.; Wang, X. Highly Sensitive and Durable Wearable Strain Sensors from a Core-Sheath Nanocomposite Yarn. *Composites Part B: Engineering* **2020**, *183* (October 2019), 107683.

(136) Wang, X.; Li, J.; Song, H.; Huang, H.; Gou, J. Highly Stretchable and Wearable Strain Sensor Based on Printable Carbon Nanotube Layers/Polydimethylsiloxane Composites with Adjustable Sensitivity. *ACS Applied Materials and Interfaces* **2018**, *10* (8), 7371–7380.

(137) Li, W.; Xu, F.; Liu, W.; Gao, Y.; Zhang, K.; Zhang, X.; Qiu, Y. Flexible Strain Sensor Based on Aerogel-Spun Carbon Nanotube Yarn with a Core-Sheath Structure. *Composites Part A: Applied Science and Manufacturing* **2018**, *108* (November 2017), 107–113.

(138) He, Z.; Zhou, G.; Byun, J. H.; Lee, S. K.; Um, M. K.; Park, B.; Kim, T.; Lee, S. B.; Chou, T. W. Highly Stretchable Multi-Walled Carbon Nanotube/Thermoplastic Polyurethane Composite Fibers for Ultrasensitive, Wearable Strain Sensors. *Nanoscale* **2019**, *11* (13), 5884–5890.

(139) Yamada, T.; Hayamizu, Y.; Yamamoto, Y.; Yomogida, Y.; Izadi-Najafabadi, A.; Futaba, D. N.; Hata, K. A Stretchable Carbon Nanotube Strain Sensor for Human-Motion Detection. *Nature Nanotechnology* **2011**, *6* (5), 296–301. https://doi.org/10.1038/nnano.2011.36.

(140) Aouraghe, M. A.; Xu, F.; Liu, X.; Qiu, Y. Flexible, Quickly Responsive and Highly Efficient E-Heating Carbon Nanotube Film. *Composites Science and Technology* **2019**, *183* (August).

(141) Zhang, L.; Baima, M.; Andrew, T. L. Transforming Commercial Textiles and Threads into Sewable and Weavable Electric Heaters. *ACS Applied Materials and Interfaces* **2017**, *9* (37), 32299–32307.

(142) Ma, Z.; Kang, S.; Ma, J.; Shao, L.; Wei, A.; Liang, C.; Gu, J.; Yang, B.; Dong, D.; Wei, L.; Ji, Z. High-Performance and Rapid-Response Electrical Heaters Based on Ultraflexible, Heat-Resistant, and Mechanically Strong Aramid Nanofiber/Ag Nanowire Nanocomposite Papers. *ACS Nano* **2019**.

(143) Lee, Y.; Le, V. T.; Kim, J. G.; Kang, H.; Kim, E. S.; Ahn, S. E.; Suh, D. Versatile, High-Power, Flexible, Stretchable Carbon Nanotube Sheet Heating Elements Tolerant to Mechanical Damage and Severe Deformation. *Advanced Functional Materials* **2018**, *28* (8), 1–8.

(144) Zhang, M.; Wang, C.; Liang, X.; Yin, Z.; Xia, K.; Wang, H.; Jian, M.; Zhang, Y. Weft-Knitted Fabric for a Highly Stretchable and Low-Voltage Wearable Heater. *Advanced Electronic Materials* **2017**, *3* (9).

(145) Hao, Y.; Tian, M.; Zhao, H.; Qu, L.; Zhu, S.; Zhang, X.; Chen, S.; Wang, K.; Ran, J. High Efficiency Electrothermal Graphene/Tourmaline Composite Fabric Joule Heater with Durable Abrasion Resistance via a Spray Coating Route. *Industrial and Engineering Chemistry Research* **2018**, *57* (40), 13437–13448.

(146) Liu, P.; Li, Y.; Xu, Y.; Bao, L.; Wang, L.; Pan, J.; Zhang, Z.; Sun, X.; Peng, H. Stretchable and Energy-Efficient Heating Carbon Nanotube Fiber by Designing a Hierarchically Helical Structure. *Small* **2018**, *14* (4), 1–6.

(147) Dudchenko, A. V.; Chen, C.; Cardenas, A.; Rolf, J.; Jassby, D. Frequency-Dependent Stability of CNT Joule Heaters in Ionizable Media and Desalination Processes. *Nature Nanotechnology* **2017**, *12* (6), 557–563.

(148) Ning, W.; Wang, Z.; Liu, P.; Zhou, D.; Yang, S.; Wang, J.; Li, Q.; Fan, S.; Jiang, K. Multifunctional Super-Aligned Carbon Nanotube/Polyimide Composite Film Heaters and Actuators. *Carbon* **2018**, *139*, 1136–1143.

(149) Jung, D.; Han, M.; Lee, G. S. Flexible Transparent Conductive Heater Using Multiwalled Carbon Nanotube Sheet. *Journal of Vacuum Science and Technology B: Microelectronics and Nanometer Structures* **2014**, *32* (4). https://doi.org/10.1116/1.4876127.

(150) Levitt, A.; Hegh, D.; Phillips, P.; Uzun, S.; Anayee, M.; Razal, J. M.; Gogotsi, Y.; Dion, G. 3D Knitted Energy Storage Textiles Using MXene-Coated Yarns. *Materials Today* **2020**, *34* (xx), 17–29.

(151) Wang, Z.; Qin, S.; Seyedin, S.; Zhang, J.; Wang, J.; Levitt, A.; Li, N.; Haines, C.; Ovalle-Robles, R.; Lei, W.; Gogotsi, Y.; Baughman, R. H.; Razal, J. M. High-Performance Biscrolled MXene/Carbon Nanotube Yarn Supercapacitors. *Small* **2018**, *14* (37), 1–9.

(152) Mun, T. J.; Kim, S. H.; Park, J. W.; Moon, J. H.; Jang, Y.; Huynh, C.; Baughman, R. H.; Kim, S. J. Wearable Energy Generating and Storing Textile Based on Carbon Nanotube Yarns. *Advanced Functional Materials* **2020**, *2000411*, 1–8.

(153) Park, J. W.; Lee, D. Y.; Kim, H.; Hyeon, J. S.; De Andrade, M. J.; Baughman, R. H.; Kim, S. J. Highly Loaded MXene/Carbon Nanotube Yarn Electrodes for Improved Asymmetric Supercapacitor Performance. *MRS Communications* **2019**, *9* (1), 114–121.

(154) Levitt, A.; Zhang, J.; Dion, G.; Gogotsi, Y.; Razal, J. M. MXene-Based Fibers, Yarns, and Fabrics for Wearable Energy Storage Devices. *Advanced Functional Materials* **2020**, *2000739*, 1–22.

(155) Zhang, J.; Seyedin, S.; Gu, Z.; Yang, W.; Wang, X.; Razal, J. M. MXene: A Potential Candidate for Yarn Supercapacitors. *Nanoscale* **2017**, *9* (47), 18604–18608. https://doi.org/10.1039/c7nr06619h.

(156) Sun, S.; Liao, C.; Hafez, A. M.; Zhu, H.; Wu, S. Two-Dimensional MXenes for Energy Storage. *Chemical Engineering Journal* **2018**, *338* (October 2017), 27–45.

(157) Muralidharan, N.; Teblum, E.; Westover, A. S.; Schauben, D.; Itzhak, A.; Muallem, M.; Nessim, G. D.; Pint, C. L. Carbon Nanotube Reinforced Structural Composite Supercapacitor. *Scientific Reports* **2018**, *8* (1), 1–9.

(158) Hunter, L. Durability of Fabrics and Garments. In *Engineering Apparel Fabrics and Garments*; Fan, J., Hunter, L., Eds.; Woodhead Publishing, 2009; pp 161–195.

(159) Bide, M. Testing Textile Durability. In *Understanding and Improving the Durability of Textiles*; Annis, P., Ed.; Woodhead Publishing, 2012; pp 126–142.

(160) Molla, M. T. I.; Compton, C.; Dunne, L. E. Launderability of Surface-Insulated Cut and Sew E-Textiles. *Proceedings - International Symposium on Wearable Computers, ISWC* **2018**, 104–111. https://doi.org/10.1145/3267242.3267255.

(161) Zeagler, C.; Gilliland, S.; Audy, S.; Starner, T. Can i Wash It?: The Effect of Washing Conductive Materials Used in Making Textile Based Wearable Electronic Interfaces. *ISWC 2013 - Proceedings of the 2013 ACM International Symposium on Wearable Computers* **2013**, 143–144. https://doi.org/10.1145/2493988.2494341.

(162) Zaman, S.; Tao, X.; Cochrane, C.; Koncar, V. Launderability of Conductive Polymer Yarns Used for Connections of E-Textile Modules: Mechanical Stresses. *Fibers and Polymers* **2019**, *20* (11), 2355–2366. https://doi.org/10.1007/s12221-019-9325-x.

(163) Tao, X.; Koncar, V.; Huang, T. H.; Shen, C. L.; Ko, Y. C.; Jou, G. T. How to Make Reliable, Washable, and Wearable Textronic Devices. *Sensors (Switzerland)* **2017**, *17* (4). https://doi.org/10.3390/s17040673.

(164) Zaman, S. U.; Tao, X.; Cochrane, C.; Koncar, V. Market Readiness of Smart Textile Structures - Reliability and Washability. *IOP Conference Series: Materials Science and Engineering* **2018**, *459* (1). https://doi.org/10.1088/1757-899X/459/1/012071.

(165) Ismar, E.; Zaman, S. uz; Tao, X.; Cochrane, C.; Koncar, V. Effect of Water and Chemical Stresses on the Silver Coated Polyamide Yarns. *Fibers and Polymers* **2019**, *20* (12), 2604–2610.

(166) Du, D.; Tang, Z.; Ouyang, J. Highly Washable E-Textile Prepared by Ultrasonic Nanosoldering of Carbon Nanotubes onto Polymer Fibers. *Journal of Materials Chemistry C* **2018**, *6* (4), 883–889. https://doi.org/10.1039/c7tc05179d.

(167) Alimohammadi, F.; Gashti, M. P.; Shamei, A. A Novel Method for Coating of Carbon Nanotube on Cellulose Fiber Using 1,2,3,4-Butanetetracarboxylic Acid as a Cross-Linking Agent. *Progress in Organic Coatings* **2012**, *74* (3), 470–478.

(168) Iijima, S. Helical Microtubules of Graphitic Carbon. *Nature* **1991**, *354* (6348), 56–58.

(169) Cai, G.; Yang, M.; Pan, J.; Cheng, D.; Xia, Z.; Wang, X.; Tang, B. Large-Scale Production of Highly Stretchable CNT/Cotton/Spandex Composite Yarn for Wearable Applications. *ACS Applied Materials and Interfaces* **2018**, *10* (38), 32726–32735.

(170) Yang, M.; Pan, J.; Luo, L.; Xu, A.; Huang, J. CNT / Cotton Composite Yarn for Electro- CNT / Cotton Composite Yarn for Electro- Thermochromic Textiles. *Smart Materials and Structures* **2019**, *28*.

(171) Yang, M.; Fu, C.; Xia, Z.; Cheng, D.; Cai, G.; Tang, B.; Wang, X. Conductive and Durable CNT-Cotton Ring Spun Yarns. *Cellulose* **2018**, *25* (7), 4239–4249.

(172) Zhang, X.; Li, Q.; Holesinger, T. G.; Arendt, P. N.; Huang, J.; Kirven, P. D.; Clapp, T. G.; DePaula, R. F.; Liao, X.; Zhao, Y.; Zheng, L.; Peterson, D. E.; Zhu, Y. Ultrastrong, Stiff, and Lightweight Carbon-Nanotube Fibers. *Advanced Materials* **2007**, *19* (23), 4198–4201.

(173) Behabtu, N.; Young, C. C.; Tsentalovich, D. E.; Kleinerman, O.; Wang, X.; Ma, A. W. K.; Bengio, E. A.; Ter Waarbeek, R. F.; De Jong, J. J.; Hoogerwerf, R. E.; Fairchild, S. B.; Ferguson, J. B.; Maruyama, B.; Kono, J.; Talmon, Y.; Cohen, Y.; Otto, M. J.; Pasquali, M. Strong, Light, Multifunctional Fibers of Carbon Nanotubes with Ultrahigh Conductivity. *Science* **2013**, *339* (6116), 182–186. https://doi.org/10.1126/science.1228061.

(174) Li, Q.; Zhang, X.; DePaula, R. F.; Zheng, L.; Zhao, Y.; Stan, L.; Holesinger, T. G.; Arendt, P. N.; Peterson, D. E.; Zhu, Y. T. Sustained Growth of Ultralong Carbon Nanotube Arrays for Fiber Spinning. *Advanced Materials* **2006**, *18* (23), 3160–3163. https://doi.org/10.1002/adma.200601344.

(175) Li, Y. L.; Kinloch, I. A.; Windle, A. H. Direct Spinning of Carbon Nanotube Fibers from Chemical Vapor Deposition Synthesis. *Science* **2004**, *304* (5668), 276–278. https://doi.org/10.1126/science.1094982.

(176) Li, Y.; Shang, Y.; He, X.; Peng, Q.; Du, S.; Shi, E.; Wu, S. Overtwisted , Resolvable Carbon Nanotube Yarn Entanglement as Strain Sensors and Rotational Actuators. **2013**, No. 9, 8128–8135. https://doi.org/10.1021/nn403400c.

(177) Tang, Z.; Jia, S.; Shi, S.; Wang, F.; Li, B. Coaxial Carbon Nanotube/Polymer Fibers as Wearable Piezoresistive Sensors. *Sensors and Actuators, A: Physical* **2018**, *284*, 85–95. https://doi.org/10.1016/j.sna.2018.10.012.

(178) Liu, K.; Sun, Y.; Zhou, R.; Zhu, H.; Wang, J.; Liu, L.; Fan, S.; Jiang, K. Carbon Nanotube Yarns with High Tensile Strength Made by a Twisting and Shrinking Method. *Nanotechnology* **2010**, *21* (4). https://doi.org/10.1088/0957-4484/21/4/045708.

(179) Sears, K.; Skourtis, C.; Atkinson, K.; Finn, N.; Humphries, W. Focused Ion Beam Milling of Carbon Nanotube Yarns to Study the Relationship between Structure and Strength. *Carbon* **2010**, *48* (15), 4450–4456. https://doi.org/10.1016/j.carbon.2010.08.004.

(180) Chawla, S.; Naraghi, M.; Davoudi, A. Effect of Twist and Porosity on the Electrical Conductivity of Carbon Nanofiber Yarns. *Nanotechnology* **2013**, *24* (25). https://doi.org/10.1088/0957-4484/24/25/255708.

(181) Liang, X.; Gao, Y.; Duan, J.; Liu, Z.; Fang, S.; Baughman, R. H.; Jiang, L.; Cheng, Q. Enhancing the Strength, Toughness, and Electrical Conductivity of Twist-Spun Carbon Nanotube Yarns by π Bridging. *Carbon* **2019**, *150*, 268–274.

(182) Shang, Y.; Wang, Y.; Li, S.; Hua, C.; Zou, M.; Cao, A. High-Strength Carbon Nanotube Fibers by Twist-Induced Self-Strengthening. *Carbon* **2017**, *119*, 47–55. https://doi.org/10.1016/j.carbon.2017.03.101.

(183) Cho, H.; Lee, H.; Oh, E.; Lee, S. H.; Park, J.; Park, H. J.; Yoon, S. B.; Lee, C. H.; Kwak, G. H.; Lee, W. J.; Kim, J.; Kim, J. E.; Lee, K. H. Hierarchical Structure of Carbon Nanotube Fibers, and the Change of Structure during Densification by Wet Stretching. *Carbon* **2018**, *136*, 409–416. https://doi.org/10.1016/j.carbon.2018.04.071.

(184) Misak, H. E.; Mall, S. Electrical Conductivity, Strength and Microstructure of Carbon Nanotube Multi-Yarns. *Materials and Design* **2015**, *75*, 76–84. https://doi.org/10.1016/j.matdes.2015.03.020.

(185) Anike, J. C.; Belay, K.; Abot, J. L. Effect of Twist on the Electromechanical Properties of Carbon Nanotube Yarns. *Carbon* **2019**, *142*, 491–503. https://doi.org/10.1016/j.carbon.2018.10.067.

(186) Inoue, Y.; Hayashi, K.; Karita, M.; Nakano, T.; Shimamura, Y.; Shirasu, K.; Yamamoto, G.; Hashida, T. Study on the Mechanical and Electrical Properties of Twisted CNT Yarns Fabricated from CNTs with Various Diameters. *Carbon* **2021**, *176*, 400–410. https://doi.org/10.1016/j.carbon.2021.01.139.

(187) Tran, C. D.; Humphries, W.; Smith, S. M.; Huynh, C.; Lucas, S. Improving the Tensile Strength of Carbon Nanotube Spun Yarns Using a Modified Spinning Process. *Carbon* **2009**, *47* (11), 2662–2670. https://doi.org/10.1016/j.carbon.2009.05.020.

(188) Sugano, K.; Kurata, M.; Kawada, H. Evaluation of Mechanical Properties of Untwisted Carbon Nanotube Yarn for Application to Composite Materials. *Carbon* **2014**, *78*, 356–365. https://doi.org/10.1016/j.carbon.2014.07.012.

(189) Liu, K.; Sun, Y.; Zhou, R.; Zhu, H.; Wang, J.; Liu, L.; Fan, S.; Jiang, K. Carbon Nanotube Yarns with High Tensile Strength Made by a Twisting and Shrinking Method. *Nanotechnology* **2010**, *21* (4). https://doi.org/10.1088/0957-4484/21/4/045708.

(190) Jia, J.; Zhao, J.; Xu, G.; Di, J.; Yong, Z.; Tao, Y.; Fang, C.; Zhang, Z.; Zhang, X.; Zheng, L.; Li, Q. A Comparison of the Mechanical Properties of Fibers Spun from Different Carbon Nanotubes. *Carbon* **2011**, *49* (4), 1333–1339. https://doi.org/10.1016/j.carbon.2010.11.054.

(191) Lepró, X.; Aracne-Ruddle, C.; Malone, D.; Hamza, H.; Schaible, E.; Buchsbaum, S. F.; Calonico-Soto, A.; Bigelow, J.; Meshot, E.; Baxamusa, S.; Stadermann, M. Liquid-Free Covalent Reinforcement of Carbon Nanotube Dry-Spun Yarns and Free-Standing Sheets. *Carbon* **2021**, *187*. https://doi.org/10.1016/j.carbon.2021.11.012.

(192) Fang, S.; Zhang, M.; Zakhidov, A. A.; Baughman, R. H. Structure and Process-Dependent Properties of Solid-State Spun Carbon Nanotube Yarns. *Journal of Physics Condensed Matter* **2010**, *22* (33). https://doi.org/10.1088/0953-8984/22/33/334221.

(193) Headrick, R. J.; Tsentalovich, D. E.; Berdegué, J.; Bengio, E. A.; Liberman, L.; Kleinerman, O.; Lucas, M. S.; Talmon, Y.; Pasquali, M. Structure-Property Relations in Carbon Nanotube Fibers by Downscaling Solution Processing. *Advanced Materials* **2018**, *1704482*, 1–8. https://doi.org/10.1002/adma.201704482.

(194) Wang, C.; Xia, K.; Wang, H.; Liang, X.; Yin, Z.; Zhang, Y. Advanced Carbon for Flexible and Wearable Electronics. *Advanced Materials* **2019**, *1801072* (31), 1–37.

(195) Cai, G.; Yang, M.; Xu, Z.; Liu, J.; Tang, B.; Wang, X. Flexible and Wearable Strain Sensing Fabrics. *Chemical Engineering Journal* **2017**, *325*, 396–403.

(196) Wang, B.; Facchetti, A. Mechanically Flexible Conductors for Stretchable and Wearable E-Skin and E-Textile Devices. *Advanced Materials* **2019**, *1901408*, 1–53. https://doi.org/10.1002/adma.201901408.

(197) Kwak, S. S.; Yoon, H. J.; Kim, S. W. Textile-Based Triboelectric Nanogenerators for Self-Powered Wearable Electronics. *Advanced Functional Materials* **2019**, *29* (2), 1–26.

(198) Keum, H.; Mccormick, M.; Liu, P.; Zhang, Y.; Omenetto, F. G. Epidermal Electronics. *Science* **2011**, *333*, 838–843.

(199) Kaltenbrunner, M.; Sekitani, T.; Reeder, J.; Yokota, T.; Kuribara, K.; Tokuhara, T.; Drack, M.; Schwödiauer, R.; Graz, I.; Bauer-Gogonea, S.; Bauer, S.; Someya, T. An Ultra-Lightweight Design for Imperceptible Plastic Electronics. *Nature* **2013**, *499* (7459), 458–463.

(200) Li, P.; Jin, Z.; Xiao, D. A Phytic Acid Etched Ni/Fe Nanostructure Based Flexible Network as a High-Performance Wearable Hybrid Energy Storage Device. *Journal of Materials Chemistry A* **2017**, *5* (7), 3274–3283.

(201) Yu, D.; Goh, K.; Wang, H.; Wei, L.; Jiang, W.; Zhang, Q.; Dai, L.; Chen, Y. Scalable Synthesis of Hierarchically Structured Carbon Nanotube-Graphene Fibres for Capacitive Energy Storage. *Nature Nanotechnology* **2014**, *9* (7), 555–562. https://doi.org/10.1038/nnano.2014.93.

(202) Xie, S.; Li, T.; Xu, Z.; Wang, Y.; Liu, X.; Guo, W. A High-Response Transparent Heater Based on a CuS Nanosheet Film with Superior Mechanical Flexibility and Chemical Stability. *Nanoscale* **2018**, *10* (14), 6531–6538.

(203) An, B. W.; Gwak, E. J.; Kim, K.; Kim, Y. C.; Jang, J.; Kim, J. Y.; Park, J. U. Stretchable, Transparent Electrodes as Wearable Heaters Using Nanotrough Networks of Metallic Glasses with Superior Mechanical Properties and Thermal Stability. *Nano Letters* **2016**, *16* (1), 471–478.

(204) Takei, K.; Takahashi, T.; Ho, J. C.; Ko, H.; Gillies, A. G.; Leu, P. W.; Fearing, R. S.; Javey, A. Nanowire Active-Matrix Circuitry for Low-Voltage Macroscale Artificial Skin. *Nature Materials* **2010**, *9* (10), 821–826.

(205) Chu, H.; Hu, X.; Wang, Z.; Mu, J.; Li, N.; Zhou, X.; Fang, S.; Haines, C. S.; Park, J. W.; Qin, S.; Yuan, N.; Xu, J.; Tawfick, S.; Kim, H.; Conlin, P.; Cho, M.; Cho, K.; Oh, J.; Nielsen, S.; Alberto, K. A.; Razal, J. M.; Foroughi, J.; Spinks, G. M.; Kim, S. J.; Ding, J.; Leng, J.; Baughman, R. H. Unipolar Stroke, Electroosmotic Pump Carbon Nanotube Yarn Muscles. *Science* **2021**, *371* (6528), 494–498.

(206) Boutry, C. M.; Negre, M.; Jorda, M.; Vardoulis, O.; Chortos, A.; Khatib, O.; Bao, Z. A Hierarchically Patterned, Bioinspired e-Skin Able to Detect the Direction of Applied Pressure for Robotics. *Science Robotics* **2018**, *3* (24), 1–10.

(207) He, Z.; Zhou, G.; Byun, J.; Lee, S.; Um, M.; Park, B.; Kim, T.; Lee, S. B.; Chou, T. Highly Stretchable Multi-Walled Carbon Nanotube/Thermoplastic Polyurethane Composite Fibers for Ultrasensitive, Wearable Strain Sensors. *Nanoscale* **2019**, *1000* (11), 5884–5890. https://doi.org/10.1039/c9nr01005j.

(208) Lee, J.; Shin, S.; Lee, S.; Song, J.; Kang, S.; Han, H.; Kim, S.; Kim, S.; Seo, J.; Kim, D.; Lee, T. Highly Sensitive Multifilament Fiber Strain Sensors with Ultrabroad Sensing Range for Textile Electronics. *ACS Nano* **2018**, *12* (5), 4259–4268.

(209) Li, Y.; Li, Y.; Su, M.; Li, W.; Li, Y.; Li, H.; Qian, X.; Zhang, X.; Li, F.; Song, Y. Electronic Textile by Dyeing Method for Multiresolution Physical Kineses Monitoring. *Advanced Electronic Materials* **2017**, *3* (10), 1–7.

(210) Heo, J. S.; Eom, J.; Kim, Y. H.; Park, S. K. Recent Progress of Textile-Based Wearable Electronics: A Comprehensive Review of Materials, Devices, and Applications. *Small* **2018**, *14* (3), 1–16.

(211) Jin, H.; Nayeem, M. O. G.; Lee, S.; Matsuhisa, N.; Inoue, D.; Yokota, T.; Hashizume, D.; Someya, T. Highly Durable Nanofiber-Reinforced Elastic Conductors for Skin-Tight Electronic Textiles. *ACS Nano* **2019**, *13* (7), 7905–7912.

(212) Lima, R. M. A. P.; Alcaraz-Espinoza, J. J.; Da Silva, F. A. G.; De Oliveira, H. P. Multifunctional Wearable Electronic Textiles Using Cotton Fibers with Polypyrrole and Carbon Nanotubes. *ACS Applied Materials and Interfaces* **2018**, *10* (16), 13783–13795.

(213) De Volder, M. F. L.; Tawfick, S. H.; Baughman, R. H.; Hart, A. J. Carbon Nanotubes: Present and Future Commercial Applications. *Science* **2013**, *339* (6119), 535–539.

(214) Di, J.; Zhang, X.; Yong, Z.; Zhang, Y.; Li, D.; Li, R.; Li, Q. Carbon-Nanotube Fibers for Wearable Devices and Smart Textiles. *Advanced Materials* **2016**, *28* (47), 10529–10538.

(215) Zhang, L.; Wang, X.; Xu, W.; Zhang, Y.; Li, Q.; Bradford, P. D.; Zhu, Y. Strong and Conductive Dry Carbon Nanotube Films by Microcombing. *Small* **2015**, *11* (31), 3830–3836.

(216) Alvarez, N. T.; Miller, P.; Haase, M. R.; Lobo, R.; Malik, R.; Shanov, V. Tailoring Physical Properties of Carbon Nanotube Threads during Assembly. *Carbon* **2019**, *144*, 55–62.

(217) Foroughi, J.; Spinks, G. M.; Aziz, S.; Mirabedini, A.; Jeiranikhameneh, A.; Wallace, G. G.; Kozlov, M. E.; Baughman, R. H. Knitted Carbon-Nanotube-Sheath/Spandex-Core Elastomeric Yarns for Artificial Muscles and Strain Sensing. *ACS Nano* **2016**, *10* (10), 9129–9135.

(218) Zhang, D.; Miao, M.; Niu, H.; Wei, Z. Core-Spun Carbon Nanotube Yarn Supercapacitors for Wearable Electronic Textiles. *ACS Nano* **2014**, *8* (5), 4571–4579.

(219) Seyedin, S.; Moradi, S.; Singh, C.; Razal, J. M. Continuous Production of Stretchable Conductive Multifilaments in Kilometer Scale Enables Facile Knitting of Wearable Strain Sensing Textiles. *Applied Materials Today* **2018**, *11*, 255–263.

(220) Inoue, Y.; Kakihata, K.; Hirono, Y.; Horie, T.; Ishida, A.; Mimura, H. One-Step Grown Aligned Bulk Carbon Nanotubes by Chloride Mediated Chemical Vapor Deposition. *Applied Physics Letters* **2008**, *92* (21).

(221) Faraji, S.; L. Stano, K.; Yildiz, O.; Li, A.; Zhu, Y.; Bradford, P. D. Ultralight Anisotropic Foams from Layered Aligned Carbon Nanotube Sheets. *Nanoscale* **2015**, *7* (40), 17038–17047.

(222) Zhao, J.; Zhang, X.; Huang, Y.; Zou, J.; Liu, T.; Liang, N.; Yu, F.; Pan, Z.; Zhu, Y.; Miao, M.; Li, Q. A Comparison of the Twisted and Untwisted Structures for One-Dimensional Carbon Nanotube Assemblies. *Materials and Design* **2018**, *146*, 20–27.

(223) Khoshnevis, H.; Tran, T. Q.; Mint, S. M.; Zadhoush, A.; Duong, H. M.; Youssefi, M. Effect of Alignment and Packing Density on the Stress Relaxation Process of Carbon Nanotube Fibers Spun from Floating Catalyst Chemical Vapor Deposition Method. *Colloids and Surfaces A: Physicochemical and Engineering Aspects* **2018**, *558* (July), 570–578.

(224) Fu, K.; Yildiz, O.; Bhanushali, H.; Wang, Y.; Stano, K.; Xue, L.; Zhang, X.; Bradford, P. D. Aligned Carbon Nanotube-Silicon Sheets: A Novel Nano-Architecture for Flexible Lithium Ion Battery Electrodes. *Advanced Materials* **2013**, *25* (36), 5109–5114.

(225) Mi, H. Y.; Jing, X.; Salick, M. R.; Cordie, T. M.; Turng, L. S. Carbon Nanotube (CNT) and Nanofibrillated Cellulose (NFC) Reinforcement Effect on Thermoplastic Polyurethane (TPU) Scaffolds Fabricated via Phase Separation Using Dimethyl Sulfoxide (DMSO) as Solvent. *Journal of the Mechanical Behavior of Biomedical Materials* **2016**, *62*, 417–427.

(226) Ji, M.; Deng, H.; Yan, D.; Li, X.; Duan, L.; Fu, Q. Selective Localization of Multi-Walled Carbon Nanotubes in Thermoplastic Elastomer Blends: An Effective Method for Tunable Resistivity-Strain Sensing Behavior. *Composites Science and Technology* **2014**, *92*, 16–26.

(227) de León, A. S.; Domínguez-Calvo, A.; Molina, S. I. Materials with Enhanced Adhesive Properties Based on Acrylonitrile-Butadiene-Styrene (ABS)/Thermoplastic Polyurethane (TPU) Blends for Fused Filament Fabrication (FFF). *Materials and Design* **2019**, *182*, 108044.

(228) Liu, H.; Dong, M.; Huang, W.; Gao, J.; Dai, K.; Guo, J.; Zheng, G.; Liu, C.; Shen, C.; Guo, Z. Lightweight Conductive Graphene/Thermoplastic Polyurethane Foams with Ultrahigh Compressibility for Piezoresistive Sensing. *Journal of Materials Chemistry C* **2017**, *5* (1), 73–83.

(229) Lund, A.; van der Velden, N. M.; Persson, N. K.; Hamedi, M. M.; Müller, C. Electrically Conducting Fibres for E-Textiles: An Open Playground for Conjugated Polymers and Carbon Nanomaterials. *Materials Science and Engineering R: Reports*. Elsevier Ltd April 1, 2018, pp 1–29. https://doi.org/10.1016/j.mser.2018.03.001.

(230) Truong, T. K.; Lee, Y.; Suh, D. Multifunctional Characterization of Carbon Nanotube Sheets, Yarns, and Their Composites. *Current Applied Physics* **2016**, *16* (9), 1250–1258.

(231) Bai, Y.; Zhang, R.; Ye, X.; Zhu, Z.; Xie, H.; Shen, B.; Cai, D.; Liu, B.; Zhang, C.; Jia, Z.; Zhang, S.; Li, X.; Wei, F. Carbon Nanotube Bundles with Tensile Strength over 80 GPa. *Nature Nanotechnology* **2018**, *13* (7), 589–595.

(232) Sun, Y.; Hou, K.; Zhang, D.; Chang, S.; Ye, L.; Cao, A.; Shang, Y. High Performance Carbon Nanotube/Polymer Composite Fibers and Water-Driven Actuators. *Composites Science and Technology* **2021**, 108676. https://doi.org/10.1016/j.compscitech.2021.108676.

(233) Levitt, A.; Hegh, D.; Phillips, P.; Uzun, S.; Anayee, M.; Razal, J. M.; Gogotsi, Y.; Dion, G. 3D Knitted Energy Storage Textiles Using MXene-Coated Yarns. *Materials Today* **2020**, *34* (xx), 17–29.

(234) Ahmed, A.; Jalil, M. A.; Hossain, M. M.; Moniruzzaman, M.; Adak, B.; Islam, M. T.; Parvez, M. S.; Mukhopadhyay, S. A PEDOT:PSS and Graphene-Clad Smart Textile-Based Wearable Electronic Joule Heater with High Thermal Stability. *Journal of Materials Chemistry C* **2020**, *8* (45), 16204–16215. https://doi.org/10.1039/d0tc03368e.

(235) Ahmed, A.; Jalil, M. A.; Hossain, M. M.; Moniruzzaman, M.; Adak, B.; Islam, M. T.; Parvez, M. S.; Mukhopadhyay, S. A PEDOT:PSS and Graphene-Clad Smart Textile-Based Wearable Electronic Joule Heater with High Thermal Stability. *Journal of Materials Chemistry C* **2020**, *8* (45), 16204–16215. https://doi.org/10.1039/d0tc03368e.

(236) Lian, Y.; Yu, H.; Wang, M.; Yang, X.; Li, Z.; Yang, F.; Wang, Y.; Tai, H.; Liao, Y.; Wu, J.; Wang, X.; Jiang, Y.; Tao, G. A Multifunctional Wearable E-Textile: Via Integrated

Nanowire-Coated Fabrics. *Journal of Materials Chemistry C* **2020**, *8* (25), 8399–8409. https://doi.org/10.1039/d0tc00372g.

(237) Zheng, X.; Shen, J.; Hu, Q.; Nie, W.; Wang, Z.; Zou, L.; Li, C. Vapor Phase Polymerized Conducting Polymer/MXene Textiles for Wearable Electronics. *Nanoscale* **2021**, *13* (3), 1832–1841. https://doi.org/10.1039/d0nr07433k.

(238) Zhu, S.; Wang, M.; Qiang, Z.; Song, J.; Wang, Y.; Fan, Y.; You, Z.; Liao, Y.; Zhu, M.; Ye, C. Multi-Functional and Highly Conductive Textiles with Ultra-High Durability through 'Green' Fabrication Process. *Chemical Engineering Journal* **2021**, *406*. https://doi.org/10.1016/j.cej.2020.127140.

(239) Maity, S.; Chatterjee, A.; Singh, B.; Pal Singh, A. Polypyrrole Based Electro-Conductive Textiles for Heat Generation. *Journal of the Textile Institute* **2014**, *105* (8), 887–893. https://doi.org/10.1080/00405000.2013.861149.

(240) Lee, S.; Park, C. H. Electric Heated Cotton Fabrics with Durable Conductivity and Self-Cleaning Properties. *RSC Advances* **2018**, *8* (54), 31008–31018. https://doi.org/10.1039/C8RA05530K.

(241) Wang, Q. W.; Zhang, H. bin; Liu, J.; Zhao, S.; Xie, X.; Liu, L.; Yang, R.; Koratkar, N.; Yu, Z. Z. Multifunctional and Water-Resistant MXene-Decorated Polyester Textiles with Outstanding Electromagnetic Interference Shielding and Joule Heating Performances. *Advanced Functional Materials* **2019**, *29* (7). https://doi.org/10.1002/adfm.201806819.

(242) Zhang, L.; Baima, M.; Andrew, T. L. Transforming Commercial Textiles and Threads into Sewable and Weavable Electric Heaters. *ACS Applied Materials and Interfaces* **2017**, *9* (37), 32299–32307. https://doi.org/10.1021/acsami.7b10514.

(243) Moraes, M. R.; Alves, A. C.; Toptan, F.; Martins, M. S.; Vieira, E. M. F.; Paleo, A. J.; Souto, A. P.; Santos, W. L. F.; Esteves, M. F.; Zille, A. Glycerol/PEDOT:PSS Coated Woven Fabric as a Flexible Heating Element on Textiles. *Journal of Materials Chemistry C* **2017**, *5* (15), 3807–3822. https://doi.org/10.1039/C7TC00486A.

(244) Yeon, C.; Kim, G.; Lim, J. W.; Yun, S. J. Highly Conductive PEDOT:PSS Treated by Sodium Dodecyl Sulfate for Stretchable Fabric Heaters. *RSC Advances* **2017**, *7* (10), 5888–5897. https://doi.org/10.1039/c6ra24749k.

(245) Hsu, P. C.; Liu, X.; Liu, C.; Xie, X.; Lee, H. R.; Welch, A. J.; Zhao, T.; Cui, Y. Personal Thermal Management by Metallic Nanowire-Coated Textile. *Nano Letters* **2015**, *15* (1), 365–371. https://doi.org/10.1021/nl5036572.

(246) Ali, A.; Baheti, V.; Militky, J.; Khan, Z.; Gilani, S. Q. Z. Comparative Performance of Copper and Silver Coated Stretchable Fabrics. *Fibers and Polymers* **2018**, *19* (3), 607–619. https://doi.org/10.1007/s12221-018-7917-5.

(247) Kim, H.; Lee, S.; Kim, H. Electrical Heating Performance of Electro-Conductive Para-Aramid Knit Manufactured by Dip-Coating in a Graphene/Waterborne Polyurethane Composite. *Scientific Reports* **2019**, *9* (1). https://doi.org/10.1038/s41598-018-37455-0.

(248) Kongahge, D.; Foroughi, J.; Gambhir, S.; Spinks, G. M.; Wallace, G. G. Fabrication of a Graphene Coated Nonwoven Textile for Industrial Applications. *RSC Advances* **2016**, *6* (77), 73203–73209. https://doi.org/10.1039/c6ra15190f.

(249) Liu, X.; Qin, Z.; Dou, Z.; Liu, N.; Chen, L.; Zhu, M. Fabricating Conductive Poly(Ethylene Terephthalate) Nonwoven Fabrics Using an Aqueous Dispersion of Reduced Graphene Oxide as a Sheet Dyestuff. *RSC Advances* **2014**, *4* (45), 23869–23875. https://doi.org/10.1039/c4ra01645a.

(250) Pan, J.; Yang, M.; Luo, L.; Xu, A.; Tang, B.; Cheng, D.; Cai, G.; Wang, X. Stretchable and Highly Sensitive Braided Composite Yarn@Polydopamine@Polypyrrole for Wearable Applications. *ACS Applied Materials and Interfaces* **2019**, *11* (7), 7338–7348. https://doi.org/10.1021/acsami.8b18823.

(251) Lima, R. M. A. P.; Alcaraz-Espinoza, J. J.; da Silva, F. A. G.; de Oliveira, H. P. Multifunctional Wearable Electronic Textiles Using Cotton Fibers with Polypyrrole and Carbon Nanotubes. *ACS Applied Materials and Interfaces* **2018**, *10* (16), 13783–13795. https://doi.org/10.1021/acsami.8b04695.

(252) Yang, M.; Pan, J.; Xu, A.; Luo, L.; Cheng, D.; Cai, G.; Wang, J.; Tang, B.; Wang, X. Conductive Cotton Fabrics for Motion Sensing and Heating Applications. *Polymers* **2018**, *10* (6). https://doi.org/10.3390/polym10060568.

(253) Ilanchezhiyan, P.; Zakirov, A. S.; Kumar, G. M.; Yuldashev, S. U.; Cho, H. D.; Kang, T. W.; Mamadalimov, A. T. Highly Efficient CNT Functionalized Cotton Fabrics for Flexible/Wearable Heating Applications. *RSC Advances* **2015**, *5* (14), 10697–10702. https://doi.org/10.1039/c4ra10667a.

(254) Ma, C.; Yuan, Q.; Du, H.; Ma, M. G.; Si, C.; Wan, P. Multiresponsive MXene (Ti3C2T x)-Decorated Textiles for Wearable Thermal Management and Human Motion Monitoring. *ACS Applied Materials and Interfaces* **2020**, *12* (30), 34226–34234. https://doi.org/10.1021/acsami.0c10750.

(255) Liu, X.; Jin, X.; Li, L.; Wang, J.; Yang, Y.; Cao, Y.; Wang, W. Air-Permeable, Multifunctional, Dual-Energy-Driven MXene-Decorated Polymeric Textile-Based Wearable Heaters with Exceptional Electrothermal and Photothermal Conversion Performance. *Journal of Materials Chemistry A* **2020**, *8* (25), 12526–12537. https://doi.org/10.1039/d0ta03048a.

(256) Sadeqi, A.; Rezaei Nejad, H.; Alaimo, F.; Yun, H.; Punjiya, M.; Sonkusale, S. R. Washable Smart Threads for Strain Sensing Fabrics. *IEEE Sensors Journal* **2018**, *18* (22), 9137–9144. https://doi.org/10.1109/JSEN.2018.2870640.

(257) Karim, N.; Afroj, S.; Tan, S.; He, P.; Fernando, A.; Carr, C.; Novoselov, K. S. Scalable Production of Graphene-Based Wearable E-Textiles. *ACS Nano* **2017**, *11* (12), 12266–12275. https://doi.org/10.1021/acsnano.7b05921.

(258) Yun, Y. J.; Hong, W. G.; Choi, N. J.; Kim, B. H.; Jun, Y.; Lee, H. K. Ultrasensitive and Highly Selective Graphene-Based Single Yarn for Use in Wearable Gas Sensor. *Scientific Reports* **2015**, *5*, 1–7. https://doi.org/10.1038/srep10904.

(259) Cai, G.; Yang, M.; Xu, Z.; Liu, J.; Tang, B.; Wang, X. Flexible and Wearable Strain Sensing Fabrics. *Chemical Engineering Journal* **2017**, *325*, 396–403. https://doi.org/10.1016/j.cej.2017.05.091.

(260) Cai, G.; Yang, M.; Pan, J.; Cheng, D.; Xia, Z.; Wang, X.; Tang, B. Large-Scale Production of Highly Stretchable CNT/Cotton/Spandex Composite Yarn for Wearable Applications. *ACS Applied Materials and Interfaces* **2018**, *10* (38), 32726–32735. https://doi.org/10.1021/acsami.8b11885.

(261) Cao, R.; Pu, X.; Du, X.; Yang, W.; Wang, J.; Guo, H.; Zhao, S.; Yuan, Z.; Zhang, C.; Li, C.; Wang, Z. L. Screen-Printed Washable Electronic Textiles as Self-Powered Touch/Gesture Tribo-Sensors for Intelligent Human-Machine Interaction. *ACS Nano* **2018**, *12* (6), 5190–5196. https://doi.org/10.1021/acsnano.8b02477.

(262) Cui, J.; Zhou, S. Highly Conductive and Ultra-Durable Electronic Textiles via Covalent Immobilization of Carbon Nanomaterials on Cotton Fabric. *Journal of Materials Chemistry C* **2018**, *6* (45), 12273–12282. https://doi.org/10.1039/C8TC04017F.

(263) Krucińska, I.; Skrzetuska, E.; Urbaniak-Domagala, W. Prototypes of Carbon Nanotube-Based Textile Sensors Manufactured by the Screen Printing Method. *Fibres and Textiles in Eastern Europe* **2012**, *91* (2), 79–83.

(264) Karim, N.; Afroj, S.; Malandraki, A.; Butterworth, S.; Beach, C.; Rigout, M.; Novoselov, K. S.; Casson, A. J.; Yeates, S. G. All Inkjet-Printed Graphene-Based Conductive Patterns for Wearable e-Textile Applications. *Journal of Materials Chemistry C* **2017**, *5* (44), 11640–11648. https://doi.org/10.1039/c7tc03669h.

(265) Jeon, J. W.; Cho, S. Y.; Jeong, Y. J.; Shin, D. S.; Kim, N. R.; Yun, Y. S.; Kim, H. T.; Choi, S. B.; Hong, W. G.; Kim, H. J.; Jin, H. J.; Kim, B. H. Pyroprotein-Based Electronic Textiles with High Stability. *Advanced Materials* **2017**, *29* (6), 1–6. https://doi.org/10.1002/adma.201605479.

(266) Afroj, S.; Karim, N.; Wang, Z.; Tan, S.; He, P.; Holwill, M.; Ghazaryan, D.; Fernando, A.; Novoselov, K. S. Engineering Graphene Flakes for Wearable Textile Sensors via Highly Scalable and Ultrafast Yarn Dyeing Technique. *ACS Nano* **2019**, *13* (4), 3847–3857. https://doi.org/10.1021/acsnano.9b00319.

(267) Son, D.; Kang, J.; Vardoulis, O.; Kim, Y.; Matsuhisa, N.; Oh, J. Y.; To, J. W.; Mun, J.; Katsumata, T.; Liu, Y.; McGuire, A. F.; Krason, M.; Molina-Lopez, F.; Ham, J.; Kraft, U.; Lee, Y.; Yun, Y.; Tok, J. B. H.; Bao, Z. An Integrated Self-Healable Electronic Skin System Fabricated via Dynamic Reconstruction of a Nanostructured Conducting Network. *Nature Nanotechnology* **2018**, *13* (11), 1057–1065. https://doi.org/10.1038/s41565-018-0244-6.

(268) Gao, Y.; Yu, L.; Yeo, J. C.; Lim, C. T. Flexible Hybrid Sensors for Health Monitoring: Materials and Mechanisms to Render Wearability. *Advanced Materials* **2020**, *32* (15), 1–31. https://doi.org/10.1002/adma.201902133.

(269) Yamamoto, Y.; Yamamoto, D.; Takada, M.; Naito, H.; Arie, T.; Akita, S.; Takei, K. Efficient Skin Temperature Sensor and Stable Gel-Less Sticky ECG Sensor for a Wearable Flexible Healthcare Patch. *Advanced Healthcare Materials* **2017**, *6* (17). https://doi.org/10.1002/adhm.201700495.

(270) Kim, T.; Park, J.; Sohn, J.; Cho, D.; Jeon, S. Bioinspired, Highly Stretchable, and Conductive Dry Adhesives Based on 1D-2D Hybrid Carbon Nanocomposites for All-in-One ECG Electrodes. *ACS Nano* **2016**, *10* (4), 4770–4778. https://doi.org/10.1021/acsnano.6b01355.

(271) Liu, Y.; McGuire, A. F.; Lou, H. Y.; Li, T. L.; Tok, J. B. H.; Cui, B.; Bao, Z. Soft Conductive Micropillar Electrode Arrays for Biologically Relevant Electrophysiological Recording. *Proceedings of the National Academy of Sciences of the United States of America* **2018**, *115* (46), 11718–11723. https://doi.org/10.1073/pnas.1810827115.

(272) Huang, C. Y.; Chiu, C. W. Facile Fabrication of a Stretchable and Flexible Nanofiber Carbon Film-Sensing Electrode by Electrospinning and Its Application in Smart Clothing for ECG and EMG Monitoring. *ACS Applied Electronic Materials* **2021**, *3* (2), 676–686. https://doi.org/10.1021/acsaelm.0c00841.

(273) Sinha, S. K.; Noh, Y.; Reljin, N.; Treich, G. M.; Hajeb-Mohammadalipour, S.; Guo, Y.; Chon, K. H.; Sotzing, G. A. Screen-Printed PEDOT:PSS Electrodes on Commercial Finished Textiles for Electrocardiography. *ACS Applied Materials and Interfaces* **2017**, *9* (43), 37524–37528. https://doi.org/10.1021/acsami.7b09954.

(274) Zhao, Y.; Zhang, S.; Yu, T.; Zhang, Y.; Ye, G.; Cui, H.; He, C.; Jiang, W.; Zhai, Y.; Lu, C.; Gu, X.; Liu, N. Ultra-Conformal Skin Electrodes with Synergistically Enhanced Conductivity for Long-Time and Low-Motion Artifact Epidermal Electrophysiology. *Nature Communications* **2021**, *12* (1), 1–12. https://doi.org/10.1038/s41467-021-25152-y.

(275) Qiu, J.; Yu, T.; Zhang, W.; Zhao, Z.; Zhang, Y.; Ye, G.; Zhao, Y.; Du, X.; Liu, X.; Yang, L.; Zhang, L.; Qi, S.; Tan, Q.; Guo, X.; Li, G.; Guo, S.; Sun, H.; Wei, D.; Liu, N. A Bioinspired, Durable, and Nondisposable Transparent Graphene Skin Electrode for Electrophysiological Signal Detection. *ACS Materials Letters* **2020**, *2* (8), 999–1007. https://doi.org/10.1021/acsmaterialslett.0c00203.

(276) Ferrari, L. M.; Sudha, S.; Tarantino, S.; Esposti, R.; Bolzoni, F.; Cavallari, P.; Cipriani, C.; Mattoli, V.; Greco, F. Ultraconformable Temporary Tattoo Electrodes for Electrophysiology. *Advanced Science* **2018**, *5* (3), 1–11. https://doi.org/10.1002/advs.201700771.

(277) Leleux, P.; Johnson, C.; Strakosas, X.; Rivnay, J.; Hervé, T.; Owens, R. M.; Malliaras, G. G. Ionic Liquid Gel-Assisted Electrodes for Long-Term Cutaneous Recordings. *Advanced Healthcare Materials* **2014**, *3* (9), 1377–1380. https://doi.org/10.1002/adhm.201300614.

(278) Fayyaz Shahandashti, P.; Pourkheyrollah, H.; Jahanshahi, A.; Ghafoorifard, H. Highly Conformable Stretchable Dry Electrodes Based on Inexpensive Flex Substrate for Long-Term Biopotential (EMG/ECG) Monitoring. *Sensors and Actuators, A: Physical* **2019**, *295*, 678–686. https://doi.org/10.1016/j.sna.2019.06.041.

(279) Stauffer, F.; Thielen, M.; Sauter, C.; Chardonnens, S.; Bachmann, S.; Tybrandt, K.; Peters, C.; Hierold, C.; Vörös, J. Skin Conformal Polymer Electrodes for Clinical ECG and EEG Recordings. *Advanced Healthcare Materials* **2018**, *7* (7), 1–10. https://doi.org/10.1002/adhm.201700994.

(280) Wang, Y.; Yin, L.; Bai, Y.; Liu, S.; Wang, L.; Zhou, Y.; Hou, C.; Yang, Z.; Wu, H.; Ma, J.; Shen, Y.; Deng, P.; Zhang, S.; Duan, T.; Li, Z.; Ren, J.; Xiao, L.; Yin, Z.; Lu, N.; Huang, Y. A. Electrically Compensated, Tattoo-like Electrodes for Epidermal Electrophysiology at Scale. *Science Advances* **2020**, *6* (43). https://doi.org/10.1126/sciadv.abd0996.

(281) Ershad, F.; Thukral, A.; Yue, J.; Comeaux, P.; Lu, Y.; Shim, H.; Sim, K.; Kim, N. I.; Rao, Z.; Guevara, R.; Contreras, L.; Pan, F.; Zhang, Y.; Guan, Y. S.; Yang, P.; Wang, X.; Wang, P.; Wu, X.; Yu, C. Ultra-Conformal Drawn-on-Skin Electronics for Multifunctional Motion Artifact-Free Sensing and Point-of-Care Treatment. *Nature Communications* **2020**, *11* (1), 1–13. https://doi.org/10.1038/s41467-020-17619-1.

(282) Nawrocki, R. A.; Jin, H.; Lee, S.; Yokota, T.; Sekino, M.; Someya, T. Self-Adhesive and Ultra-Conformable, Sub-300 Nm Dry Thin-Film Electrodes for Surface Monitoring of Biopotentials. *Advanced Functional Materials* **2018**, *28* (36), 1–11. https://doi.org/10.1002/adfm.201803279.

(283) Sim, K.; Ershad, F.; Zhang, Y.; Yang, P.; Shim, H.; Rao, Z.; Lu, Y.; Thukral, A.; Elgalad, A.; Xi, Y.; Tian, B.; Taylor, D. A.; Yu, C. An Epicardial Bioelectronic Patch Made from Soft Rubbery Materials and Capable of Spatiotemporal Mapping of Electrophysiological Activity. *Nature Electronics* **2020**, *3* (12), 775–784. https://doi.org/10.1038/s41928-020-00493-6.

(284) Deng, J.; Yuk, H.; Wu, J.; Varela, C. E.; Chen, X.; Roche, E. T.; Guo, C. F.; Zhao, X. Electrical Bioadhesive Interface for Bioelectronics. *Nature Materials* **2021**, *20* (2), 229–236. https://doi.org/10.1038/s41563-020-00814-2.

(285) Zhang, L.; Kumar, K. S.; He, H.; Cai, C. J.; He, X.; Gao, H.; Yue, S.; Li, C.; Seet, R. C. S.; Ren, H.; Ouyang, J. Fully Organic Compliant Dry Electrodes Self-Adhesive to Skin for Long-Term Motion-Robust Epidermal Biopotential Monitoring. *Nature Communications* **2020**, *11* (1), 1–13. https://doi.org/10.1038/s41467-020-18503-8.

(286) Wicaksono, I.; Tucker, C. I.; Sun, T.; Guerrero, C. A.; Liu, C.; Woo, W. M.; Pence, E. J.; Dagdeviren, C. A Tailored, Electronic Textile Conformable Suit for Large-Scale Spatiotemporal Physiological Sensing in Vivo. *npj Flexible Electronics* **2020**, *4* (1). https://doi.org/10.1038/s41528-020-0068-y.

(287) Jin, H.; Nayeem, M. O. G.; Lee, S.; Matsuhisa, N.; Inoue, D.; Yokota, T.; Hashizume, D.; Someya, T. Highly Durable Nanofiber-Reinforced Elastic Conductors for Skin-Tight Electronic Textiles. *ACS Nano* **2019**, *13* (7), 7905–7912. https://doi.org/10.1021/acsnano.9b02297.

(288) Li, B. M.; Mills, A. C.; Flewwellin, T. J.; Herzberg, J. L.; Bosari, A. S.; Lim, M.; Jia, Y.; Jur, J. S. Influence of Armband Form Factors on Wearable ECG Monitoring Performance. *IEEE Sensors Journal* **2021**, *21* (9), 11046–11060. https://doi.org/10.1109/JSEN.2021.3059997.

(289) Wang, L.; Wang, L.; Zhang, Y.; Pan, J.; Li, S.; Sun, X.; Zhang, B.; Peng, H. Weaving Sensing Fibers into Electrochemical Fabric for Real-Time Health Monitoring. *Advanced Functional Materials* **2018**, *28* (42), 1–8. https://doi.org/10.1002/adfm.201804456.

(290) Jin, H.; Matsuhisa, N.; Lee, S.; Abbas, M.; Yokota, T.; Someya, T. Enhancing the Performance of Stretchable Conductors for E-Textiles by Controlled Ink Permeation. *Advanced Materials* **2017**, *29* (21). https://doi.org/10.1002/adma.201605848.

(291) Yapici, M. K.; Alkhidir, T.; Samad, Y. A.; Liao, K. Graphene-Clad Textile Electrodes for Electrocardiogram Monitoring. *Sensors and Actuators B: Chemical* **2015**, *221*, 1469–1474. https://doi.org/10.1016/j.snb.2015.07.111.

(292) Wang, C.; Xia, K.; Wang, H.; Liang, X.; Yin, Z.; Zhang, Y. Advanced Carbon for Flexible and Wearable Electronics. *Advanced Materials* **2019**, *31* (9), 1–37. https://doi.org/10.1002/adma.201801072.

(293) Trovato, V.; Teblum, E.; Kostikov, Y.; Pedrana, A.; Re, V.; Nessim, G. D.; Rosace, G. Sol-Gel Approach to Incorporate Millimeter-Long Carbon Nanotubes into Fabrics for the Development of Electrical-Conductive Textiles. *Materials Chemistry and Physics* **2020**, *240* (March 2019), 122218. https://doi.org/10.1016/j.matchemphys.2019.122218.

(294) Yang, J. C.; Mun, J.; Kwon, S. Y.; Park, S.; Bao, Z.; Park, S. Electronic Skin: Recent Progress and Future Prospects for Skin-Attachable Devices for Health Monitoring, Robotics, and Prosthetics. *Advanced Materials* **2019**, *31* (48), 1–50. https://doi.org/10.1002/adma.201904765.

(295) Lee, S. M.; Byeon, H. J.; Lee, J. H.; Baek, D. H.; Lee, K. H.; Hong, J. S.; Lee, S. H. Self-Adhesive Epidermal Carbon Nanotube Electronics for Tether-Free Long-Term Continuous Recording of Biosignals. *Scientific Reports* **2014**, *4* (1), 6074. https://doi.org/10.1038/srep06074.

(296) Liu, B.; Tang, H.; Luo, Z.; Zhang, W.; Tu, Q.; Jin, X. Wearable Carbon Nanotubes-Based Polymer Electrodes for Ambulatory Electrocardiographic Measurements. *Sensors and Actuators, A: Physical* **2017**, *265*, 79–85. https://doi.org/10.1016/j.sna.2017.08.036.

(297) Liu, B.; Luo, Z.; Zhang, W.; Tu, Q.; Jin, X. Silver Nanowire-Composite Electrodes for Long-Term Electrocardiogram Measurements. *Sensors and Actuators, A: Physical* **2016**, *247*, 459–464. https://doi.org/10.1016/j.sna.2016.06.008.

(298) Koo, J. H.; Jeong, S.; Shim, H. J.; Son, D.; Kim, J.; Kim, D. C.; Choi, S.; Hong, J. I.; Kim, D. H. Wearable Electrocardiogram Monitor Using Carbon Nanotube Electronics and Color-Tunable Organic Light-Emitting Diodes. *ACS Nano* **2017**, *11* (10), 10032–10041. https://doi.org/10.1021/acsnano.7b04292.

(299) Li, B. M.; Yildiz, O.; Mills, A. C.; Flewwellin, T. J.; Bradford, P. D.; Jur, J. S. Iron-on Carbon Nanotube (CNT) Thin Films for Biosensing E-Textile Applications. *Carbon* **2020**, *168*, 673–683. https://doi.org/10.1016/j.carbon.2020.06.057.

(300) Taylor, L. W.; Williams, S. M.; Yan, J. S.; Dewey, O. S.; Vitale, F.; Pasquali, M. Washable, Sewable, All-Carbon Electrodes and Signal Wires for Electronic Clothing. *Nano Letters* **2021**, *21* (17), 7093–7099. https://doi.org/10.1021/acs.nanolett.1c01039.

(301) Aly, K.; Li, A.; Bradford, P. D. Strain Sensing in Composites Using Aligned Carbon Nanotube Sheets Embedded in the Interlaminar Region. *Composites Part A: Applied*

Science and Manufacturing **2016**, *90*, 536–548. https://doi.org/10.1016/j.compositesa.2016.08.003.

(302) He, N.; Yildiz, O.; Pan, Q.; Zhu, J.; Zhang, X.; Bradford, P. D.; Gao, W. Pyrolytic-Carbon Coating in Carbon Nanotube Foams for Better Performance in Supercapacitors. *Journal of Power Sources* **2017**, *343*, 492–501. https://doi.org/10.1016/j.jpowsour.2017.01.091.

(303) Aly, K.; Bradford, P. D. Real-Time Impact Damage Sensing and Localization in Composites through Embedded Aligned Carbon Nanotube Sheets. *Composites Part B: Engineering* **2019**. https://doi.org/10.1016/j.compositesb.2018.12.104.

(304) Anike, J. C.; Belay, K.; Abot, J. L. Effect of Twist on the Electromechanical Properties of Carbon Nanotube Yarns. *Carbon* **2019**, *142*, 491–503. https://doi.org/10.1016/j.carbon.2018.10.067.

(305) Xu, W.; Chen, Y.; Zhan, H.; Wang, J. N. High-Strength Carbon Nanotube Film from Improving Alignment and Densification. *Nano Letters* **2016**, *16* (2), 946–952. https://doi.org/10.1021/acs.nanolett.5b03863.

(306) Luo, X.; Weng, W.; Liang, Y.; Hu, Z.; Zhang, Y.; Yang, J.; Yang, L.; Yang, S.; Zhu, M.; Cheng, H. M. Multifunctional Fabrics of Carbon Nanotube Fibers. *Journal of Materials Chemistry A* **2019**, *7* (15), 8790–8797. https://doi.org/10.1039/c9ta01474h.

(307) Uzun, S.; Seyedin, S.; Stoltzfus, A. L.; Levitt, A. S.; Alhabeb, M.; Anayee, M.; Strobel, C. J.; Razal, J. M.; Dion, G.; Gogotsi, Y. Knittable and Washable Multifunctional MXene-Coated Cellulose Yarns. *Advanced Functional Materials* **2019**, *29* (45), 1–13. https://doi.org/10.1002/adfm.201905015.

(308) Maziz, A.; Concas, A.; Khaldi, A.; Stålhand, J.; Persson, N. K.; Jager, E. W. H. Knitting and Weaving Artificial Muscles. *Science Advances* **2017**, *3* (1), 1–11.

(309) Li, B. M.; Yildiz, O.; Mills, A. C.; Flewwellin, T. J.; Bradford, P. D.; Jur, J. S. Iron-on Carbon Nanotube (CNT) Thin Films for Biosensing E-Textile Applications. *Carbon* **2020**, *168*, 673–683. https://doi.org/10.1016/j.carbon.2020.06.057.

(310) Lee, S. M.; Byeon, H. J.; Lee, J. H.; Baek, D. H.; Lee, K. H.; Hong, J. S.; Lee, S. H. Self-Adhesive Epidermal Carbon Nanotube Electronics for Tether-Free Long-Term Continuous Recording of Biosignals. *Scientific Reports* **2014**, *4*. https://doi.org/10.1038/srep06074.

(311) Taylor, L. W.; Williams, S. M.; Yan, J. S.; Dewey, O. S.; Vitale, F.; Pasquali, M. Washable, Sewable, All-Carbon Electrodes and Signal Wires for Electronic Clothing. *Nano Letters* **2021**, *21* (17), 7093–7099. https://doi.org/10.1021/acs.nanolett.1c01039.

(312) O'Mahony, C.; Grygoryev, K.; Ciarlone, A.; Giannoni, G.; Kenthao, A.; Galvin, P. Design, Fabrication and Skin-Electrode Contact Analysis of Polymer Microneedle-Based ECG Electrodes. *Journal of Micromechanics and Microengineering* **2016**, *26* (8). https://doi.org/10.1088/0960-1317/26/8/084005.

(313) Zhou, W.; Song, R.; Pan, X.; Peng, Y.; Qi, X.; Peng, J.; Hui, K. S.; Hui, K. N. Fabrication and Impedance Measurement of Novel Metal Dry Bioelectrode. *Sensors and Actuators, A: Physical* **2013**, *201*, 127–133. https://doi.org/10.1016/j.sna.2013.06.025.

(314) Xu, X.; Luo, M.; He, P.; Yang, J. Washable and Flexible Screen Printed Graphene Electrode on Textiles for Wearable Healthcare Monitoring. *Journal of Physics D: Applied Physics* **2020**, *53* (12). https://doi.org/10.1088/1361-6463/ab5f4a.

(315) Achilli, A.; Bonfiglio, A.; Pani, D. Design and Characterization of Screen-Printed Textile Electrodes for ECG Monitoring. *IEEE Sensors Journal* **2018**, *18* (10), 4097–4107. https://doi.org/10.1109/JSEN.2018.2819202.

(316) Trindade, I. G.; Martins, F.; Baptista, P. High Electrical Conductance Poly(3,4-Ethylenedioxythiophene) Coatings on Textile for Electrocardiogram Monitoring. *Synthetic Metals* **2015**, *210*, 179–185. https://doi.org/10.1016/j.synthmet.2015.09.024.

(317) Ankhili, A.; Tao, X.; Cochrane, C.; Koncar, V.; Coulon, D.; Tarlet, J. M. Comparative Study on Conductive Knitted Fabric Electrodes for Long-Term Electrocardiography Monitoring: Silver-Plated and PEDOT:PSS Coated Fabrics. *Sensors (Switzerland)* **2018**, *18* (11). https://doi.org/10.3390/s18113890.

(318) Takamatsu, S.; Lonjaret, T.; Crisp, D.; Badier, J. M.; Malliaras, G. G.; Ismailova, E. Direct Patterning of Organic Conductors on Knitted Textiles for Long-Term Electrocardiography. *Scientific Reports* **2015**, *5*. https://doi.org/10.1038/srep15003.

(319) Shathi, M. A.; Chen, M.; Khoso, N. A.; Rahman, M. T.; Bhattacharjee, B. Graphene Coated Textile Based Highly Flexible and Washable Sports Bra for Human Health Monitoring. *Materials and Design* **2020**, *193*. https://doi.org/10.1016/j.matdes.2020.108792.

(320) Akter Shathi, M.; Minzhi, C.; Khoso, N. A.; Deb, H.; Ahmed, A.; Sai Sai, W. All Organic Graphene Oxide and Poly (3, 4-Ethylene Dioxythiophene) - Poly (Styrene Sulfonate)

Coated Knitted Textile Fabrics for Wearable Electrocardiography (ECG) Monitoring. *Synthetic Metals* **2020**, *263*. https://doi.org/10.1016/j.synthmet.2020.116329.

(321) Yokus, M. A.; Jur, J. S. Fabric-Based Wearable Dry Electrodes for Body Surface Biopotential Recording. *IEEE Transactions on Biomedical Engineering* **2016**, *63* (2), 423–430. https://doi.org/10.1109/TBME.2015.2462312.

(322) Rajanna, R. R.; Sriraam, N.; Vittal, P. R.; Arun, U. Performance Evaluation of Woven Conductive Dry Textile Electrodes for Continuous ECG Signals Acquisition. *IEEE Sensors Journal* **2020**, *20* (3), 1573–1581. https://doi.org/10.1109/JSEN.2019.2946058.

(323) Lee, E.; Cho, G. PU Nanoweb-Based Textile Electrode Treated with Single-Walled Carbon Nanotube/Silver Nanowire and Its Application to ECG Monitoring. *Smart Materials and Structures* **2019**, *28* (4). https://doi.org/10.1088/1361-665X/ab06e0.

(324) Yapici, M. K.; Alkhidir, T.; Samad, Y. A.; Liao, K. Graphene-Clad Textile Electrodes for Electrocardiogram Monitoring. *Sensors and Actuators B: Chemical* **2015**, *221*, 1469–1474. https://doi.org/10.1016/j.snb.2015.07.111.

(325) Chlaihawi, A. A.; Narakathu, B. B.; Emamian, S.; Bazuin, B. J.; Atashbar, M. Z. Development of Printed and Flexible Dry ECG Electrodes. *Sensing and Bio-Sensing Research* **2018**, *20*, 9–15. https://doi.org/10.1016/j.sbsr.2018.05.001.

(326) Saleh, S. M.; Jusob, S. M.; Harun, F. K. C.; Yuliati, L.; Wicaksono, D. H. B. Optimization of Reduced GO-Based Cotton Electrodes for Wearable Electrocardiography. *IEEE Sensors Journal* **2020**, *20* (14), 7774–7782. https://doi.org/10.1109/JSEN.2020.2981262.

(327) Moreno, A.; Walton, R. D.; Bayer, J. D. Stretchable Conductive Fabric for Cardiac Electrophysiology Applications. *ACS Applied Bio Materials* **2020**, *3* (5), 3114–3122. https://doi.org/10.1021/acsabm.0c00155.

(328) Xu, X.; Luo, M.; He, P.; Yang, J. Washable and Flexible Screen Printed Graphene Electrode on Textiles for Wearable Healthcare Monitoring. *Journal of Physics D: Applied Physics* **2020**, *53* (12). https://doi.org/10.1088/1361-6463/ab5f4a.

(329) Xu, X.; Xie, S.; Zhang, Y.; Peng, H. The Rise of Fiber Electronics. *Angewandte Chemie* **2019**, *131* (39), 13778–13788. https://doi.org/10.1002/ange.201902425.

(330) Zulan, L.; Zhi, L.; Lan, C.; Sihao, C.; Dayang, W.; Fangyin, D. Reduced Graphene Oxide Coated Silk Fabrics with Conductive Property for Wearable Electronic Textiles

Application. *Advanced Electronic Materials* **2019**, *5* (4). https://doi.org/10.1002/aelm.201800648.

(331) Zeng, W.; Shu, L.; Li, Q.; Chen, S.; Wang, F.; Tao, X. M. Fiber-Based Wearable Electronics: A Review of Materials, Fabrication, Devices, and Applications. *Advanced Materials*. Wiley-VCH Verlag August 20, 2014, pp 5310–5336. https://doi.org/10.1002/adma.201400633.

(332) Huang, Y.; Hu, H.; Huang, Y.; Zhu, M.; Meng, W.; Liu, C.; Pei, Z.; Hao, C.; Wang, Z.; Zhi, C. From Industrially Weavable and Knittable Highly Conductive Yarns to Large Wearable Energy Storage Textiles. *ACS Nano* **2015**, *9* (5), 4766–4775. https://doi.org/10.1021/acsnano.5b00860.

(333) Araromi, O. A.; Graule, M. A.; Dorsey, K. L.; Castellanos, S.; Foster, J. R.; Hsu, W. H.; Passy, A. E.; Vlassak, J. J.; Weaver, J. C.; Walsh, C. J.; Wood, R. J. Ultra-Sensitive and Resilient Compliant Strain Gauges for Soft Machines. *Nature* **2020**, *587* (7833), 219–224. https://doi.org/10.1038/s41586-020-2892-6.

(334) Wu, R.; Ma, L.; Hou, C.; Meng, Z.; Guo, W.; Yu, W.; Yu, R.; Hu, F.; Liu, X. Y. Silk Composite Electronic Textile Sensor for High Space Precision 2D Combo Temperature–Pressure Sensing. *Small* **2019**, *15* (31). https://doi.org/10.1002/smll.201901558.

(335) Fan, W.; He, Q.; Meng, K.; Tan, X.; Zhou, Z.; Zhang, G.; Yang, J.; Lin Wang, Z. *Machine-Knitted Washable Sensor Array Textile for Precise Epidermal Physiological Signal Monitoring*; 2020; Vol. 6.

(336) Wang, L.; Fu, X.; He, J.; Shi, X.; Chen, T.; Chen, P.; Wang, B.; Peng, H. Application Challenges in Fiber and Textile Electronics. *Advanced Materials*. Wiley-VCH Verlag February 1, 2020. https://doi.org/10.1002/adma.201901971.

(337) Weng, W.; Sun, Q.; Zhang, Y.; Lin, H.; Ren, J.; Lu, X.; Wang, M.; Peng, H. Winding Aligned Carbon Nanotube Composite Yarns into Coaxial Fiber Full Batteries with High Performances. *Nano Letters* **2014**, *14* (6), 3432–3438. https://doi.org/10.1021/nl5009647.

(338) Shi, J.; Liu, S.; Zhang, L.; Yang, B.; Shu, L.; Yang, Y.; Ren, M.; Wang, Y.; Chen, J.; Chen, W.; Chai, Y.; Tao, X. Smart Textile-Integrated Microelectronic Systems for Wearable Applications. *Advanced Materials*. Wiley-VCH Verlag February 1, 2020. https://doi.org/10.1002/adma.201901958.

(339) Cui, J.; Zhou, S. Highly Conductive and Ultra-Durable Electronic Textiles via Covalent Immobilization of Carbon Nanomaterials on Cotton Fabric. *Journal of Materials Chemistry C* **2018**, *6* (45), 12273–12282. https://doi.org/10.1039/C8TC04017F.

(340) Wang, Q. W.; Zhang, H. bin; Liu, J.; Zhao, S.; Xie, X.; Liu, L.; Yang, R.; Koratkar, N.; Yu, Z. Z. Multifunctional and Water-Resistant MXene-Decorated Polyester Textiles with Outstanding Electromagnetic Interference Shielding and Joule Heating Performances. *Advanced Functional Materials* **2019**, *29* (7). https://doi.org/10.1002/adfm.201806819.

(341) Wang, J. N.; Luo, X. G.; Wu, T.; Chen, Y. High-Strength Carbon Nanotube Fibre-like Ribbon with High Ductility and High Electrical Conductivity. *Nature Communications* **2014**, *5*. https://doi.org/10.1038/ncomms4848.

(342) Lu, W.; Zu, M.; Byun, J. H.; Kim, B. S.; Chou, T. W. State of the Art of Carbon Nanotube Fibers: Opportunities and Challenges. *Advanced Materials*. April 10, 2012, pp 1805–1833. https://doi.org/10.1002/adma.201104672.

(343) Dalton, A. B. ; Collins, S. ; Munoz, E. ;; Razal, J. M. *Super-Tough Carbon-Nanotube Fibres*; 2003; Vol. 12.

(344) Behabtu, N.; Young, C. C.; Tsentalovich, D. E.; Kleinerman, O.; Wang, X.; Ma, A. W. K.; Bengio, E. A.; ter Waarbeek, R. F.; de Jong, J. J.; Hoogerwerf, R. E.; Fairchild, S. B.; Ferguson, J. B.; Maruyama, B.; Kono, J.; Talmon, Y.; Cohen, Y.; Otto, M. J.; Pasquali, M. Strong, Light, Multifunctional Fibers of Carbon Nanotubes with Ultrahigh Conductivity. *Science* **2013**, *339* (6116), 182–186. https://doi.org/10.1126/science.1228061.

(345) Zhang, M.; Atkinson, K. R.; Baughman, R. H. Multifunctional Carbon Nanotube Yarns by Downsizing an Ancient Technology. *Science* **2004**, *306* (5700), 1358–1361. https://doi.org/10.1126/science.1104276.

(346) Li, Y. L.; Kinloch, I. A.; Windle, A. H. Direct Spinning of Carbon Nanotube Fibers from Chemical Vapor Deposition Synthesis. *Science* **2004**, *304* (5668), 276–278. https://doi.org/10.1126/science.1094982.

(347) Yamada, T.; Hayamizu, Y.; Yamamoto, Y.; Yomogida, Y.; Izadi-Najafabadi, A.; Futaba, D. N.; Hata, K. A Stretchable Carbon Nanotube Strain Sensor for Human-Motion Detection. *Nature Nanotechnology* **2011**, *6* (5), 296–301. https://doi.org/10.1038/nnano.2011.36.

(348) Li, Y.; Shang, Y.; He, X.; Peng, Q.; Du, S.; Shi, E.; Wu, S.; Li, Z.; Li, P.; Cao, A. Overtwisted, Resolvable Carbon Nanotube Yarn Entanglement as Strain Sensors and

Rotational Actuators. *ACS Nano* **2013**, *7* (9), 8128–8135. https://doi.org/10.1021/nn403400c.

(349) Zhou, J.; Xu, X.; Xin, Y.; Lubineau, G. Coaxial Thermoplastic Elastomer-Wrapped Carbon Nanotube Fibers for Deformable and Wearable Strain Sensors. *Advanced Functional Materials* **2018**, *28* (16). https://doi.org/10.1002/adfm.201705591.

(350) Wang, C.; Zhang, M.; Xia, K.; Gong, X.; Wang, H.; Yin, Z.; Guan, B.; Zhang, Y. Intrinsically Stretchable and Conductive Textile by a Scalable Process for Elastic Wearable Electronics. *ACS Applied Materials and Interfaces* **2017**, *9* (15), 13331–13338. https://doi.org/10.1021/acsami.7b02985.

(351) Lee, D. W.; Kim, H.; Moon, J. H.; Jeong, J. H.; Sim, H. J.; Kim, B. J.; Hyeon, J. S.; Baughman, R. H.; Kim, S. J. Orthogonal Pattern of Spinnable Multiwall Carbon Nanotubes for Electromagnetic Interference Shielding Effectiveness. *Carbon* **2019**, *152*, 33–39. https://doi.org/10.1016/j.carbon.2019.05.052.

(352) Kim, S. H.; Haines, C. S.; Li, N.; Kim, K. J.; Mun, T. J.; Choi, C.; Di, J.; Oh, Y. J.; Oviedo, J. P.; Bykova, J.; Fang, S.; Jiang, N.; Liu, Z.; Wang, R.; Kumar, P.; Qiao, R.; Priya, S.; Cho, K.; Kim, M.; Lucas, M. S.; Drummy, L. F.; Maruyama, B.; Lee, D. Y.; Lepró, X.; Gao, E.; Albarq, D.; Ovalle-Robles, R.; Kim, S. J.; Ray, †; Baughman, H. *Harvesting Electrical Energy from Carbon Nanotube Yarn Twist*; 2017; Vol. 357.

(353) Zhang, D.; Miao, M.; Niu, H.; Wei, Z. Core-Spun Carbon Nanotube Yarn Supercapacitors for Wearable Electronic Textiles. *ACS Nano* **2014**, *8* (5), 4571–4579. https://doi.org/10.1021/nn5001386.

(354) Seyedin, S.; Uzun, S.; Levitt, A.; Anasori, B.; Dion, G.; Gogotsi, Y.; Razal, J. M. MXene Composite and Coaxial Fibers with High Stretchability and Conductivity for Wearable Strain Sensing Textiles. *Advanced Functional Materials* **2020**, *30* (12). https://doi.org/10.1002/adfm.201910504.

(355) Wang, Q.; Wu, Y.; Li, T.; Zhang, D.; Miao, M.; Zhang, A. High Performance Two-Ply Carbon Nanocomposite Yarn Supercapacitors Enhanced with a Platinum Filament and in Situ Polymerized Polyaniline Nanowires. *Journal of Materials Chemistry A* **2016**, *4* (10), 3828–3834. https://doi.org/10.1039/c5ta10667b.

(356) Levitt, A.; Hegh, D.; Phillips, P.; Uzun, S.; Anayee, M.; Razal, J. M.; Gogotsi, Y.; Dion, G. 3D Knitted Energy Storage Textiles Using MXene-Coated Yarns. *Materials Today* **2020**, *34*, 17–29. https://doi.org/10.1016/j.mattod.2020.02.005.

(357) Liu, L. X.; Chen, W.; Zhang, H. bin; Wang, Q. W.; Guan, F.; Yu, Z. Z. Flexible and Multifunctional Silk Textiles with Biomimetic Leaf-Like MXene/Silver Nanowire Nanostructures for Electromagnetic Interference Shielding, Humidity Monitoring, and Self-Derived Hydrophobicity. *Advanced Functional Materials* **2019**, *29* (44). https://doi.org/10.1002/adfm.201905197.

(358) Zhang, X.; Wang, X.; Lei, Z.; Wang, L.; Tian, M.; Zhu, S.; Xiao, H.; Tang, X.; Qu, L. Flexible MXene-Decorated Fabric with Interwoven Conductive Networks for Integrated Joule Heating, Electromagnetic Interference Shielding, and Strain Sensing Performances. *ACS Applied Materials and Interfaces* **2020**, *12* (12), 14459–14467. https://doi.org/10.1021/acsami.0c01182.

(359) Liu, X.; Jin, X.; Li, L.; Wang, J.; Yang, Y.; Cao, Y.; Wang, W. Air-Permeable, Multifunctional, Dual-Energy-Driven MXene-Decorated Polymeric Textile-Based Wearable Heaters with Exceptional Electrothermal and Photothermal Conversion Performance. *Journal of Materials Chemistry A* **2020**, *8* (25), 12526–12537. https://doi.org/10.1039/d0ta03048a.

(360) Wang, Z.; Qin, S.; Seyedin, S.; Zhang, J.; Wang, J.; Levitt, A.; Li, N.; Haines, C.; Ovalle-Robles, R.; Lei, W.; Gogotsi, Y.; Baughman, R. H.; Razal, J. M. High-Performance Biscrolled MXene/Carbon Nanotube Yarn Supercapacitors. *Small* **2018**, *14* (37). https://doi.org/10.1002/smll.201802225.

(361) Park, J. W.; Lee, D. Y.; Kim, H.; Hyeon, J. S.; de Andrade, M. J.; Baughman, R. H.; Kim, S. J. Highly Loaded MXene/Carbon Nanotube Yarn Electrodes for Improved Asymmetric Supercapacitor Performance. *MRS Communications* **2019**, *9* (1), 114–121. https://doi.org/10.1557/mrc.2019.7.

(362) Yu, C.; Gong, Y.; Chen, R.; Zhang, M.; Zhou, J.; An, J.; Lv, F.; Guo, S.; Sun, G. A Solid-State Fibriform Supercapacitor Boosted by Host–Guest Hybridization between the Carbon Nanotube Scaffold and MXene Nanosheets. *Small* **2018**, *14* (29). https://doi.org/10.1002/smll.201801203.

(363) Uzun, S.; Seyedin, S.; Stoltzfus, A. L.; Levitt, A. S.; Alhabeb, M.; Anayee, M.; Strobel, C. J.; Razal, J. M.; Dion, G.; Gogotsi, Y. Knittable and Washable Multifunctional MXene-Coated Cellulose Yarns. *Advanced Functional Materials* **2019**, *29* (45). https://doi.org/10.1002/adfm.201905015.

(364) Faraji, S.; L. Stano, K.; Yildiz, O.; Li, A.; Zhu, Y.; Bradford, P. D. Ultralight Anisotropic Foams from Layered Aligned Carbon Nanotube Sheets. *Nanoscale* **2015**, *7* (40), 17038–17047. https://doi.org/10.1039/c5nr03899e.

(365) Alhabeb, M.; Maleski, K.; Anasori, B.; Lelyukh, P.; Clark, L.; Sin, S.; Gogotsi, Y. Guidelines for Synthesis and Processing of Two-Dimensional Titanium Carbide (Ti3C2Tx MXene). *Chemistry of Materials* **2017**, *29* (18), 7633–7644. https://doi.org/10.1021/acs.chemmater.7b02847.

(366) Ning, H.; Ma, Z.; Zhang, Z.; Zhang, D.; Wang, Y. A Novel Multifunctional Flame Retardant MXene/Nanosilica Hybrid for Poly(Vinyl Alcohol) with Simultaneously Improved Mechanical Properties. *New Journal of Chemistry* **2021**, *45* (9), 4292–4302. https://doi.org/10.1039/d0nj04897f.

(367) Sun, K.; Wang, F.; Yang, W.; Liu, H.; Pan, C.; Guo, Z.; Liu, C.; Shen, C. Flexible Conductive Polyimide Fiber/MXene Composite Film for Electromagnetic Interference Shielding and Joule Heating with Excellent Harsh Environment Tolerance. *ACS Applied Materials & Interfaces* **2021**, *13* (42), 50368–50380. https://doi.org/10.1021/acsami.1c15467.

(368) Biccai, S.; Boland, C. S.; Odriscoll, D. P.; Harvey, A.; Gabbett, C.; Osuilleabhain, D. R.; Griffin, A. J.; Li, Z.; Young, R. J.; Coleman, J. N. Negative Gauge Factor Piezoresistive Composites Based on Polymers Filled with MoS2 Nanosheets. *ACS Nano* **2019**, *13* (6), 6845–6855. https://doi.org/10.1021/acsnano.9b01613.

(369) Cai, Y.; Shen, J.; Ge, G.; Zhang, Y.; Jin, W.; Huang, W.; Shao, J.; Yang, J.; Dong, X. Stretchable Ti3C2Tx MXene/Carbon Nanotube Composite Based Strain Sensor with Ultrahigh Sensitivity and Tunable Sensing Range. *ACS Nano* **2018**, *12* (1), 56–62. https://doi.org/10.1021/acsnano.7b06251.

(370) Li, H.; Du, Z. Preparation of a Highly Sensitive and Stretchable Strain Sensor of MXene/Silver Nanocomposite-Based Yarn and Wearable Applications. *ACS Applied*

Materials and Interfaces **2019**, *11* (49), 45930–45938. https://doi.org/10.1021/acsami.9b19242.

(371) Yang, Y.; Shi, L.; Cao, Z.; Wang, R.; Sun, J. Strain Sensors with a High Sensitivity and a Wide Sensing Range Based on a Ti 3 C 2 T x (MXene) Nanoparticle–Nanosheet Hybrid Network. *Advanced Functional Materials* **2019**, *29* (14). https://doi.org/10.1002/adfm.201807882.